Modelling haematopoietic malignancies using zebrafish

Oscar A Peña

A thesis submitted for the degree of Doctor of Philosophy

University College London

November, 2018

Declaration

I, Oscar Andrés Peña Cabello confirm that the work presented in this thesis is my own. Where information has been derived from other sources, I confirm that this has been indicated in the thesis.

Signed:

Date:

Abstract

Primitive and definitive haematopoiesis were studied during embryonic and larval development in three zebrafish models of human haematological diseases: TEL-AML1 expressing acute lymphoblastic leukaemia (ALL), GATA2 haploinsufficient disorders, and MDS with isolated del(5q) (MDS5q).

The t(12;21)(p13;q22) chromosomal translocation resulting in the TEL-AML1 fusion gene is the most common translocation in childhood ALL. The translocation arises *in utero* and can be found in approximately 1% of new-born infants. However, less than 1% of these children develop leukaemia and this translocation is not observed in adult ALL. This suggests that the cell of origin resulting in the eventual transformation to BCP-ALL is present and disrupted early during development. Early developmental haematopoiesis was studied in transgenic zebrafish expressing the human TEL-AML1 fusion protein. The numbers of granulocytes are transiently increased by the expression of TEL-AML1 fusion protein in these animals.

The *GATA2* gene encodes a transcription factor that plays a major role in haematopoiesis. Recently, germline GATA2 mutations have been identified as the cause of a range of haemato-vascular disorders including Emberger syndrome, Monomac and DCML deficiency all with predisposition to MDS. We took advantage of the presence of two GATA2 paralogs (*gata2a* and *gata2b*) in zebrafish to dissect the role of GATA2 in early haematopoietic and vascular development. Gata2a and Gata2b were shown to have different functions in haematopoiesis. Gata2a regulates primitive myeloid cell development and vascular morphogenesis. The first wave of lymphocytes and haematopoietic progenitors derived from the dorsal aorta are also affected. A novel role for the Gata2b was identified, in the development of myeloid cells in the caudal haematopoietic tissue. Double heterozygous fish carrying mutations in both *gata2a* and *gata2b* were used to model germinal mutations in *GATA2* found in patients.

Ribosomal protein gene 14 (*RPS14*), located on 5q, has been shown to be the likely genetic determinant of anaemia in patients with MDS5q. Our group has used TALENs to generate an *rps14* mutant zebrafish. Fish carrying a heterozygous mutation in *rps14* gene show defects in erythropoiesis and granulopoiesis, and the

severity of these defects is enhanced by haemolytic or cold stress. The rescuing effects of a TLR7/8 agonist, imiquimod, identified previously in a small molecule screen for modifiers of the anaemia phenotype associated with Rps14 loss, were studied in *rps14* mutant fish. Pharmacological evidence suggests a role for TLR7 in erythroid development, as exposure to a TLR7 agonist partially rescues the phenotype of heterozygous *rps14* mutant fish, while treatment with a TLR8 agonist has no effect.

Impact Statement

In this work, developmental haematopoiesis was studied in zebrafish models of haematopoietic malignancies. The findings presented in this thesis contribute to the understanding of the role of *gata2a*, *gata2b*, and *rps14* genes in developmental haematopoiesis.

Through the analysis of developmental haematopoiesis in fish carrying mutations in *gata2a* and *gata2b* genes, distinctive functions for both zebrafish paralogs of the human GATA2 gene were defined. These findings show that the *gata2a* gene has a role in the differentiation of primitive macrophages during primitive haematopoiesis, in addition to its role in vascular morphogenesis. On the other hand, *gata2b* is shown to have a role in the development of granulocytes at the start of definitive haematopoiesis. Additionally, new stable zebrafish lines carrying mutations in the *gata2b* gene were produced, which will serve as a tool to both study the function of the zebrafish *gata2b* gene and to model GATA2 haploinsufficiency in zebrafish.

The characterization of developmental haematopoiesis in *rps14* mutant fish showed subtle perturbations elicited by haploinsufficient levels of Rps14. However, heterozygous mutant larvae show anaemia under conditions of stress. Low temperature elicits poor haemoglobinization of erythrocytes. Similarly, recovery after haemolytic stress is also reduced in heterozygotes. Further experiments building on previous work in our group allowed the identification of TLR7 activation as an important pathway that regulates the development of erythroid cells. These findings validate the use of heterozygous *rps14* mutant fish as a model of MDS with loss of 5q. The combined use of CRISPR applications and NGS will allow the development of zebrafish models of increasing complexity to study the genetic interactions of *rps14* with other genes affected by this chromosomal alteration.

A complete understanding of the early events that precede overt disease is key to the development of new tools for diagnosis and treatment. Although the scope of this work does not include work with human samples, the examples of conservation of the molecular mechanisms between experimental animal models and human patients are numerous. The findings presented in chapter 6 (Modelling MDS with loss of 5q using *rps14* mutants) are a good example of the discovery of candidate

pathways for the future development of strategies of treatment. Additional work with samples derived from patients has allowed the validation of these findings. However, extensive research on the underlying mechanisms of the rescue of anaemia induced by *rps14* haploinsufficiency by TLR7 activation will be necessary to develop a treatment based on these findings.

Dedication

A mi madre y a mi padre, por la perseverancia y la fortaleza.
Les debo todo.

A mi hermana, por el coraje para seguir el camino propio.

Y a Jasmine, que me rescató de la oscuridad justo a tiempo.

Table of Contents

List of figures

List of tables

List of Supplementary Figures

List of Supplementary Tables

Abbreviations

%GC	percentage of guanine-cytosine content
4-OH	4-hydroxytamoxifen
aa	amino acid
AA	branchial arches
AGM	aorta-gonad mesonephros
ALL	acute lymphoblastic leukaemia
ALPM	anterior lateral plate mesoderm
AML	acute myeloid leukaemia
AML1	acute myeloid leukaemia 1 protein
ANOVA	analysis of variance
ASXL1	Additional sex combs-like 1 gene
B-ALL	B cell acute lymphoblastic leukaemia
BCIP	5-bromo-4-chloro-3-indolyl-phosphate
bHLH	basic helix-loop-helix
bp	base pair
BSA	bovine serum albumin
CA	caudal artery
Cas9	CRISPR associated protein 9
CBFβ	core binding factor β
CDKN2A	cyclin dependent kinase inhibitor 2A
CDR	commonly deleted region
cebpα	CCAAT/enhancer-binding protein alpha

CFP	cyan fluorescent protein
CHT	caudal haematopoietic tissue
CI	confidence interval
CMML	chronic myelomonocytic leukaemia
cpa5	carboxypeptidase A5
CRISPR	clustered regularly interspaced short palindromic repeats
CRLF2	cytokine receptor like factor 2
crRNA	CRISPR RNA
csf1r	macrophage colony-stimulating factor receptor
CV	caudal vein
DCML	dendritic cells, monocytes, B and natural killer lymphoid cells deficiency
DLAV	dorsal longitudinal anastomotic vessel
DMSO	Dimethyl sulfoxide
DNA	deoxyribonucleic acid
dNTP	deoxynucleoside triphosphate
dpf	days post-fertilization
dsDNA	double-stranded DNA
EBF1	early B cell factor 1
EDTA	ethylenediaminetetraacetic acid
EGFP	enhanced green fluorescent protein
ELANE	elastase, neutrophil expressed
ELB	embryo lysis buffer
EMP	erythromyeloid progenitor

ETO	eight twenty-one
ETS	E-Twenty-Six
ETV6	ETS variant 6
EVI1	ecotropic virus integration site 1 protein homolog
FBS	foetal bovine serum
GFP	green fluorescent protein
GLRA1	glycine receptor alpha 1
GRCz10	Genome Reference Consortium Zebrafish Build 10
GTF2I	general transcription factor IIi
HA	hypobranchial artery
HBB	haemoglobin subunit beta
hESC	human embryonic stem cell
HM	hybridization mix
hpf	hours post-fertilization
HSC	haematopoietic stem cell
HSPC	haematopoietic stem and progenitor cell
ICM	intermediate cellular mass
IGH	immunoglobulin heavy locus
IKZF1	IKAROS family zinc finger 1
INSDC	International Nucleotide Sequence Database Collaboration
itga2b	integrin, alpha 2b
kb	kilo-base pair
kdrl	kinase insert domain receptor like

klf2a	Kruppel-like factor 2a
lck	T-cell specific tyrosine kinase
lmo2	LIM domain only 2
LPL	leukocyte-plastin
lyz	lysozyme C
Mb	mega base pairs
MDS	myelodysplastic syndrome
miRNAs	microRNAs
MITF	melanogenesis associated transcription factor
mitfa	microphthalmia-associated transcription factor a
mKOκ	monomeric Kusabira orange kappa
monoMAC	monocytopenia with atypical mycobacterial infections
mpeg1.1	macrophage expressed 1, tandem duplicate 1
mpo	myeloperoxidase
mpx	myeloid peroxidase
NBT	4-Nitro blue tetrazolium chloride
nCas9n	NLS-Cas9-NLS
NGS	next-generation sequencing
NK	natural killer
NLS	nuclear localization signal
PAM	protospacer adjacent motif
PAX5	paired box 5
PBI	posterior blood island

PBS	phosphate-buffered saline
PBST	phosphate-buffered saline with 0.1% v/v Tween 20
PCR	polymerase chain reaction
PDGFRβ	beta-type platelet-derived growth factor receptor
PFA	paraformaldehyde
PHS	primary head synus
PHZ	phenylhydrazine
PICA	primitive internal carotid arteries
PLPM	posterior lateral plate mesoderm
PRC2	polycomb repressive complex 2
PTU	1-phenyl-2-thiourea
rag1	recombination activating gene 1
rag2	recombination activating gene 2
rcf	relative centrifugal force
RFP	red fluorescent protein
RhoGAP	Rho GTPase activating proteins
RNA	ribonucleic acid
RPS14	ribosomal protein S-14
RPS19	ribosomal protein S-19
RPS20	ribosomal protein S-20
RUNX1	Runt-related transcription factor 1
RUNX1T1	RUNX1 translocation partner 1
Se	intersegmental vessel

SEM	standard error of the mean
SETBP1	SET binding protein 1
sgRNA	small guide RNA
spi1b	Spi-1 proto-oncogene b
ss	somite stage
SSC	saline-sodium citrate
ssDNA	single-stranded DNA
TALEN	transcription activator-like effector nucleases
TBE	Tris-Borate-EDTA
TEL	translocation, ETS, leukaemia
TLR	Toll-like receptor
TLR4	Toll-like receptor 4
TLR7	Toll-like receptor 7
TLR8	Toll-like receptor 8
tnnt2a	troponin T type 2a
tracrRNA	trans-activating crRNA
UTR	untranslated region
VA	ventral aorta
VEGFR2	vascular endothelial growth factor receptor 2
WISH	whole mount *in situ* hybridization
YFP	yellow fluorescent protein
ZFIN	Zebrafish Information Network

Introduction

1.1 Developmental haematopoiesis in zebrafish

1.1.1 Primitive haematopoiesis in zebrafish embryos

Haematopoietic and endothelial cells in zebrafish (*Danio rerio*) have a common origin, haemato-vascular progenitors derived from the mesoderm during early development (Gering et al., 2003). During somitogenesis, haemato-vascular progenitors can be observed as two anterolateral pairs of stripes of cells expressing markers like *lmo2* (LIM domain only 2) and *runx1* (Runt-related transcription factor 1) genes (Gering et al., 2003; Kalev-Zylinska et al., 2002; Patterson et al., 2007). Haemato-vascular progenitors in the pair of stripes located in the anterior part of the embryo form the anterior lateral plate mesoderm (ALPM), that generates primitive myeloid cells (Herbomel et al., 1999; Lieschke et al., 2002). Similarly, the haemato-vascular progenitors located in the posterior pair of stripes form the posterior lateral plate mesoderm (PLPM), and their cells generate primarily primitive erythroid cells and some myeloid cells (Detrich et al., 1995; Lieschke et al., 2002).

The first myeloid cells in the zebrafish embryo differentiate directly from haemato-vascular progenitors in the ALPM (Herbomel et al., 1999), forming two anterolateral groups of cells that express markers like *spi1b* (Spi-1 proto-oncogene b, previously known as *pu.1*) (Lieschke et al., 2001) and *cebpα* (Thisse et al., 2001). Differentiation of these groups of myeloid cells is followed by their ventral migration over the yolk. As a result, by 18 ss (somite stage) the primitive macrophages are found laterally over the surface of the yolk (Herbomel et al., 1999; Lieschke et al., 2002). Independently from primitive macrophages derived from the ALPM, primitive erythroid cells originate from progenitors in the PLPM (Detrich et al., 1995; Lieschke et al., 2002). The stripes of cells of the PLPM converge in the intermediate cellular mass (ICM) during embryogenesis (Detrich et al., 1995). These first erythroid cells in the ICM later enter the blood circulation between 24 and 26 hpf (Long et al., 1997).

1.1.2 Second wave of primitive haematopoiesis

In the first wave of primitive haematopoiesis, myeloid and erythroid cells are produced by direct differentiation of cells from the ALPM and PLPM (Detrich et al., 1995; Herbomel et al., 1999; Lieschke et al., 2002).Bertrand and colleagues (2007) showed the presence of transient erythromyeloid progenitors (EMP) that co-express *gata1a* and *lmo2* in the PBI (posterior blood island). EMPs arise autonomously from *lmo2*$^{+}$ mesoderm in the PBI and can be detected by 30 hpf as a *lmo2*$^{+}$ *gata1a*$^{+}$ cell population. This *lmo2*$^{+}$ *gata1a*$^{+}$ population of cells was shown to express both myeloid and erythroid markers, and *in vitro* experiments demonstrate that EMPs have both erythroid and myeloid potential, but they do not exhibit lymphoid potential (Bertrand et al., 2007). EMPs are transient, as they cannot be found in the PBI after 72 hpf, and they do not colonize the kidney marrow (Bertrand et al., 2007; Carroll and North, 2014), where definitive haematopoiesis proceeds until adulthood (Traver et al., 2003).

The first granulocytes, detected by peroxidase activity, are observed in the PBI by 31 hpf (Lieschke et al., 2001). Similarly, granulocytes that accumulate Sudan Black, presumably neutrophils, are found in the PBI between 33 hpf and 35 hpf (Le Guyader et al., 2008), suggesting that they derive from the EMPs. Other myeloid cells, the mast cells, have been shown to be derived from the EMPs (Da'as et al., 2012; Dobson et al., 2008).

1.1.3 Onset of definitive haematopoiesis

Definitive haematopoiesis generates mature blood cells from multi-potent progenitor cells which will ultimately result in the establishment of haematopoietic stem cells that persist during the entire life of the organism (Bertrand et al., 2010, 2008; Kissa et al., 2007; Kissa and Herbomel, 2010; Murayama et al., 2006). Definitive haematopoiesis is initiated from haematopoietic stem cells (HSC) that differentiate from the endothelium of the dorsal aorta in a process known as endothelial to haematopoietic transition (EHT). HSCs derive from the haemogenic endothelium in the ventral wall of the dorsal aorta (DA) (Bertrand et al., 2010; Kissa and Herbomel, 2010), in a process dependent of blood flow (North et al., 2009). Once the HSCs emerge, they enter the blood circulation through the caudal vein

(CV) (Kissa et al., 2007), and later they seed the caudal haematopoietic tissue (CHT) (Murayama et al., 2006). The CHT seeded by HSCs then becomes a transient niche of definitive haematopoiesis, where erythroid and myeloid cells are produced transiently (Kissa et al., 2007; Murayama et al., 2006) widely accepted as similar to the fetal liver in mammals. At a later stage, some of the HSCs in the CHT enter the blood circulation and seed the pronephros, the precursor of the kidney which becomes the site of definitive haematopoiesis until adulthood (Bertrand et al., 2008; Langenau et al., 2004; Murayama et al., 2006), like the bone marrow in mammals.

In zebrafish, the development of T lymphocytes occurs through two different mechanisms. Tian and colleagues (2017) show that the first wave of lymphocytes is derived from progenitors that emerge from the haemogenic endothelium of the DA, which later enter the blood circulation in the AGM region and exit the vasculature in the head and migrate interstitially and colonize the thymic rudiments (Hess and Boehm, 2012; Kissa et al., 2007). From 5 dpf, another mechanism slowly takes over, where HSCs colonize both thymi and originate T lymphocytes (Tian et al., 2017).

1.2 TEL-AML1 fusion protein and childhood acute lymphoblastic leukaemia

1.2.1 A chromosomal translocation generates the *TEL-AML1* fusion gene

B-cell precursor acute lymphoblastic leukaemia (BCP-ALL) is a heterogeneous disease characterized by the acquisition of mutations and other genetic lesions, followed by the clonal expansion of transformed haematopoietic cells whose differentiation is arrested (Ghazavi et al., 2015). In approximately 75% of BCP-ALL patients a chromosomal alteration is found, which include abnormal chromosome number, chromosomal translocations and deletions (Ghazavi et al., 2015; Jaffe et al., 2011).

The t(12;21)(p13;q22) chromosomal translocation is the most common translocation in BCP-ALL and is found in approximately 25% of paediatric BCP-ALL cases (Ghazavi et al., 2015; Jaffe et al., 2011). This translocation fuses *TEL* (translocation, ETS, leukaemia), also known as *ETV6* (ETS variant 6), and *AML1* (acute myeloid leukaemia 1 protein), also known as *RUNX1* (Romana et al., 1995). The t(12;21)(p13;q22) chromosomal translocation generates a chimeric protein named TEL-AML1 (also known as ETV6-RUNX1) (Romana et al., 1995). *TEL-AML1*-positive patients have a good prognosis and their 5-year survival rates exceed 85%, although late relapse is possible (De Braekeleer et al., 2012; Ghazavi et al., 2015). However, cancer therapy applied at an early age has late effects that become apparent years later. Many different sequelae of treatment have been reported, such as neurocognitive deficits, cardiotoxicity and secondary malignancies (Jaffe et al., 2011).

The *TEL* and *AML1* genes are involved in several chromosomal translocations that are found in different myeloid and lymphoid leukaemias (De Braekeleer et al., 2012; Ichikawa et al., 2013). Indeed, both *TEL* and *AML1* genes were first identified in fusions to other genes. The first described translocation involving the *TEL* gene was identified in its fusion to *PDGFRβ* (beta-type platelet-derived growth factor receptor) in the t(5;12)(q33;p13) chromosomal translocation in a patient with chronic myelomonocytic leukaemia (CMML) (Golub et al., 1994). Similarly, translocations involving *AML1* fused to the *ETO* (eight twenty-one) gene

(*RUNX1T1,* RUNX1 translocation partner 1) were identified in an AML patient with the t(8;21)(q22;q22) chromosomal translocation (Miyoshi et al., 1991). *TEL* and *AML1* genes encode transcription factors that are critical for definitive haematopoiesis. *TEL* encodes a nuclear protein that belongs to the ETS (E-Twenty-Six) family and plays an important role in haematopoiesis. TEL contains two major domains, an amino-terminal basic helix-loop-helix (bHLH) domain and an ETS domain, located in its C-terminus. The bHLH domain allows TEL to homodimerize while the ETS binding domain is responsible for binding to specific DNA sequences. Functional studies show that TEL acts as a strong transcriptional repressor by recruitment of proteins involved in the histone-deacetylase pathway although deacetylase-independent repression has also been reported (De Braekeleer et al., 2012). *AML1* encodes a transcription factor that is critical for definitive haematopoiesis and for the generation of haematopoietic stem cells (HSC). AML1 contains a highly conserved Runt domain near its N-terminus responsible for AML1 heterodimerization with CBFβ (core binding factor β). Binding to CBFβ enhances AML1's affinity to DNA and protects AML1 from ubiquitination and proteasomal degradation (Ichikawa et al., 2013).

The TEL-AML1 fusion protein contains domains of TEL amino-terminal to the ETS DNA binding domain, including the bHLH domain, typical in transcription factors that dimerise, and all known functional domains of AML1, including the RUNT DNA binding domain (Zelent et al., 2004). This makes TEL-AML1 chimeric protein different from other AML1 fusion proteins, like AML1-ETO and AML1-EVI1 (EVI1, ecotropic virus integration site 1 protein homolog), which contain the Runt DNA binding domain but lack the C-terminal domains that mediate interactions with other proteins (Ichikawa et al., 2013; Zelent et al., 2004). Given that the TEL-AML1 gene fuses the sequences encoding bHLH and repression domains of TEL protein with those encoding the RUNT DNA binding domain of AML1, TEL-AML1 is thought to act by repressing AML1's transcriptional targets, and also by interfering with normal TEL functions through heterodimerization (De Braekeleer et al., 2012; Ghazavi et al., 2015; Zelent et al., 2004).

1.2.2 TEL-AML1 fusion protein arises *in utero*

The *TEL-AML1* fusion gene arises *in utero* (Wiemels et al., 1999), and evidence shows that TEL-AML1-positive cells are present at birth (Greaves, 2009; Zelent et al., 2004). Although the precise position of the breakpoint is different in each patient's cells, making them all unique, most of the breakpoints are scattered throughout intron 5 (12 kb) of the *TEL* gene and intron 1 (100 kb, approximately) of the *AML1* gene (Greaves and Wiemels, 2003; Romana et al., 1995). Twins sharing the same *TEL-AML1* breakpoint indicate that the t(12;21)(p13;q22) translocation originates in a single cell. Therefore leukaemia is presumed to arise only from an *in utero* event, when either the conditions are permissive to leukaemia onset, or a cell type prone to leukaemia is present.

Interestingly, although a *TEL-AML1* fusion gene can be found in approximately 1% of new-born infants, less than 1% of these children eventually develop leukaemia. Similarly, the rate of concordance in *TEL-AML1*-positive twins is approximately 10% (Greaves, 2009), indicating that additional events are necessary for leukaemia onset, and that the fitness of TEL-AML1 expressing cells must in the majority of cases be outcompeted by wild-type cells. Consistent with this idea, TEL-AML1-positive clones generated *in utero* can still be found in individuals up to the age of 15 without leukaemia (Zelent et al., 2004). Additional evidence is provided by animal models where TEL-AML1 expression alone is not enough to trigger overt ALL (Fischer et al., 2005; Schindler et al., 2009; van der Weyden et al., 2011). However, most of these animal models fail to recapitulate the genetic effects of t(12;21)(p13;q22) translocation, particularly the expression pattern of TEL-AML1 (Fischer et al., 2005; Morrow et al., 2004; Sabaawy et al., 2006; Tsuzuki et al., 2004), where *TEL-AML1* expression is controlled by the *TEL* gene promoter. In addition these models do not include the effect of the loss of the translocated copy of the *TEL* gene (Fischer et al., 2005; Morrow et al., 2004; Sabaawy et al., 2006; Tsuzuki et al., 2004; van der Weyden et al., 2011), which could be crucial, given the tumour suppressor function attributed to TEL (Rompaey et al., 2000).

1.2.3 Additional genetic lesions

Additional recurrent genetic lesions have been found in TEL-AML1-positive patients, such as deletions of *TEL*, *PAX5* (paired box 5), *EBF1* (early B cell factor 1) and *CDKN2A* (cyclin dependent kinase inhibitor 2A), among other genes (Ghazavi et al., 2015). The loss of the non-translocated copy of the *TEL* gene is the most common deletion in TEL-AML1-positive patients (Attarbaschi et al., 2004). Studies in twins show that *TEL* gene deletions are subclonal to *TEL-AML1*-positive clones and their boundaries are different in twins, which suggest loss of *TEL* is a secondary event occurring after chromosomal translocation. The loss of the *TEL* gene is thought to promote leukaemogenesis by a direct tumour suppressor function of TEL (Rompaey et al., 2000) or indirect, via heterodimerization with TEL-AML1 that could reduce its transforming activity (Zelent et al., 2004).

A two-step model has been proposed according to these data, where the chimeric fusion gene constitutes a first hit that initiates subtle changes in haematopoietic compartments, a covert pre-leukaemic state, but is not sufficient to trigger leukaemia. During the covert pre-leukaemic state period, additional genetic lesions are acquired by the clone that eventually starts overt ALL (Zelent et al., 2004).

1.2.4 Animal models expressing TEL-AML1 fusion protein

TEL-AML1 fusion protein expression has been shown to have effects on haematopoiesis *in vivo* (Fischer et al., 2005; Schindler et al., 2009; Tsuzuki et al., 2004) and differentiation *in vitro* (Böiers et al., 2018; Fuka et al., 2012; Morrow et al., 2004), mainly increasing the numbers of progenitors, without complete block of B-cell differentiation, and with variable effects on myeloid cells. Although TEL-AML1 expression alone is not sufficient to initiate ALL (Schindler et al., 2009; van der Weyden et al., 2011), animal models have shown TEL-AML1's leukaemogenic potential in combination with additional genetic lesions (Bernardin et al., 2002; Swaminathan et al., 2015; van der Weyden et al., 2011). TEL-AML1 seems to act in the earliest B-cell progenitor cells, because TEL-AML1 expression controlled by *rag2* (recombination activating 2) and *IGH* (immunoglobulin heavy locus) gene promoters fails to induce leukaemia (Sabaawy et al., 2006; Zelent et al., 2004).

Therefore, it has been proposed that TEL-AML1 affects a primitive, as yet undefined B or pre-B cell progenitor during development, which may be the cellular origin of leukaemia. Consistent with this hypothesis, expression of TEL-AML1 in early haematopoietic compartments increases the number of HSCs and maintains them quiescent in mice (Schindler et al., 2009), presumably giving them the opportunity to accumulate further mutations. Similarly, embryonic stem cells engineered to express TEL-AML1 fusion protein from the endogenous locus exhibit a partial block in B-cell differentiation *in vitro*, and show instead a myeloid gene expression profile indicating a propensity to aberrant B-cell differentiation associated with TEL-AML1 (Böiers et al., 2018). Although there is convincing evidence supporting a TEL-AML1 role in the establishment of a pre-leukaemic clone, there is conflicting evidence about the role of TEL-AML1 in leukaemic cells. Some studies have failed to find a significant impact of TEL-AML1 knockdown on cell cycle, survival or transcriptional profile of cell lines expressing TEL-AML1 (Andreasson et al., 2001; Zaliova et al., 2011), suggesting that TEL-AML1 may be dispensable for survival of leukaemic cells once leukaemia has been established. In contrast, other groups have reported that knockdown of TEL-AML1 in cell lines impairs cell engraftment in mice (Fuka et al., 2012; Mangolini et al., 2013), and affects cell cycle and survival, and causes major transcriptional changes in cell lines (Diakos et al., 2007; Fuka et al., 2012, 2011; Mangolini et al., 2013). These data suggest that TEL-AML1 expression is required for maintenance of REH cells *in vitro*, a cell line that expresses TEL-AML1 fusion protein (Uphoff et al., 1997), but none of these studies shows evidence of TEL-AML1 dependency in leukaemic cells in an animal model.

1.2.5 Zebrafish model expressing TEL-AML1 fusion protein

A transgenic zebrafish expressing hTEL-AML1 (human TEL-AML1) chimeric protein fused to GFP, and under the control of zebrafish *β-actin* gene promoter (Sabaawy et al., 2006) *ZBA-EGFP-TA* provides an interesting animal model for TEL-AML1 leukaemia, because approximately 3% of these fish develop B-cell leukaemia without the need to experimentally induce additional genetic lesions (Sabaawy et al., 2006). Additionally, a zebrafish model of disease provides the advantage of its external development and small size, which make it possible to

carry out chemical screens. Given that the disease is initiated *in utero* (Wiemels et al., 1999), the use of zebrafish allows study of the earliest phases of development.

Although the *ZBA-EGFP-TA* model recapitulates some aspects of TEL-AML1 leukaemia (Sabaawy et al., 2006), it has some drawbacks. Most of these drawbacks involve its differences at the molecular level with the t(12;21)(p13;q22) chromosomal translocation.

In contrast to patients carrying the t(12;21)(p13;q22) chromosomal translocation, where hTEL-AML1 fusion protein expression is controlled by the *TEL* gene promoter, in *Tg(ZβA:EGFP-hTEL-AML1$^{+/-}$)* transgenic fish the expression of *hTEL-AML1* is controlled by a fragment of the zebrafish *β-actin* gene promoter (Higashijima et al., 1997; Sabaawy et al., 2006). However, the zebrafish *β-actin* promoter used in *Tg(ZβA:EGFP-hTEL-AML1)* transgenic fish drives expression mainly in the skin (Higashijima et al., 1997; Traver et al., 2003) and at low levels in blood cells (Mosimann et al., 2011).

Finally, although the reported low incidence of overt leukaemia in *ZBA-EGFP-TA* fish (3%) (Sabaawy et al., 2006) is in close agreement with the low percentage of patients carrying *hTEL-AML1* fusion gene that develop overt leukaemia (Zelent et al., 2004), a model with higher penetrance of leukaemia and shorter latency periods would be much more useful for research.

1.3 GATA2 transcription factor and GATA2 deficiency

1.3.1 The GATA family of transcription factors

GATA is a family of highly conserved transcription factors, with important roles in cell growth and differentiation of different cell lineages (Charron and Nemer, 1999; Gillis et al., 2009). The GATA transcription factors bind the consensus DNA sequence (A/T)GATA(A/G) through two highly conserved zinc finger domains (Ko and Engel, 1993). Transcription factors from the GATA family have been found in the genomes of vertebrates, invertebrates, fungi and plants (Lowry and Atchley, 2000). The genomes of mammals encode six different GATA genes, evolutionarily related, that have been divided into two different classes based on phylogenetic evidence: GATA-1, -2, -3 class (GATA123), and GATA-4, -5, -6 (GATA456) (Gillis et al., 2009). Interestingly, these groups are also similar in terms of expression. Mammalian *GATA1*, *GATA2*, and *GATA3* are mainly expressed by haematopoietic cells (Orkin, 1995; Simon, 1995), while *GATA4, GATA5* and *GATA6* are expressed in tissues derived from the mesoderm and endoderm, such as liver, heart and gut (Charron and Nemer, 1999; Molkentin, 2000). Phylogenetic analysis shows that the GATA genes found in current vertebrates have evolved through a series of events of genome duplication and the loss and retention of some of the resulting genes (Gillis et al., 2009; Liu et al., 2016).

Phylogenetic analysis suggests that the GATA123 family was generated by consecutive events of duplication, retention and loss of genes during the evolution of vertebrates (Gillis et al., 2009). Analysis of modern genomes suggests that the GATA123 paralogon in the ancestor of chordates underwent two different events of genome duplication. The first genome duplication originated the GATA-1 and the GATA-2/3 paralogons, and a second genome duplication generated GATA-1 and GATA-1b, and GATA-2 and GATA-3 (Gillis et al., 2009). The paralogon GATA-1 was retained and it is found in modern vertebrates, while the paralogon GATA-1b (also referred in literature as -ogm, ohnolog-gone-missing) was lost (Liu et al., 2016). According to this model, both GATA-2 and GATA-3 derived from the duplication of the GATA-2/3 paralogon (Gillis et al., 2009; Liu et al., 2016). Gillis and colleagues propose a similar mechanism for the evolution of GATA456 paralogon into the GATA-4, GATA-5, and GATA-6 genes found in modern vertebrates (Gillis et al., 2009).

Once the amniotes and teleosts diverged, an event of genome duplication early in the teleost fish lineage had a major importance in their later evolution (Amores et al., 1998; Glasauer and Neuhauss, 2014; Postlethwait et al., 1998). Phylogenetic evidence suggests that this genome duplication originated from two GATA-2 paralogons found in the genomes of teleost fish, GATA-2a and GATA2b (Gillis et al., 2009; Liu et al., 2016). Both paralogs are also found in the zebrafish genome, *gata2a* and *gata2b* (Postlethwait et al., 1998). The rate of mutations calculated in GATA-2a and GATA-2b of different teleost fish suggest that the ancestral GATA-2 gene was more similar to modern GATA-2a genes, although the sequences of both zinc finger domains is extremely conserved (Liu et al., 2016).

1.3.2 Structure of GATA2

In the human genome, the *GATA2* gene (ENSG00000179348) is located in chromosome 3 and has 6 exons. Two different mRNAs have been described, of 3484 bp and 3263 bp (Vicente et al., 2012). Interestingly, all *GATA*-1 (Ito et al., 1993), *GATA*-2 (Minegishi et al., 1998), and *GATA*-3 (Asnagli et al., 2002) genes contain two first exons that encode tissue specific 5'-untranslated regions (UTR), and that are used differentially. In the case of *GATA2*, the transcription of *GATA2* mRNAs starts from two different exons. Transcription of *GATA2* starting in the first exon, also known as distal or IS exon, is limited to haematopoietic and neuronal cells; while *GATA2* transcription starting in the second exon, also known as proximal or IG exon, occurs in all cell types expressing *GATA2* (Minegishi et al., 1998; Pan et al., 2000).

GATA2, as other transcription factors of the GATA family, binds DNA through two highly conserved zinc finger domains (Vicente et al., 2012). Additionally, to zinc finger domains, other domains have been described in GATA2. Two transactivation domains, one negative regulatory domain, a nuclear localization signal, and regions that are thought to be involved in GATA2 protein degradation, have been described (Minegishi et al., 2003; Vicente et al., 2012; Viger et al., 2008).

1.3.3 GATA2 has a pivotal role in definitive haematopoiesis

GATA2 has a key role in haematopoiesis in mammals. Diverse studies in mutant animals, chimaeras, and *in vitro* experiments show that GATA2 is crucial for definitive haematopoiesis. Homozygous *Gata2*$^{-/-}$ knockout mice die of severe anaemia by E11.5. Close morphological examination of the embryos suggested normal development of the heart and endothelial cells (Tsai et al., 1994). However, experiments in chimeric mice showed that *Gata2*$^{-/-}$ cells are able to contribute to primitive haematopoietic cells, but not to haematopoietic lineages derived from the foetal liver (Tsai et al., 1994). These results suggest that while GATA2 is dispensable for primitive haematopoiesis, the transient wave of definitive haematopoiesis in the foetal liver of embryos requires GATA2 activity. In agreement with these findings, after birth, chimeric mice contained no *Gata2*$^{-/-}$ haematopoietic cells, although *Gata2*$^{-/-}$ cells did contribute to other organs (Tsai et al., 1994). Further *in vitro* experiments show that *Gata2*$^{-/-}$ cells fail to produce haematopoietic lineages, although GATA2 is dispensable for *in vitro* terminal differentiation of erythrocytes and macrophages (Tsai et al., 1994; Tsai and Orkin, 1997).

Given that *Gata2*$^{-/-}$ knockout mice display a lethal phenotype by E11.5 (Tsai et al., 1994), later studies used conditional mutants to study the role of GATA2 in different cell types during development. De Pater and colleagues (2013) used conditional *GATA2* mutant mice in which the fifth coding exon is excised by Cre, to show that GATA2 activity is required for EHT, and therefore the production of the first HSCs. Consistently, zebrafish *gata2b* morphants display a severe disruption in EHT (Butko et al., 2015). Experiments in mice with conditional *Gata2* mutation in their HSCs show that GATA2 is also required for the survival of HSCs after EHT (de Pater et al., 2013). A series of *in vitro* experiments with *GATA2*$^{-/-}$ human embryonic stem cells (hESC) show a partially impaired EHT and a decreased generation of HSPCs (haematopoietic stem and progenitor cells) (Huang et al., 2015), confirming the previous findings in conditional mutant mice (de Pater et al., 2013).

The role in haematopoiesis and development of zebrafish *gata2a* and *gata2b* genes is described in the sections 4.1.3 and 5.1.3, respectively.

1.3.4 *GATA2* mutations and disease

In 2011, a series of research articles reported the discovery of mutations in the *GATA2* gene in cohorts of patients of different diseases with a wide variety of manifestations (Dickinson et al., 2011; Hahn et al., 2011; Hsu et al., 2011; Ostergaard et al., 2011), all of them sharing defects in the haematopoietic compartment (Bigley et al., 2011; Emberger et al., 1979; Vinh et al., 2010). Ostergaard and colleagues (2011) recruited unrelated patients of Emberger syndrome (Emberger et al., 1979) and found underlying heterozygous *GATA2* mutations. In patients with DCML (dendritic cell, monocyte, B, and natural killer lymphoid deficiency) (Bigley et al., 2011), exome sequencing identified mutations in the *GATA2* gene (Dickinson et al., 2011). Similarly, Hsu and colleagues (2011) identified *GATA2* mutations in a cohort of monoMAC patients (monocytopenia and mycobacterial infections syndrome) (Vinh et al., 2010). In the same year, *GATA2* mutations were also found in patients with familial predisposition to myelodysplastic syndrome (MDS) and acute myeloid leukaemia (AML) (Hahn et al., 2011).

GATA2 deficiency, elicited by diverse mutant alleles, both as heterozygous germinal mutations and as somatic mutations, has a wide spectrum of manifestations, haematologic, infectious, pulmonary, dermatologic, neoplastic, lymphatic, and other diverse symptoms such as hearing loss, miscarriage, and hypothyroidism. Among the haematologic manifestations of *GATA2* deficiency the most common are profound B lymphocytopenia, natural killer lymphocytopenia, and monocytopenia, but neutropenia and CD4 lymphocytopenia are also observed (Bigley et al., 2011; Emberger et al., 1979; Hahn et al., 2011; Spinner et al., 2014; Vinh et al., 2010; Wlodarski et al., 2016).

Many of the *GATA2* mutations found in patients are concentrated in the regions encoding the two zinc finger domains, however, mutations in regions encoding other domains closer to the amino terminal end of GATA2 have also been described (Dickinson et al., 2011; Hahn et al., 2011; Hsu et al., 2011; Ostergaard et al., 2011). Mutations in the enhancer region in intron 5 have also been found (Hsu et al., 2011; Spinner et al., 2014). A wide variety of mutations has been described, deletion and insertions, both in frame and leading to frameshifts, together with missense mutations (Spinner et al., 2014). Additionally, Spinner and

colleagues (2014) studied the correlation between genotype and phenotype among patients and found that lymphedema has only been observed in patients with null or regulatory mutations, but not in those that have missense mutations.

1.4 Myelodysplastic syndrome with del(5q) and RPS14 deficiency

1.4.1 Myelodysplastic syndrome with del(5q)

MDS with loss of all or part of chromosome 5q (del(5q)), also known as 5q- syndrome, is the only type of MDS defined cytogenetically (Komrokji et al., 2013). Patients with a distinct haematological disorder, consisting in macrocytic anaemia, megakaryocytic dysplasia and erythroid dysplasia were found to carry heterozygous interstitial deletion in the long arm of chromosome 5 (Dana and Wasmuth, 1982; Van Den Berghe et al., 1974).

The MDS clone carrying del(5q) is initiated in HSCs (Tehranchi et al., 2010), and extensive work has been focused on defining the commonly deleted region (CDR) (Boultwood et al., 1994; Jaju et al., 1998; Le Beau et al., 1996; Zhao et al., 1997). Initially, work carried out in MDS and AML patients restricted the CDR to a 1.5Mb (mega base pairs) region in chromosome 5 (Zhao et al., 1997). Other studies used samples from 5q- syndrome patients exhibiting the symptoms described originally to define the limits of the CDR (Boultwood et al., 1994; Jaju et al., 1998; Le Beau et al., 1996). Currently, the accepted CDRs consist of a proximal CDR in 5q31 (Liu et al., 2007), and a distal CDR of 1.5Mb in 5q32-33, between the marker D5S413 and the gene *GLRA1* (glycine receptor alpha 1) (Boultwood et al., 2002). However, this does not imply that chromosome 5 in 5q- patients has two deletions, on the contrary, many 5q- patients have deletions that overlap with both described CDRs (Komrokji et al., 2013).

Historically the proximal CDR has been associated with additional cytogenetic alterations and progression towards AML, however recent studies suggest paradoxically that both CDRs can be found in MDS del(5q) patients, while progression to AML is linked to the distal CDRs, in 5q32-33 (Douet-Guilbert et al., 2012). The distal CDR in 5q32-33 also contains the ribosomal protein S-14 (*RPS14*) gene, and three microRNAs (miR-143, miR-145, and miR-146). Current evidence shows that heterozygous deletion of *RPS14* gene is crucial to the anaemia that characterizes the 5q- syndrome.

1.4.2 Role of RPS14 deficiency in MDS with del(5q)

The *RPS14* gene in chromosome 5 encodes a structural component of the 40S subunit of the ribosome (Dana and Wasmuth, 1982; Nakamichi et al., 1986; Rhoads et al., 1986). Through an *in vitro* RNA interference screen, Ebert and colleagues (2008) showed that decreased expression of *RPS14* induced a decreased survival of human $CD34^+$ umbilical cord blood cells, and a disrupted erythroid proliferation. Interestingly, work carried out in animal models shows that disruption of the biogenesis of ribosomes induces anaemic phenotypes similar to the anaemia found in 5q- syndrome (Craven et al., 2005; McGowan et al., 2008; Narla et al., 2014; Payne et al., 2012). For example, mice carrying mutations in ribosomal protein S-19 (*RPS19*) and ribosomal protein S-20 (*RPS20*) genes, identified in a large-scale chemical mutagenesis screen, show a phenotype of erythroid hypoplasia (McGowan et al., 2008). Conditional *Rps14* mutant mice exhibit an age-dependent progressive anaemia and megakaryocyte dysplasia (Schneider et al., 2016). Similarly, zebrafish embryos injected with *rps14* and *rps19* morpholinos display a phenotype of severe anaemia (Narla et al., 2014; Payne et al., 2012).

Abundant evidence shows that the effects of disruption of ribosomal biogenesis on the development of erythroid cells are dependent on Tp53 (Barlow et al., 2010; McGowan et al., 2008; Momand et al., 1992; Narla et al., 2014; Schneider et al., 2016). Findings reported by different groups suggest the activation of p53 by the accumulation of free ribosomal proteins via a MDM2 (mouse double minute 2) dependent mechanism. Haploinsufficiency for ribosomal proteins, such as RPS14, interferes with ribosomal assembly, and induces an increase in the number of free ribosomal proteins (Ferreira-Cerca and Hurt, 2009). It has been shown that ribosomal proteins L5, L11, L23 and S7, are capable of binding the zinc finger domain of MDM2 (Narla and Ebert, 2010). MDM2 is an important regulator of the activity of p53. MDM2 is a E3-ubiquitin ligase with a zinc finger domain that allows it to bind the DNA binding site of p53. In this way, MDM2 interferes with p53's transcriptional activity and induces its proteasomal degradation by ubiquitination (Momand et al., 1992). Therefore, the liberation of free ribosomal proteins has two effects: the binding of MDM2 to the ribosomal proteins, inducing auto-ubiquitination; and the release of MDM2-dependent repression of p53 (Ferreira-Cerca and Hurt, 2009; Narla and Ebert, 2010).

The role of p53 activation has been shown in murine models of del(5q). Barlow and her colleagues (2010) developed mice carrying a deletion in a region of chromosome 11, a region with synteny to human chromosome 5, containing the *Rps14* gene. Mice haploinsufficient for this chromosomal region show a macrocytic anaemia phenotype that could be rescued by crossing with p53-deficient mice (Barlow et al., 2010). Similar results have been reported in a murine model of del(5q) with conditional inactivation of *Rps14* (Schneider et al., 2016). Schneider and her colleagues show that *Rps14* inactivation induces a defect in erythroid cell differentiation that is dependent on p53, as *Trp53* haploinsufficiency partially rescues survival of *Rps14* haploinsufficient mice and their erythroid differentiation defect (Schneider et al., 2016).

In contrast, work carried out in zebrafish embryos using morpholinos targeting *rps14*, and *rps19*, suggest involvement of other pathways in addition to p53. Payne and her colleagues tested the effects of L-leucine, a known activator of mRNA translation, on *rps14* and *rps19* morphant zebrafish embryos (Payne et al., 2012). Treatment with L-leucine induced a rescue in the phenotype of both *rps14* and *rps19* morphant embryos, suggesting that increased translation of these mRNAs is sufficient to counteract the effects of haploinsufficiency. Further work on these models of ribosomopathies shows that the effect of L-leucine is independent from p53 (Narla et al., 2014). Importantly, p53 activation does not account for some of the aspects of disease. In fact, *rps14* or *rps19* knock down using morpholinos in *p53* mutant zebrafish still show severe anaemia (Narla et al., 2014), demonstrating that pathways other than p53 activation are involved in disease.

2 Materials and Methods

2.1 Fish husbandry

2.1.1 Wild type, mutant and transgenic zebrafish lines used

Zebrafish (*Danio rerio*) larvae were obtained in UCL fish facility by natural spawning according to standard procedures (Westerfield, 2000). Wild type zebrafish strains used were AB and TL.

Transgenic strains used were: *Tg(gata1a:dsRed)sd2* (Traver et al., 2003), *Tg(itga2b:GFP)la2Tg* (previously known as *Tg(cd41:GFP)*) (Lin et al., 2005). Additionally, the transgenic fish line *Tg(lyz:nfsB-mCherry)sh260* (data not published), a kind gift from Dr Stephen Renshaw, was used. To produce it, a DNA construct where *lyz* gene promoter (Hall et al., 2007; Wang et al., 2014) controls the expression of *nfsB* and *mCherry* genes, lyz:nfsB-mCherry, was generated by Gateway cloning. The transgenic line was produced using the Tol2kit as previously described (Kwan et al., 2007; Nüsslein-Volhard and Dahm, 2002).

The mutant strain *casper* (White et al., 2008), which is a double mutant of *nacre* (mutation in *mitfa* gene, microphthalmia-associated transcription factor a) and *roy orbison* (a mutant not mapped yet), was used due to its lack of pigmentation.

All embryos were collected by natural spawning and raised at 28.5 °C in E3 medium (see Table 2.1 for details) in Petri dishes.

Table 2.1 | E3 composition.

reagent	Final concentration
NaCl	5 mM
KCl	0.17 mM
$CaCl_2$	0.33 mM
$MgSO_4$	0.3 mM
Methylene blue	0.1% v/v
pH 7.0 (at 25 °C)	-

Pigment formation was avoided by supplementing E3 medium with phenylthiourea (PTU) (Sigma) 0.2 mM from 24 hpf. All animals used in this work were anesthetized with ethyl 3-aminobenzoate methanesulfonate (E10521, Sigma) before each experiment.

2.1.2 Staging of embryos and larvae

Embryos and larvae were staged according to Kimmel *et al*. (Kimmel et al., 1995), and larval ages are expressed in somites (ss), hours post-fertilization (hpf), and days post-fertilization (dpf).

2.2 Whole mount *in situ* hybridization (WISH)

2.2.1 Fixation, permeabilization, and dehydration of embryos and larvae for WISH

Embryos and larvae were fixed by overnight incubation in 4% w/v PFA at 4 °C. Embryos and larvae older than 18 hpf (18ss) were dechorionated with forceps prior to incubation in PFA, while embryos at 18 ss stage (18 hpf) or younger were dechorionated after the incubation in PFA. After washes with 1x PBST, samples were treated with 10 µg/mL proteinase K during different periods of time according to their developmental stage (see Table 2.2), and washed again with 1x PBST to be then fixed overnight in 4% w/v PFA at 4 °C.

Table 2.2 | Proteinase K treatments used for each developmental stage.

Developmental stage	Time of digestion [minutes]
10 ss – 18 ss	3
18 ss – 24 hpf	5
2 dpf	15
3 dpf	25
4 dpf	35

Following fixation, samples were dehydrated by incubating them in solutions of PBST with increasing concentrations of methanol (75% v/v PBST, 25% v/v methanol; 50% v/v PBST, 50% v/v methanol; 25% v/v PBST, 75% v/v methanol), to be then stored in 100% v/v methanol at -20 °C for at least one night, to inactivate endogenous alkaline phosphatases.

2.2.2 *In situ* hybridization procedure

WISH procedure was started by rehydrating the samples through a series of 5 minutes washes with solutions of PBST with decreasing concentrations of methanol (25% v/v PBST, 75% v/v methanol; 50% v/v PBST, 50% v/v methanol; 75% v/v PBST, 25% v/v methanol). Samples were then washed 3 times with 1x PBST for 5 minutes.

Following rehydration, samples were prepared for the hybridization step by incubating them first in HM- (hybridization mix: 50% v/v deionized formamide, 5x SSC (saline-sodium citrate), and 0.1% v/v Tween 20, adjusted to pH 6.0 by adding citric acid) solution for 15 minutes at 65 °C. Then HM- solution was replaced by HM+ (50% v/v deionized formamide, 5x SSC, 0.1% v/v Tween 20, 50 µg/ml of heparin, 500 µg/ml of RNase-free tRNA adjusted to pH 6.0 by adding citric acid) and the samples were incubated at 65 °C for 4 hours.

Hybridization with the probe was carried out by overnight incubation at 65 °C in 200 µL of HM+ solution with 50 – 100 ng of RNA probe labelled with digoxigenin.

After the hybridization, the probes were recovered and washed at 65 °C with solutions with decreasing concentrations of SSCT (1x SSC, 0.1% v/v Tween 20). First, samples were washed twice with a solution of 2x SSCT, 50% v/v formamide for 30 minutes. Then the samples were washed with 2x SSCT for 15 minutes. This wash was followed by 2 washes of 30 minutes with 0.2x SSCT.

To prepare the samples for the blocking process, the samples were washed three times with MABT (100 mM maleic acid, 150 mM NaCl, Tris-HCl, 0.1% v/v Tween 20, pH 9.5) for 5 minutes at room temperature. Then the samples were blocked by incubation with blocking solution (1x PBST, 2% v/v sheep serum, 2 mg/ml BSA) for 1 to 4 hours at room temperature. After blocking, the samples were incubated

overnight with anti-digoxigenin antibody (1333089001, Roche) (1:5000) diluted in blocking solution at 4 °C with gentle rocking.

The samples were washed three times with MABT solution for 30 minutes at room temperature. Then the samples were prepared for the detection phase.

2.2.3 Detection and preparation of samples for imaging

All probes used were labelled with digoxigenin, and the anti-digoxigenin antibody used had alkaline phosphatase activity. The samples were washed 4 times in AP buffer (100 mM Tris-HCl, 50 mM $MgCl_2$, 100 mM NaCl, 0.1% v/v Tween 20, and pH 9.5). For detection, samples were incubated in a reaction of 337.5 µg/mL NBT (4-Nitro blue tetrazolium chloride) and 175 µg/mL BCIP (5-bromo-4-chloro-3-indolyl-phosphate) in AP buffer in dark for variable periods of time. The detection reaction was stopped by washing the samples three times in stop solution (1x PBS, 1 mM EDTA, 0.1% v/v Tween 20, pH 5.5) during 15 minutes at room temperature.

For imaging, the samples were transferred into 80% v/v glycerol in PBST through a series of washes: 20% v/v Glycerol, 80% v/v PBST; 40% v/v Glycerol, 60% v/v PBST; 60% v/v Glycerol, 40% v/v PBST; and 80% v/v Glycerol, 20% v/v PBST.

2.3 Sudan Black staining

Sudan Black staining was used to label granulocytes in zebrafish embryos and larvae. Sudan black B (SB), is a lipid stain that labels granules in neutrophils, eosinophils and monocytes (Sheehan and Storey, 1946). Zebrafish embryos and larvae were stained as previously described (Le Guyader et al., 2008). Larvae were fixed in 4% w/v PFA for 2 hours. Then larvae were incubated in Sudan Black staining reagent (CAT 3801, Sigma) during 20 minutes with gentle rocking. After the incubation, the Sudan Black staining reagent was discarded, and background staining was removed by washing twice with 70% v/v ethanol for 5 minutes. Larvae were then washed 3 times with 1x PBST to prevent staining loss, and pigments were removed as described in section 2.5. All steps were carried out at room temperature.

2.4 *o*-dianisidine staining

O-dianisidine staining was used to label erythrocytes in zebrafish larvae. Larvae were incubated in staining mix (0.7 mg/mL o-dianisidine (D9143, Sigma); 12 mM sodium acetate; 0.7% v/v H_2O_2) during 20 minutes in dark with very gentle rocking. Larvae were then washed three times with 1x PBST and fixed with 4% w/v PFA for 1 hour at room temperature. Finally, larvae were washed again three times with 1x PBST.

2.5 Bleaching of embryos

Pigments in fixed embryos and larvae older than 24 hpf were removed by incubation in (5% v/v deionised formamide, 0.5x SSC, 5% H_2O_2) at room temperature. Incubation time varied according to the developmental stage of embryos and larvae. After bleaching, the embryos and larvae were washed three times during 5 minutes with 1x PBST.

2.6 Microinjection

Morpholinos, or mRNAs and sgRNAs were microinjected into 1-cell stage zebrafish embryos to pull down the expression of specific genes (see section 6.2.4) or to edit the genome and generate new zebrafish mutant lines (see section 5.2.5), respectively.

To obtain large numbers of 1-cell stage embryos for microinjections, the couples of adult fish were left overnight in breeding boxes with a divider to keep males and females separated during the night. The next morning, as soon as the lights of the facility turned on, the dividers were removed from a group of breeding boxes, and the fish were allowed to breed. The dividers of other groups of breeding boxes were removed during the morning to obtain 1-cell stage embryos during 2 to 3 hours.

Embryos were carefully aligned in an agarose mould made for microinjection. This mould was made of 1% w/v agarose (50004, SLS) dissolved in E3 medium, poured into a 10 cm plastic petri dish, then the injection mould was carefully placed on the

agarose and it was allowed to solidify. Moulds for microinjection made in this way were kept at 4 °C with E3, and wrapped in parafilm (PF002, Generon) to prevent dehydration of the agarose.

2.7 Standard Polymerase Chain Reaction (PCR)

Standard polymerase chain reaction (PCR) was used as part of genotyping protocols for *gata2a*^{um27} (see section 4.2.2), *gata2b* mutants (see sections 5.2.8 and 5.2.9), and *rps14*^{E8fs} (see section 6.2.2) mutant fish, and as a part of sequencing protocol to identify mutations generated by CRISPR (Clustered Regularly Interspaced Short Palindromic Repeats, and CRISPR associated protein 9, respectively) (see section 5.2.6).

The DNA polymerase used for routine PCR was *Taq* DNA polymerase (M0273S, NEB) together with Standard *Taq* Buffer (B9014S, NEB). The composition of the Standard *Taq* Buffer is shown in Table 2.3:

Table 2.3 | 1x Standard *Taq* Reaction Buffer composition.

reagent	Final concentration
KCl	50 mM
Tris-HCl	10 mM
$MgCl_2$	1.5 mM
pH 8.3 (at 25 °C)	-

Deoxynucleosides triphosphate (dNTP) were acquired separately as 100 mM stocks: dATP (R0141, Thermo Scientific), dCTP (R0151, Thermo Scientific), dGTP (R0161, Thermo Scientific), and dTTP (R0171, Thermo Scientific). A 10 mM solution with all four dNTPs was prepared and aliquoted.

2.8 Design of primers

All primers used were designed in Geneious version 7.1.9 (http://www.geneious.com) (Kearse et al., 2012), that uses Primer3 2.3.4 (http://primer3.sourceforge.net/releases.php/) for primer design.

2.9 DNA digestion with restriction enzymes

Digestion of DNA with restriction enzymes was carried out typically for genotyping purposes (see sections 4.2.2, 5.2.8, and 6.2.2) but also as part of cloning and to linearize plasmid DNA to be used as template for *in vitro* transcription reactions (see section 5.2.4).

In the case of digestions of PCR products with restriction enzymes to genotype fish, the typical reaction was carried out in a total volume of 20 µL, with 2 units of restriction enzyme and variable concentrations of template DNA. Given that genotyping of samples usually involved large number of samples (24 – 96), a large master mix containing nuclease free water, the enzyme buffer, and the enzyme was prepared first, and then aliquoted in the tubes for all the samples. In these cases, the DNA to be digested was a PCR product, and was added last, followed by a short spin in a microcentrifuge to mix the components of the digestion. The Table 2.4 shows the volumes and concentrations of each component used in the mix of a standard restriction digestion for genotyping:

Table 2.4 | Reaction mix of a standard restriction digestion for genotyping.

Reagent	Volume per reaction [µL]	Final concentration
10x enzyme buffer	2	1x
Enzyme	0.2	2 units
template DNA	10	variable
nuclease free water	7.8	-

In the case of genotyping protocols for *gata2a*^{um27} (section 4.2.2) and *gata2b*^{u5008} (section 5.2.8) mutations, the enzymes used CutSmart buffer (B7204S, NEB):

Table 2.5 | 1x CutSmart buffer composition.

Reagent	Final concentration
Potassium Acetate	50 mM
Tris-acetate	20 mM
Magnesium Acetate	10 mM
BSA (bovine serum albumin)	100 µg/mL
pH 7.9 (at 25 °C)	-

Incubations times and temperatures used for digestions with restriction enzymes were those recommended by their manufacturers, including an incubation period of 20 minutes at 65 °C to inactivate the restriction enzymes.

On the other hand, in the case of digestions carried out on plasmid DNA to be used for cloning or *in vitro* transcription reactions, restriction digestion reactions were carried out in a total volume of 50 µL, where 1 µg of DNA was digested using 10 – 20 units of restriction enzyme. In these cases, the restriction enzyme was the last component added to the reaction. The Table 2.6 summarizes the components of the restriction digestions of plasmid DNA and their concentrations:

Table 2.6 | Reaction mix of a restriction digestion of plasmid DNA.

Reagent	Volume per reaction [µL]	Final concentration
10x enzyme buffer	5	1x
Enzyme	variable	10 - 20 units
plasmid DNA	variable	1 µg/50 µL
nuclease free water	variable	-

As mentioned before, incubations times and temperatures used for digestions with restriction enzymes were those recommended by their manufacturers.

2.10 Gel electrophoresis in agarose gels

Electrophoresis in agarose gels was used to visualise both DNA and RNA, and the concentration of the gels used varied between 0.8% w/v and 3% w/v depending on the size of the nucleic acids to be resolved.

Agarose gels were prepared by dissolving agarose powder (50004, SLS) in TBE (Tris-Borate-EDTA) under intense heat.

As molecular weight marker, HyperLadder 50bp (BIO-33040, Bioline) and HypperLadder 1kb (BIO-33053, Bioline) were used for DNA fragments under and over 1 kb, respectively.

2.11 Genotyping

In all experiments carried out with mutant fish or their cells, genotyping for the mutations studied was carried out on each sample after data acquisition. The overall strategy consisted in the extraction of genomic DNA from cells, fin clips, or whole embryos and larvae; followed by the amplification by PCR of a region around the mutation, and a digestion of the PCR products with a restriction enzyme; finally, the genotypes are read from the digestion pattern observed by gel electrophoresis. The details of each specific genotyping protocol are provided in their respective chapters (see section 4.2.2 for *gata2a*^{um27} genotyping; sections 5.2.8 and 5.2.9 for genotyping of *gata2b* mutations; and section 6.2.2 for genotyping of *rps14*^{E8fs} mutations).

In the following sections, the different methods used to extract genomic DNA from fin clips from adult fish (section 2.11.2), embryos and larvae (section 2.11.3), and cells (section 2.11.4) are described in detail.

2.11.1 Fin clipping of adult fish

Adult fish were fin clipped to obtain genomic DNA for genotyping. Genomic DNA was extracted from this tissue cells as described in section 2.11.2, and used as template in genotyping protocols (details about genotyping protocols in sections 2.11.5, 4.2.2, 5.2.8, 5.2.9, and 6.2.2).

Each fish was anesthetized by transfer into a small breeding box with 0.08 g/L 3-aminobenzoate methanesulfonate, and after 1 to 2 minutes, the fish was taken from the box with anaesthesia and placed on a piece of parafilm, lying on its side. A piece of the fin was cut using scissors. The tissue of each adult fish was placed in a separate PCR tube. After the procedure, each fish was put back into a tank without anaesthesia for recovery, and later, in a separate compartment of a 24-compartment tank designed for this purpose (DC-96, R&D Aquatics).

2.11.2 Extraction of genomic DNA from fin clips of adult fish

The protocol used for extraction of genomic DNA from fin clips obtained from adult fish consisted in cell lysis, followed by a long step of digestion with a proteinase. First, the cell lysis is carried out by incubation of each of fin clips, placed in PCR tubes, in 40 µL of embryo lysis buffer (ELB, see Table 2.7 for details of its composition) for 10 minutes at 98 °C.

Table 2.7 | Embryo lysis buffer composition.

reagent	Final concentration
KCl	50 mM
Tris-HCl	10 mM
Tween 20	0.3% v/v
NP40	0.3% v/v
pH 8.3 (at 25 °C)	-

After incubation of the fin clips with ELB, the digestion of the samples is started by adding 10 µL of 10 mg/mL proteinase K to each fin clip. The samples were

incubated 16 hours at 55 °C for digestion, followed by 10 minutes at 98 °C to inactivate proteinase K. DNA obtained by this method was diluted to 1 – 10 ng/µL and used directly for PCR without further purification.

2.11.3 Extraction of genomic DNA from embryos and larvae

Genomic DNA from embryos and larvae was obtained using a KOH based method. Each time, a fresh 1:50 dilution was prepared from each 50x Base solution and 50x Neutralisation solution (see Table 2.8 for details on the composition of both solutions). Embryos and larvae are placed in PCR tubes, liquid is removed and replaced by 25 µL of 1x Base solution. Samples were incubated at 95 °C for 30 minutes, and then cooled down at 4 °C for 20 minutes. The solution is neutralised by adding 25 µL of 1x Neutralisation solution. This solution was then diluted to 1 – 10 ng/µL and used for PCR without further purification.

Table 2.8 | Composition of 50x Base solution and 50x Neutralisation solution used in genomic DNA extraction.

50x Base solution	
reagent	**Final concentration**
KOH	1.25 M
EDTA	10 mM

50x Neutralisation solution	
reagent	**Final concentration**
Tris-HCl	2 M

2.11.4 Extraction of genomic DNA from cells

Genomic DNA was extracted from cells to identify *gata2b* mutations in the gamete cells of F0 fish (see sections 5.2.6 and 5.2.7), and to genotype larvae after flow cytometry experiments (see section 6.2.9), using a small remaining volume of cells in suspension.

The cell suspensions were centrifuged at 400 rcf for 5 minutes to precipitate cells, and the supernatant was discarded. Then 10 µL of a 75 mM NaOH solution were added to each sample, followed by a short incubation of 2 minutes at 95 °C in a thermocycler. Then the samples were cooled down to 10 °C for 5 minutes, and 1.5 µL of Tris-HCl (pH 8.0) solution were added to each sample to neutralize the base. Finally, the samples were centrifuged again at 400 rcf for 5 minutes, and the supernatant was diluted to 1 – 10 ng/µL and used directly for PCR without further purification.

2.11.5 Genotyping of *Tg(itga2b:GFP)* transgenic fish

In experiments where itga2b:GFP$^+$ cells were quantified or the presence/absence of itga2b:GFP$^+$ cells was recorded, those fish showing no fluorescent cells were later genotyped for the *Tg(itga2b:GFP)* transgene, to confirm that all fish in the experiment were transgenic *Tg(itga2b:GFP)* fish. The genotyping strategy was based on the amplification by PCR of a 126 bp fragment of DNA in the region coding for GFP with the following primers:

Table 2.9 | Primers used for genotyping of *Tg(itga2b:GFP)* transgenic fish.

Primer name	Sequence (5' to 3')	Length	%GC	Tm
gp009	AACTCCAGCAGGACCATGTG	20	55.0	60.0
op006	CTACCAGCAGAACACCCCCA	20	60.0	61.5

The primers in Table 2.9 were used in a PCR reaction to amplify a fragment of the sequence encoding GFP from the genomic DNA of the fish. Table 2.10 shows the components and concentrations of the PCR reaction used:

Table 2.10 | Components and concentrations of PCR for genotyping of *Tg(itga2b:GFP)* transgene.

Reagent	Volume per reaction [µL]	Final concentration
10x Standard Taq buffer	2.5	1x
10 mM dNTPs	0.5	200 µM
10 µM gp009	0.5	0.2 µM
10 µM op006	0.5	0.2 µM
Standard Taq Polymerase	0.125	0.625 units
genomic DNA	2	variable
nuclease free water	18.875	-

The PCR described in Table 2.10 to identify the presence of the GFP coding sequence was carried out under the cycling conditions detailed in Table 2.11:

Table 2.11 | Cycling conditions used in PCR for *Tg(itga2b:GFP)* transgene genotyping.

phase		temperature [°C]	time [s]
initial denaturation		95	30
34 cycles	denaturation	95	15
	annealing	64	30
	extension	68	30
final extension		68	5 minutes

The results of the PCR reaction were visualised by electrophoresis in 3% w/v agarose gels. The presence of a 126 bp DNA band indicated the presence of the GFP coding sequence in the genomic DNA, from *Tg(itga2b:GFP)* transgene, in this case.

2.12 Imaging and image processing

Live embryos and larvae were imaged in E3 medium with ethyl 3-aminobenzoate methanesulfonate while fixed embryos and larvae were imaged either in 1x PBST or 80% v/v glycerol. All images were acquired using a Leica M205 FA fluorescent dissecting stereoscope equipped with a Leica DFC 365 FX camera. Images were processed using Fiji version v1.49u software (Schindelin et al., 2012).

2.13 Statistical analysis

Data are presented as boxplots and error bars show minimum and maximum data points in each group. Additional statistical information is provided in Supplementary Tables for quantitative data. Sample size, mean, standard deviation, standard error of the mean and 95% confidence interval of the mean are shown in the Supplementary Tables. In those cases where inferential statistics were used, Supplementary Tables also provide *p*-values of tests used, including normality tests, and *post-hoc* tests.

Statistical analysis was performed using GraphPad Prism version 5.00 for Windows software (GraphPad Software, San Diego, CA, USA). The probability level for statistical significance was $p < 0.05$ and all tests used were two-tailed. When necessary, each group of data was tested using D'Agostino & Pearson omnibus normality test to assess whether parametric analysis could be used. Groups of data whose sample size was smaller than 8 were not checked for normality and non-parametric analysis was carried out instead.

2.14 Nomenclature used for genes, proteins, transgenics and mutants

GRCz10 (Genome Reference Consortium Zebrafish Build 10), INSDC (International Nucleotide Sequence Database Collaboration) Assembly GCA_000002035.3, released in September 2014, was used as reference zebrafish genome, and all genomic coordinates shown refer to GRCz10. The reference sequence for zebrafish *gata2b* gene throughout this work is the Ensembl sequence

ENSDARG00000009094.7. Similarly, the sequence for zebrafish *rps14* gene used as a reference throughout this work is the sequence ENSDARG00000036629.5, from the Ensembl database.

Zebrafish genes, proteins, and mutations, and also transgenic and mutant zebrafish lines are referred to following the updated nomenclature conventions for zebrafish found at ZFIN's (Zebrafish Information Network) website (http://zfin.org/). The new mutant lines generated in this work were designated according to previously published guidelines (den Dunnen et al., 2016).

Human genes and proteins are referred to following the guidelines of the HUGO Gene Nomenclature Committee (HGNC) (Wain et al., 2002), also available in https://www.genenames.org/about/guidelines.

Mouse genes and proteins are referred to following the updated guidelines available in http://www.informatics.jax.org/mgihome/nomen/gene.shtml, of the previously published guidelines (Eppig, 2007).

3 Effect of the expression of human TEL-AML1 fusion protein in zebrafish haematopoiesis

3.1 Introduction

3.1.1 Expression of TEL-AML1 is not sufficient to initiate leukaemia

TEL-AML1 fusion protein results from the t(12;21)(p13;q22) chromosomal translocation, which is the most common translocation found in paediatric BCP-ALL patients (Ghazavi et al., 2015; Jaffe et al., 2011). Both TEL and AML1 are transcription factors that have major roles in haematopoiesis The resulting chimeric protein contains the amino-terminal domains of TEL, and all known functional domains of AML1 (Zelent et al., 2004), and it is thought to act as a transcriptional repressor of both AML1's and TEL's transcriptional targets (Ghazavi et al., 2015; Zelent et al., 2004).

A range of animal models have been developed to study the effects of TEL-AML1 expression on haematopoiesis, recapitulating some of the observations made in patients carrying the t(12;21)(p13;q22) translocation (Andreasson et al., 2001; Bernardin et al., 2002; Fischer et al., 2005; Morrow et al., 2004; Sabaawy et al., 2006; Schindler et al., 2009; Tsuzuki et al., 2004; van der Weyden et al., 2011). In most of these animal models the expression of TEL-AML1 fusion protein is not sufficient to induce overt BCP-ALL, and no gross changes in haematopoietic compartments are observed (Andreasson et al., 2001; Fischer et al., 2005; Morrow et al., 2004; Schindler et al., 2009; Tsuzuki et al., 2004; van der Weyden et al., 2011), in agreement with the low frequency of overt leukaemia observed in patients carrying the *TEL-AML1* fusion (Greaves and Wiemels, 2003).

The low rate of concordance found in *TEL-AML1* twins, and the long latency of the disease have suggested that additional genetic changes are necessary for onset of leukaemia (Greaves and Wiemels, 2003; Zelent et al., 2004). Such genetic lesions have been observed in *TEL-AML1*-positive patients, the deletion of the other copy of *TEL* gene being the most frequent (Attarbaschi et al., 2004). Consistent with this, overt BCP-ALL, and other types of leukaemias, have been

reported in a mouse model where TEL-AML1 expression is combined with the expression of a *Sleeping Beauty* transposon array, that was used to carry out insertional mutagenesis, thus inducing additional hits in other genes (van der Weyden et al., 2011). Similarly, lymphoid malignancies have been reported in a murine model of TEL-AML1 expression after ENU mutagenesis (Schindler et al., 2009), which shows the necessity for a secondary genetic lesion. Additionally, in the same study it was found that expression of TEL-AML1 in the HSCs is required to induce its oncogenic activity, supporting the idea of a pre-leukaemic state induced by TEL-AML1.

It is important to note that the deletions of the wild type copy of the *TEL* gene observed in patients, which are linked to poorer prognosis (Romana et al., 1995), are subclonal to the *TEL-AML1*-positive clones (Romana et al., 1996), suggesting that the non-translocated copy of the *TEL* gene is lost after the chromosomal translocation. These data have led to the proposal of a two-step model, where the expression of TEL-AML1 chimeric protein induces subtle changes in haematopoietic cells, and an additional genetic lesion elicits overt leukaemia (Zelent et al., 2004).

3.1.2 TEL-AML1 induces subtle changes in haematopoiesis

Studies carried out using animal models expressing TEL-AML1 fusion protein (Schindler et al., 2009; van der Weyden et al., 2011), or transplanted with cells expressing it (Andreasson et al., 2001; Bernardin et al., 2002; Fischer et al., 2005; Morrow et al., 2004; Tsuzuki et al., 2004), show that the expression of TEL-AML1 fusion protein causes subtle changes in different haematopoietic compartments.

The B-cell compartment is affected by TEL-AML1 expression in most animal models studied. There is evidence supporting the notion that the expression of TEL-AML1 leads to an impaired differentiation in the pro-B-cell compartment (Fischer et al., 2005; Morrow et al., 2004; Schindler et al., 2009; Tsuzuki et al., 2004), however, no blockage of B-cell differentiation has been observed, and some studies have reported no effects on the B-cell compartment (Bernardin et al., 2002; van der Weyden et al., 2011).

The expression of TEL-AML1 has been shown to increase the number of HSCs and to maintain them in a quiescent state (Schindler et al., 2009). However, there is conflicting evidence regarding whether TEL-AML1 confers on HSCs a competitive advantage over wild type HSCs (Morrow et al., 2004) or not (Schindler et al., 2009).

Animal models also provide evidence of an effect of TEL-AML1 expression on the myeloid compartment. Two reports have shown increased myeloid potential induced by TEL-AML1 expression, without observable defects in differentiation (Morrow et al., 2004; Tsuzuki et al., 2004). Despite the conflicting evidence provided by animal models, it is important to point out that there are no records of *TEL-AML1*-positive patients developing AML (De Braekeleer et al., 2012).

3.1.3 Rationale for the study of early haematopoiesis in a zebrafish model expressing the human TEL-AML1 fusion protein

A transgenic zebrafish model that expresses human TEL-AML1 fusion protein under the control of a ubiquitous promoter, *ZBA-EGFP-TA*, has been shown to lead to B-lineage ALL in 3% of the transgenic fish (Sabaawy et al., 2006), consistent with the low frequency of leukaemia found in *TEL-AML1*-positive patients (Greaves and Wiemels, 2003). In the same study, the researchers report that expression of TEL-AML1 under the control of the *rag2* gene promoter, leading to expression in B and T-cell progenitors, fails to induce leukaemia (Sabaawy et al., 2006), in keeping with what has been reported in a murine model where TEL-AML1 expression is under the control of the *IGH* promoter (Andreasson et al., 2001). Additionally, *ZBA-EGFP-TA* transgenic fish show signs of B-cell differentiation arrest (Sabaawy et al., 2006), as has been observed in other animal models (Fischer et al., 2005; Morrow et al., 2004; Schindler et al., 2009; Tsuzuki et al., 2004).

These similarities between the zebrafish model and murine models, together with the fact that adult zebrafish develop overt leukaemia, strongly suggest that human TEL-AML1 fusion protein is active in zebrafish. Therefore, it was reasoned that the advantages of zebrafish to study early development could be used to investigate the early effects of TEL-AML1 expression on haematopoiesis, using *Tg(ZβA:GFP-*

hTEL-AML1) transgenic fish. Importantly, such a study would not only shed light on the early events that precede the onset of leukaemia, but it would also allow the identification of haematopoietic phenotypes suitable for the design of a chemical screen in a next phase.

3.1.4 Aims of the experiments described in this chapter

1. To determine the effect of hTEL-AML1 expression on primitive haematopoiesis in zebrafish.
2. To determine the effect of hTEL-AML1 expression on definitive haematopoiesis in zebrafish.

3.2 Methods

3.2.1 Fish Husbandry

Transgenic fish carrying the sequence encoding human TEL-AML1 fusion protein under the control of the zebrafish *β-actin* gene promoter, *Tg(ZβA:GFP-hTEL-AML1)*, were kindly provided by Dr Hatem Sabaawy. Experiments were carried out using embryos and larvae obtained by outcrossing adult hemizygous *Tg(ZβA:GFP-hTEL-AML1)*$^{+/-}$ fish to wild type, other transgenic lines, or *casper* mutant fish (see section 2.1 for details). The hemizygous *Tg(ZβA:GFP-hTEL-AML1)*$^{+/-}$ embryos and larvae (herein named - / TA) obtained in this way were identified by the expression of GFP and were raised in Petri dishes together with wild type siblings (herein named - / -), which were used as controls.

3.3 Results

3.3.1 Expression of GFP-hTEL-AML1 in *Tg(ZβA:GFP-hTEL-AML1)* fish

In the transgenic zebrafish line used to model the effects of t(12;21)(p13;q22) chromosomal translocation in early haematopoiesis, *Tg(ZβA:GFP-hTEL-AML1)*, the expression of the human TEL-AML1 fusion protein is controlled by the promoter of the zebrafish *β-actin* gene, while in the patients the t(12;21)(p13;q22) chromosomal translocation results in the expression of the TEL-AML1 fusion protein under the control of the *TEL* gene promoter. Taking advantage of the fact that in the *Tg(ZβA:GFP-hTEL-AML1)* transgenic fish hTEL-AML1 fusion protein is fused to GFP, the expression pattern of hTEL-AML1 was studied during embryonic and larval development by fluorescence microscopy of live transgenic fish. To perform imaging on hemizygous *Tg(ZβA:GFP-hTEL-AML1)*$^{+/-}$ fish and wild type fish at equivalent developmental stages, adult hemizygous *Tg(ZβA:GFP-hTEL-AML1)*$^{+/-}$ fish were crossed to wild type AB fish. The embryos obtained were raised in Petri dishes and separated only before imaging. Figure 3.1 shows *in vivo* imaging of representative *Tg(ZβA:GFP-hTEL-AML1)*$^{+/-}$ fish at 24, 48 and 72 hpf. Hemizygous *Tg(ZβA:GFP-hTEL-AML1)*$^{+/-}$ fish display normal morphology and embryonic development (see Figure 3.1 a, c and e), and are indistinguishable from their wild type siblings. hTEL-AML1 expression, revealed by the accumulation of GFP, changes through larval development. At 24 hpf, GFP-hTEL-AML1 expression can be seen in skin cells (Figure 3.1 a') and in a small number of cells in the intermediate cellular mass (ICM) and in the posterior blood island (PBI) (Figure 3.1 b', white arrowhead). Interestingly, from this stage GFP$^+$ cells can be observed occasionally circulating through the dorsal aorta and the caudal vein (CV) (data not shown). This suggests that some haematopoietic cells express GFP-hTEL-AML1. Later, at 48 hpf, the number of GFP$^+$ cells in the caudal haematopoietic tissue (CHT) increases (see Figure 3.1 d'). However, at 72 hpf the number of GFP$^+$ cells found in the CHT of *Tg(ZβA:GFP-hTEL-AML1)*$^{+/-}$ larvae is significantly reduced when compared to that of 48 hpf embryos (compare Figure 3.1 d' and f').

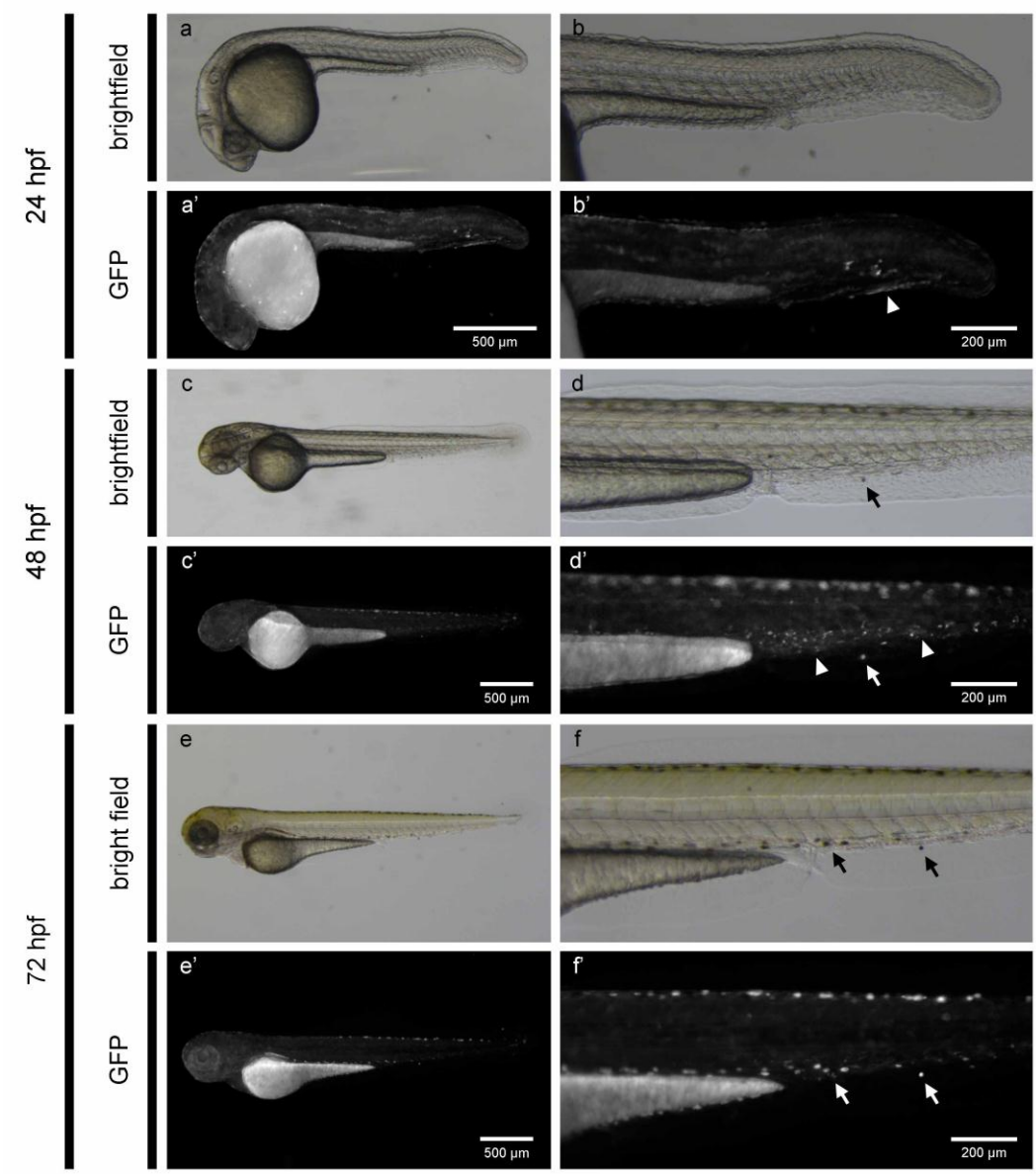

Figure 3.1 | Expression of GFP-hTEL-AML1 in *Tg(ZβA:GFP-hTEL-AML1)*$^{+/-}$ fish during development.

Bright field **(a-f)** and GFP fluorescence **(a'-f')** images of 24 hpf **(a, b, a', b')**, 48 hpf **(c, d, c', d')**, and 72 hpf **(e, f, e', f')** fish. Notice the GFP-hTEL-AML1^{+} cells in the PBI at 24 hpf **(b', white arrowhead)** whose number increases in the CHT by 48 hpf **(d', white arrowheads)**. By 72 hpf most of fluorescence in the CHT comes from pigmented cells **(f', white arrows)** which can be seen also in the bright field image **(f, black arrows)**. Scale bars: **(a and a')** 500 µm;

(b and b') 200 µm; **(c and c')** 500 µm; **(d and d')** 200 µm; **(e and e')** 500 µm; **(f and f')** 200 µm.

3.3.2 Emergence of haematopoietic stem cells in hemizygous *Tg(ZβA:GFP-hTEL-AML1)*$^{+/-}$ embryos

To study the effect of GFP-hTEL-AML1 expression on the start of definitive haematopoiesis, the emergence of haematopoietic stem cells (HSC) was analysed. HSCs develop from the ventral wall of the dorsal aorta in a process dependent on Runx1 (Bertrand et al., 2010; Kissa and Herbomel, 2010). HSCs in *Tg(ZβA:GFP-hTEL-AML1)*$^{+/-}$ embryos were labelled by WISH for *runx1* gene expression at 24 hpf. Figure 3.2 shows images of wild type (Figure 3.2 a-b) and *Tg(ZβA:GFP-hTEL-AML1)*$^{+/-}$ (Figure 3.2 c-d) embryos. The expression of *runx1* can be observed in cranial ganglia (Figure 3.2 a and c) as previously described (Gau et al., 2017), and also along the dorsal aorta (Figure 3.2 b and d). *Tg(ZβA:GFP-hTEL-AML1)*$^{+/-}$ embryos show normal *runx1* expression, suggesting that the expression of hTEL-AML1 fusion protein does not interfere in their emergence from endothelial cells.

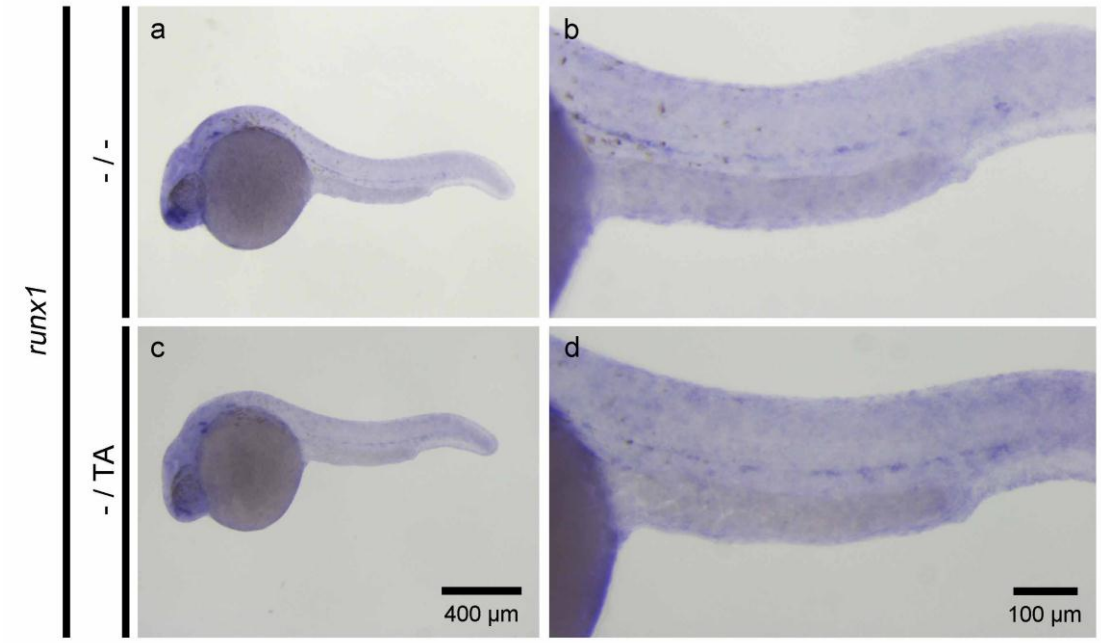

Figure 3.2 | Emergence of haematopoietic stem cells in the dorsal aorta of *Tg(ZβA:GFP-hTEL-AML1)*$^{+/-}$ embryos.

The expression of *runx1* gene was studied by WISH to label newly generated HSCs along the dorsal aorta in 24 hpf embryos. Whole mount **(a and c)**, and lateral views of the trunk **(b and d)** are shown for both wild type **(a-b)** and *Tg(ZβA:GFP-hTEL-AML1)*$^{+/-}$ **(b-d)** embryos. Scale bars: **(a-c)**, 400 µm; **(b-d)**, 100 µm.

3.3.3 Primitive erythroid cells develop normally in embryos expressing GFP-hTEL-AML1

The development of primitive erythroid cells in *Tg(ZβA:GFP-hTEL-AML1)* fish was studied by WISH. The expression of the *gata1a* gene was used as a marker for the specification of early erythroid cells in the intermediate cellular mass (ICM) that are derived from the posterior lateral plate mesoderm (PLPM) (Detrich et al., 1995; Lieschke et al., 2002) and produce the first circulating erythroid cells (Long et al., 1997). Figure 3.3 shows the expression of *gata1a* in 18 hpf (18ss) *Tg(ZβA:GFP-hTEL-AML1)*$^{+/-}$ embryos (Figure 3.3 c and d) and their wild type siblings (Figure 3.3 a and b). In wild type embryos, *gata1a* is expressed in the ICM, from the yolk sac to the PBI (Figure 3.3 b). Hemizygous *Tg(ZβA:GFP-hTEL-AML1)*$^{+/-}$ embryos exhibit

the same expression pattern (Figure 3.3 d), suggesting that primitive erythroid cell development is undisturbed by the expression of GFP-hTEL-AML1. Consistent with the results shown in the Figure 3.3, by 24 - 28 hpf *Tg(ZβA:GFP-hTEL-AML1)*$^{+/-}$ embryos display normal blood circulation (data not shown).

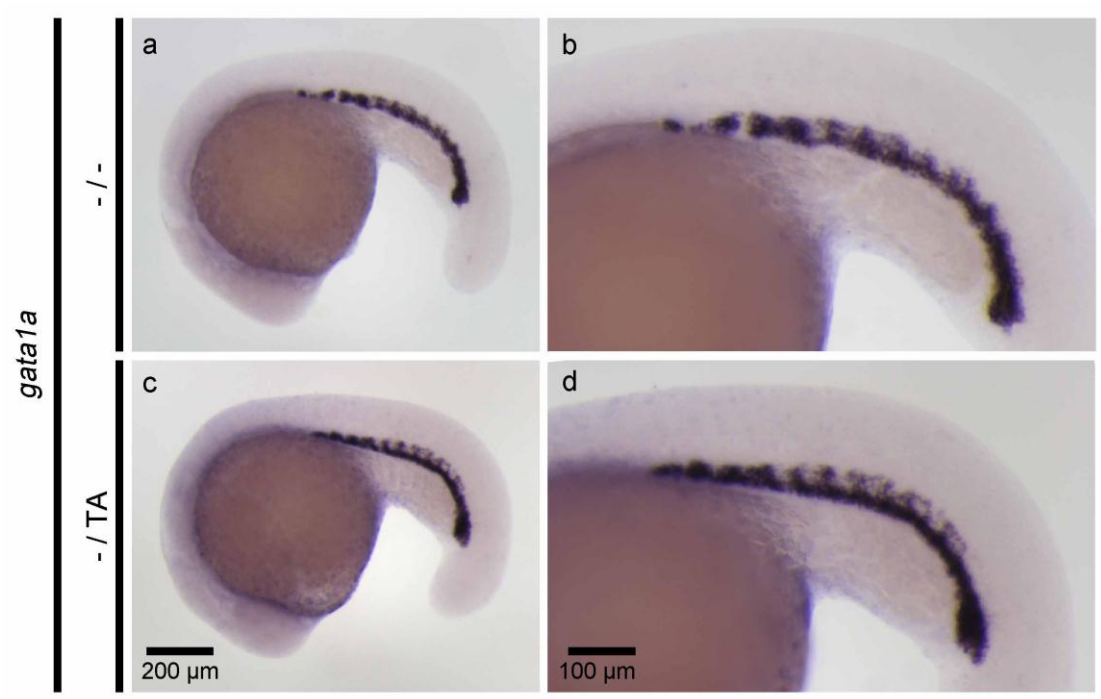

Figure 3.3 | Early erythroid development in *Tg(ZβA:GFP-hTEL-AML1)*$^{+/-}$ fish.

Early erythroid development was studied by WISH for *gata1a* gene expression. The expression pattern of the *gata1a* gene at 18 hpf is shown in wild type **(a-b)** and *Tg(ZβA:GFP-hTEL-AML1)*$^{+/-}$ **(c-d)** embryos. All images are lateral views with anterior to the left. Scale bars: **(a and c)**, 200 µm; **(b and d)**, 100 µm.

3.3.4 Development of definitive erythroid cells in *Tg(ZβA:GFP-hTEL-AML1)* fish

The development of definitive erythroid cells was monitored using a transgenic reporter line *Tg(gata1a:dsRed)*, that expresses dsRed fluorescent protein under the control of the *gata1a* gene promoter, labelling almost exclusively erythroid cells

(Traver et al., 2003). Compound transgenic fish were obtained by outcrossing adult transgenic *Tg(ZβA:GFP-hTEL-AML1)*$^{+/-}$ fish to homozygous transgenic *Tg(gata1a:dsRed)*$^{+/+}$ fish. Both - / - and - / TA larvae obtained were imaged under identical conditions. Figure 3.4 shows that larvae expressing hTEL-AML1 fusion protein (Figure 3.4 a'-f') develop erythroid cells that perfuse the heart, dorsal aorta (DA), CV, the intersegmental vessels (Se) and other vessels in the head, in the same way as observed in wild type larvae (Figure 3.4 a-f). Also, both - / - and - / TA larvae exhibit a population of stationary dsRed^{+} cells in the CHT, between the dorsal aorta and the CV. No noticeable differences were found between transgenic *Tg(ZβA:GFP-hTEL-AML1)*$^{+/-}$ fish and their wild type siblings. Similarly, imaging at 72 hpf shows no significant difference between both groups (see Supplementary Figure 9.1), supporting the idea that hTEL-AML1 expression does not affect erythroid development in *Tg(ZβA:GFP-hTEL-AML1)*$^{+/-}$ fish.

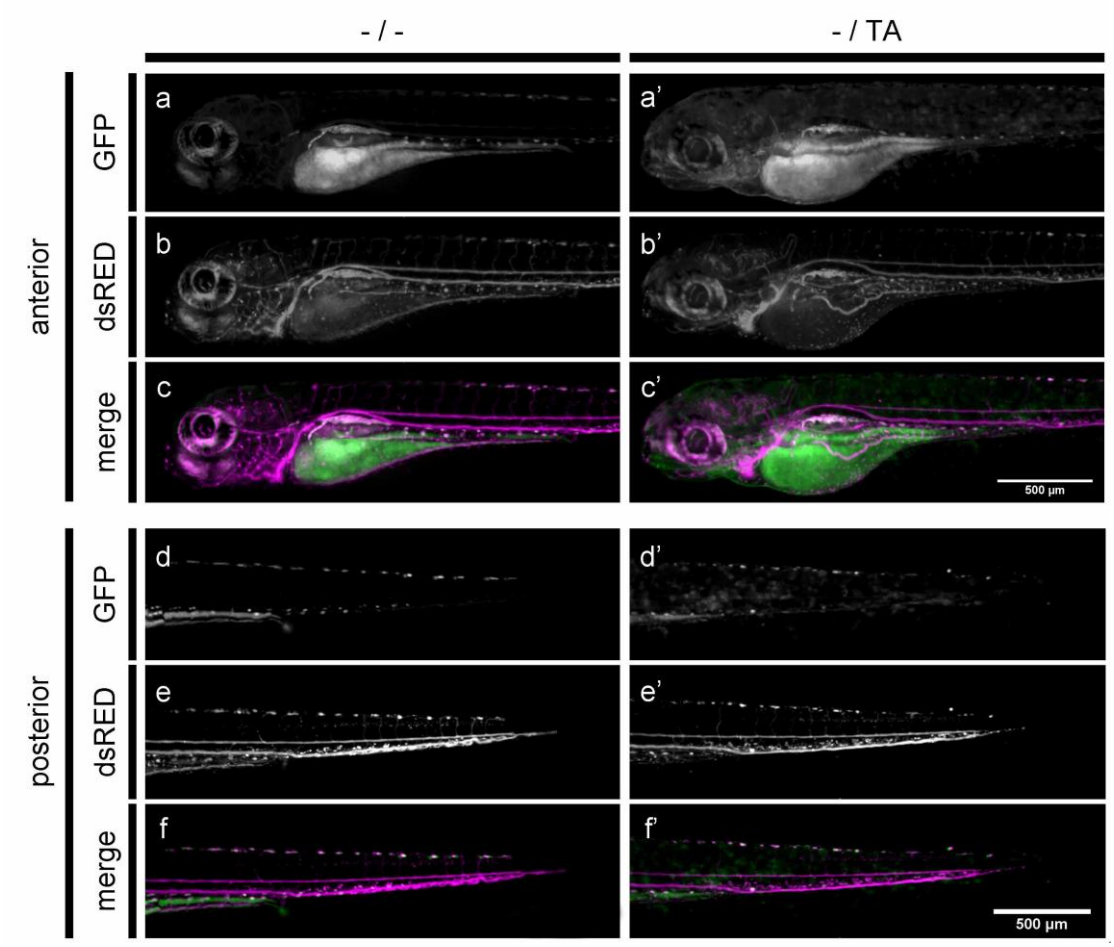

Figure 3.4 | Definitive erythroid cells develop normally in *Tg(ZβA:GFP-hTEL-AML1)*$^{+/-}$ fish.

The transgenic reporter line *Tg(gata1a:dsRed)* was used to study erythroid cells in transgenic *Tg(ZβA:GFP-hTEL-AML1)*$^{+/-}$ larvae. Wild type **(a-f)** and *Tg(ZβA:GFP-hTEL-AML1)*$^{+/-}$ **(a'-f')** fish were imaged at 4 dpf. Images of the anterior **(a-c and a'-c')** and posterior **(d-f and d'-f')** halves of larvae are shown. GFP **(a, a', d, d')** and dsRed **(b, b', e, e')** channels are shown in addition to images of both channels merged **(c, c', f, f')**. Scale bars: **(a-c and a'-c')**, 500 µm; **(d-f and d'-f')**, 500 µm.

Imaging of larvae carrying the transgenic reporter *Tg(gata1a:dsRed)* shows that definitive erythrocytes develop normally in *Tg(ZβA:GFP-hTEL-AML1)*$^{+/-}$ larvae (Figure 3.4 and Supplementary Figure 9.1). Therefore, a histological technique, *o*-

dianisidine (see section 2.4 for more details), was used to detect haemoglobin in erythrocytes of *Tg(ZβA:GFP-hTEL-AML1)*$^{+/-}$ fish at 5 dpf. Figure 3.5 shows images of 5 dpf wild type and *Tg(ZβA:GFP-hTEL-AML1)*$^{+/-}$ larvae that have been stained with *o*-dianisidine. Haemoglobinization pattern in larvae expressing GFP-hTEL-AML1 (Figure 3.5 b, d, f, h, and j) is normal compared to that of wild type larvae (Figure 3.5 a, c, e, g, and i). *Tg(ZβA:GFP-hTEL-AML1)*$^{+/-}$ larvae exhibit normal haemoglobinization in erythroid cells in heart, and major vessels of the head, like the primary head synus (PHS), ventral aorta (VA), branchial arches (AA), and hypobranchial artery (HA) (compare Figure 3.5 c and d). Erythroid cells containing haemoglobin can also be observed in the caudal artery (CA), CV, and intersegmental vessel (Se) (see Figure 3.5 g-j).

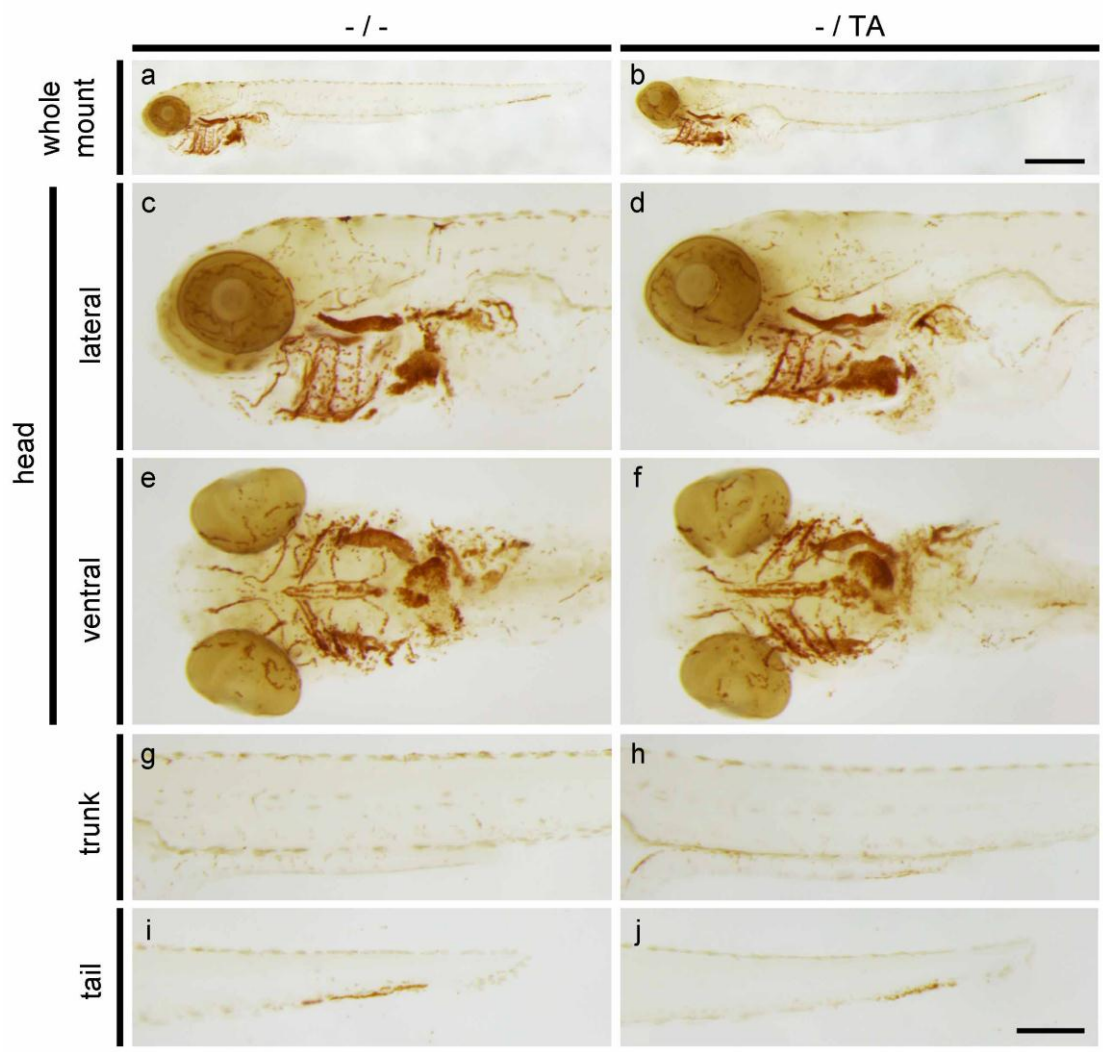

Figure 3.5 | Haemoglobinization in *Tg(ZβA:GFP-hTEL-AML1)*$^{+/-}$ fish at 5 dpf.

O-dianisidine staining was used to label haemoglobin in erythrocytes in 5 dpf *Tg(ZβA:GFP-hTEL-AML1)*$^{+/-}$ fish. Images of wild type **(a, c, e, g, and i)** and *Tg(ZβA:GFP-hTEL-AML1)*$^{+/-}$ **(b, d, f, h, and j)** larvae are shown. **(a-b)** Whole mount images of larvae. **(c-f)** Heads of larvae are shown in lateral **(c-d)** and ventral **(e-f)** views. Lateral views of the trunk **(g-h)** and the tail **(i-j)** are shown. All images show anterior to the left. Scale bars: **(a-b)**, 500 µm; **(c-j)**, 200 µm.

3.3.5 Myeloid cell development is transiently affected by hTEL-AML1 expression

Primitive myeloid development was studied using WISH for the *ikaros* gene. At early stages the *ikaros* gene is expressed in two different cell types: in primitive myeloid cells in the yolk sac, and in erythroid cells in the haematopoietic tissue of the ICM (Willett et al., 2001). Figure 3.6 shows the expression of the *ikaros* gene in embryos expressing GFP-hTEL-AML1 at 18 hpf. At 18 hpf (18ss), *ikaros* expression can be observed along the ICM until the PBI (Figure 3.6 a-b and d-e). Embryos carrying 2 copies of GFP-hTEL-AML1 transgene show a normal expression pattern of *ikaros* in the ICM, suggesting that primitive haematopoiesis is not affected by hTEL-AML1 expression at this stage.

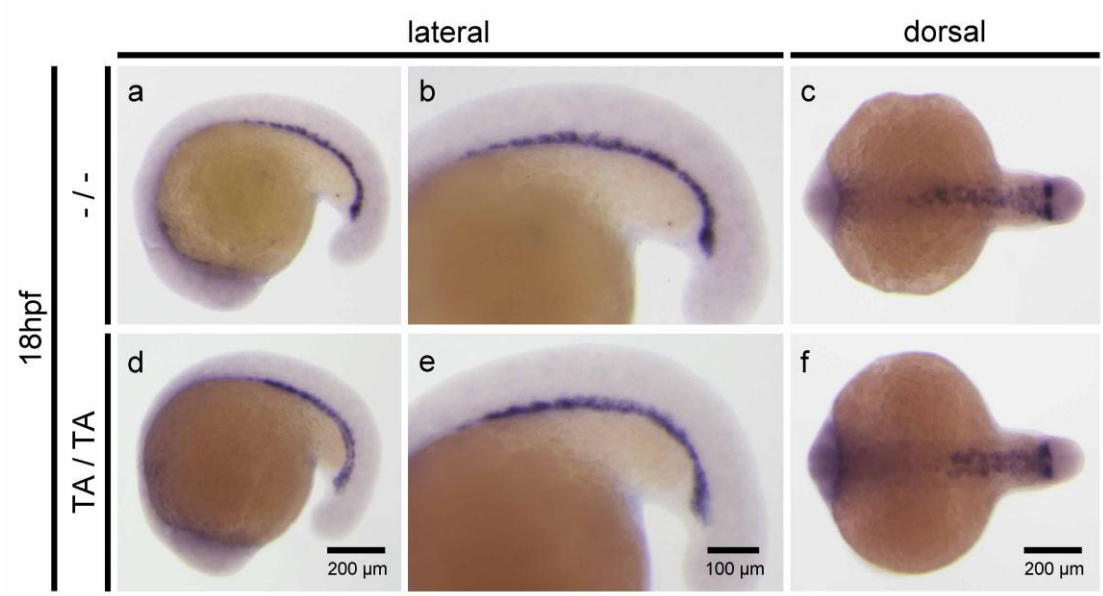

Figure 3.6 | Expression of *ikaros* gene in *Tg(ZβA:GFP-hTEL-AML1)* embryos at 18 hpf.

Expression analysis of *ikaros* by WISH in 18 hpf **(a-f)** transgenic embryos. Images of wild type **(a-c)**, and *Tg(ZβA:GFP-hTEL-AML1)*$^{+/+}$ **(d-f)** embryos are shown. Lateral **(a, b, d, and e)** and dorsal **(c, and f)** views are shown with anterior to the left. Scale bars: **(a and d)**, 200 µm; **(b and e)**, 100 µm; **(c and f)**, 200 µm.

Later, by 22 hpf, *ikaros* expression is found in the ICM (Figure 3.7 a and b) and in myeloid cells over the yolk sac (Figure 3.7 c). *Tg(ZβA:GFP-hTEL-AML1)*$^{+/-}$ embryos show normal expression of the *ikaros* gene by 22 hpf in both the ICM (Figure 3.7 a' and b') and the cells in the yolk (Figure 3.7 c'). Myeloid cells expressing *ikaros* over the yolk sac were quantified in 22 hpf *Tg(ZβA:GFP-hTEL-AML1)*$^{+/-}$ and wild type embryos, and no statistically significant difference was found (Figure 3.7 d). These results suggest that primitive myeloid cells derived from the rostral blood island (RBI) are not affected by the expression of GFP-hTEL-AML1. Similarly, results show that *Tg(ZβA:GFP-hTEL-AML1)*$^{+/-}$ embryos have normal *ikaros* expression in the ICM, suggesting that haematopoietic cells derived from the posterior lateral plate mesoderm (PLPM) are not perturbed by GFP-hTEL-AML1 expression.

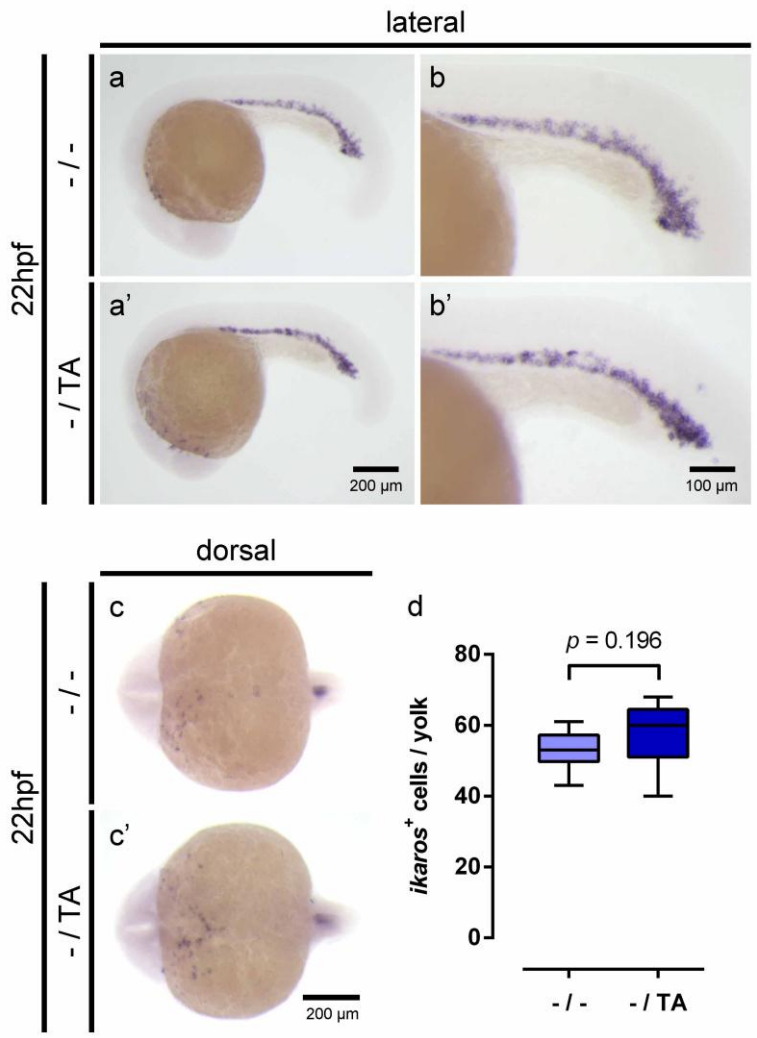

Figure 3.7 | Expression of *ikaros* in 22 hpf embryos suggests normal development of myeloid cells in *Tg(ZβA:GFP-hTEL-AML1)* embryos.

Expression analysis of *ikaros* by WISH in 22 hpf transgenic embryos. Images of wild type **(a-c)**, and *Tg(ZβA:GFP-hTEL-AML1)*$^{+/-}$ **(a'-c')** embryos are shown. Lateral **(a, b, a', and b')** and dorsal **(c and c')** views are shown with anterior to the left. Scale bars: **(a and a')**, 200 µm; **(b and b')**, 100 µm; **(c and c')**, 200 µm. **(d)** Quantification of the number of *ikaros*$^{+}$ cells in the yolk of 22 hpf wild type and *Tg(ZβA:GFP-hTEL-AML1)*$^{+/-}$ embryos. Statistical comparison was carried out by unpaired parametric t test. See Supplementary Table 9.1 for more details.

To study granulopoiesis in zebrafish embryos expressing GFP-hTEL-AML1, a histological technique was used, Sudan Black (see section 2.3 for more details), that stains primary granules in the granulocytes (Sheehan and Storey, 1946), mainly neutrophils in zebrafish embryos (Le Guyader et al., 2008). Embryos obtained from outcrosses of *Tg(ZβA:GFP-hTEL-AML1)*$^{+/-}$ adult fish and wild type fish were raised together in Petri dishes, and separated in groups according to their expression of GFP before Sudan Black staining. Figure 3.8 a-l shows images of 24-72 hpf embryos stained with Sudan Black, where neutrophils appear as black dots (Le Guyader et al., 2008). From 24 hpf to 72 hpf, most of neutrophils reside in the ventral side of the tail, first called the posterior blood island (PBI) and later called the caudal haematopoietic tissue (CHT), where definitive haematopoiesis transiently takes place (Murayama et al., 2006). However, by 24 hpf most neutrophils are not visible by Sudan Black staining (Le Guyader et al., 2008), probably due to low accumulation of primary granules and therefore low levels of Sudan Black stain being retained. Consistently, only a few Sudan Black^{+} neutrophils were observed at 24 hpf, even at high magnification (see Figure 3.8 a-d). However, no statistical difference was found in the numbers of Sudan Black^{+} neutrophils in the PBI of 24 hpf embryos expressing GFP-hTEL-AML1 when compared to wild types (Figure 3.9 a). This is consistent with previous results showing normal expression pattern of the gene *ikaros,* and normal numbers of *ikaros*$^{+}$ cells on the yolk sac in *Tg(ZβA:GFP-hTEL-AML1)*$^{+/-}$ embryos (Figure 3.7 c, c' and d).

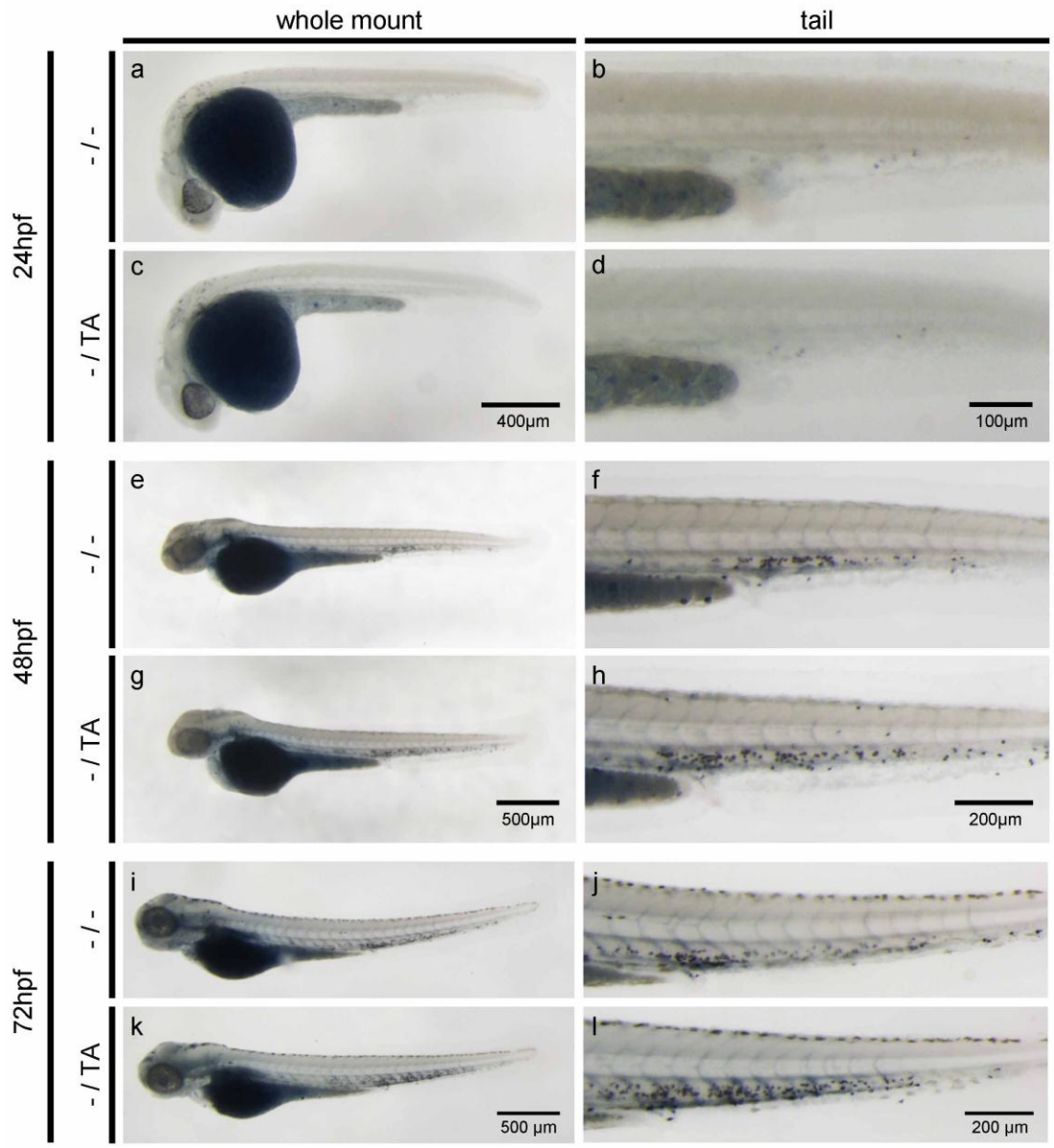

Figure 3.8 | Sudan Black^{+} granulocytes in the CHT of *Tg(ZβA:GFP-hTEL-AML1)*$^{+/-}$ larvae at 24 hpf, 48 hpf and 72 hpf.

Sudan Black was used to label the granulocytes of *Tg(ZβA:GFP-hTEL-AML1)*$^{+/-}$ fish between 24 hpf and 7 dpf. Images of wild type **(a, b, e, f, i, and j)** and *Tg(ZβA:GFP-hTEL-AML1)*$^{+/-}$ fish **(c, d, g, h, k, and l)** at 24 hpf **(a-d)**, 48 hpf **(e-h)**, and 72 hpf **(i-l)** are shown with anterior to the left. Scale bars: **(a and c)**, 400 µm; **(b and d)**, 100 µm; **(e and g)**, 500 µm; **(f and h)**, 200 µm; **(i and k)**, 500 µm; **(j and l)**, 200 µm.

Later, by 48 hpf, images of stained embryos (Figure 3.8 e-h) suggest the presence of increased numbers of neutrophils in the CHT of embryos expressing GFP-hTEL-AML1. Quantifications of Sudan Black^{+} granulocytes in the CHT of 48 hpf embryos (Figure 3.9 b) show this increase is statistically significant. Similarly, images of 72 hpf larvae stained with Sudan Black suggest that there is a higher number of neutrophils in the CHT of *Tg(ZβA:GFP-hTEL-AML1)*$^{+/-}$ fish (Figure 3.8 h) than in the CHT of wild type larvae (Figure 3.8 f). Quantifications carried out in 72 hpf larvae confirm this observation (Figure 3.9 c), supporting a role for GFP-hTEL-AML1 expression affecting granulopoiesis in the CHT.

Interestingly, quantification of Sudan Black^{+} neutrophils in the CHT of 4 dpf larvae (Figure 3.9 d) shows no significant difference between *Tg(ZβA:GFP-hTEL-AML1)*$^{+/-}$ larvae and their wild type siblings. Similar results were obtained from quantifications carried out in 7 dpf larvae (Figure 3.9 e), suggesting that the effect of GFP-hTEL-AML1 on granulopoiesis in the CHT of *Tg(ZβA:GFP-hTEL-AML1)*$^{+/-}$ larvae is transient.

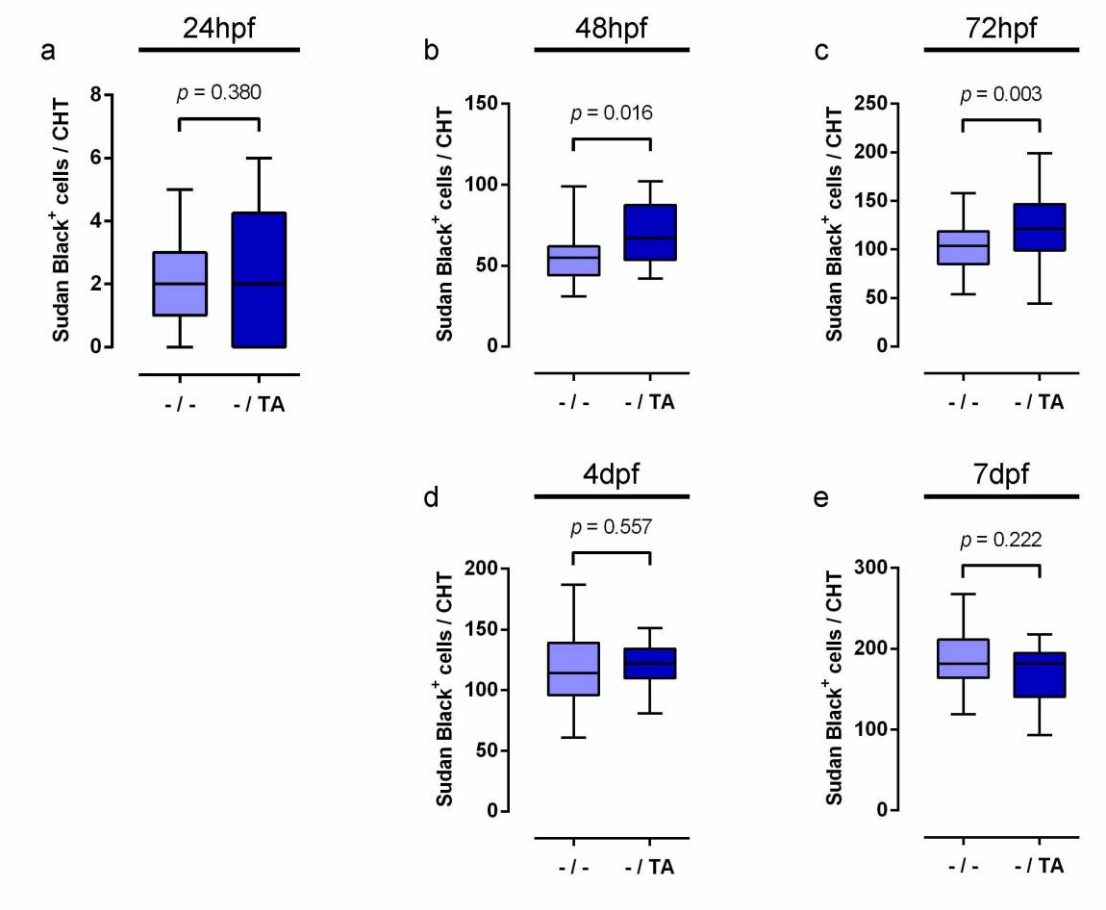

Figure 3.9 | Expression of GFP-hTEL-AML1 induces a transient increase in the number of granulocytes in the CHT.

In **(a-e)**, quantifications of the number of Sudan Black^{+} granulocytes in the CHT in *Tg(ZβA:GFP-hTEL-AML1)*$^{+/-}$ fish at 24 hpf **(a)**, 48 hpf **(b)**, 72 hpf **(c)**, 4 dpf **(d)**, and 7 dpf **(e)** are shown. Statistical comparisons in **(a-e)** were carried out by unpaired t test. See Supplementary Table 9.2 – 9.6 for more details.

3.3.6 T-Lymphoid development is unaffected in fish expressing hTEL-AML1 protein

The development of thymocytes and lymphoid cells in *Tg(ZβA:GFP-hTEL-AML1)*$^{+/-}$ fish was studied using three different markers: *gata3* (GATA binding protein 3), *rag1* (recombination activating gene 1) and *lck* (T-cell specific tyrosine kinase). To avoid the interference of developmental differences other than those elicited by

hTEL-AML1 expression, *Tg(ZβA:GFP-hTEL-AML1)*$^{+/-}$ fish were outcrossed to wild type AB fish, and their embryos were raised together in Petri dishes until 4 dpf, when larvae were split in groups according to the expression, or lack of, GFP, and fixed for WISH as described in section 2.3.

The development of early thymocytes in *Tg(ZβA:GFP-hTEL-AML1)*$^{+/-}$ fish was studied using the expression of *gata3*, a zinc-finger transcription factor that is expressed in haematopoietic cells, the kidney and nervous system (Neave et al., 1995). In haematopoietic cells, *gata3* expression is restricted to thymocytes and T lymphocytes, and it has been shown to be required in early development of T cells (Ma et al., 2013; Ting et al., 1996). The expression of *gata3* in 4 dpf *Tg(ZβA:GFP-hTEL-AML1)*$^{+/-}$ larvae is compared to that of their wild type siblings in Figure 3.10 a-f. At 4 dpf, zebrafish larvae express *gata3* in early thymocytes, anterior branchial arches and structures in the midbrain (Thisse et al., 2001). Expression of *gata3* is normal in *Tg(ZβA:GFP-hTEL-AML1)*$^{+/-}$ larvae (Figure 3.10 d) compared to that of wild type larvae (Figure 3.10 a). Lateral views of the heads of larvae show normal expression of *gata3* in the midbrain and anterior branchial arches (Figure 3.10 b compared to Figure 3.10 e). In Figure 3.10 c (black arrowheads) the expression of *gata3* in thymocytes can be observed in both thymi. Transgenic larvae expressing hTEL-AML1 exhibit normal *gata3* expression (Figure 3.10 f, black arrowheads), suggesting normal development of thymocytes in both thymi.

The expression of *rag1* and *lck* were used as markers of immature T-cells in 4 dpf larvae. Although *rag1* is expressed from 4 hpf in zebrafish (Thisse et al., 2001), its expression in the thymi can be observed from 72 hpf (Ma et al., 2013; Thisse et al., 2001). Similarly, *lck* expression is observable in the thymi from 4 dpf (Jones et al., 2015; Ma et al., 2013). Figure 3.10 shows the expression patterns of *rag1* (Figure 3.10 g-l) and *lck* (Figure 3.10 m-r) in 4 dpf larvae expressing hTEL-AML1 and their wild type siblings. In both cases, the expression is found in immature T cells in the bilateral thymic lobes at this stage. Larvae expressing hTEL-AML1 display normal expression patterns for both thymic markers (Figure 3.10 j-l and p-r), suggesting that colonization of thymi by haematopoietic progenitors and further T cell development are not disrupted by hTEL-AML1 expression in transgenic larvae.

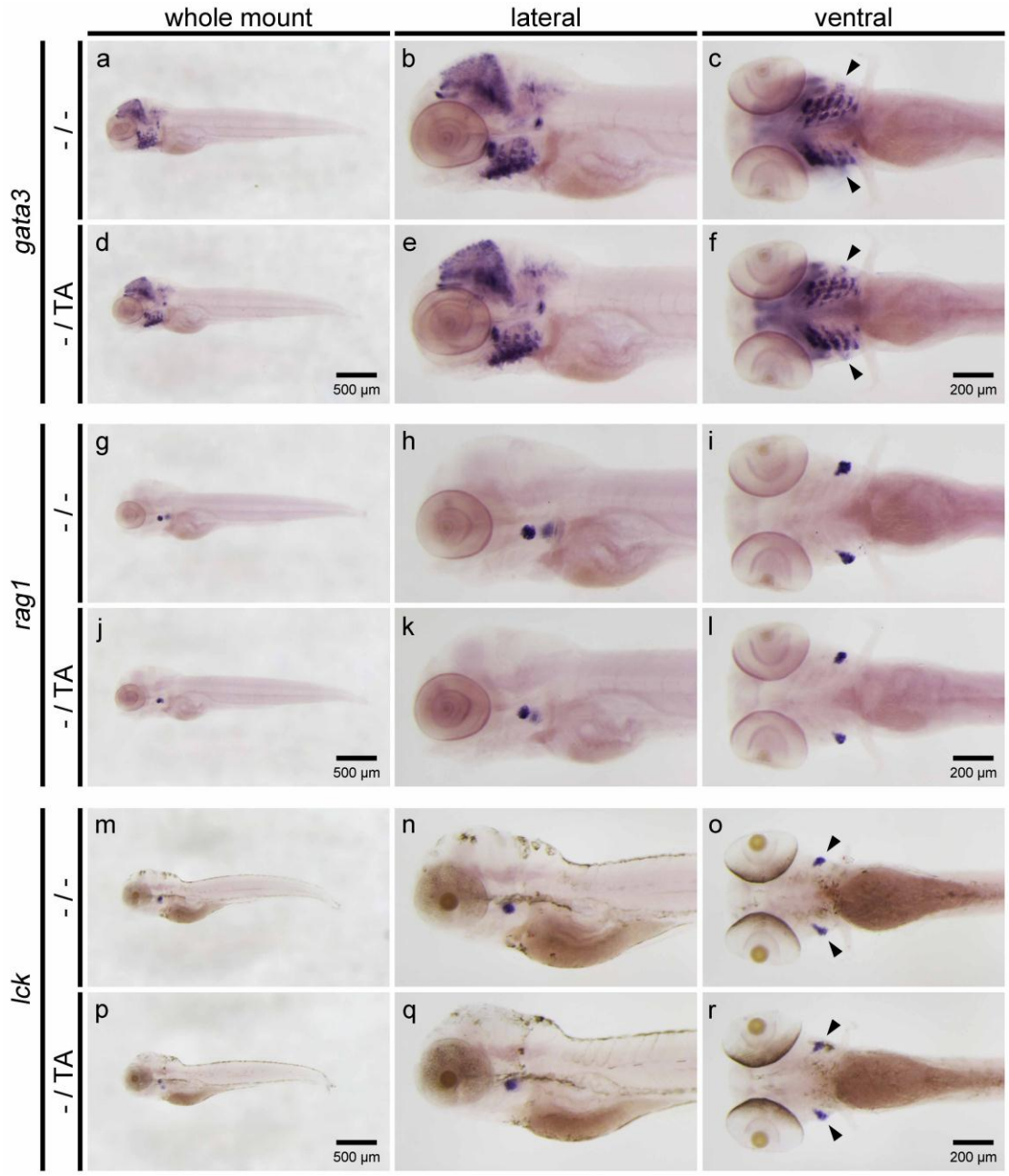

Figure 3.10 | Normal development of thymocytes and T lymphocytes in *Tg(ZβA:GFP-hTEL-AML1)*$^{+/-}$ fish.

The expression of thymic markers was analysed by WISH in 4 dpf *Tg(ZβA:GFP-hTEL-AML1)*$^{+/-}$ fish. The expression of *gata3* **(a-f)**, *rag1* **(g-l)** and *lck* **(m-r)** genes is compared in *Tg(ZβA:GFP-hTEL-AML1)*$^{+/-}$ fish (- / TA, in **d-f**, **j-l**, and **p-r**) and their wild type siblings (- / -, in **a-c**, **g-l**, and **m-o**). All images show anterior to the left. Left and middle columns show lateral views of larvae, and right column pictures show

larvae from ventral view, making both thymi visible. Scale bars: left column, 500 µm; middle and right columns, 200 µm.

3.4 Discussion

The Table 3.1 summarizes the main results of section 3.3, that are discussed in this section.

Table 3.1 | Summary of haematopoietic phenotype of *Tg(ZβA:GFP-hTEL-AML1)*$^{+/-}$ fish.

Lineage	Phenotype observed
HSCs	Normal levels of expression of *runx1* at 24 hpf.
Erythroid cells	Normal levels of expression of *gata1a* at 18 hpf. Normal levels of *Tg(gata1a:dsRed)*+ cells at 4 dpf. Normal levels of *o*-dianisidine staining at 5 dpf.
Myeloid cells	Normal numbers of *ikaros*+ cells in the yolk at 22 hpf. Increased numbers of Sudan Black+ cells at 48 and 72 hpf.
Lymphoid cells	Normal levels of expression of *gata3, rag1,* and *lck* at 4 dpf.

3.4.1 Effects of human *TEL-AML1* expression in primitive haematopoiesis in zebrafish

The first haematopoietic cells in vertebrates differentiate directly from haemato-vascular progenitors derived from the mesoderm (Carroll and North, 2014). Haemato-vascular progenitors in the lateral plate mesoderm (LPM) generate both the primitive myeloid and erythroid cells, from the anterior and posterior lateral plate mesoderm, respectively (Carroll and North, 2014; Lieschke et al., 2002). Although the establishment of haemato-vascular mesoderm (previously known as haemangioblasts) was not assessed directly in embryos expressing GFP-hTEL-AML1, it is possible to infer that haemato-vascular mesoderm in *Tg(ZβA:GFP-hTEL-AML1)* embryos is correctly established from experiments that show no perturbations in primitive haematopoietic cells derived from it. Experiments carried out at between 18 hpf and 24 hpf stages suggest normal development of haematopoietic cells derived from the primitive wave of haematopoiesis (Figure 3.3, Figure 3.6, and Figure 3.7).

By 10 ss, the haemato-vascular progenitors form two pairs of stripes of cells that express early haematopoietic markers, including *lmo2* and *runx1* genes (Kalev-Zylinska et al., 2002; Patterson et al., 2007). The progenitors located in the anterior part of the embryo form the anterior lateral plate mesoderm (ALPM) and generate primitive myeloid cells (Herbomel et al., 1999). In contrast, primitive erythroid cells, are generated from the posterior lateral plate mesoderm (PLPM) (Detrich et al., 1995; Lieschke et al., 2002). Results obtained regarding both primitive erythroid and myeloid cells strongly suggest normal primitive haematopoiesis in *Tg(ZβA:GFP-hTEL-AML1)* embryos. Expression of *ikaros* in cells on the yolk sac (Figure 3.7) and Sudan Black stainings (Figure 3.8 and Figure 3.9) show no difference in the number of primitive myeloid cells in embryos expressing GFP-hTEL-AML1. Similarly, results of expression analysis of the haematopoietic markers *ikaros* (Figure 3.6 and Figure 3.7) and *gata1a* (Figure 3.3) in the ICM show normal development of haematopoietic cells derived from the posterior lateral plate mesoderm (PLPM) in embryos expressing GFP-hTEL-AML1.

A transient wave of primitive haematopoiesis has been described in the caudal haematopoietic tissue, before the emergence of haematopoietic stem cells. These cells, termed erythromyeloid progenitors (EMP), demonstrate erythroid and myeloid potential *in vitro* (Bertrand et al., 2007). However, EMPs do not have lymphoid potential, and cells derived from them have not been observed to colonise the kidney (Bertrand et al., 2007; Carroll and North, 2014). This wave of haematopoiesis is followed by the emergence of haematopoietic stem cells (HSC) from endothelial cells in the ventral wall of the dorsal aorta (Bertrand et al., 2010; Kissa and Herbomel, 2010). HSCs then migrate to the caudal haematopoietic tissue (CHT), where they generate myeloid and erythroid cells (Le Guyader et al., 2008; Murayama et al., 2006). The development of EMPs in *Tg(ZβA:GFP-hTEL-AML1)* embryos was not studied. Zebrafish EMPs have been shown to reside in the PBI and to express *gata1a* and *lmo2* genes (Bertrand et al., 2007), therefore, although *gata1a* expression in the PBI of *Tg(ZβA:GFP-hTEL-AML1)* embryos is normal at 18 hpf (Figure 3.3), it is not possible to rule out the possibility that EMPs number or function is affected by hTEL-AML1 expression.

3.4.2 Expression of hTEL-AML1 induces a transient increase in the number of granulocytes

Both EMPs and HSCs transiently produce myeloid and erythroid cells in the CHT (Bertrand et al., 2007; Murayama et al., 2006). Experiments on transgenic *Tg(ZβA:GFP-hTEL-AML1)* larvae show normal development of erythroid cells by 72 hpf (Supplementary Figure 9.1) and 4 dpf (Figure 3.4). In contrast, myeloid cells are affected in larvae expressing the *Tg(ZβA:GFP-hTEL-AML1)* transgene (Figure 3.8 and Figure 3.9). Sudan Black experiments on *Tg(ZβA:GFP-hTEL-AML1)*$^{+/-}$ larvae show a transient increase in the number of granulocytes in the CHT at 48 hpf and 72 hpf, however, by 4 dpf, their number is indistinguishable from that of wild type larvae (Figure 3.9). Given that myeloid cells found in the CHT between 48 hpf and 72 hpf potentially arise from different progenitors, including myeloid cells produced during the primitive wave of haematopoiesis, it is difficult to definitively determine the origin of the increased number of Sudan Black^{+} cells. Further experiments are necessary to dissect whether GFP-hTEL-AML1 expression affects haemato-vascular progenitors, EMPs, or HSCs in *Tg(ZβA:GFP-hTEL-AML1)* transgenic fish.

The increased number of granulocytes found in the CHT of *Tg(ZβA:GFP-hTEL-AML1)* transgenic larvae at 48 hpf and 72 hpf show that the degree of conservation between human and zebrafish allows the human TEL-AML1 fusion protein to regulate gene transcription, and to induce changes in the haematopoietic compartment. Given that Sabaawy and colleagues did not investigate early haematopoiesis in *ZBA-EGFP-TA* transgenic fish (Sabaawy et al., 2006), it is not known whether the overt leukaemia in adult fish that they report was preceded by increased numbers of myeloid cells during larval development.

It is interesting to note that the transient increase in the number of Sudan Black^{+} granulocytes in the CHT (Figure 3.9) is observed almost concomitantly with an also transient presence of cells expressing GFP-hTEL-AML1 in the CHT (Figure 3.1). These observations suggest that the levels of expression of human TEL-AML1 fused to GFP could be directly correlated with the changes observed in the haematopoietic compartment. Previous reports in zebrafish and murine models expressing TEL-AML1 have shown that the levels of expression, and the promoter controlling the expression of TEL-AML1 fusion protein have a major impact on the

effects observed in the haematopoietic compartments (Andreasson et al., 2001; Sabaawy et al., 2006). Interestingly, Sabaawy and colleagues report that while the expression of human TEL-AML1 fusion protein under the control of the *β-actin* gene leads to overt leukaemia in zebrafish, the expression of the same transgene under the control of the *rag2* gene promoter does not induce leukaemia (Sabaawy et al., 2006). These findings suggest that the effects of TEL-AML1 expression are cell autonomous and that they are restricted to a delimited time window during haematopoietic development.

It is important to consider that the quantifications of Sudan Black^{+} cells carried out in *Tg(ZβA:GFP-hTEL-AML1)* transgenic fish (Figure 3.9) include only those cells residing in the CHT, while the granulocytes infiltrating other tissues and those in the blood stream were not quantified. However, imaging of *Tg(ZβA:GFP-hTEL-AML1)*$^{+/-}$ fish at 48 hpf and 72 hpf shows normal distribution of Sudan Black-labelled granulocytes and no abnormal accumulations of granulocytes were found. All these data together show that there is robust evidence supporting that there is an increased number of granulocytes residing in the CHT of *Tg(ZβA:GFP-hTEL-AML1)*$^{+/-}$ fish at 48 hpf and 72 hpf. It would be interesting to carry out quantifications of total numbers of granulocytes (i. e. using flow cytometry in transgenic embryos) to determine whether this difference is due to differences in total numbers of granulocytes or caused by differences in their location. If the quantifications show that there is an increment in the total number of granulocytes in *Tg(ZβA:GFP-hTEL-AML1)*$^{+/-}$ larvae, further experiments will be necessary to assess the possibility of increased number of progenitors, increased differentiation of progenitors into granulocytes, or decreased cell death in the granulocytes. On the other hand, if the total numbers of granulocytes are not changed in *Tg(ZβA:GFP-hTEL-AML1)*$^{+/-}$ larvae, the increased number of granulocytes in the CHT could be caused by a defective mobilization of granulocytes into the blood circulation, defective differentiation of granulocytes, or abnormal localization of their progenitors.

Similar experiments would be necessary to determine whether by 4 dpf the numbers of granulocytes return to those observed in the wild type fish or the developmental changes, entry into the blood stream, and granulopoiesis in the kidney, are responsible for masking the differences between wild type and *Tg(ZβA:GFP-hTEL-AML1)*$^{+/-}$ transgenic fish.

The observed transient increase in the number of granulocytes in the CHT of *Tg(ZβA:GFP-hTEL-AML1)*$^{+/-}$ transgenic fish at 48 hpf and 72 hpf (Figure 3.8 and Figure 3.9) raises additional questions. Given that Sudan Black staining in zebrafish larvae labels mostly neutrophils (Le Guyader et al., 2008), it is still unknown whether expression of GFP-hTEL-AML1 also affects other myeloid cells present at this developmental stage, like macrophages (Herbomel et al., 1999) and mast cells (Dobson et al., 2008). Further experiments would be needed to determine whether GFP-hTEL-AML1 expression also affects other myeloid cells, their progenitors, or it biases the fate of the cells produced. Additionally, it is possible that the number or function of either progenitor cells or HSCs are affected in *Tg(ZβA:GFP-hTEL-AML1)*$^{+/-}$ transgenic fish.

3.4.3 Lymphoid development in fish expressing hTEL-AML1

Lymphoid markers like *rag1* and *lck* have been used in the past as an indirect way to determine whether HSCs are affected by an experimental condition (Jones et al., 2015; Kwan et al., 2016). This has been done under the assumption that all lymphoid cells in the thymi are derived from the definitive wave of haematopoiesis and therefore, from HSCs, given that it has been shown that EMPs do not have lymphoid potential (Bertrand et al., 2007). However, a recent report shows that lymphoid cells found in the zebrafish thymi at 4 dpf stage come entirely from the cells from the hemogenic endothelium in a transient wave of lymphopoiesis independent of HSCs (Tian et al., 2017), and that lymphoid cells derived from HSCs do not appear in the thymi until 8 dpf. Similarly, studies carried out in mice show that HSCs do not initiate the seeding of the thymic rudiment (Luis et al., 2016). Experiments shown in Figure 3.10 were designed to indirectly assess HSC function, but considering these new findings, the interpretation of their results is now very different. Given that all lymphoid cells at this stage come from progenitors generated in the hemogenic endothelium that enter the blood circulation and seed the developing thymus (Hess and Boehm, 2012; Kissa et al., 2007; Tian et al., 2017), results in Figure 3.10 show that these processes are normal in *Tg(ZβA:GFP-hTEL-AML1)*$^{+/-}$ transgenic larvae, suggesting as well that hemogenic endothelium is functional. It does not specifically assess the output from AGM derived HSC.

We were not able to assess the development of B cells in *Tg(ZβA:GFP-hTEL-AML1)*$^{+/-}$ larvae because zebrafish B cells are not clearly distinguishable prior to 3 weeks of development (Page et al., 2013). However, VDJ rearrangements are detectable by 4 dpf suggesting B cell precursors are present during early development without clear surface markers to delineate expression (Danilova and Steiner, 2002). In mice, early lympho-myeloid progenitors have been described arising in the foetal liver at E11.5. These progenitors arise independently from HSCs and are defined by the expression of $Lin^{-}Kit^{+}Flt3^{+}IL7R\alpha^{+}$ (Böiers et al., 2013). Consistently, progenitors with lymphoid potential independent of HSCs have been also described in zebrafish (Tian et al., 2017). To determine if these lympho-myeloid progenitors were present in zebrafish, the expression of *il7r* was analysed during development by WISH. However, we were unable to detect *il7r* transcripts before its expression in T cells at 4 dpf (data not shown). The presence of such cells cannot be excluded due to the sensitivity limitations of the WISH technique.

4 Defining the role of Gata2a in developmental haematopoiesis

4.1 Introduction

4.1.1 Mammalian GATA2 plays a critical role in haematopoiesis

GATA2 belongs to the GATA family of nuclear proteins, that bind a consensus DNA sequence due to the presence of two highly conserved zinc finger domains (Trainor et al., 1996). In mammals, the GATA family is composed of six members, GATA1-6, which are divided into two different subfamilies (Lowry and Atchley, 2000), that are expressed in different cell types (Vicente et al., 2012). While the proteins GATA1, GATA2, and GATA3 are mainly expressed in haematopoietic cells (Orkin, 1995; Simon, 1995); GATA4, GATA5 and GATA6 are expressed in cells derived from the endoderm and mesoderm (Charron and Nemer, 1999; Molkentin, 2000). *Gata2* is expressed in a broad range of tissues, including the central nervous system, foetal liver, endothelial cells, the heart, and haematopoietic cells (Simon, 1995). Expression of *Gata2* in haematopoietic cells has been found mainly in early haematopoietic progenitors, mast cells, and megakaryocytes (Tsai et al., 1994; Tsai and Orkin, 1997), consistent with its critical role in haematopoiesis.

Studies using *Gata2* knockout mice showed that homozygous *Gata2*$^{-/-}$ mice died before the foetal liver stage (E11.5) as a consequence of severe anaemia caused by failure of definitive haematopoiesis (Tsai et al., 1994). In contrast, heterozygous knockout *Gata2* mice are born healthy (Tsai et al., 1994), and display normal numbers of cells in the major haematopoietic compartments (Rodrigues et al., 2005). Interestingly, double *Gata1*$^{-/-}$*; Gata2*$^{-/-}$ knockout mice show an almost complete lack of primitive erythroid cells, while loss of either gene alone has lesser impact on primitive erythroid cells, suggesting functional redundancy between GATA1 and GATA2, and a role for GATA2 in primitive haematopoiesis (Fujiwara et al., 2004).

Due to the lethal phenotype of homozygous *Gata2* knockout mice, the role of GATA2 in haematopoiesis has been studied using chimaeras carrying *Gata2*$^{-/-}$ cells (Tsai et al., 1994), conditional mutants (de Pater et al., 2013; Lim et al., 2012)

and transplantation assays (Ling et al., 2004; Rodrigues et al., 2008, 2005). Chimaeras obtained by injection of homozygous *Gata2*$^{-/-}$ embryonic stem cells into wild type blastocysts show that *Gata*$^{-/-}$ cells contribute to primitive haematopoietic lineages, but fail to contribute to any of the lineages derived from definitive haematopoiesis (Tsai et al., 1994). Additionally, *Gata2*$^{+/-}$ bone marrow cells exhibit a decreased capacity to engraft in wild type irradiated hosts (Rodrigues et al., 2008, 2005). Closer examination of haematopoiesis in wild type recipients transplanted with heterozygous *Gata2*$^{+/-}$ cells shows that production of HSCs in the AGM is reduced, while the numbers of HSCs in the yolk sac, foetal liver and adult bone marrow remain unaffected (Ling et al., 2004), suggesting a requirement for GATA2 activity during HSC emergence. Further experiments using conditional knockout mice dissected a dual role for GATA2: conditional deletion of the *Gata2* gene in vascular cells showed that GATA2 activity is required for the emergence of HSCs via EHT; and deletion of the *Gata2* gene in HSCs demonstrates that GATA2 is necessary for the survival of HSCs (de Pater et al., 2013).

4.1.2 GATA2 gene is duplicated in teleost fish

The zebrafish genome encodes two *gata2* ohnologs, *gata2a* and *gata2b*, which have also been found in other teleost fish (Gillis et al., 2009; Liu et al., 2016). Phylogenetic analysis and the presence of syntenic regions strongly suggests that *gata2a* and *gata2b* were originated via a chromosomal duplication event (Gillis et al., 2009).

Phylogenetic analysis suggests that the evolutionary rate of *gata2b* has been faster than that of *gata2a*, suggesting that the current *gata2a* gene is more similar to the common ancestor of both genes (Liu et al., 2016). Consistent with this, alignments of the protein sequences of Gata2a and Gata2b together with human and murine GATA2 protein sequences show that the sequence of the C-terminal zinc finger of Gata2a is more similar to that of both mammals, which are identical (Butko et al., 2015).

Analysis of the expression patterns of *gata2a* and *gata2b* genes shows that *gata2b* is expressed in branchiomotor neurons (20 hpf), in the DA (from 16 hpf), and later in haematopoietic cells in the CHT (50 hpf and 72 hpf) (Butko et al., 2015). In

contrast, *gata2a* expression is found in a wide range of cell lineages from earlier developmental stages: by 8 ss, *gata2a* is expressed in the PLPM (Brown et al., 2000; Butko et al., 2015; Detrich et al., 1995); in ventral neurons of the spinal cord by 24 hpf (Andrzejczuk et al., 2018); in the central nervous system and the pituitary gland (Quiroz et al., 2012); the DA, the CV, and primitive erythrocytes (25 hpf) (Butko et al., 2015); and in adults, *gata2a* expression has been detected in eosinophils found in the kidney marrow (Balla et al., 2010; Traver et al., 2003). These data suggest that *gata2a* retains the wide expression pattern observed in *Gata2* in mice, supporting the idea that *gata2a* has conserved some of the functions in haematopoiesis observed in mammalian GATA2.

4.1.3 Role of Gata2a in vascular and haematopoietic development

The zebrafish *gata2a* gene is expressed in different tissues, and in addition to its role in vascular and haematopoietic development, it has been shown to have important roles in the development of the nervous system. By using *gata2a*^{um27} mutant fish (Zhu et al., 2011), Andrzejczuk and colleagues show that *gata2a* is required for the development of particular groups of ventral spinal cord neurons (Andrzejczuk et al., 2018). Additionally, *gata2a* morphants display loss of thyrotrope cells in the pituitary gland, demonstrating the critical role of Gata2a in pituitary development (Quiroz et al., 2012).

Expression analysis of *gata2a* suggested a role in embryonic haematopoiesis (Detrich et al., 1995), and studies in *gata2a* morphants showed that, although no alteration of the expression of key myeloid and erythroid genes was detected, *gata2a* morphants exhibit decreased numbers of blood cells (Galloway et al., 2005). Later work showed that *gata2a* downregulation is critical for erythroid maturation (Pase et al., 2009).

The generation of the zebrafish *gata2a*^{um27} mutant line uncovered the role of Gata2a in vascular development (Zhu et al., 2011). Zhu and colleagues showed that homozygous *gata2a*$^{um27/um27}$ mutants have defects in the DA leading to lack of blood circulation in the trunk of most (94%) homozygous mutants by 48 hpf (Zhu et al., 2011). These suggest a role for Gata2a in definitive haematopoiesis through

its action on endothelial cells, as it has been shown in mice with conditional mutants (de Pater et al., 2013; Lim et al., 2012).

4.1.4 Aims of the experiments described in this chapter

1. To determine the role of Gata2a in primitive haematopoiesis in zebrafish.
2. To determine the role of Gata2a in definitive haematopoiesis in zebrafish.

4.2 Methods

4.2.1 Mutant and transgenic zebrafish lines used

To study the role of Gata2a in developmental haematopoiesis, a mutant fish line carrying a 10 bp deletion in the *gata2a* gene was used (Zhu et al., 2011). This 10 bp deletion causes a frameshift and a premature stop codon, and the *gata2a*^{um27} mutant allele encodes a 297aa protein without the two zinc-finger domains of Gata2a (Zhu et al., 2011).

Additionally, the transgenic zebrafish line *Tg(kdrl:GFP)la116*, originally published as *Tg(flk1:GFP)*^{la116} (Choi et al., 2007), was used to visualise the development of the vasculature in *gata2a*^{um27} mutant fish. This line was a kind gift from Nathan Lawson.

4.2.2 Genotyping of *gata2a*^{um27} mutant fish

The genotyping strategy for *gata2a*^{um27} mutants is based on the amplification by PCR of a 409 bp DNA fragment of *gata2a* gene around the region of the deletion. The PCR product obtained this way was then digested with MspA1I enzyme, and the digestion pattern was analysed by gel electrophoresis. Wild type PCR products are cut, generating two fragments (151 bp and 258 bp), and mutant PCR products are not cut, as the 11 bp deletion removes the restriction site, giving one DNA band (409 bp).

Genomic DNA obtained from embryos or fin clips from adult fish (see section 2.11.3) was used as a template for a PCR with the primers shown in the Table 4.1:

Table 4.1 | Primers used for genotyping of *gata2a*^{um27} mutants.

Primer name	Sequence (5' to 3')	Length	%GC	Tm
gata2 for digest geno	GGCCAGAACGTGGCTTTTCCG	21	61.9	64.6
gata2 rev digest geno	GGGGATCACCAGGGGGTGAG	20	70	63.8

The Table 4.2 shows the components and concentrations of the PCR for *gata2a*^{um27} genotyping. Volumes shown are calculated for one 25 µL reaction and were scaled up for large numbers of samples. Details about dNTPs, the DNA polymerase used, and its reaction buffer are available in section 2.7.

Table 4.2 | Components of PCR for *gata2a*^{um27} genotyping.

Reagent	Volume per reaction [µL]	Final concentration
10x Standard Taq buffer	2.5	1x
10 mM dNTPs	0.5	200 µM
10 µM gata2 for digest geno	0.5	0.2 µM
10 µM gata2 rev digest geno	0.5	0.2 µM
Standard Taq Polymerase	0.125	0.625 units
genomic DNA	2	variable
nuclease free water	18.875	-

As controls, additional samples with genomic DNA from wild type embryos as DNA template and nuclease free water instead of DNA template were used in each experiment. The PCR described above was ran under the cycling conditions described in the Table 4.3.

Table 4.3 | Cycling conditions used in PCR for *gata2a*^{um27} genotyping.

Phase		temperature [°C]	time [s]
initial denaturation		95	30
35 cycles	denaturation	95	15
	annealing	64	30
	extension	68	30
final extension		68	5 minutes

The results from this PCR reactions were checked by electrophoresis in agarose gels. 5µL of the PCR products were run in a 3% (w/v) agarose gel. A single 409 bp band is expected, but a double band was observed in heterozygous DNA samples (see Figure 4.1 and text for details). A possible explanation is that one of the double bands correspond to homodimers of both wild type and mutant PCR products, that have similar electrophoretic migration, given their similar size; and the other corresponds to heterodimers of wild type and mutant PCR product, that migrate in the gel as a larger DNA fragment would do, due to the mismatch caused by the *gata2a*^{um27} deletion.

The PCR products were then digested using the restriction enzyme MspA1I (Cat. R0577S, NEB). The Table 4.4 shows the components and concentrations for the digestion of the PCR products with MspA1I enzyme:

Table 4.4 | Reaction mix for MspA1I digestion.

Reagent	Volume per reaction [µL]	Final concentration
10x CutSmart buffer	2	1x
MspA1I enzyme	0.2	2 units
PCR product	10	variable
nuclease free water	7.8	-

The MspA1I digestion mix were incubated 2 hours at 37 °C and 20 minutes at 65 °C for restriction enzyme inactivation. The DNA digestions were then analysed by electrophoresis in agarose gels. 10 µL of the digested DNA were ran in a 3% (w/v) agarose gel. The genotypes were read from the digestion pattern as explained in the Table 4.5.

Table 4.5 | *gata2a*^{um27} genotypes and MspA1I digestion patterns.

gata2a^{um27} genotype	Number of bands	Band sizes [bp]
Wild type (+/+)	2	258 151
Heterozygote (+/um27)	3	398 258 151
Homozygote (um27/um27)	1	398

An example of this genotyping protocol is shown in the Figure 4.1, where the genotyping of a group of 8 embryos after WISH at 22 hpf is shown. In Figure 4.1 a, the image of the gel electrophoresis of the PCR for genotyping is shown. As explained before, PCR products from wild type DNA have an expected size of 409 bp, while the PCR products amplified from mutant DNA are expected to be 398 bp. Given the difference between these two amplicons is only 11 bp, they are not expected to be resolved in this gel. Interestingly, in lanes 1, 2, 4, 5, and 8, an additional band is observed under 500 bp. Then in Figure 4.1 b, the MspA1I digestion of the same embryos is shown. Digestion patterns observed are consistent with the expected patterns in Table 4.5. Notice that the digestion shows that embryo in lane 7 is a homozygous *gata2a*$^{um27/um27}$ mutant, and that gel electrophoresis of the PCR shows a single band, as expected. It is also interesting to notice that all embryos that exhibited an additional band in the PCR (1, 2, 4, 5, and 8) in Figure 4.1 a, are heterozygous *gata2a*$^{+/um27}$ mutants according to the digestion (Figure 4.1 b).

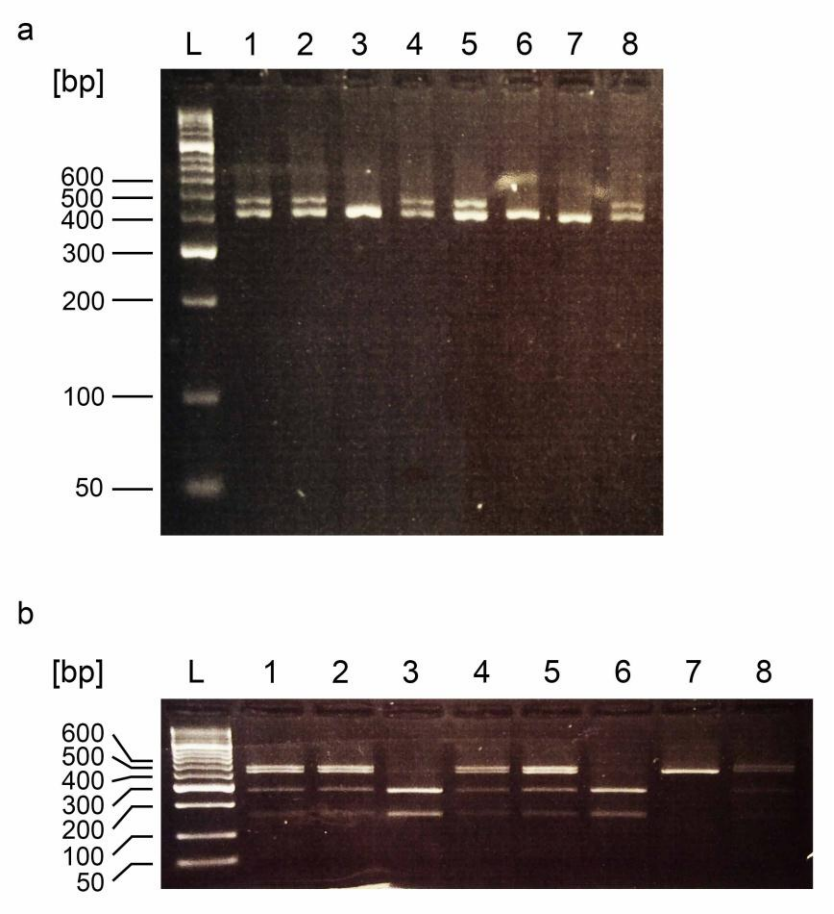

Figure 4.1 | Example of *gata2a*^{um27} genotyping.

Images of gel electrophoresis of the PCR **(a)** and the MspA1I digestion **(b)** done to genotype 22 hpf *gata2a*^{um27} mutant embryos after WISH. In **(a)**, PCR products obtained from the genomic DNA of 8 different embryos are shown in lanes 1 – 8. Amplicons from wild type DNA are expected to be 409 bp, and those from mutant DNA are expected to be 398 bp. Notice the double bands in lanes 1, 2, 4, 5, and 8. In **(b)**, the digestion patterns of the same embryos shown in **(a)** can be observed. Digestion patterns show that embryos in lanes 3, and 6 are wild types, while those in lanes 1, 2, 4, 5, and 8 are heterozygous *gata2a*$^{+/um27}$ mutants. The embryo in lane 7 is a homozygous *gata2a*$^{um27/um27}$ mutant. Notice that all embryos displaying a double band in the PCR, in **(a)**, are heterozygous, as shown by the digestions, in **(b)**. L, HypperLadder 50bp. The numbers in the column in the centre of the figure show the size in bp of relevant bands of the molecular weight marker.

4.3 Results

4.3.1 Haemato-vascular progenitors develop normally in *gata2a*^{um27} mutant embryos

The development of the haemato-vascular progenitors, from which the first haematopoietic cells derive (Vogeli et al., 2006), was studied in *gata2a*^{um27} mutant embryos by WISH. Haemato-vascular progenitors were studied by using the expression of *lmo2* and *runx1* as markers. Figure 4.2 shows images of WISH for these genes carried out in 10ss *gata2a*^{um27} mutant embryos. In wild type embryos, *lmo2* is expressed in the haemato-vascular progenitors in both the ALPM (Figure 4.2 a) and the PLPM (Figure 4.2 d) (Patterson et al., 2007), which later generate primitive myeloid and erythroid cells, respectively (Detrich et al., 1995; Lieschke et al., 2002). In the case of the haemato-vascular progenitors in the ALPM, the expression patterns show a degree of variability that was observed among wild type embryos, and also among both heterozygous *gata2a*$^{+/um27}$ and homozygous *gata2a*$^{um27/um27}$ embryos (Figure 4.2 a-c), suggesting normal development of progenitors in the ALPM. In the case of the haemato-vascular progenitors in the PLPM, the expression of *runx1* (Figure 4.2 g-i) was used as a marker (Patterson et al., 2007), in addition to that of *lmo2* (Figure 4.2 d-f). Both *lmo2* and *runx1* expression patterns are normal in both heterozygous *gata2a*$^{+/um27}$ and homozygous *gata2a*$^{um27/um27}$ embryos, suggesting that haemato-vascular progenitors in the PLPM develop normally in the mutant embryos.

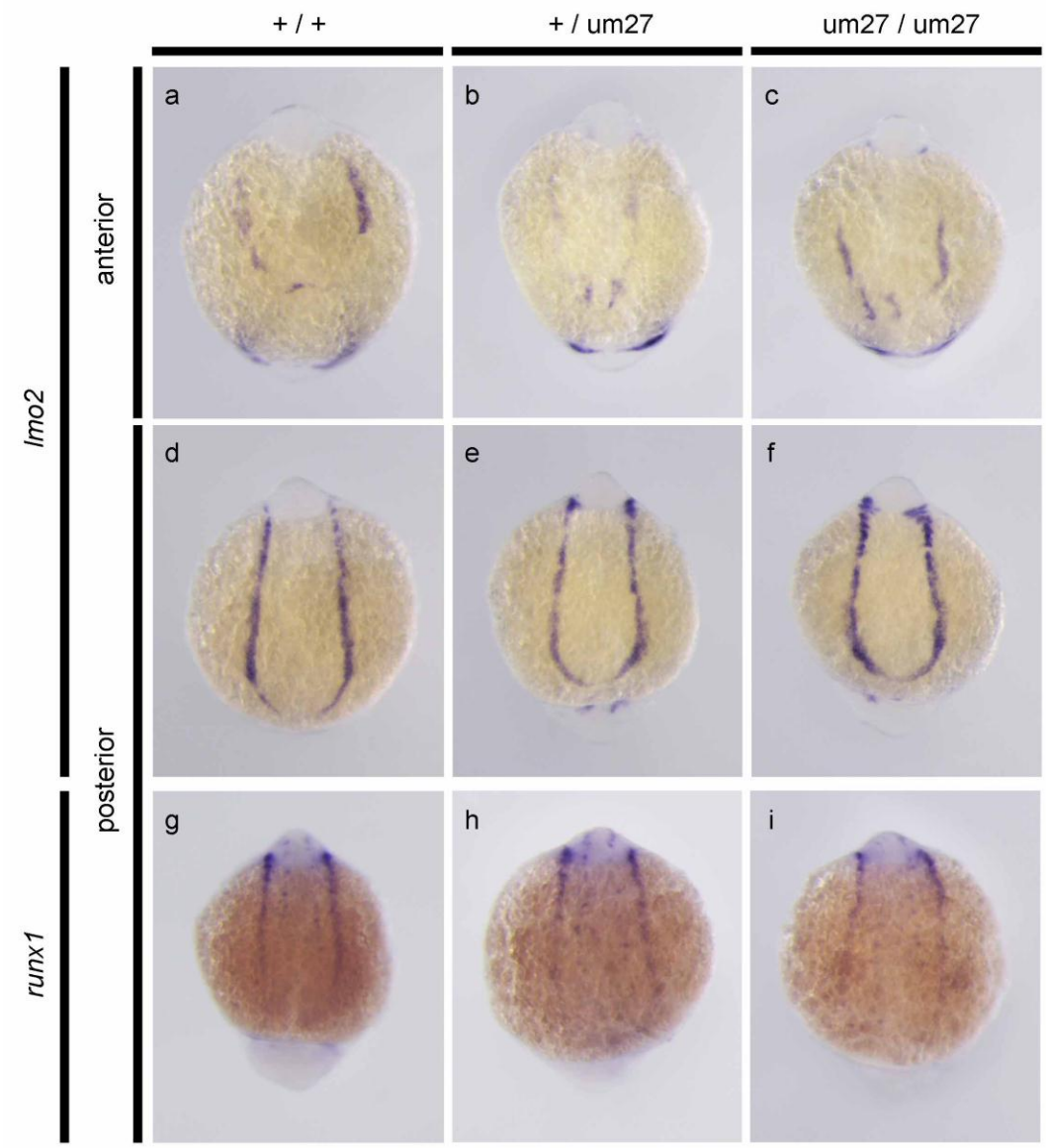

Figure 4.2 | Expression patterns of *lmo2* and *runx1* show normal specification of haemato-vascular progenitors in *gata2a*^{um27} mutant embryos.

Images of *lmo2* **(a-f)** and *runx1* **(g-i)** WISH on 10 ss *gata2a*^{um27} mutant embryos showing haemato-vascular progenitors in the anterior **(a-c)** and posterior **(d-i)** side of the embryos. All images show dorsal to the top.

4.3.2 Primitive erythroid development in *gata2*^{um27} mutant embryos

The development of the erythroid cells from the primitive wave of haematopoiesis was studied using WISH with a probe for *gata1a* gene. Gata1a is a transcription factor that plays a critical role in primitive haematopoiesis by directing lineage fate decisions in myeloid and erythroid cells (Galloway et al., 2005). The primitive erythroid cells are derived from the PLPM (Detrich et al., 1995; Lieschke et al., 2002), whose two stripes of cells converge during embryogenesis in the ICM (Detrich et al., 1995). Figure 4.3 shows the expression of *gata1a* in 18 hpf *gata2a*^{um27} mutant embryos. At this stage, *gata1a* is normally expressed in cells in the ICM over the yolk sac and in the PBI (Detrich et al., 1995). Both heterozygous *gata2a*$^{+/um27}$ (Figure 4.3 b) and homozygous *gata2a*$^{um27/um27}$ (Figure 4.3 c) mutant embryos exhibit normal *gata1a* expression in the ICM and PBI, suggesting that *gata2a*^{um27} mutant embryos have a normal erythroid development at this stage.

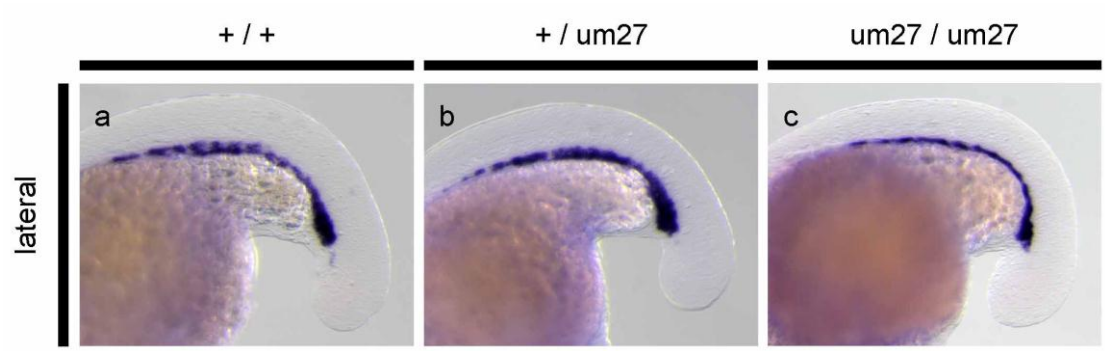

Figure 4.3 | Expression of *gata1a* shows normal development of primitive erythroid cells.

Lateral views of *gata1a* WISH on 18 hpf *gata2a*^{um27} embryos. Wild type (+ / +) **(a)**, heterozygous (+ / um27) **(b)**, and homozygous mutant (um27 / um27) **(c)** embryos are displayed with anterior to the left.

The progenitors in the PLPM produce the first primitive erythroid cells, that later enter into the blood circulation, which starts between 24 – 26 hpf (Long et al., 1997). A histochemical technique, *o*-dianisidine staining, was used to label the haemoglobin in the maturing erythroid cells of *gata2a*^{um27} mutant embryos at 28

hpf (Figure 4.4). In wild type embryos, *o*-dianisidine^{+} cells are abundant in the heart and the duct of Cuvier (Figure 4.4 a), and some cells can be found scattered in the PBI (Figure 4.4 a'). Images in Figure 4.4 b and b' show that haemoglobinization in erythroid cells of heterozygous *gata2a*$^{+/um27}$ embryos is normal compared to that of wild type embryos. However, homozygous *gata2a*$^{um27/um27}$ embryos display an abnormal distribution of *o*-dianisidine^{+} cells (Figure 4.4 c and c'). Haemoglobinization of erythroid cells is not disturbed in homozygous mutant embryos, suggesting that Gata2a is not necessary for this process (Figure 4.4 c and c'). Although haemoglobinization is not affected, the erythroid cells are abnormally distributed. The heart and duct of Cuvier have decreased numbers of labelled cells (Figure 4.4 c), while a big accumulation of *o*-dianisidine^{+} cells is found in the PBI (Figure 4.4 c' arrowhead), suggesting that the blood circulation problems previously reported at 48 hpf (Zhu et al., 2011) are already present by 28 hpf.

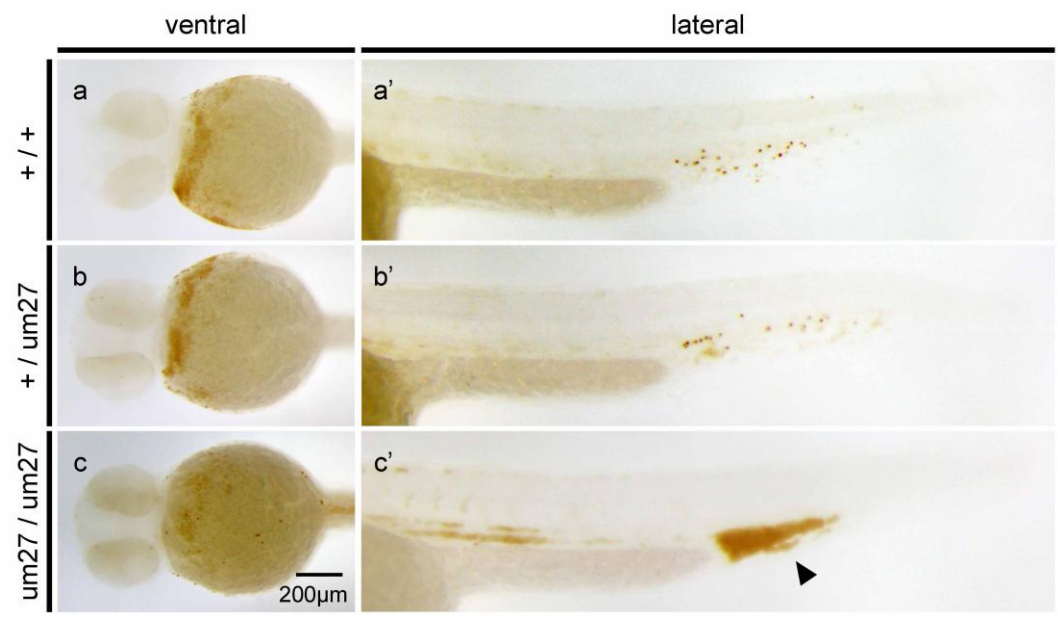

Figure 4.4 | Haemoglobinization of erythroid cells in 28 hpf *gata2a*^{um27} embryos.

o-dianisidine was used to label haemoglobin in erythroid cells of 28 hpf *gata2a*^{um27} embryos. Images of ventral views of the heads **(a-c)** and lateral views of the tails **(a'-c')** of wild type **(a and a')**, heterozygous **(b and b')**, and homozygous mutant **(c and c')** embryos are shown. Notice the accumulation of erythroid cells in the PBI of the homozygous mutant embryo **(c', black arrowhead)**. All embryos are displayed with anterior to the left. Scale bar in **(a-c)**, 200 µm.

4.3.3 Role of Gata2a in myeloid cell development

The first myeloid cells differentiate directly from the haemato-vascular progenitors in the ALPM (Herbomel et al., 1999; Lieschke et al., 2002). It has been shown that these first myeloid cells start expressing *spi1b* transcripts at 6 ss (12 hpf) (Lieschke et al., 2002). Therefore, the expression of *spi1b* was used to label the myeloid cells derived from progenitors in the ALPM in 10 ss (14 hpf) *gata2a*^{um27} mutant embryos (Figure 4.5). Wild type embryos at this stage express *spi1b* in two anterolateral groups of cells in the ALPM (Figure 4.5 a), and both heterozygous *gata2a*$^{+/um27}$ (Figure 4.5 b) and homozygous *gata2a*$^{um27/um27}$ (Figure 4.5 c) mutant embryos

exhibit normal *spi1b* expression pattern, suggesting normal development of primitive myeloid cells at this stage.

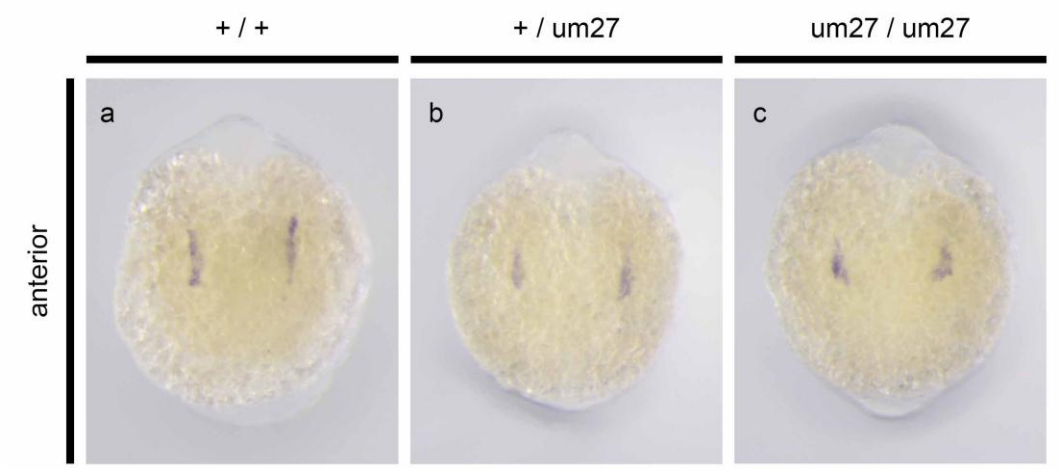

Figure 4.5 | WISH analysis of *spi1b* gene shows normal development of primitive myeloid cells.

Images of *spi1b* WISH on *gata2a*^{um27} mutants at 10 ss **(a, b, and c)** stage. All the images show the anterior part of the embryos with dorsal to the top.

After the differentiation of the first myeloid cells from the ALPM, the two groups of *spi1b*$^{+}$ cells produced (see Figure 4.5 a) coalesce and migrate ventrally scattering on both sides of the surface of the yolk (Lieschke et al., 2002). Figure 4.6 shows the expression of *spi1b* gene in 18 hpf (18ss) *gata2a*^{um27} mutant embryos. In wild type embryos, the expression of *spi1b* is found in two different territories (Lieschke et al., 2002): myeloid cells scattered on the yolk sac (Figure 4.6 a), and in lower levels in the PBI (Figure 4.6 e). Embryos carrying the *gata2a*^{um27} mutant allele show normal expression pattern in cells in both the yolk (Figure 4.6 b and c) and the PBI (Figure 4.6 f and g). The caudal expression of *spi1b* observed in the embryos was variable regardless of their *gata2a* genotype, and it could reflect subtle developmental differences, as it has been shown that the expression of *spi1b* decreases until it is not observable in the PBI by 22 – 24 hpf (Bennett et al., 2001; Lieschke et al., 2002).

The migration of the primitive myeloid cells scatters them and thus allows their quantification. Figure 4.6 d shows the results, the numbers of *spi1b*$^{+}$ cells on the yolk of 18 hpf *gata2a*^{um27} mutant embryos. No statistically significant differences were found (Figure 4.6 and Supplementary Table 9.7), suggesting that the development of primitive myeloid cells is not affected by *gata2a*^{um27} mutation.

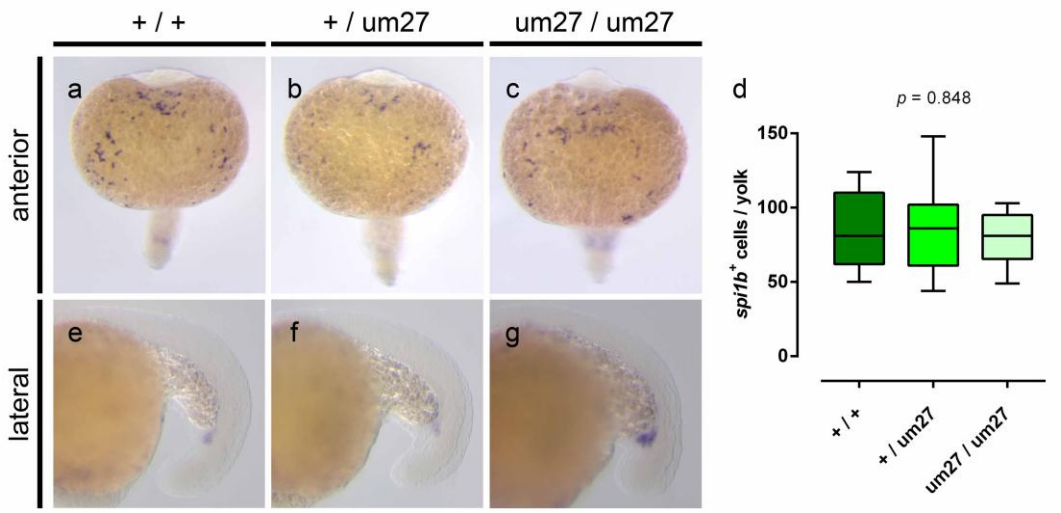

Figure 4.6 | Expression of *spi1b* gene at 18 hpf shows normal numbers of primitive myeloid cells in the yolk.

Images of *spi1b* WISH on *gata2a*^{um27} mutants at 18 hpf **(a-c, and e-g)** stages. Rostral views **(a-c)** and lateral views **(e-g)** of wild type **(a and e)**, heterozygous **(b and f)**, and homozygous mutant **(c and g)** embryos are shown. In **(d)**, quantification of *spi1b*$^{+}$ cells in the yolk of 18 hpf *gata2a*^{um27} mutant embryos. Statistical comparison was carried out by one-way ANOVA. See Supplementary Table 9.7 for more details.

After the 18 hpf stage, the level of expression of *spi1b* decreases both in the cells in the yolk and in the PBI, and only a few labelled cells are visible by 24 hpf (Lieschke et al., 2002). In further experiments, the levels of expression of both *ikaros* and *spi1b* in the PBI in 22 hpf *gata2a*^{um27} embryos (Figure 4.7 a-f) show a great variability with poor correlation with their *gata2a* genotype. Quantifications of *spi1b*$^{+}$ cells were carried out to overcome these difficulties (Figure 4.7 g-j).

Interestingly, despite the variability observed, the total number of *spi1b*$^{+}$ cells in *gata2a*^{um27} mutant embryos is not significantly different from that of their wild type siblings (Figure 4.7 g). No significant differences were found in the numbers of *spi1b*$^{+}$ cells in the yolk, the AGM, or the PBI of *gata2a*^{um27} mutant embryos (Figure 4.7 h-j), suggesting that the total number of myeloid cells and their distribution are not affected in *gata2a*^{um27} mutants.

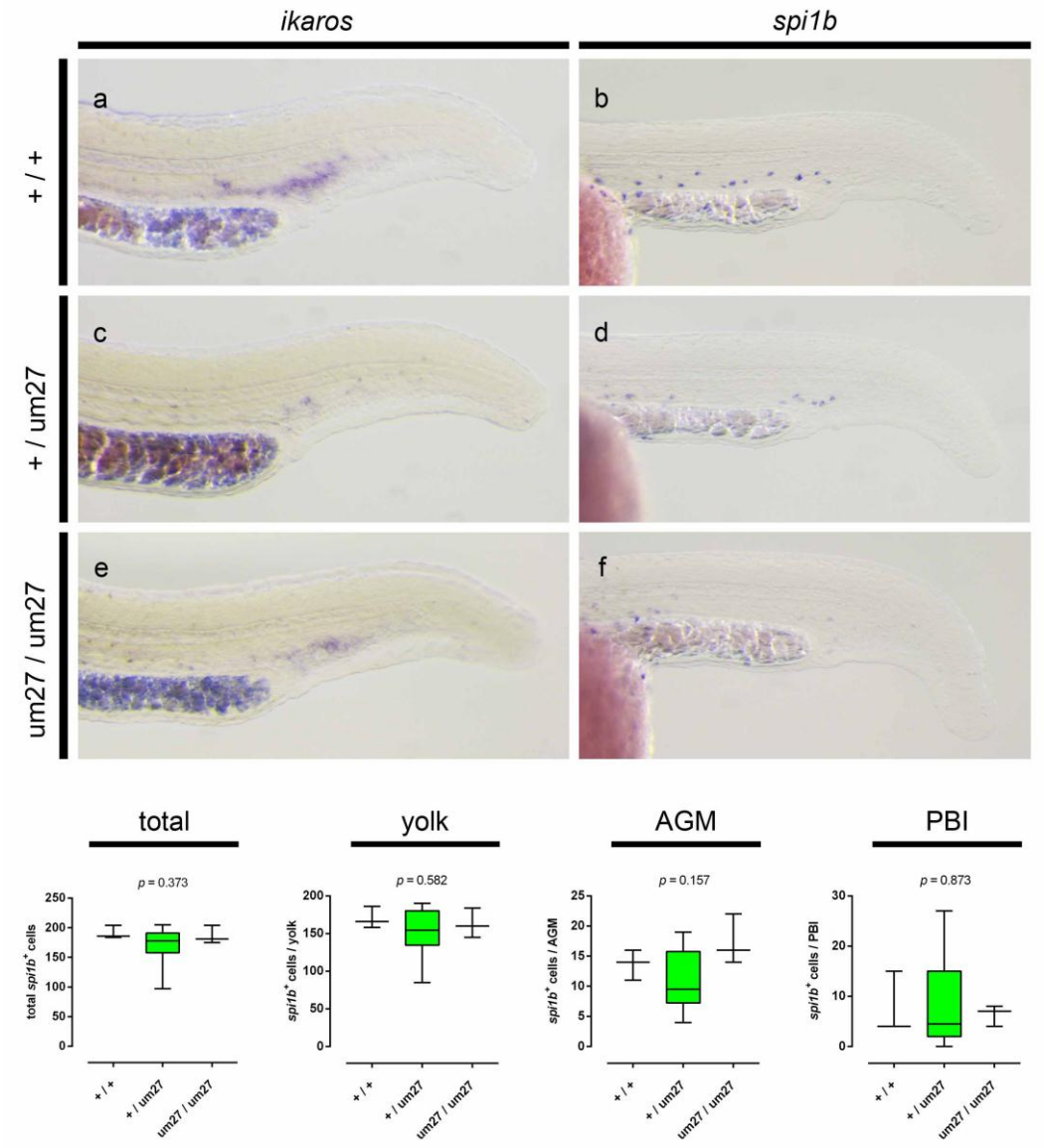

Figure 4.7 | Normal numbers of myeloid cells in the PBI of *gata2a*^{um27} mutant embryos by 22 hpf.

Lateral views of the tails of *ikaros* **(a, c, and e)** and *spi1b* **(b, d, and f)** WISH on *gata2a*^{um27} mutants at 22 hpf stage. Wild type (+ / +) **(a and b)**, heterozygous (+ / um27) **(c and d)**, and homozygous (um27 / um27) **(e and f)** mutant embryos are displayed with anterior to the left. Notice that *ikaros* and *spi1b* expression patterns suggest a decreased amount in myeloid cells in the PBI of the embryos. In **(g-j)**, quantifications of *spi1b*$^{+}$ cells in 22 hpf *gata2a*^{um27} embryos in the entire body **(g)**, the yolk **(h)**, the AGM **(i)**, and the PBI **(j)**. Statistical comparisons in **(g-i)** were carried out by Kruskal-Wallis test, and their

p-values are shown in each graph. See Supplementary Table 9.8 – 9.15 for more details.

Later during development, the expression of the *spi1b* gene appears again in myeloid cells in the PBI (Lieschke et al., 2002), possibly derived from EMPs or HSCs (Bertrand et al., 2007; Murayama et al., 2006). WISH with a *spi1b* probe was carried out in 32 hpf *gata2a*^{um27} embryos, and results are shown in the Figure 4.8. The expression of *spi1b* in the 32 hpf *gata2a*^{um27} mutants suggests a dose dependent decrease in the expression of *spi1b* in cells in the PBI (Figure 4.8 a-c). Notice the decrease in the intensity of staining in the heterozygous embryos displayed in Figure 4.8 b, compared to that of the representative wild type embryo shown in Figure 4.8 a.

The *spi1b*$^{+}$ cells were quantified along the AGM and in the PBI, the results are shown in Figure 4.8 d and Figure 4.8 e. As the images in Figure 4.8 a-c suggest, the quantifications carried out in the AGM show that homozygous *gata2a*$^{um27/um27}$ mutants have a significantly lower number of *spi1b*$^{+}$ cells in their AGM than heterozygous *gata2a*$^{+/um27}$ embryos (*p*-value = 0.015, Figure 4.8 d). The *p*-value for the comparison between wild type *gata2a*$^{+/+}$ embryos and homozygous *gata2a*$^{um27/um27}$ mutant embryos is 0.060 (Supplementary Table 9.12), suggesting that further experiments are necessary to determine whether this difference is a significant difference or not.

In contrast to what the imaging of *spi1b* WISH suggests (Figure 4.8 a-c), quantification of *spi1b*$^{+}$ cells in the PBI of 32 hpf *gata2a*^{um27} mutant embryos shows that there are no significant differences across all genotypes (Figure 4.8 e and Supplementary Table 9.13).

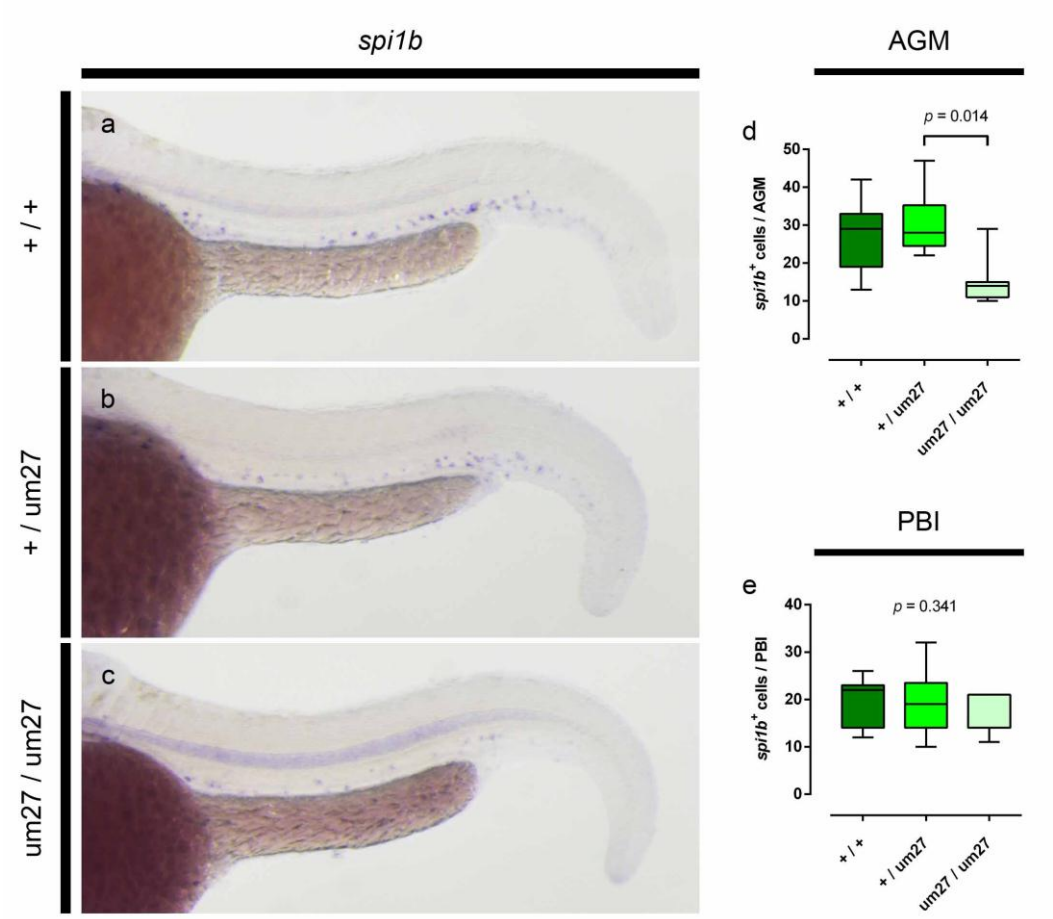

Figure 4.8 | Expression of *spi1b* in 32 hpf *gata2a*^{um27} embryos.

In **(a-c)**, lateral views of the tails of *spi1b* WISH on 32 hpf *gata2a*^{um27} embryos. In **(d)**, quantification of *spi1b*$^{+}$ cells in the AGM region of embryos. In **(e)**, quantification of *spi1b*$^{+}$ cells in the PBI of embryos. Statistical comparisons in **(d and e)** were carried out by Kruskal-Wallis test followed by Dunn's multiple comparison test. See Supplementary Table 9.12 and Supplementary Table 9.13 for more details about **(d)** and **(e)**, respectively.

Previous results suggest that Gata2a has a role in the development of myeloid cells (Figure 4.8). Therefore, the expression of *cebpα* was studied by WISH in *gata2a*^{um27} mutant embryos, given that *cebpα* is a myeloid transcription factor crucial for granulopoiesis (Dai et al., 2016) and that it has been suggested that *Cebpa* is a transcriptional target of *Gata2* (Cooper et al., 2015). In the figure below, images of *cebpα* WISH on 22 hpf *gata2a*^{um27} mutant embryos are shown (Figure

4.9). As previously described (Lyons et al., 2001; Thisse et al., 2001), wild type embryos have *cebpα* expression along the pronephric duct (Figure 4.9 a) and also in a group of cells in the PBI (Figure 4.9 a'), presumably myeloid cells (Dobson et al., 2008). Images of the PBI of *gata2a*^{um27} embryos suggest decreased numbers of *cebpα+* cells in the PBI of both heterozygous and homozygous mutant embryos (Figure 4.9 b' and c'). Cells expressing *cebpα* in the PBI of 22 hpf embryos were quantified, and the results show a dose dependent decrease in the number of labelled cells in heterozygous *gata2a*$^{+/um27}$ and homozygous *gata2a*$^{um27/um27}$ mutant embryos (Figure 4.9 d and Supplementary Table 9.14). These results suggest that Gata2a has a role in the development of these cells or in the control of *cebpα* expression in them.

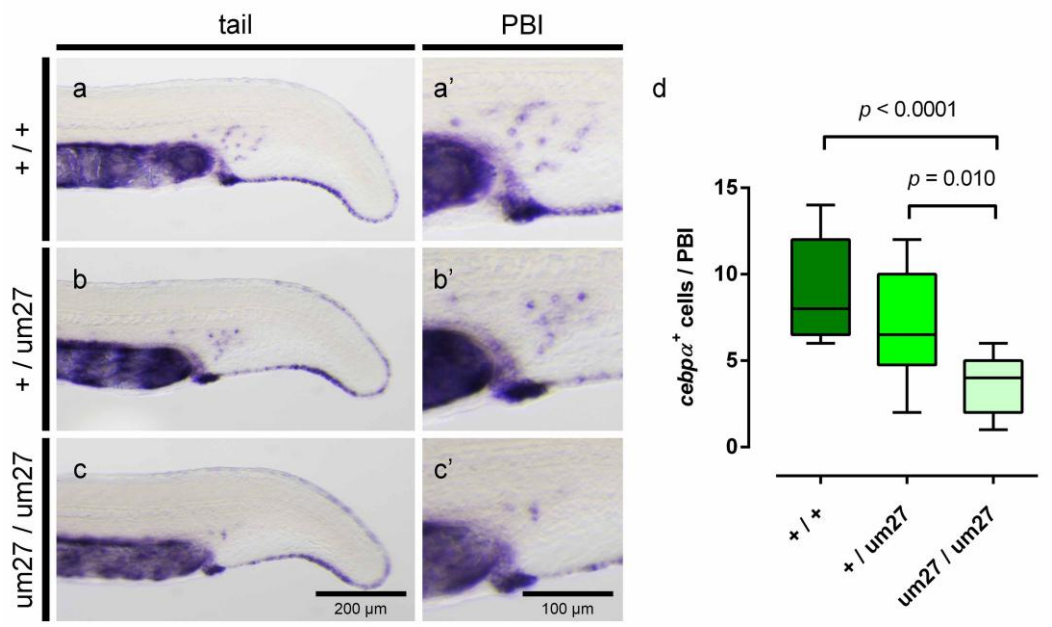

Figure 4.9 | Decreased numbers of *cebpα*$^{+}$ cells in the PBI of 22 hpf *gata2a*^{um27} embryos.

Images of *cebpα* WISH on *gata2a*^{um27} mutants at 22 hpf stage. Lateral views of the tail **(a-c)**, and the PBI **(a'-c')** of the embryos are displayed. In **(d)**, a quantification of *cebpα*$^{+}$ cells in the PBI of 22 hpf *gata2a*^{um27} embryos. Statistical comparison in **(d)** was carried out by one-way ANOVA ($p < 0.0001$) followed by Tukey's multiple comparisons test. See Supplementary Table 9.14 for more details.

The expression of *cebpα* in *gata2a*^{um27} mutant embryos was studied further at earlier developmental stages to determine whether mutations in *gata2a* gene affect *cebpα* expression in the rostral primitive myeloid cells or in the PLPM. The images in Figure 4.10 show *cebpα* WISH in 10 ss *gata2a*^{um27} mutant embryos. At this stage, *cebpα* is expressed in two groups of primitive myeloid cells derived from the ALPM (Figure 4.10 a) and in the PLPM (Figure 4.10 d) (Jing et al., 2013; Thisse et al., 2001). Images of *cebpα* WISH show that both heterozygous *gata2a*$^{+/um27}$ and homozygous *gata2a*$^{um27/um27}$ mutant embryos have normal expression of *cebpα* in both the rostral primitive myeloid cells (Figure 4.10 b and c), and in the PLPM (Figure 4.10 e and f). This suggests that *gata2a*^{um27} mutation has no effect on *cebpα* expression at this developmental stage.

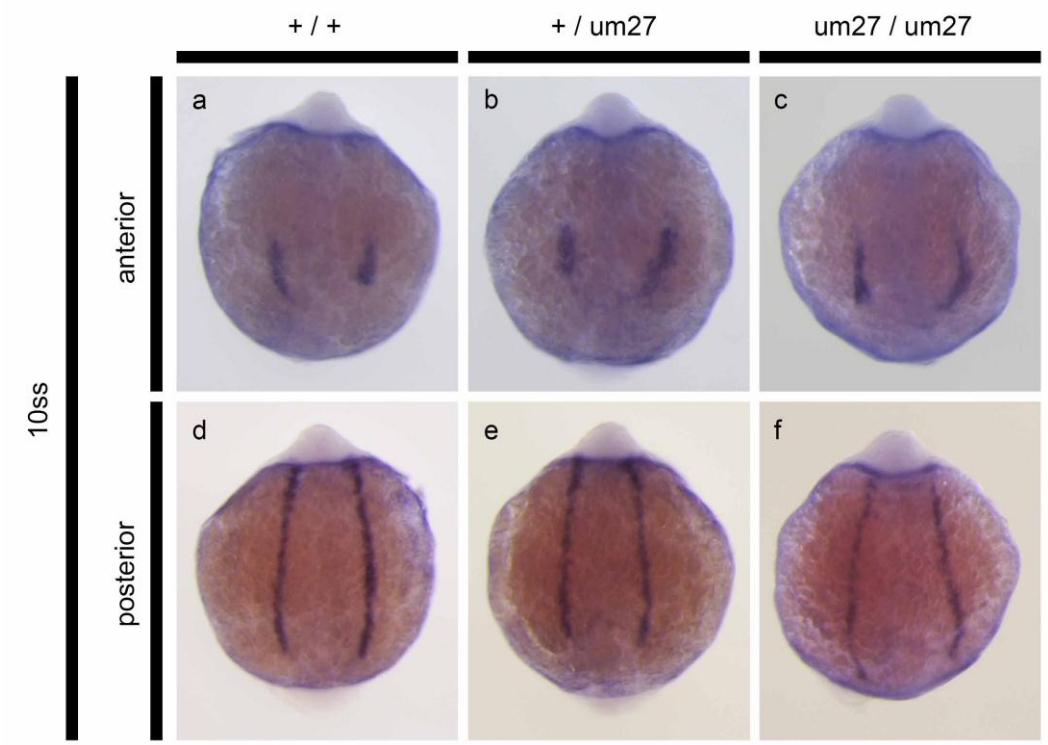

Figure 4.10 | Expression pattern of *cebpα* shows normal development of haemato-vascular progenitors in both ALPM and PLPM of *gata2a*^{um27} mutants.

Images of *cebpα* WISH on *gata2a*^{um27} mutants at 10 ss stage. Dorsal images of anterior **(a-c)** and posterior **(d-f)** part of the embryos are displayed. Images of wild type **(a and d)**, heterozygous mutants (+ /

um27, shown in **(b and e)**, and homozygous mutants (um27 / um27, shown in **(c and f)** are shown.

The study of the expression of *cebpα* in *gata2a*^{um27} was continued in 18 hpf embryos. As mentioned previously, the primitive myeloid cells derived from the ALPM migrate over the yolk sac ventrally, and during this process, they scatter themselves over the yolk (Lieschke et al., 2002). The expression of *cebpα* was analysed by WISH in 18 hpf *gata2a*^{um27} mutant embryos (Figure 4.11), and the *cebpα*$^{+}$ cells in the yolk sac were quantified (Figure 4.11 d). The normal expression of *cebpα,* as that of *spi1b* (Lieschke et al., 2002), includes expression in rostral primitive myeloid cells (Figure 4.11 a) and also caudal expression in the ICM (Figure 4.11 e) (Jing et al., 2013; Thisse et al., 2001). Imaging of *cebpα* WISH in *gata2a*^{um27} mutants shows that both heterozygotes (Figure 4.11 b and f) and homozygotes (Figure 4.11 c and g) for *gata2a*^{um27} mutation have normal *cebpα* expression in both territories. Consistently, the quantification of *cebpα*$^{+}$ cells in the yolk of *gata2a*^{um27} mutant embryos shows no statistically significant differences across genotypes (Figure 4.11 d, and Supplementary Table 9.15), suggesting that *gata2a*^{um27} mutation does not affect rostral primitive myeloid cells and haematopoietic cells in the ICM at this developmental stage. Additionally, this suggests that the phenotype observed in *cebpα*$^{+}$ cells in the PBI of 22 hpf *gata2a*^{um27} mutant embryos (Figure 4.9) arises between this time point, 18 hpf, and 22 hpf, while in the haemato-vascular progenitors labelled at 10 ss no differences were detected (Figure 4.10).

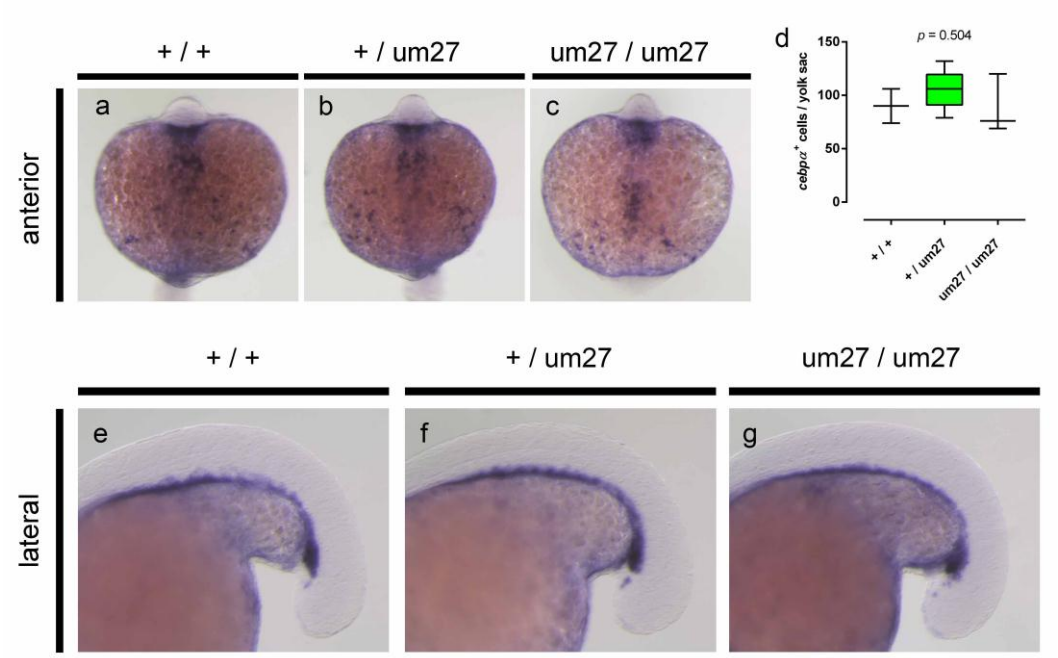

Figure 4.11 | Expression of *cebpα* at 18 hpf shows normal development of primitive myeloid cells and haemato-vascular progenitors in the PLPM of *gata2a*^{um27} mutants.

Images of *cebpα* WISH on *gata2a*^{um27} mutants at 18 hpf stage. Dorsal views of the anterior **(a-c)** part of the embryos are displayed. In **(d)**, a quantification of *cebpα*$^{+}$ cells in the yolk of 18 hpf *gata2a*^{um27} embryos. In **(e-g)**, lateral views of 18 hpf embryos with anterior to the left are shown. Statistical comparison in **(d)** was carried out by Kruskal-Wallis test (p = 0.5044) (see Supplementary Table 9.15 for more details).

The results depicted in Figure 4.9 show that the number of *cebpα*$^{+}$ cells in the PBI at 22 hpf depends on Gata2a. It was hypothesized that these cells correspond to myeloid cells, therefore the expression of the *l-plastin* gene was monitored by WISH in 22 hpf *gata2a*^{um27} mutant embryos. L-plastin, the actin-bundling protein leukocyte plastin, is a cytosolic protein involved in cell motility and its transcripts have been shown to be expressed in early embryonic macrophages at this stage (Herbomel et al., 2001, 1999), both in the macrophages in the yolk sac and in those residing in the PBI. Figure 4.12 shows quantifications of *l-plastin*$^{+}$ cells in 22 hpf *gata2a*^{um27} mutant embryos. Quantifications show that the total number of *l-plastin*$^{+}$ cells is significantly reduced in homozygous *gata2a*$^{um27/um27}$ mutant embryos

compared to that of their heterozygous *gata2a*$^{+/um27}$ siblings (Figure 4.12 a). Similarly, quantifications of *l-plastin*$^{+}$ cells in the yolk show the same results (Figure 4.12 b). Considering that most of *l-plastin*$^{+}$ cells of the embryos at this stage reside in the yolk (86% in the case of heterozygous *gata2a*$^{+/um27}$ embryos and 91% in the wild type embryos, Supplementary Table 9.16 and Supplementary Table 9.17), these results suggest that the rostral primitive macrophages are severely affected by *gata2a*^{um27} mutations. The *l-plastin*$^{+}$ macrophages (Herbomel et al., 1999) were also quantified along the AGM (Figure 4.12 c) and in the PBI (Figure 4.12 d) in *gata2a*^{um27} mutants. In the case of the quantifications carried out in the AGM (Figure 4.12 c), the Kruskal-Wallis test shows that there is at least one group with a significantly different median to the others, however, the *post-hoc* tests do not have enough statistical power to determine which one (Supplementary Table 9.18). Interestingly, the number of *l-plastin*$^{+}$ cells in the PBI of 22 hpf *gata2a*^{um27} shows no significant changes across genotypes (Figure 4.12 d). In contrast to the results found for rostral primitive macrophages, the numbers of macrophages found in the PBI are not affected by *gata2a*^{um27} mutation.

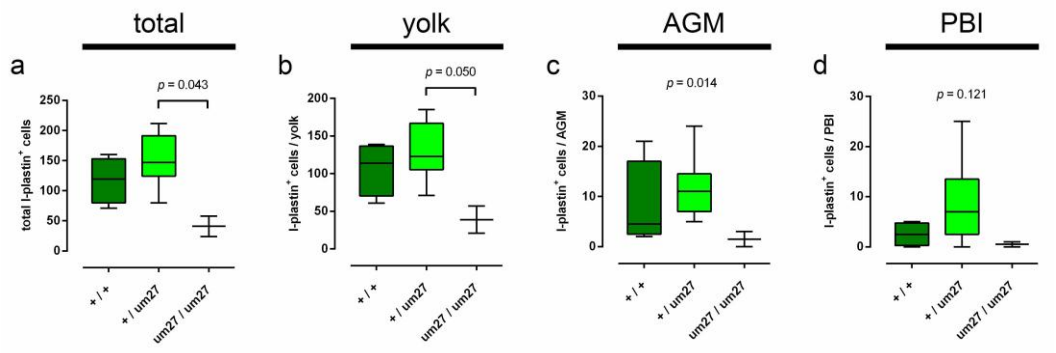

Figure 4.12 | Quantification of *l-plastin*$^{+}$ cells in 22 hpf *gata2a*^{um27} mutant embryos.

Expression of *l-plastin* was analysed by WISH in 22 hpf *gata2a*^{um27} mutant embryos. The number of *l-plastin*$^{+}$ cells was quantified in the entire embryo **(a)**, the yolk **(b)**, AGM **(c)**, and the PBI **(d)**. Statistical comparisons were carried out by Kruskal-Wallis test followed by the Dunn's multiple comparisons test. In **(a and b)**, Kruskal-Wallis test showed significant differences among the medians of the groups (*p*-values 0.017 and 0.030, respectively) so the *p*-values of *post-hoc* tests are shown. In **(c)**, Kruskal-Wallis test shows statistically

significant difference among the groups (*p*-value shown), but the *post-hoc* tests show no significant difference. In **(d)**, medians of the groups showed no statistically significant difference, so *p*-value of the Kruskal-Wallis test is shown instead. See Supplementary Table 9.16 – 9.19 for more details.

In addition to macrophages, the primitive wave haematopoiesis also generates neutrophils. However, experiments using cell-tracing techniques have shown that neutrophils originate from the ventral gastrula, whose cells populate the ICM, in contrast to macrophages, which originate from cells in the dorsal gastrula that populate the RBI (Warga et al., 2009). Zebrafish embryonic neutrophils have been shown to express *mpx,* myeloperoxidase gene (also known as *mpo*, myeloperoxidase), gene (Bennett et al., 2001; Lieschke et al., 2001). The expression of *mpx* is first detectable at 18 ss, as a diffuse labelling in cells in the ICM, and it becomes visible in individual cells by 22 hpf (Bennett et al., 2001). However, peroxidase activity is not detectable by histochemical techniques until 33 hpf (Lieschke et al., 2001). The development of neutrophils was studied by WISH for *mpx*, in 32 hpf *gata2a*^{um27} mutant embryos. As shown previously for *l-plastin* (Figure 4.12) and *spi1b* (Figure 4.7) -positive cells, the number of *mpx*$^{+}$ cells was quantified in the entire embryos, the yolk, AGM, and in the PBI (Figure 4.13).

Figure 4.13 a shows that *gata2a*^{um27} mutant embryos have normal numbers of total *mpx*$^{+}$ cells, neutrophils, in contrast to what has been observed in primitive macrophages (Figure 4.12 a). Similarly, quantifications of *mpx*$^{+}$ neutrophils in the yolk (Figure 4.13 b) and the AGM (Figure 4.13 c) show no statistically significant differences among genotypes. However, it is important to notice that a closer analysis to the quantifications carried out in the yolk (Figure 4.13 b) suggests that it is possible that homozygous *gata2a*$^{um27/um27}$ mutant embryos have significantly more *mpx*$^{+}$ cells in the yolk than their wild type siblings, but further experiments are needed to clarify this point due to low statistical power (see Supplementary Table 9.21). In contrast, quantifications of *mpx*$^{+}$ cells carried out in the PBI of *gata2a*^{um27} mutant embryos show that homozygous *gata2a*$^{um27/um27}$ mutant embryos have a significantly decreased number of neutrophils in the PBI (Figure 4.13 d).

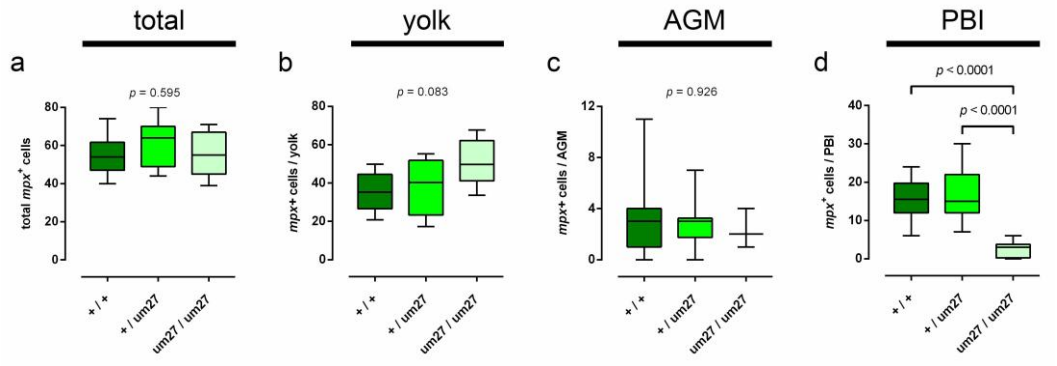

Figure 4.13 | Quantification of *mpx*⁺ cells in 32 hpf *gata2a*^{um27} mutant embryos.

Expression of *mpx* was analysed by WISH in 32 hpf *gata2a*^{um27} mutant embryos. The number of *mpx*⁺ cells was quantified in the entire embryos **(a)**, the yolk **(b)**, AGM **(c)**, and the PBI **(d)**. Statistical comparisons in **(a, b, and c)** were carried out by Kruskal-Wallis test followed by the Dunn's multiple comparisons test, while in **(d)** one-way ANOVA followed by Tukey's multiple comparisons test was used. See Supplementary Table 9.20 – 9.23 for more details.

It has been shown that by 31 hpf, peroxidase activity can be detected in embryonic neutrophils (Lieschke et al., 2001). Later, Sudan Black accumulation in granulocytes has been reported between 33 and 35 hpf (Le Guyader et al., 2008), although Figure 3.8 shows Sudan Black⁺ cells at 24 hpf. Neutrophils were studied in 48 hpf *gata2a*^{um27} mutant embryos by using Sudan Black staining (Figure 4.14). Images of 48 hpf *gata2a*^{um27} mutant embryos stained with Sudan Black are shown in Figure 4.14 a-f. In wild type embryos, some of Sudan Black⁺ neutrophils are scattered in tissue in the head, but not in the brain or retina, (Figure 4.14 a) as previously described (Le Guyader et al., 2008). However, most of neutrophils labelled with Sudan Black reside in the CHT at this stage (Figure 4.14 b). Images of heterozygous *gata2a*$^{+/um27}$ mutant embryos show that they have normal distribution of Sudan Black⁺ neutrophils, both in the head (Figure 4.14 c) and their CHT (Figure 4.14 d). In contrast, while homozygous *gata2a*$^{um27/um27}$ mutant embryos have normal distribution of labelled neutrophils in the head (Figure 4.14 e), their CHT lacks almost entirely of Sudan Black⁺ neutrophils (Figure 4.14 f).

The number of Sudan Black^{+} neutrophils in the CHT of 48 hpf *gata2a*^{um27} mutant embryos was quantified, and the results are shown in Figure 4.14 g. The homozygous *gata2a*$^{um27/um27}$ mutant embryos show severely decreased numbers of labelled neutrophils in the CHT (Figure 4.14 g, and Supplementary Table 9.24), consistently with data shown in Figure 4.13 d.

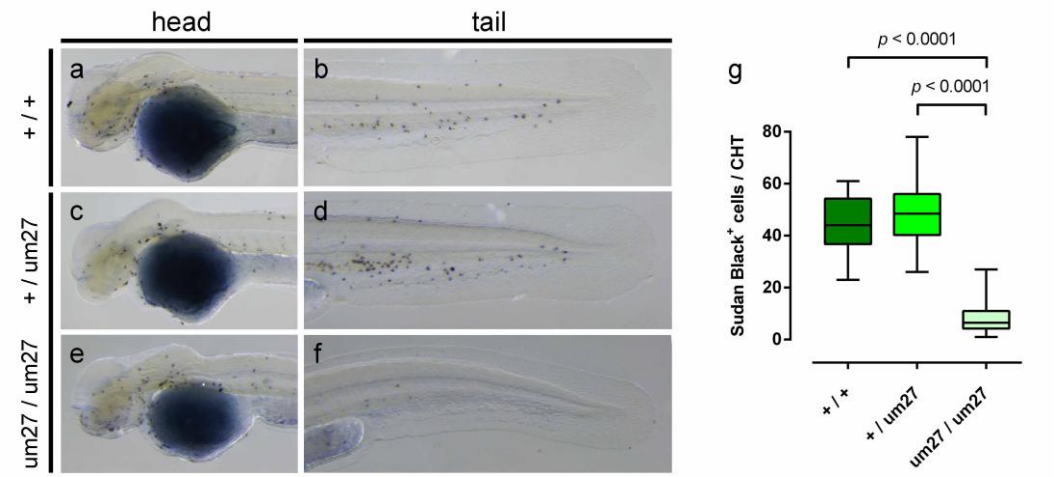

Figure 4.14 | Granulocytes in *gata2a*^{um27} mutant embryos at 48 hpf.

Granulocytes were labelled with Sudan Black in 48 hpf *gata2a*^{um27} embryos. Images of the heads **(a, c, and e)** and the tails **(b, d, and f)** of wild type **(a-b)**, heterozygous mutant **(c-d)**, and homozygous mutant **(e-f)** embryos stained with Sudan Black are shown. **(g)** Quantification of Sudan Black^{+} granulocytes in the CHT of 48 hpf *gata2a*^{um27} embryos. Statistical comparison was carried out by Kruskal-Wallis test ($p < 0.0001$) followed by the Dunn's multiple comparisons test. No statistically significant difference between wild type (+ / +) and heterozygous (+ / um27) embryos was found ($p > 0.999$). See Supplementary Table 9.24 for more details.

4.3.4 Vascular development in *gata2a*^{um27} mutants

The primitive wave of haematopoiesis generates myeloid and erythroid cells (Detrich et al., 1995; Lieschke et al., 2002), and it is followed by a transient wave of definitive haematopoiesis. This wave consists of *lmo2*$^{+}$ *gata1*$^{+}$ double positive

progenitors of erythromyeloid potential residing in the PBI (Bertrand et al., 2007). In a third wave of haematopoiesis, HSCs arise from the ventral wall of the dorsal aorta in the AGM region (Bertrand et al., 2010; Kissa and Herbomel, 2010), enter the blood circulation through the CV (Kissa et al., 2007) and migrate to the CHT (Murayama et al., 2006), where they establish a transient niche of haematopoiesis, that is seen as the teleost equivalent to mammalian foetal liver (Ciau-Uitz et al., 2014). Later in development, HSCs residing in the CHT migrate and seed the definitive haematopoietic organs, both the thymus and the kidney (Murayama et al., 2006).

A previous report shows that by 48 hpf, 94% of homozygous *gata2a*$^{um27/um27}$ mutant embryos display a phenotype of blood circulation in the head but no blood circulation in the trunk, consistent with abnormal gaps observed in the dorsal aorta, labelled by the expression of the *Tg(kdrl:GFP)la116* transgene (Zhu et al., 2011). Consistently, Butko and colleagues report abnormal accumulations of *o*-dianisidine^{+} erythroid cells and also extravascular erythrocytes (labelled by the *Tg(gata1a:dsRed)* expression) in the trunk and the head of 48 hpf homozygous *gata2a*$^{um27/um27}$ mutant embryos (Butko et al., 2015).

These reports are consistent with the results shown in the Figure 4.4, supporting a role for Gata2a in vascular development. Additionally, given that HSCs arise from haemogenic endothelium in the ventral wall of the dorsal aorta (Bertrand et al., 2010; Kissa and Herbomel, 2010), it was hypothesized that definitive haematopoiesis dependent on HSCs is perturbed in *gata2a*^{um27} mutant fish.

To study the time of the onset of the vascular defect in *gata2a*^{um27} mutants, the expression of *kdrl* gene (kinase insert domain receptor like) was studied by WISH in 18 hpf *gata2a*^{um27} mutant embryos. Figure 4.15 shows that the expression of *kdrl* in *gata2a*^{um27} mutants, both heterozygous (Figure 4.15 b) and homozygous (Figure 4.15 c), is indistinguishable from that of their wild type siblings (Figure 4.15 a). These results suggest that vascular development is affected by *gata2a*^{um27} mutation at a later developmental stage.

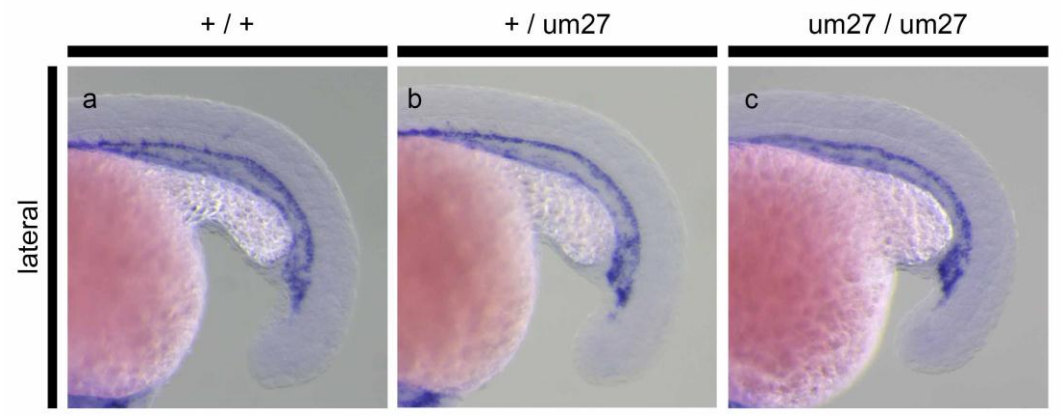

Figure 4.15 | Expression of *kdrl* at 18 hpf shows normal vascular development in *gata2a*^{um27} mutants.

Images of *kdrl* WISH on *gata2a*^{um27} mutants at 18 hpf stage. Lateral views of the tails **(a-c)** of the embryos are displayed with anterior to the left.

In order to define the vascular phenotype observed in homozygous *gata2a*$^{um27/um27}$ mutant embryos, it is relevant to mention that previous research carried out in our laboratory shows delayed development of the intersegmental vessels as early as 24 hpf (Umamahesan, 2014)[1]. At 24 hpf *gata2a*^{um27} mutant embryos carrying the *Tg(kdrl:GFP)la116* transgenic insertion, that expresses GFP in vascular cells, were imaged (Figure 4.16). Imaging of *gata2a*^{um27}*; Tg(kdrl:GFP)* transgenic mutant embryos at 24 hpf (Umamahesan, 2014) showed normal development of vasculature in the tail and the CV plexus in embryos of all genotypes (Figure 4.16 a-i), suggesting that the major blood vessels in the trunk, whose structure is disrupted in homozygous *gata2a*$^{um27/um27}$ mutant embryos by 48 hpf (Zhu et al., 2011), are not affected at the 24 hpf stage.

Additionally, Umamahesan (2014) reports a delayed development of Se vessels in homozygous *gata2a*$^{um27/um27}$ mutant embryos by 24 hpf. Figure 4.16 j shows the number of completely developed Se, those that have elongated dorsally and connected to the dorsal longitudinal anastomotic vessels (DLAV), in each embryo.

[1] Data represented in Figure 4.16 are part of Chianna Umamahesan MSc's work under the supervision of Dr Elspeth Payne at the UCL Cancer Institute, and are reproduced here with permission of the author.

Homozygous *gata2a*$^{um27/um27}$ mutant embryos have a significantly decreased number of completely developed Se vessels, suggesting that *gata2a*^{um27} mutation has an impact on vasculature development as early as 24 hpf, and therefore highlighting the possibility of an effect on the emergence of HSCs and early lymphocytes.

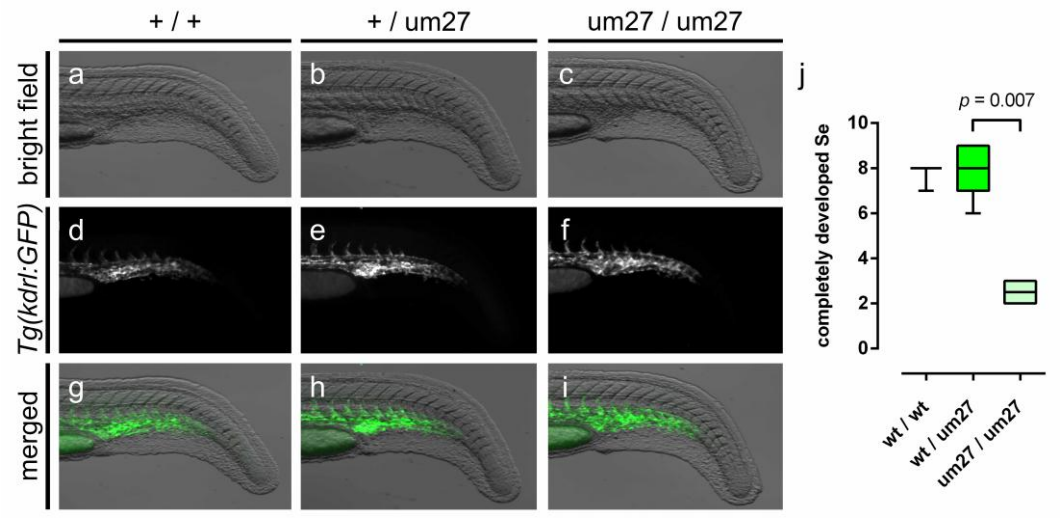

Figure 4.16 | Vasculature in 24 hpf *gata2a*^{um27} mutant embryos expressing the *Tg(kdrl:GFP)* transgene, modified from Umamahesan, 2014.

Imaging of transgenic mutant embryos *gata2a*^{um27}*; Tg(kdrl:GFP)* at 24 hpf **(a-i)**. Laterals views of the tails of wild type **(a, d, and g)**, heterozygous *gata2a*$^{+/um27}$ **(b, e, and h)**, and homozygous *gata2a*$^{um27/um27}$ mutant embryos **(c, f, and i)** are shown in bright field **(a-c)**, and *Tg(kdrl:GFP)* **(d-f)** channels. Additionally, **(g-i)** shows both channels merged. In all images, anterior is shown to the left. In **(j)**, quantification of completely developed Se vessels at 24 hpf. Statistical comparison was carried out by Kruskal-Wallis test ($p < 0.0020$) followed by the Dunn's multiple comparisons test. See Supplementary Table 9.25 for more details. Modified from (Umamahesan, 2014).

Further imaging of *gata2a*^{um27} mutant embryos carrying the *Tg(kdrl:GFP)* transgenic reporter was performed to determine the time window where the first defects in the development of the DA happen in the homozygous *gata2a*$^{um27/um27}$ mutant embryos (Figure 4.17). Heterozygous *gata2a*$^{+/um27}$ adult fish were crossed with *gata2a*$^{+/um27}$*; Tg(kdrl:GFP)*$^{+/-}$ adult fish, and the embryos obtained were screened for GFP expression. Hemizygous *Tg(kdrl:GFP)*$^{+/-}$ embryos were imaged at 30 hpf, and genotyped for *gata2a*^{um27} mutation. Figure 4.17 shows representative embryos of each genotype. Similarly to what was observed in 24 hpf embryos in Figure 4.16 (Umamahesan, 2014), by 30 hpf heterozygous *gata2a*$^{+/um27}$ mutant embryos have a normal development of their vasculature (Figure 4.17 d-f), without noticeable differences from the wild type *gata2a*$^{+/+}$ embryos (Figure 4.17 a-c).

In contrast, homozygous *gata2a*$^{um27/um27}$ mutant embryos exhibit a wide range of phenotypes that combine different defects (Figure 4.17 g-o). At this stage, some homozygotes *gata2a*$^{um27/um27}$ with apparently normal development of the vasculature were found (Figure 4.17 g-i). Figure 4.17 j-l shows a homozygous *gata2a*$^{um27/um27}$ mutant embryo that has pericardial oedema (Figure 4.17 j, arrowhead) together with a severe defect in its antero-posterior axis, that is bent ventrally at a point near the end of the extension of the yolk (Figure 4.17 j, arrow). Fluorescence imaging shows there are absent Se, and a gap in the DLAV around the point where the axis of the embryo is angled (Figure 4.17 k, arrowhead). In Figure 4.17 m-o, another homozygous *gata2a*$^{um27/um27}$ mutant embryo is shown, with pericardial oedema (Figure 4.17 m, arrowhead) and a defect in the tail (Figure 4.17 m, arrow). The tip of the tail of this embryo is ventrally curved, and its caudal fin (Figure 4.17 m) is smaller than in wild type (Figure 4.17 a), and heterozygous (Figure 4.17 d) embryos. In this embryo the CV plexus is abnormally developed (Figure 4.17 n, arrowhead), with dense vasculature and less gaps than the wild type embryos (Figure 4.17 b). All three homozygous *gata2a*$^{um27/um27}$ mutant embryos lacked blood circulation in the trunk and tail.

These results show that the defects in the development of the vasculature reported previously (Zhu et al., 2011), arise between 24 hpf and 30 hpf, concomitantly with the emergence of the first HSCs from the DA (Bertrand et al., 2010; Kissa and Herbomel, 2010).

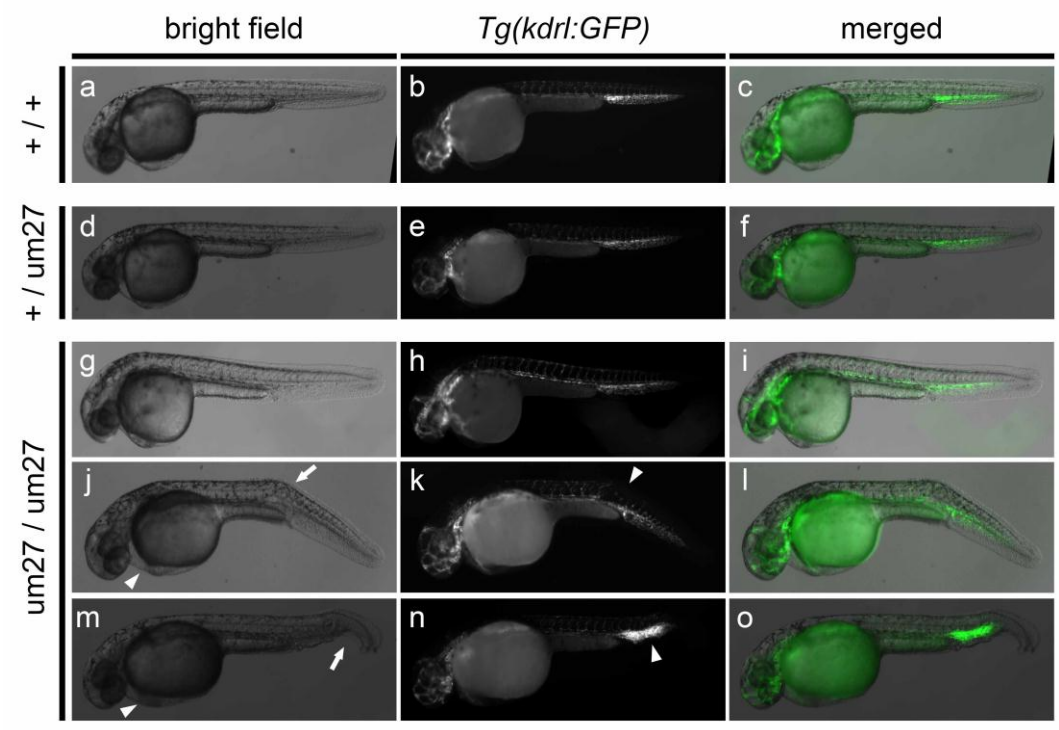

Figure 4.17 | Diverse defects in the development of the vasculature of 30 hpf homozygous *gata2a*$^{um27/um27}$ mutants.

Hemizygous transgenic *Tg(kdrl:GFP)*$^{+/-}$ embryos carrying the *gata2a*^{um27} mutation were obtained by outcross of *gata2a*$^{+/um27}$; *Tg(kdrl:GFP)*$^{+/-}$ and *gata2a*$^{+/um27}$ adult fish. **(a-o)** Imaging of GFP^{+} embryos was carried out at 30 hpf on the bright field **(a, d, g, j, and m)** and the GFP **(b, e, h, k, and n)** channels. In **(c, f, I, l, and o)**, images of bright field and GFP channels merged are shown. Development of vasculature in heterozygous *gata2a*$^{+/um27}$ embryos **(d-f)** shows no differences from that of their wild type siblings **(a-b)**. In contrast, homozygous *gata2a*$^{um27/um27}$ mutant embryos **(g-o)** exhibit different phenotypes, ranging from normal vasculature **(g-i)**, to defective development of the DA and some of the Se in the trunk **(j-l)**, and severe abnormalities in the CV plexus **(m-o)**. See the text for more details.

4.3.5 Onset of definitive haematopoiesis in *gata2a*^{um27} mutants

Inflammatory signalling derived from primitive myeloid cells has been shown to have a role in the emergence of HSCs both in zebrafish and mouse (Espín-Palazón et al., 2014; He et al., 2015; Li et al., 2014; Sawamiphak et al., 2014). Given that the findings presented in section 4.3.3 suggest that *gata2a*^{um27} mutation induces changes in the primitive myeloid compartment, it was hypothesized that abnormal development of myeloid cells in *gata2a*^{um27} mutant embryos may affect the posterior emergence of HSCs.

Quantifications of myeloid cells, and HSCs and progenitors were carried out at different developmental stages in heterozygous *gata2a*$^{+/um27}$ mutant embryos and their wild type siblings in order to determine whether HSCs, and progenitors, emergence is affected in *gata2a*$^{+/um27}$ heterozygotes, and whether this phenotype correlates with an abnormal number of myeloid cells in the CHT (Figure 4.18). The transgenic reporter *Tg(lyz:nfsB-mCherry)* labels myeloid cells, while in the transgenic line *Tg(itga2b:GFP)*, where HSPC express low levels of GFP (GFP^{low}) and thrombocytes express high levels of GFP (GFP^{high}) (Lin et al., 2005). Compound double transgenic *gata2a*^{um27} mutant embryos expressing both *Tg(lyz:nfsB-mCherry)* and *Tg(itga2b:GFP)* transgenes were obtained by outcross, and were kept in individual wells. Fish were imaged at 28 hpf, 52 hpf and 72 hpf (Figure 4.18 a-f). The number of lyz:nfsB-mCherry^{+} cells in the PBI or CHT of each fish was recorded at 28 hpf, 52 hpf and 72 hpf (Figure 4.18 g). Additionally, the number of itga2b:GFP^{low} cells in the CHT was quantified in each larva at 52 hpf and 72 hpf (Figure 4.18 h).

Figure 4.18 a-f shows lateral views of the tails of a heterozygous *gata2a*$^{+/um27}$ mutant larva (Figure 4.18 d-f) and one of its wild type siblings (Figure 4.18 a-c). The images show no major differences between wild type and heterozygous fish, and only a big increase in the number of lyz:nfsB-mCherry^{+} cells is noticeable from 28 hpf to 52 hpf in both wild type and heterozygous fish. Quantification of lyz:nfsB-mCherry^{+} cells in the PBI and CHT of these fish confirms that there is no statistically significant difference between wild type and heterozygous *gata2a*$^{+/um27}$ mutant fish at the developmental stages studied (Figure 4.18 g and Supplementary Table 9.26).

Additionally, the number of itga2b:GFP^{low} cells in the CHT was quantified at 52 hpf and 72 hpf in the same embryos analysed in Figure 4.18 g (Figure 4.18 h). Interestingly, heterozygous *gata2a*$^{+/um27}$ mutant larvae exhibit a decreased number of itga2b:GFP^{low} cells in the CHT at 52 hpf, and later, at 72 hpf, no significant difference is found (Figure 4.18 h and Supplementary Table 9.27).

These results show that Gata2a haploinsufficiency is sufficient to induce a transient decrease in the number of HSCs and progenitors in the CHT without a concomitant decrease in the number of myeloid cells found in the CHT.

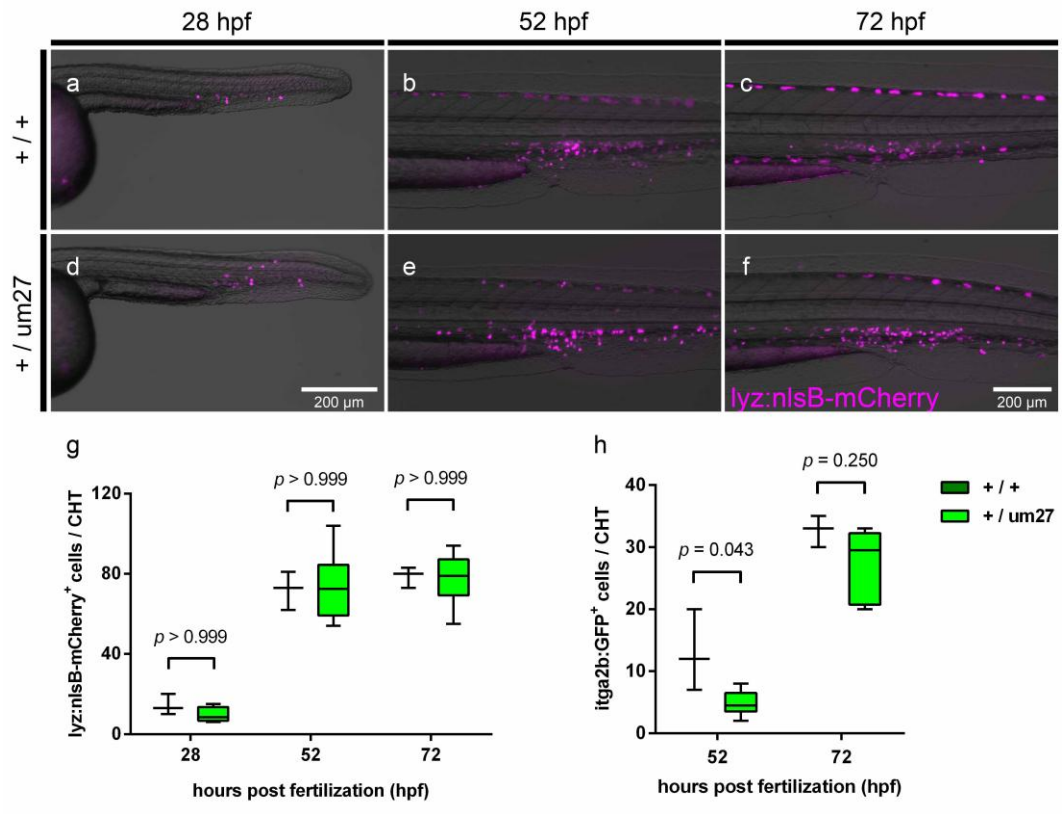

Figure 4.18 | Quantification of lyz:nfsB-mCherry⁺ and itga2b:GFP⁺ cells in the CHT of *gata2a*^{um27} embryos.

Compound transgenic mutant embryos *gata2a*^{um27}*; Tg(lyz:nfsB-mCherry); Tg(itga2b:GFP)* were imaged at 28 hpf **(a and d)**, 52 hpf **(b and e)**, and 72 hpf **(c and f)** stages. In **(a-f)**, lateral views of the tails of wild type **(a-c)** and heterozygous **(d-f)** mutant embryos are shown. *Tg(lyz:nfsB-mCherry)*, displayed in magenta, and bright field channels are shown merged with anterior to the left. Scale bars in **(a and d)**, 200 µm; **(b, c, e, and f)**, 200 µm. In **(g)**, Tg(lyz:nfsB-mCherry)$^{+}$ cells were quantified in the PBI / CHT of a group of *gata2a*^{um27} embryos at 28 hpf, 52 hpf, and 72 hpf. In **(h)**, itga2b:GFP^{low} cells were quantified in the CHT of the same group of *gata2a*^{um27} embryos analysed in **(g)**, at 52 hpf and 72 hpf. Statistical comparisons in **(g and h)** were carried out by repeated measures two-way ANOVA, followed by Bonferroni's multiple comparisons test. See Supplementary Table 9.26 and Supplementary Table 9.27 for more details.

The development of HSCs was studied later during larval development by using 4 dpf *gata2a*^{um27} mutant larvae carrying the *Tg(itga2b:GFP)* transgenic insertion (Lin et al., 2005). Figure 4.19 shows lateral views of the trunks and tails of representative 4 dpf transgenic mutant *gata2a*^{um27}*; Tg(itga2b:GFP)* larvae. In wild type larvae, both labelled thrombocytes (GFP^{high}), and labelled HSCs and progenitors in the CHT (GFP^{low}), can be observed (Figure 4.19 a). Thrombocytes, characterized by the expression of high levels of GFP, are found both in the CHT and in the blood stream, and can be seen in Figure 4.19 a as GFP^{+} lines due to their fast movement. The *Tg(itga2b:GFP)* transgene also drives the expression of GFP to HSCs and progenitors that reside in the CHT, and can be observed in Figure 4.19 a as GFP^{low} cells. Heterozygous *gata2a*$^{+/um27}$ mutant larvae (Figure 4.19 b) exhibit a similar phenotype to that of wild type larvae (Figure 4.19 a), with GFP^{high} cells in the blood circulation and residing in the CHT, in addition to GFP^{low} cells in the CHT.

In contrast, two different phenotypes with similar penetrance were found in homozygous *gata2a*$^{um27/um27}$ mutant larvae (Figure 4.19 c and d). Some of *gata2a*$^{um27/um27}$ mutant larvae (54%) completely lack GFP^{+} cells (Figure 4.19 c), suggesting complete absence of thrombocytes, HSCs and other haematopoietic progenitors. These larvae were later genotyped for the *Tg(itga2b:GFP)* transgene, to confirm that they were transgenic (see section 2.11.5). Interestingly, 46% of homozygous *gata2a*$^{um27/um27}$ mutant larvae have GFP^{high} cells in their blood circulation and GFP^{low} cells residing in the CHT (Figure 4.19 d), although their numbers seem to be lower than that observed in wild type larvae. These results show that emergence of HSCs is not completely impeded in homozygous *gata2a*$^{um27/um27}$ mutant larvae, suggesting the possibility that Gata2a function could be dispensable for HSC emergence, or its lack rescued by a redundant mechanism, such as Gata2b and other GATA factors. Additionally, the known fact that the emergence of HSCs from the haemogenic endothelium depends on blood flow (North et al., 2009), together with the reported lack of blood circulation in the trunk and tail of *gata2a*$^{um27/um27}$ mutant embryos (Zhu et al., 2011), suggest that decreased or absent HSCs could be, at least in part, a secondary consequence of the effect of lack of blood flow on HSCs emergence.

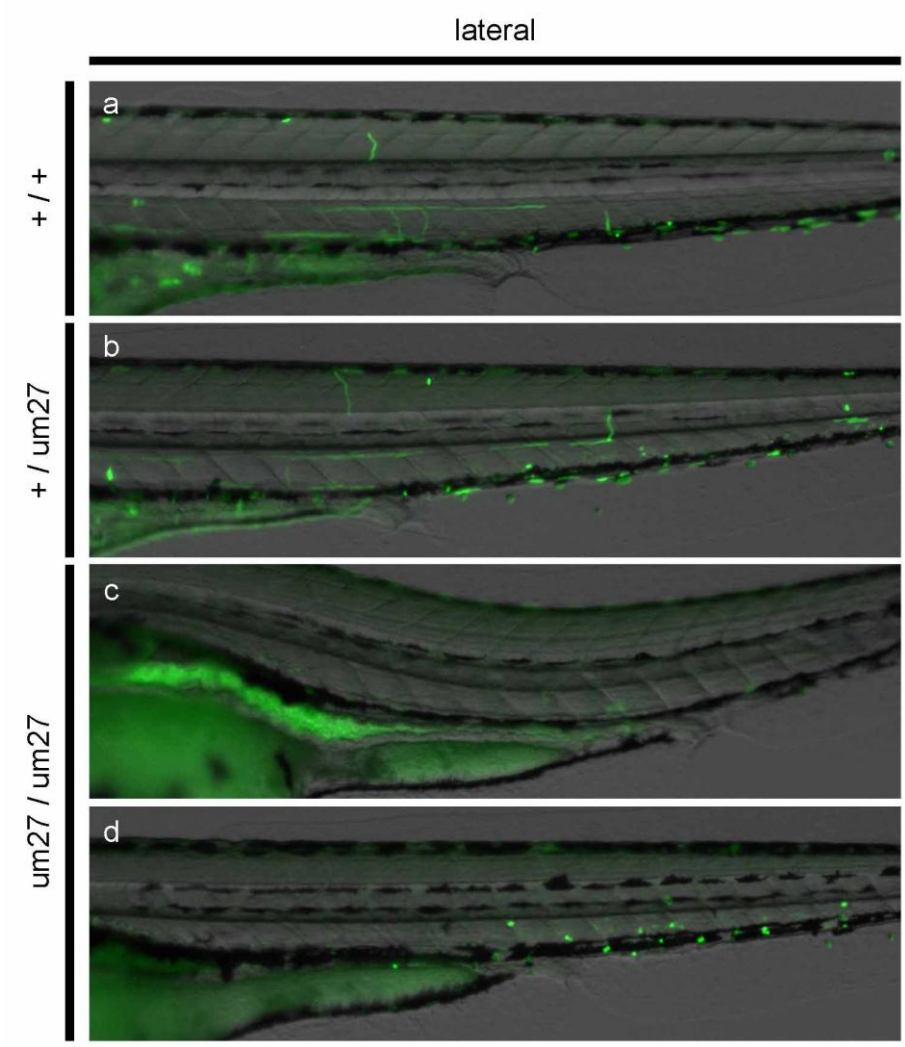

Figure 4.19 | Imaging of 4 dpf *gata2a^{um27}; Tg(itga2b:GFP)* transgenic mutant larvae.

In **(a-d)**, lateral views of the trunk and tail of *gata2a^{um27}* mutant larvae carrying the *Tg(itga2b:GFP)* transgenic insertion, that labels HSCs and progenitors, and thrombocytes (Lin et al., 2005). GFP and bright field channels are shown merged in all images. Representative wild type **(a)**, heterozygous *gata2a$^{+/um27}$* **(b)**, and homozygous *gata2a$^{um27/um27}$* mutant larvae **(c and d)**, are shown. Notice that in the case of homozygous *gata2a$^{um27/um27}$* mutant larvae, two representative images are shown with examples of the two different phenotypes observed in homozygous mutant larvae. All images show anterior to the left and dorsal to the top.

Imaging of homozygous mutant *gata2a*$^{um27/um27}$*; Tg(itga2b:GFP)* larvae at 4 dpf (Figure 4.19 c and d) suggests that the previously reported phenotype of lack of blood circulation in the trunk and tail of *gata2a*$^{um27/um27}$ larvae (Zhu et al., 2011) could affect the emergence of HSCs, as previously shown (North et al., 2009).

In Table 4.6, the presence of blood circulation and the presence of GFP^{+} cells of 4 dpf *gata2a*^{um27}*; Tg(itga2b:GFP)* transgenic mutant larvae were recorded to determine whether there is a correlation between the phenotype of lack of blood circulation and the phenotype of lack of GFP^{+} cells in homozygous mutant *gata2a*$^{um27/um27}$ larvae. Results in Table 4.6 are color-coded to facilitate their reading, so presence of blood circulation or GFP^{+} cells is marked with a + sign, and the cell is coloured green, and absence of blood circulation or GFP^{+} cells is marked with a – sign, and the cell is coloured red.

Table 4.6 shows that all wild type and heterozygous *gata2a*$^{+/um27}$ mutant larvae analysed had blood circulation both in the trunk and the tail, and that they possessed GFP^{+} cells, consistently with results shown in Figure 4.19, a and b. In contrast, homozygous *gata2a*$^{um27/um27}$ mutant larvae exhibit three phenotypes, ranging from apparently normal blood circulation with presence of GFP^{+} cells (Table 4.6, larvae b1, b4, c2, and c3) to complete absence of blood circulation and no GFP^{+} cells found (Table 4.6, larvae b7 and b10). An intermediate phenotype was also observed, where larvae have blood circulation in the trunk and the head, but not in the tail, with complete absence of GFP^{+} cells (Table 4.6, larvae b2 and c5). All those larvae with absent GFP^{+} cells were later genotyped as described in section 2.11.5, and were confirmed to carry the *Tg(itga2b:GFP)* transgenic insertion. Interestingly, there is a complete correlation between the lack of blood circulation in the tail and the absence of GFP^{+} cells, suggesting that the presence or absence of HSCs in homozygous *gata2a*$^{um27/um27}$ mutant larvae is linked to their vascular phenotype. It is important to notice that the penetrance reported for the phenotype of lack of blood circulation in the tail is 94% at 48 hpf (Zhu et al., 2011), however, Table 4.6 shows that only 50% of homozygous *gata2a*$^{um27/um27}$ mutant larvae exhibit this phenotype. Given that the mortality of *gata2a*^{um27} is negligible until 5 dpf (data not shown), these results suggest that some of homozygous mutant larvae acquire blood circulation in the tail later during larval development.

Table 4.6 | Presence of blood circulation and circulating itga2b:GFP^{+} cells in 4 dpf *gata2a^{um27}* larvae.

genotype	embryo	blood circulation			GFP^{+} cells
		anywhere	trunk	tail	
+ / +	b6	+	+	+	+
	c4	+	+	+	+
+ / um27	b3	+	+	+	+
	b8	+	+	+	+
	b9	+	+	+	+
	c1	+	+	+	+
um27 / um27	b1	+	+	+	+
	b2	+	+	-	-
	b4	+	+	+	+
	b7	-	-	-	-
	b10	-	-	-	-
	c2	+	+	+	+
	c3	+	+	+	+
	c5	+	+	-	-

Homozygous *gata2a$^{um27/um27}$* mutant embryos have been shown to have a phenotype of lack of blood circulation (Zhu et al., 2011), however, there is a discrepancy between the reported penetrance of this phenotype at 48 hpf (94%), and the penetrance found by 4 dpf (50%, Table 4.6). These results suggest that some of the homozygous *gata2a$^{um27/um27}$* mutant fish that do not have blood circulation in their tails by 48 hpf, acquire blood circulation later during development.

Figure 4.20 shows the progression of the presence of blood circulation in the tail of a group of *gata2a^{um27}* mutant fish that were checked every day until 5 dpf. For each fish, the presence or absence of blood circulation was recorded every day and the lines in Figure 4.20 represent its progression over time. Data from fish were coloured according to their genotype (see caption of Figure 4.20). The progression of wild type (purple) and heterozygous *gata2a$^{+/um27}$* (blue) mutant fish seem similar: some embryos already display blood circulation in the tail by 1 dpf (24 hpf); by 2 dpf all embryos have blood circulation in the tail; and no changes are observed until 5 dpf.

In contrast, none of homozygous *gata2a$^{um27/um27}$* mutant embryos has blood circulation in the tail by 2 dpf, consistently with a previous report (Zhu et al., 2011).

However, by 3 dpf one larva has blood circulation in the tail, and by 5 dpf, another larva acquires it. It is important to notice that although both fish had blood circulation in their tails, in both the blood flow was interrupted at some point in the dorsal aorta, and the blood continued flowing towards the tail through the Se vessels to the DLAV. In both fish the blood flow reached the CV or the dorsal aorta through another Se, and went back to the heart through the CV.

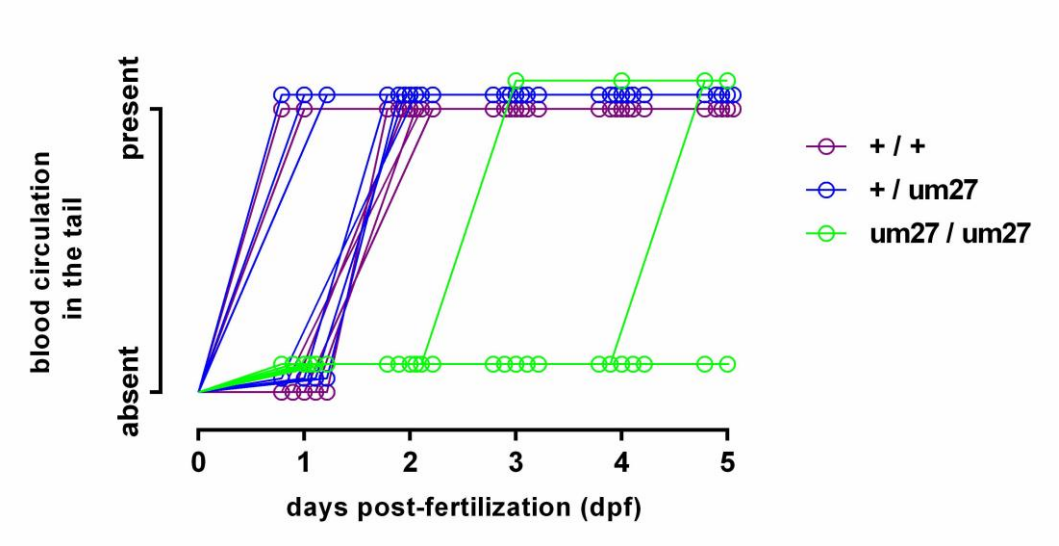

Figure 4.20 | Onset of blood circulation in *gata2a*^{um27} mutant fish.

The presence or absence of blood circulation in the tail of a group of *gata2a*^{um27} mutant fish was recorded each day until 5 dpf. Wild type (+/+) fish are shown in purple, heterozygous *gata2a*$^{+/um27}$ fish are shown in blue, and homozygous *gata2a*$^{um27/um27}$ mutant fish are shown in green.

4.3.6 T-Lymphoid development in *gata2a*^{um27} mutant larvae

The development of lymphoid cells in *gata2a*^{um27} mutant larvae was studied by WISH by using *lck* marker. The expression of *lck* has been reported in zebrafish larvae by 4 dpf in immature T-cells in the thymi (Jones et al., 2015; Ma et al., 2013). Figure 4.21 a-c shows images of *lck* WISH on 4 dpf *gata2a*^{um27} larvae. The ventral views displayed make visible both bilateral thymic lobes. Given that at least three

phenotypes were found, their frequency was recorded, and the results are shown in Figure 4.21 d.

At 4 dpf stage, symmetric *lck* expression in both thymi was found in most of the wild type larvae analysed (75%) (Figure 4.21 a). Heterozygous *gata2a*$^{+/um27}$ mutant larvae show a wide range of phenotypes, ranging from normal *lck* expression in both thymi, comparable to that displayed by wild type embryos (Figure 4.21 a), to a complete absence of *lck* expression in both thymi, as observed in homozygous *gata2a*$^{um27/um27}$ mutant larvae (Figure 4.21 c). In the Figure 4.21 b, the image of a larvae with an intermediate phenotype is shown. These larvae exhibit asymmetric *lck* expression, where one thymic lobe has normal expression of *lck* gene, and the other thymic lobe has decreased or no detectable *lck* expression (Figure 4.21 b). This phenotype was observed in 44% of the heterozygous *gata2a*$^{+/um27}$ mutant larvae analysed (Figure 4.21 d). In the case of homozygous *gata2a*$^{um27/um27}$ mutant larvae, all larvae analysed showed severely decreased *lck* expression in both thymic lobes or no detectable expression of *lck* (Figure 4.21 c).

These results show abnormal T-cell development in *gata2a*^{um27} mutant embryos, and the severity and penetrance of these phenotypes suggest a dose dependent effect of *gata2a*^{um27} mutations in T-lymphoid development. Given that it has been shown that all the T-cells found at this stage are generated by a transient wave of lymphopoiesis, independently of HSCs (Luis et al., 2016; Tian et al., 2017), these results suggest a dose dependent effect of Gata2a on the colonization of thymi by haematopoietic progenitors.

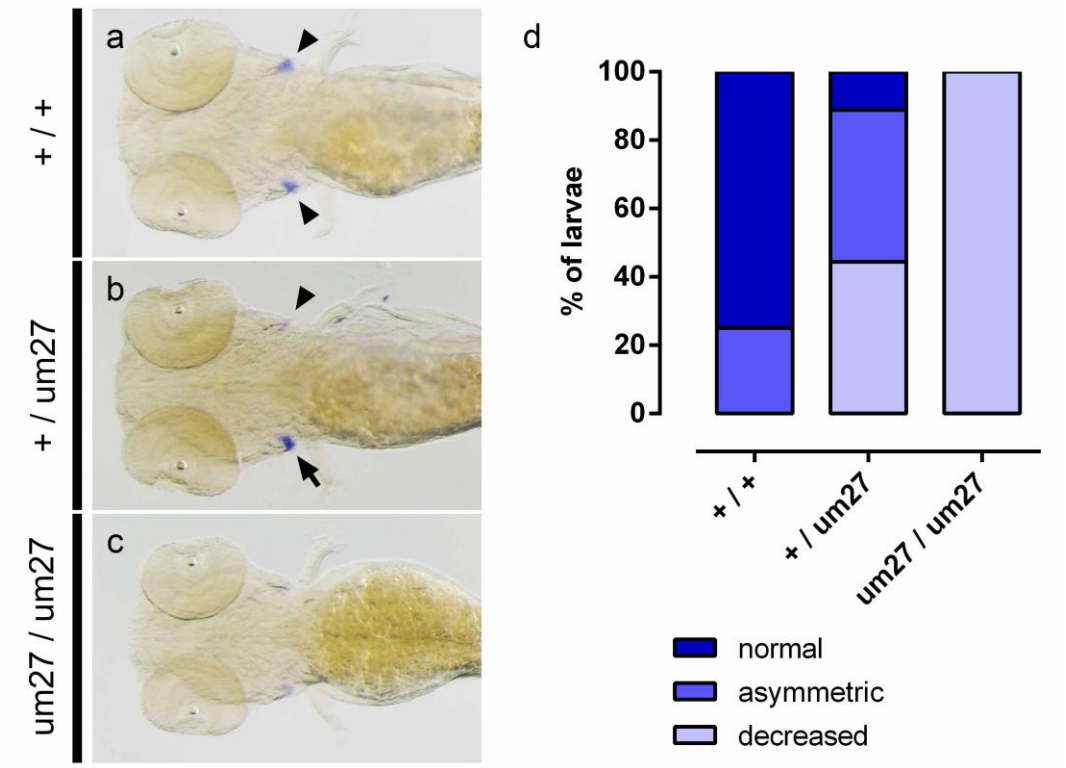

Figure 4.21 | Expression of *lck* in larval thymi shows deficient colonization by haematopoietic progenitors.

Immature T-cells were labelled by *lck* WISH on *gata2a*^{um27} WISH at 4 dpf stage. In **(a-c)**, ventral views of representative larva are shown with anterior to the left. At this stage, *lck* expression is normally found in immature T-cells in both thymi **(a, arrowheads)**. Notice asymmetric labelling in the thymi of heterozygous mutant larvae **(b, arrow and arrowhead)**. Homozygous mutant larvae exhibit severely decreased expression of *lck*, **(c)**. In **(d)**, observed frequency of different phenotypes in *lck* WISH for each genotype.

4.4 Discussion

The Table 4.7 summarizes the main phenotypes of *gata2a*^{um27} mutants shown in the section 4.3, that are discussed in this section.

Table 4.7 | Summary of haematopoietic phenotype of *gata2a*^{um27} mutants.

Lineage	Phenotype observed
Haemato-vascular progenitors	Normal levels of expression of *lmo2* at 10 ss. Normal levels of expression of *runx1* at 10 ss.
HSCs	Transient decrease of *Tg(itga2b:GFP)+* cells in heterozygotes at 52 hpf. Decreased number of *Tg(itga2b:GFP)+* cells in homozygotes at 4 dpf.
Erythroid cells	Normal expression levels of *gata1a* at 18 hpf. Abnormal distribution of *o*-dianisidine+ cells in homozygotes at 28 hpf.
Myeloid cells	Normal expression levels of *spi1b* from 10 ss to 22 hpf. Decreased number of *spi1b+* cells in the PBI of homozygotes at 32 hpf. Normal expression levels of *cebpa* at 10 ss and 18 hpf. Dosis dependent decrease of *cebpa+* cells in the PBI at 22 hpf. Decreased *l-plastin+* cells in the yolk of homozygotes at 32 hpf. Decreased *mpx+* cells in the PBI of homozygotes at 32 hpf. Decreased Sudan Black+ cells in the PBI of homozygotes at 48 hpf.
Lymphoid cells	Asymmetric levels of expression of *lck* in heterozygotes at 4 dpf. Decreased or absent expression of *lck* in homozygotes at 4 dpf.

4.4.1 Primitive erythroid cell development in *gata2a* mutants

In zebrafish, the first primitive erythroid cells differentiate from haemato-vascular progenitors in the PLPM (Detrich et al., 1995; Lieschke et al., 2002). In *gata2a*^{um27} mutant embryos, the establishment of the caudal haemato-vascular progenitors is normal, as shown by the expression pattern of *lmo2* and *runx1* genes at 10 ss (Figure 4.2). At later developmental stages, expression analysis of *gata1a* by WISH and histochemical detection of haemoglobin show that primitive erythroid

cells differentiate normally in homozygous *gata2a*$^{um27/um27}$ mutant embryos (Figure 4.3 and Figure 4.4), in close agreement with findings reported in *gata2a* morphants (Galloway et al., 2005). These results suggest that Gata2a is dispensable for the development of primitive erythroid cells. Consistent with this, Tsai and colleagues carried out *in vivo* experiments that showed that primitive erythroid cells can be found in homozygous *Gata2*$^{-/-}$ knockout mice, however, despite their normal maturation, their number was significantly decreased. Furthermore, wild type chimaeras injected with homozygous *Gata2*$^{-/-}$ knockout cells contained primitive erythrocytes that were homozygous *Gata2*$^{-/-}$ mutant, although in lower numbers than what was expected from their degree of chimerism (Tsai et al., 1994). Similarly, homozygous *Gata2*$^{-/-}$ mutant cells were shown to have erythroid potential *in vitro*, however the numbers of colonies produced were significantly reduced (Tsai et al., 1994; Tsai and Orkin, 1997).

This difference between *Gata2*$^{-/-}$ mice and *gata2a*$^{um27/um27}$ zebrafish suggests the possibility that the effects of the lack of Gata2a activity in primitive erythroid cell development are rescued by a redundant mechanism in zebrafish embryos. Gata2b and Gata1 could be good candidates for that function, given that functional redundancy has been already observed between GATA proteins 1 and 2 during primitive haematopoiesis in mice (Fujiwara et al., 2004). In the case of Gata2a and Gata2b, although their complete sequences have only 57% identity and 67% similarity, closer examination of the sequences encoding the zinc finger domains shows that their N-terminal zinc finger domains have identical aminoacid sequences, and their C-terminal zinc finger domains differ in only 3 out 20aa, supporting the idea of possible functional redundancy between Gata2a and Gata2b (Butko et al., 2015). However, it should be mentioned that there is no available expression data of *gata2b* gene in zebrafish at these stages to provide additional support for this hypothesis.

It could also be hypothesized that during zebrafish embryonic development the observed robustness of primitive haematopoiesis against mutations in transcription factors known to be key for haematopoietic development (Galloway et al., 2005; Tsai et al., 1994), is based on a network of transcription factors that share some degree of functional redundancy (Fujiwara et al., 2004).

4.4.2 A possible role for Gata2a in the differentiation of primitive macrophages from primitive myeloid cells

Primitive myeloid cells are generated from haemato-vascular progenitors in the ALPM through direct differentiation (Herbomel et al., 1999), independently of the primitive erythroid cells, originated from caudal progenitors (Lieschke et al., 2002). The expression patterns of *spi1b* (Figure 4.5) and *cebpα* (Figure 4.10) in 10 ss *gata2a*^{um27} mutant embryos show that the heterozygous and homozygous mutant embryos have normal numbers of primitive myeloid cells. These results suggest that the early differentiation of myeloid cells from haemato-vascular progenitors is not affected by *gata2a*^{um27} mutations.

Differentiation of primitive myeloid cells from progenitors in the ALPM is followed by their ventral migration at both sides of the yolk sac (Herbomel et al., 1999). By 18 ss, the primitive myeloid cells are still migrating on the yolk sac, as shown by the scattered expression of the myeloid markers *spi1b* (Lieschke et al., 2002), *cebpα* and *l-plastin* (Thisse et al., 2001). Expression analysis at this stage showed that *gata2a*^{um27} mutant embryos have normal expression of *spi1b* and *cebpα*, and quantifications showed in both cases that the number of *spi1b*$^{+}$ or *cebpα*$^{+}$ cells in the yolk sac is normal in all *gata2a*^{um27} mutant embryos (Figure 4.6 and Figure 4.11). These results show that *gata2a*^{um27} mutation does not affect the migration of primitive myeloid cells, in contrast to what is observed in homozygous *cebpα* mutant embryos, in which primitive myeloid cells do not migrate and fail to differentiate into macrophages and neutrophils (Dai et al., 2016).

In contrast, at 22 hpf, the development of myeloid cells in both the yolk sac and the PBI is affected in homozygous *gata2a*$^{um27/um27}$ mutant embryos (Figure 4.9 and Figure 4.12). Interestingly, *gata2a*^{um27} mutation seems to affect myeloid cells both in the rostral and in the caudal regions.

In the case of the myeloid cells in the yolk sac, homozygous mutant embryos show decreased numbers of *l-plastin*$^{+}$ cells at 22 hpf (Figure 4.12). The possibility that these differences have been produced by differences in the location of *l-plastin* cells was ruled out by quantifications of labelled cells in the whole embryo and in the AGM and the PBI. While the numbers of *l-plastin*$^{+}$ cells in the AGM and the PBI of homozygous *gata2a*$^{um27/um27}$ mutants are normal, the total number of labelled cells in the whole embryos was significantly reduced (Figure 4.12).

In contrast to *l-plastin*$^{+}$ cells, quantifications of the number of *spi1b*$^{+}$ cells in the yolk sac of *gata2a*^{um27} mutant at this stage show no significant differences (Figure 4.7), suggesting that the number of myeloid cells is not affected in *gata2a*^{um27} mutant embryos. Previous studies show that *l-plastin*$^{+}$ cells correspond to primitive macrophages that start as primitive myeloid progenitors derived from the ALPM expressing *spi1b*, and that as they migrate in the yolk sac mature into primitive macrophages and express *l-plastin* by 18 ss (Bennett et al., 2001; Herbomel et al., 2001, 1999). Other studies have shown that at 22-24 hpf *l-plastin*$^{+}$ cells co-express *csf1r* (macrophage colony-stimulating factor receptor, also known as *c-fms*), a macrophage marker, and that they are ablated in *spi1b* morphants, in contrast to *mpx*$^{+}$ *lyz*$^{+}$ (lysozyme C) neutrophils (Su et al., 2007). All together, these results suggest that primitive myeloid cells develop normally from ALPM progenitors in homozygous *gata2a*$^{um27/um27}$ mutant embryos, but their maturation into macrophages is perturbed. Further analysis of the expression of other macrophage-specific markers, like *csf1r*, and *mpeg1.1* (macrophage expressed 1, tandem duplicate 1), would be necessary to determine whether Gata2a regulates the expression of *l-plastin*, or it has a wider role controlling the maturation of primitive macrophages.

Interestingly, mice lacking L-plastin (also known as leukocyte-plastin, LPL) display a defective response to bacteria, and impaired motility of immune cells (Todd et al., 2011; Wang et al., 2010). Consistent with studies in mice, Kell and colleagues reported that homozygous *l-plastin*$^{-/-}$ mutant zebrafish show increased mortality, particularly during the 4 to 6 weeks after fertilisation (Kell et al., 2018). The authors hypothesize that the lack of L-plastin in the immune cells of mutant fish makes them more sensitive to opportunistic infections, explaining their increased mortality (Kell et al., 2018). Recurrent viral, bacterial and fungal infections are one of the most common manifestations of GATA2 deficiency (Spinner et al., 2014). Thus, the observed reduction in *l-plastin* expression in the primitive macrophages of homozygous *gata2a*$^{um27/um27}$ mutant embryos is interesting for the understanding of human GATA2 deficiency, as it connects zebrafish *gata2a* mutations with a decreased capacity of immune cells to respond to pathogens.

4.4.3 Caudal effects of *gata2a*^{um27} mutation in myeloid cell development

The study of the myeloid cells that develop in the caudal region showed additional abnormalities in *gata2a*^{um27} mutant embryos. Expression analysis of *cebpα* by WISH in 22 hpf embryos showed that *gata2a*^{um27} mutants exhibit a dose dependent decrease in the number of *cebpα*$^{+}$ cells found in the PBI (Figure 4.9). In a similar way to what has been discussed before (see section 4.4.2), quantification of the *spi1b*$^{+}$ cells in the PBI (and AGM) of 22 hpf *gata2a*^{um27} mutant embryos shows no significant differences across genotypes (Figure 4.7), suggesting again that the number of primitive myeloid progenitor cells found in the PBI is not disturbed in *gata2a*^{um27} mutants, but their differentiation into other lineages is affected.

Dobson and colleagues showed in 2008 that mast cells develop in the PBI, and that mast cells can be detected as *cpa5*$^{+}$ (carboxypeptidase A5) cells in the PBI of zebrafish embryos since 24 hpf (Dobson et al., 2008). Importantly, the development of mast cells was shown to be dependent on Gata2a, as *gata2a* morphants lack completely *cpa5*$^{+}$ cells (Dobson et al., 2008); and mast cells were shown to originate first from EMPs, and later, from HSCs (Da'as et al., 2012). The possibility that the *cebpα*$^{+}$ cells affected by *gata2a*^{um27} mutations are mast cells, was ruled out because it has been shown that *cpa5*$^{+}$ mast cells in the PBI do not co-express *cebpα* (Dobson et al., 2008). However, the fact that both *cpa5*$^{+}$ mast cells and *cebpα*$^{+}$ cells arise simultaneously in the same tissue, and that the development of both cell types depends on Gata2a activity, suggests that both mast cells and *cebpα*$^{+}$ cells arise from the same progenitors, the EMPs (Da'as et al., 2012).

The transcription factor CEBPA is a key transcription factor in granulopoiesis in both mice (Arinobu et al., 2005; Zhang et al., 1997) and zebrafish (Dai et al., 2016), which suggests the possibility that the *cebpα*$^{+}$ cells observed in the PBI of 22 hpf embryos (Figure 4.9) could be granulocytes. Consistent with this, at a later developmental stage, 32 hpf homozygous *gata2a*$^{um27/um27}$ mutant embryos exhibit a significant decrease in the number of *mpx*$^{+}$ cells in the PBI (Figure 4.13 d), which is apparently consistent with the results in Figure 4.9. However, quantifications in Figure 4.13 a show that the total number of *mpx*$^{+}$ cells in 32 hpf embryos is not affected by *gata2a*^{um27} mutation, suggesting that the observed decrease in *mpx*$^{+}$

cells is caused by a difference in the distribution of *mpx*$^{+}$ neutrophils in different tissues. Therefore, these results suggest that *cebpα*$^{+}$ cells found in the PBI, whose number depends on Gata2a (Figure 4.9 d), are not neutrophils. It has been shown in mice that two transcription factors, CEBPA and MITF (melanogenesis associated transcription factor), control mast cell and basophil cell fates in an antagonistic fashion by directly repressing each other's expression (Qi et al., 2013). While MITF transcriptional activity induces mast cell fate, CEBPA elicits basophil cell fate (Huang et al., 2016; Qi et al., 2013). The data suggest that the *cebpα*$^{+}$ cells found in the PBI of 22 hpf embryos are granulocytes, and it could be hypothesized that they correspond to basophils.

4.4.4 Gata2a is necessary for the development of the vasculature

The most conspicuous characteristic of homozygous *gata2a*$^{um27/um27}$ mutant embryos is the phenotype of lack of blood circulation in the trunk and the tail, which by 48 hpf is detectable in 94% of the *gata2a*$^{um27/um27}$ embryos (Zhu et al., 2011). Zhu and colleagues report, using transgenic reporter lines, that cranial vessels develop normally in the homozygous *gata2a*$^{um27/um27}$ mutant embryos. Additionally, using quantum dots they showed that lumenization is not affected by *gata2a*^{um27} mutation in these vessels (Zhu et al., 2011). In contrast, they show that lateral dorsal aortae in homozygous *gata2a*$^{um27/um27}$ mutant embryos are more dilated than in their wild type siblings, and the DA is discontinuous at points in the trunk of the embryos, probably causing the observed disruptions in blood circulation in the trunk and the tail (Zhu et al., 2011).

Imaging of *gata2a*$^{um27/um27}$ mutant embryos carrying the *Tg(kdrl:GFP)* transgenic reporter showed that abnormalities in vasculature arise earlier than previously reported (Zhu et al., 2011), as soon as 24 hpf, when a transient delay in the development of Se vessels was found in homozygous *gata2a*$^{um7/um27}$ mutant embryos (Umamahesan, 2014), revealing that Gata2a is required for the development of Se by angiogenesis (Isogai et al., 2001). However, despite this delay, the development of Se in the trunk and the tail proceeds and it is completed in most homozygous *gata2a*$^{um27/um27}$ mutant embryos and in all heterozygotes by 48 hpf, as shown in Figure 4.17. Additional morphological abnormalities in vasculature were found in homozygous *gata2a*$^{um27/um27}$ mutant embryos by 30 hpf,

such as pericardial oedema and a variety of defects in the DA, the Se, and the CV plexus (Figure 4.17). Similarly, *Gata2* knockout mice were reported to exhibit enlarged pericardial sac, and the sections of the heart of E9.5 embryos show normal endothelium (Tsai et al., 1994).

A proportion of patients carrying *GATA2* mutations exhibit chronic lymphedema (Emberger et al., 1979; Ostergaard et al., 2011; Spinner et al., 2014). The development of lymphatic vasculature was not analysed in this study, and no major signs of oedema were found in heterozygous *gata2a*$^{+/um27}$ mutant juvenile or adult fish were found. There is a strong correlation of lymphoedemas with *GATA2* mutations predicted to elicit nonsense-mediated decay of mRNA and with those in the enhancer region of intron 5 (Kazenwadel et al., 2015; Ostergaard et al., 2011; Spinner et al., 2014). Lymphoedema has not been observed in patients carrying *GATA2* missense mutations and in-frame deletions in the C-terminal zinc finger domain that are predicted to result in the production of a stable mRNA product translated into a mutant protein (Spinner et al., 2014).

Together with the morphological defects observed in the DA, Se, and CV plexus of *gata2a*$^{um27/um27}$ mutant embryos (Figure 4.17), it was observed that the blood circulation in the trunk and tail of homozygotes is already interrupted by 30 hpf, and *o*-dianisidine stainings suggest that blood circulation is interrupted even earlier, by 28 hpf (Figure 4.4). Zhu and colleagues hypothesized that, given that all the defects in vascular development found in their study occur after the onset of blood circulation, it is possible that they are caused by a disruption in the mechanisms regulating mechanosensation in the endothelial cells (Zhu et al., 2011).

Previous studies have shown that mechanosensation plays an important role in vascular and lymphatic morphogenesis. Through *in vitro* studies on human cell lines, Mammoto and colleagues showed a link between mechanosensation mechanisms and transcriptional regulation of angiogenesis through GTF2I (general transcription factor IIi, also known as TFII-I) and GATA2 (Mammoto et al., 2009). External mechanical stress has been shown to regulate Rho activity through the regulation of the upstream inhibitor, p190RhoGAP (Rho GTPase activating proteins, also known as ARHGAPs) *in vitro* (Mammoto et al., 2007). p190RhoGAP integrates mechanical stimuli by regulating the balance of two transcription factors with antagonistic effects on angiogenesis, GTF2I and GATA2 (Mammoto et al.,

2009), both capable of regulating VEGFR2 (vascular endothelial growth factor receptor 2) expression (Jackson et al., 2005; Minami et al., 2004, 2001) in response to different levels of stiffness of the extracellular matrix.

As suggested by Zhu and colleagues (Zhu et al., 2011), the results obtained by *in vitro* experiments that link mechanosensation, expression of GATA2, and angiogenesis (Mammoto et al., 2009, 2007), could provide a working hypothesis to explain the vascular phenotype of homozygous *gata2a*$^{um27/um27}$ mutant embryos, based on a defective mechanosensation in endothelial cells. Zhu and colleagues support their hypothesis about mechanosensation by the observation that the vascular phenotypes found in their study occur by 48 hpf (Zhu et al., 2011), after the onset of blood circulation 24 – 26 hpf (Long et al., 1997). Although they do not elaborate and only mention a possible connection between mechanosensation and vascular development, it could be hypothesized that blood circulation provides a mechanical stimulus that acts as a developmental cue for the morphogenesis of vasculature, thus affecting its final architecture. Consistently with this idea, *tnnt2a* (troponin T type 2a) morphants, which do not have blood circulation, exhibit disruptions in DA development (Wang et al., 2011). Similarly, in *klf2a* (Kruppel-like factor 2a) morphants, which also lack blood circulation, defective development of the DA and other blood vessels has also been reported (Nicoli et al., 2010; Wang et al., 2011).

Despite the strong evidence supporting the role of KLF2 in human cell lines (Dekker et al., 2002; Huddleson et al., 2005; Parmar et al., 2006), studies carried out in zebrafish present contradictory evidence. In contrast to the phenotypes reported in *klf2a* morphants (Nicoli et al., 2010; Wang et al., 2011), homozygous *klf2a*$^{sh317/sh317}$ mutant embryos generated by TALEN (transcription activator-like effector nucleases) exhibit normal blood circulation, development of HSCs, and angiogenesis (Novodvorsky et al., 2015). Poor correlation between phenotypes observed in zebrafish morphants and mutants has already been shown in a large screening (Kok et al., 2015). This makes results in *klf2a* morphants (Nicoli et al., 2010; Wang et al., 2011) difficult to interpret, and suggests the presence of genetic compensation mechanisms (El-Brolosy and Stainier, 2017; Rossi et al., 2015).

However, the earliest effects of *gata2a*^{um27} mutation on the development of vasculature can be observed before 48 hpf, by 24 hpf, as decreased expression of the *kdrl* gene in Se in the trunk (Zhu et al., 2011), and delayed formation of Se in

the trunk can be found in homozygous *gata2a*$^{um27/um27}$ mutant embryos (Umamahesan, 2014). These results suggest that the first defects in the development of vasculature in homozygous *gata2a*$^{um27/um27}$ mutant embryos are concomitant with the onset of blood circulation rather than posterior to it. In this case, it could also be hypothesized that Gata2a deficiency disrupts mechanosensation in the endothelial cells, but it could be possible that the mechanical stimulus that endothelial cells fail to sense is not blood circulation, but the stiffness of the extracellular matrix around the endothelial cells, as suggested by *in vitro* studies (Mammoto et al., 2009). In this way, the interruption of the blood circulation could be a secondary consequence of the abnormal morphology of blood vessels, that results from the disruption of mechanosensation. It is worth mentioning that the phenotypes of *tnnt2a* and *klf2a* morphants do not include defective development of Se (Nicoli et al., 2010; Wang et al., 2011), as observed in homozygous *gata2a*$^{um27/um27}$ mutant embryos (Figure 4.16 and Figure 4.17), which suggests that the mere lack of blood circulation, or the lack of sensing of blood circulation, is not sufficient to phenocopy the abnormalities in vasculature's development observed in *gata2a*$^{um27/um27}$ homozygotes.

Finally, it is important to comment on the apparent uncoupling of endothelial differentiation and vascular morphogenesis that different observations in *gata2a*^{um27} mutant embryos suggest. Together with the defects in vascular morphology shown here (Figure 4.17) and in previous studies (Umamahesan, 2014; Zhu et al., 2011), analysis of the expression of diverse artery markers (Zhu et al., 2011) suggests that endothelial differentiation is not affected by Gata2a deficiency. Consistent with this, cells in the DA are able to undergo EHT and to produce HSCs in homozygous *gata2a*$^{um27/um27}$ mutant embryos and larvae (Figure 4.19 and Table 4.6), suggesting that endothelial differentiation and vascular morphology are uncoupled, as hypothesized previously (Zhu et al., 2011).

4.4.5 Emergence of HSC in *gata2a*^{um27} mutant fish

Definitive haematopoiesis is carried out during adulthood by HSCs that reside in the bone marrow of mammals, and in the kidney of teleost fish (Ciau-Uitz et al., 2014; Traver et al., 2003). HSCs emerge from the ventral wall of the haemogenic endothelium of the dorsal aorta through EHT (Bertrand et al., 2010; Kissa and

Herbomel, 2010). After their emergence from the DA, HSCs enter the blood circulation in the CV and eventually seed the CHT, where HSCs carry out a transient wave of haematopoiesis (Kissa et al., 2007; Murayama et al., 2006). Later, some HSCs leave the CHT and seed the kidney, where definitive haematopoiesis proceeds throughout life (Bertrand et al., 2008; Langenau et al., 2004; Murayama et al., 2006).

Given their critical role in definitive haematopoiesis, the numbers of HSCs were studied in *gata2a*^{um27} mutant larvae. Imaging of mutant larvae carrying the transgenic reporter *Tg(itga2b:GFP)* shows a significant decrease in the number of HSCs in the CHT of homozygous *gata2a*$^{um27/um27}$ mutants (Figure 4.19). This is consistent with the reported phenotype of lack of blood circulation in the trunk and tail of *gata2a*$^{um27/um27}$ homozygotes (Zhu et al., 2011), given that blood flow has been shown to affect the emergence of HSCs from the DA (North et al., 2009). These results suggest that homozygous *gata2a*$^{um27/um27}$ mutants are unable to produce HSCs, however, it is important to distinguish between the different possibilities that could explain the role of Gata2a in the emergence of HSCs. One possibility is that Gata2a is directly required for the EHT, as shown for GATA2 in mice (de Pater et al., 2013) and human cells (Huang et al., 2015), or for the survival of HSCs, which has also been shown as another function of GATA2 in mice (de Pater et al., 2013). Another possible explanation is that the emergence of HSCs is merely affected by the lack of blood circulation caused by the vascular defects observed in *gata2a*$^{um27/um27}$ mutants (Zhu et al., 2011).

In this sense, it is important to notice that ~50% of the homozygous *gata2a*$^{um27/um27}$ mutant larvae have itga2b:GFP^{+} cells in the CHT by 4 dpf (Figure 4.19), and also, a similar proportion (~50%) of *gata2a*$^{um27/um27}$ homozygotes have blood circulation in the trunk and tail. Close examination of larvae at 4 dpf shows a strong correlation between the presence of blood circulation, and itga2b:GFP^{+} cells in the CHT of *gata2a*$^{um27/um27}$ mutant larvae (Table 4.6). These results support the idea that the decreased numbers of HSCs in *gata2a*$^{um27/um27}$ homozygous mutants are at least partly a secondary effect of their lack of blood circulation or the delayed start of it.

In contrast to the phenotype observed in homozygous mutants, all the heterozygous *gata2a*$^{+/um27}$ mutant larvae analysed had normal blood circulation in the entire body. It is interesting to note that despite having normal blood circulation, heterozygous *gata2a*$^{+/um27}$ embryos transiently exhibit a significant decrease in the

number of itga2b:GFP^{+} cells in the CHT (Figure 4.18). This defect in the production of HSCs can be observed as soon as 36 hpf (Figure 5.14), as a decrease in the number of *cmyb*$^{+}$ cells along the AGM of heterozygous *gata2a*$^{+/um27}$ embryos. These findings in heterozygous embryos show that Gata2a has a role in the production of HSCs independent of the effects of *gata2a*$^{um27/um27}$ on the development of vasculature. Furthermore, the decrease in the number of *cmyb*$^{+}$ cells in the AGM region strongly suggest that *gata2a* haploinsufficiency results in defective emergence of HSCs from the DA. Thus, it could be hypothesized that Gata2a plays a role in the EHT, as previously shown in mice with conditional *GATA2* mutations (de Pater et al., 2013) and in human *GATA2*$^{-/-}$ embryonic stem cells (Huang et al., 2015).

The fact that the observed decrease in the number of HSCs in heterozygous *gata2a*$^{+/um27}$ embryos is transient, suggests that other redundant mechanisms rescue the phenotype of *gata2a*$^{+/um27}$ heterozygotes. This could explain the observations that show that by 72 hpf, *gata2a*$^{+/um27}$ heterozygous larvae have normal numbers of itga2b:GFP^{+} cells in the CHT. As discussed previously regarding primitive erythroid cell development (section 4.4.1), the high degree of conservation between Gata2a and Gata2b amino acid sequences, and in this case, the expression of *gata2b* in the ventral wall of the DA from 18 ss (Butko et al., 2015), suggest that Gata2b is likely to have this role. This possibility is discussed in detail later, in the section 5.4.4.

4.4.6 Defective lymphopoiesis in *gata2a*^{um27} mutant fish

As discussed earlier, lymphopoiesis is affected in both heterozygous *gata2a*$^{+/um27}$ and homozygous *gata2a*$^{um27/um27}$ mutant larvae, in a dose dependent manner (Figure 4.21). The expression of *lck,* analysed by WISH in 4 dpf larvae, shows that all homozygous *gata2a*$^{um27/um27}$ mutant larvae have significantly decreased numbers of *lck*$^{+}$ lymphocytes, while heterozygotes exhibit a range of phenotypes. Interestingly, 44% of heterozygotes analysed have asymmetric expression of *lck*, suggesting a defective colonization of thymi by haematopoietic progenitors.

The lymphoid cells found in zebrafish larvae at this developmental stage (4 dpf), have been shown to be produced by haematopoietic progenitors that emerge from

the endothelium and enter the blood circulation, independently from HSCs (Tian et al., 2017). These progenitors exit the blood circulation in different points near the head, and migrate towards both developing thymi (Hess and Boehm, 2012; Kissa et al., 2007).

The observed defect in lymphopoiesis is consistent with a decreased haematopoietic potential of endothelial cells as a consequence of *gata2a* haploinsufficiency. It could be hypothesized that *gata2a* deficiency in endothelial cells affects the emergence of haematopoietic progenitors from them, either by decreasing their number, disrupting their function, or both. In keeping with this hypothesis, heterozygous *gata2a*$^{+/um27}$ embryos exhibit transiently decreased numbers of HSCs in the CHT (Figure 4.18).

It is interesting to mention that the wide range of phenotypes observed in heterozygous *gata2a*$^{+/um27}$ larvae, and the apparent stochasticity of the colonization of each thymus, together with the reported normal colonization of thymi in 50% of *silent heart* mutants, that carry a mutation in *tnnt2a* gene (Hess and Boehm, 2012), which lack blood circulation, suggest that normal lymphopoiesis depends on the successful arrival of a critical number of haematopoietic progenitors to both thymi, independently.

The possibility that lack of blood circulation could cause the observed defects in lymphopoiesis was ruled out for two main reasons. First, the penetrance of the lymphoid phenotype and the frequency of defects in blood circulation are not consistent. While none of the heterozygous *gata2a*$^{+/um27}$ embryos analysed lacked blood circulation, defective lymphopoiesis was found in 89% of heterozygotes (Figure 4.21). Conversely, by 4 dpf approximately 50% of homozygous *gata2a*$^{um27/um27}$ larvae lacked blood circulation in the trunk and tail, but 100% of homozygous mutants displayed defective lymphopoiesis. Thus, defects in blood circulation in the tail of *gata2a*^{um27} mutants do not correlate with the penetrance of their defects in lymphoid cell development. An additional argument comes from the reports that show that occlusion of the PHS by laser-mediated ablation of cells, does not delay the colonization of thymus by haematopoietic progenitors (Kissa et al., 2007). Also, it has been shown using *silent heart* mutants, that colonization of the thymus by haematopoietic progenitors occurs even in the absence of blood circulation (Hess and Boehm, 2012).

Similarly to the phenotype found in *gata2a*$^{+/um27}$ mutant larvae, decreased numbers of B (in 86% of patients) and T (in 51% of patients) lymphocytes have been observed in patients carrying *GATA2* mutations (Spinner et al., 2014). However, it has been shown in zebrafish that transient lymphopoiesis, independent from HSCs, is followed by the production of lymphocytes in a HSC-dependent manner (Tian et al., 2017). Therefore, it is likely that the initial defective lymphopoiesis found in heterozygous *gata2a*$^{+/um27}$ mutant fish is only transient and that the posterior production of lymphocytes depends on the presence of HSCs (Tian et al., 2017). On the other hand, the defective lymphopoiesis observed in heterozygous *gata2a*$^{+/um27}$ mutant larvae supports the idea of a role for Gata2a in the differentiation of endothelial cells, also discussed in the section 4.4.4. Based on this, it could be hypothesized that Gata2a heterozygosity causes a defective differentiation in the endothelial cells that disrupts the emergence of the first wave of lymphocyte progenitors, described by Tian and colleagues (2017).

5 Refining a zebrafish model of GATA2 deficiency in humans

5.1 Introduction

5.1.1 Heterozygous *GATA2* mutations underlie different syndromes with haematological manifestations

Heterozygous mutations in the *GATA2* gene have been independently found in patients with different clinical syndromes. Hsu and colleagues identified both somatic and acquired *GATA2* mutations in monoMAC patients (Hsu et al., 2011). Another study identified *GATA2* mutations by exome sequencing in DCML deficiency patients (Dickinson et al., 2011). Later, other studies found *GATA2* mutations in Emberger syndrome patients (Ostergaard et al., 2011) and within cohorts of familial MDS/AML (Hahn et al., 2011).

The spectrum of manifestations was reported by Spinner and colleagues, who examined 57 patients carrying *GATA2* mutations from 40 different families (Spinner et al., 2014). Patients carrying *GATA2* mutations exhibit a wide range of symptoms, including haematological disorders like MDS and AML; viral, fungal and mycobacterial infections; pulmonary abnormalities and ventilatory defects; dermatologic symptoms like warts and panniculitis; and lymphoedemas, among many others (Spinner et al., 2014).

Among the haematological manifestations of *GATA2* mutations reported by Spinner and colleagues, the most frequent are B lymphocytopenia, NK lymphocytopenia, and monocytopenia (Spinner et al., 2014). The authors also reported CD4 lymphocytopenia and neutropenia, which were slightly less frequent and had less severity. Other less frequent haematological abnormalities have been found, like atypical megakaryocytes, hypocellular bone marrow, and some patients also met the criteria for MDS, AML or CMML (Ding et al., 2017; Hahn et al., 2011; Spinner et al., 2014).

5.1.2 Heterozygous *gata2a*$^{+/um27}$ mutation is not sufficient to replicate the symptoms of GATA2 deficiency

The study of haematopoiesis in fish carrying *gata2a*^{um27} mutations showed that Gata2a plays important roles in primitive haematopoiesis, however, the phenotype of heterozygous *gata2a*$^{+/um27}$ mutant fish does not resemble the symptoms observed in GATA2 deficiency patients. Interestingly, Gata2a is necessary for the morphogenesis of vasculature (discussed in section 4.4.4), and current evidence also suggests a role for Gata2a in the differentiation of endothelial cells (discussed in section 4.4.6). It is possible that these vascular phenotypes are related to the defects in lymphatic development observed in murine models of GATA2 deficiency (Lim et al., 2012) and in patients with Emberger syndrome (Emberger et al., 1979; Ostergaard et al., 2011).

The results presented in section 4.3.3 support a role for zebrafish Gata2a in the development of primitive macrophages, and other myeloid lineages. Consistently with these results, it has been shown that Gata2a is required for the development of mast cells from EMPs (Da'as et al., 2012; Dobson et al., 2008). Further experiments show that Gata2a is transiently required for the emergence of HSCs, however, by 72 hpf heterozygous *gata2a*$^{+/um27}$ mutant larvae display normal numbers of haematopoietic progenitors in the CHT (see section 4.3.4), suggesting that *gata2a* heterozygosity is not sufficient to induce long-lasting effects on definitive haematopoiesis. Therefore, it was hypothesized that some of the functions of mammalian GATA2 in definitive haematopoiesis, such as in the survival of HSCs (de Pater et al., 2013), could be carried out by the ohnolog, *gata2b.*

5.1.3 Requirement of *gata2b* mutations to develop a model of GATA2 deficiency in zebrafish

The findings in section 4.3 suggest that Gata2a has only some of all the functions in haematopoiesis found in murine GATA2, and that other functions could be carried out by the *gata2a* ohnolog, *gata2b.* Both *gata2a* and *gata2b* genes share a common ancestor, from which they originated by a genome duplication event (Gillis et al., 2009; Glasauer and Neuhauss, 2014). However, the expression

patterns of *gata2a* and *gata2b* show important differences (Butko et al., 2015). During embryonic development, the transcripts of *gata2a* are found in the PLPM (Brown et al., 2000; Butko et al., 2015; Detrich et al., 1995), neurons in the spinal cord (Andrzejczuk et al., 2018), pituitary gland (Quiroz et al., 2012), and blood vessels (Butko et al., 2015).

In contrast, the expression pattern of *gata2b* is restricted to branchiomotor neurons and the DA (Butko et al., 2015). Further experiments of lineage tracing using a Gal4 transgenic line with a *gata2b* promoter show that *gata2b* expression in the DA labels haemogenic endothelium, which give rise to adult haematopoietic cells during adulthood (Butko et al., 2015). Butko and colleagues (2015) also studied the function of Gata2b in developmental haematopoiesis by using morpholinos targeting *gata2b*. They showed that *gata2b* is required for the specification and emergence of HSCs from the ventral wall of the DA, without any detectable effect on the vasculature (Butko et al., 2015), in contrast to *gata2a* (Zhu et al., 2011).

It has been reported that GATA2 deficiency elicits a wide variety of symptoms that affect many cell types beyond the haematopoietic lineages (Bigley et al., 2011; Emberger et al., 1979; Spinner et al., 2014; Vinh et al., 2010). Current data suggests that while the function of Gata2b is restricted to definitive haematopoiesis (Butko et al., 2015), Gata2a plays different roles in the central nervous system (Andrzejczuk et al., 2018), endocrine signalling (Quiroz et al., 2012), vasculature (Zhu et al., 2011), and haematopoiesis (see section 4). Therefore, it was hypothesized that to develop a zebrafish model of GATA2 deficiency that replicates the symptoms observed in the patients, mutations in both *gata2a* and *gata2b* genes are required in heterozygosity.

5.1.4 Aims of the experiments described in this chapter

1. To generate a stable *gata2b* mutant line in zebrafish.
2. To study the role of Gata2b in developmental haematopoiesis in zebrafish.
3. To assess haematopoiesis in fish carrying mutations in *gata2a* and *gata2b*.

5.2 Methods

5.2.1 Transgenic and mutant zebrafish lines used

The transgenic zebrafish line *Tg(-9.0spi1b:EGFP)zdf11,* published under the name *TG(zpu.1*:*EGFP)*^{df5} (Hsu et al., 2004), was used as a reporter of myeloid cells, and in the text is referred as *Tg(spi1b:EGFP)* for simplicity.

Two zebrafish lines carrying mutations in the *gata2b* gene, *gata2b*^{u5008} and *gata2b*^{delCVN}, were used to study the role of Gata2b in developmental haematopoiesis. The generation of these mutant lines by CRISPR/Cas9 technology is described in detail in the sections 5.2.2, 5.2.3, 5.2.5, and 5.2.6; and the resulting mutant lines are described in detail in the section 5.3.1.

5.2.2 Design of small guide RNAs targeting zebrafish *gata2b* gene

To generate a stable *gata2b* mutant zebrafish line, sgRNAs (small guide RNA) were designed targeting exons 3 and 4 in *gata2b* gene. To find suitable target sites for sgRNAs in zebrafish *gata2b* gene, the web tool CHOPCHOP v2 (http://chopchop.cbu.uib.no/) was used (Labun et al., 2016). The Ensembl identifier of zebrafish *gata2b* gene (ENSDARG00000009094.7) was used as query, and options were adjusted so the 5' ends of the target sites would be GG, and PAM (protospacer adjacent motif) motif "NGG".

From the list of sites obtained, four sites with no predicted off-targets were selected, 3 of them in exon 3, and one targeting exon 4. Table 5.1 shows details about the four sgRNAs selected. The guides were named gata2b_1 to 4, and their target sequences are shown in Table 5.1, with the PAM underlined. The locations of the target sequences are shown in genomic coordinates.

Table 5.1 | sgRNAs targeting *gata2b* gene designed with CHOPCHOP v2.

sgRNA name	target sequence (5' to 3')	genomic location	exon	strand	%GC
gata2b_1	GGCTGACGGTCCATGAGCCGTGG	chr6:40798318	3	-	70
gata2b_2	GGACACATCTTTGGGCGGGGTGG	chr6:40798482	3	-	65
gata2b_3	GGTGAGTTCAGATTTCATAGCGG	chr6:40798754	3	+	40
gata2b_4	GGACGTGAATGTGTAAATTGTGG	chr6:40799561	4	+	40

The location of the sites targeted by the sgRNAs in Table 5.1 are shown in Figure 5.1. sgRNAs gata2b_1, gata2b_1, and gata2b_1 and were design targeting different sites along exon 3 (Figure 5.1 b), and sgRNA gata2b_4 bind the 5' end of exon 4 (Figure 5.1 c).

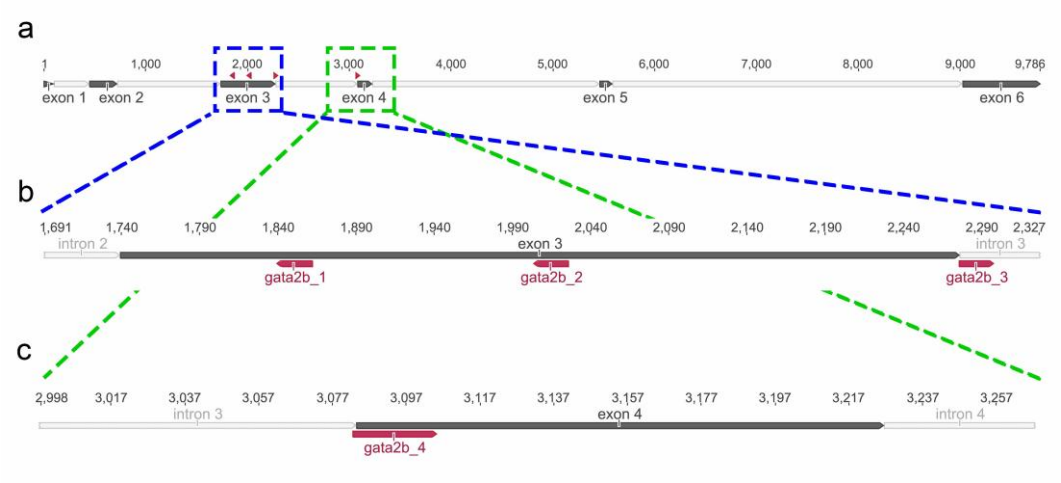

Figure 5.1 | Schematic representation of sites targeted by *gata2b* sgRNAs.

Diagrams in **(a-c)** represent the genomic structure of zebrafish *gata2b* gene, and the sites targeted by sgRNAs in Table 5.1. In all diagrams, exons are depicted as dark grey boxes, introns as light grey boxes, sgRNA binding sites as red rectangles. Numbering of the sequences in **(a-c)** is relative to the first base pair of exon 1. In **(a)**, the sites targeted by sgRNAs in Table 5.1 in the exons 3 and 4 of *gata2b* gene are shown. The region inside the blue box is shown in more detail in **(b)**, and the region in the green box is shown in **(c)**. In **(b)**, the binding sites of sgRNAs gata2b_1, gata2b_2, and gata2b_3

in exon 3 are shown. In **(c)**, the binding site of sgRNA gata2b_4 in exon 4 is shown.

5.2.3 Synthesis of CRISPR small guide RNAs

The synthesis of sgRNAs targeting zebrafish *gata2b* gene was carried out following a previously published cloning-free method (Gagnon et al., 2014). This strategy consists in the generation of a sgDNA, that later is used as a DNA template for an *in vitro* transcription reaction that produces the sgRNAs. The sgDNAs are generated by annealing of a gene-specific oligonucleotide and a constant oligonucleotide to generate ssDNAs (single-stranded DNA) that is then used as template in a T4 DNA polymerase reaction to obtain dsDNA (double-stranded DNA). The gene-specific oligonucleotides used carry the sequence of a DNA-dependent RNA polymerase, followed by the sequence of the binding site (without PAM), and followed by a constant sequence that anneals with the constant oligonucleotide. The constant oligonucleotide encodes the reverse-complement of the tracrRNA (trans-activating crRNA) tail (Gagnon et al., 2014).

In order to synthesize sgRNA targeting the sites in Table 5.1, the four gene-specific oligonucleotides and the constant oligonucleotide were purchased (IDT Technologies), as previously described (Gagnon et al., 2014). The sequences of the oligonucleotides used are shown in Table 5.2. The oligonucleotides used include the sequence of the T7 promoter (5'-TAATACGACTCACTATA-3'). Notice that the gene-specific region of the oligonucleotides (underlined in Table 5.2) does not include the PAM.

Table 5.2 | Gene-specific oligonucleotides used for sgDNA synthesis.

sgRNA name	gene-specific oligonucleotide used for sgDNA synthesis (5' to 3')
gata2b_1	TAATACGACTCACTATAGGCTGACGGTCCATGAGCCGGTTTTAGAGCTAGAAATAGCAAG
gata2b_2	TAATACGACTCACTATAGGACACATCTTTGGGCGGGGGTTTTAGAGCTAGAAATAGCAAG
gata2b_3	TAATACGACTCACTATAGGTGAGTTCAGATTTCATAGGTTTTAGAGCTAGAAATAGCAAG
gata2b_4	TAATACGACTCACTATAGGACGTGAATGTGTAAATTGGTTTTAGAGCTAGAAATAGCAAG

constant oligonucleotide used for sgDNA synthesis (5' to 3')
AAAAGCACCGACTCGGTGCCACTTTTTCAAGTTGATAACGGACTAGCCTTATTTTAACTTGCTATTTCTAGCTCTAAAAC

The oligonucleotides were resuspended in nuclease free water to a final concentration of 100 µM, and then each of the gene-specific oligonucleotides in Table 5.2 was combined with the constant oligonucleotide in the annealing reaction shown in Table 5.3:

Table 5.3 | Components of the annealing reaction.

Reagent	Volume per reaction [µL]	Final concentration
100 µM gene-specific oligonucleotide	1	10 µM
100 µM constant oligonucleotide	1	10 µM
nuclease free water	8	-

The annealing reactions described in Table 5.3 were then cooled down slowly in a thermocycler using the program described in the Table 5.4.

Table 5.4 | Annealing program.

phase	temperature range [°C]	cooling rate [°C/s]	time [s]
initial denaturation	95	-	5 minutes
first cooling phase	95 - 85	-2	5
second cooling phase	85 - 25	-0.1	10 minutes
final extension	4	-	hold

The ssDNA products obtained after the annealing reaction were then used in a T4 DNA polymerase reaction (M0203S, NEB) to get dsDNA that could be used as templates for *in vitro* transcription. All 10 µL of the annealing reaction described in Table 5.3 were used as template for the T4 DNA polymerase. The Table 5.5 shows the volumes and final concentrations of all the components in the reaction, that was incubated at 12 °C for 1 hour in a thermocycler.

Table 5.5 | Components of T4 DNA polymerase reaction.

reagent	Volume per reaction [µL]	Final concentration
10x NEB buffer 2.1	2	1x
10 mM dNTPs	2.5	1.25 mM
100x BSA NEB	0.2	1x
T4 DNA polymerase	0.5	1.5 units
annealed ssDNA	10	variable
nuclease free water	4.8	-

The 100x BSA used has a concentration of 20 mg/mL (B9000S, NEB). The components and concentrations of 10x NEB buffer 2.1 (B7202S, NEB) are shown in Table 5.6.

Table 5.6 | 10x NEB buffer 2.1 composition.

Reagent	Final concentration
Sodium chloride	50 mM
Tris-HCl	10 mM
Magnesium chloride	10 mM
BSA	100 µg/mL
pH 7.9 (at 25 °C)	-

After the T4 DNA polymerase reaction described in Table 5.5, the sgDNAs were purified using MinElute PCR purification kit (28004, QIAgen) following manufacturer's instructions. In the last step, the sgDNAs were eluted in 20 µL of nuclease free water, and their DNA concentrations were measured in a nano spectrophotometer (see Table 5.7).

Table 5.7 | Nano spectrophotometer measurements of sgDNAs.

sgDNA	concentration [ng/µL]	A_{260nm}/A_{280nm}	A_{260nm}/A_{230nm}
gata2b_1	288.14	1.87	2.44
gata2b_2	287.87	1.85	2.26
gata2b_3	238.71	1.87	2.48
gata2b_4	330.46	1.85	2.48

To confirm that the sgDNAs generated had the correct length, each of them was analysed by electrophoresis in 3% w/v agarose gels. In each case, 1 µL of sgDNA or 0.5 µL of the corresponding gene-specific oligonucleotide, was loaded together with 4 µL of 5x loading dye. HyperLadder 50bp (see section 2.10 for details) was used as molecular weight marker. Figure 5.2 shows photographs of the agarose gels. For each sgRNA being synthesized, its corresponding gene-specific oligonucleotide, labelled “oligo” in the images; and its corresponding sgDNA (labelled “sgDNA”) were ran in parallel. The images in Figure 5.2 show a single band near 50 bp in all gene-specific oligonucleotides, in agreement with their length, 60 bp (Table 5.2). In the case of the sgDNAs, a 120 bp was expected, and two bands were found in all of them: one over 100 bp and another one over 200 bp. However, the most intense band was the one near 100 bp in all four sgDNAs, suggesting that the DNA fragments with the correct length were dominant in all cases.

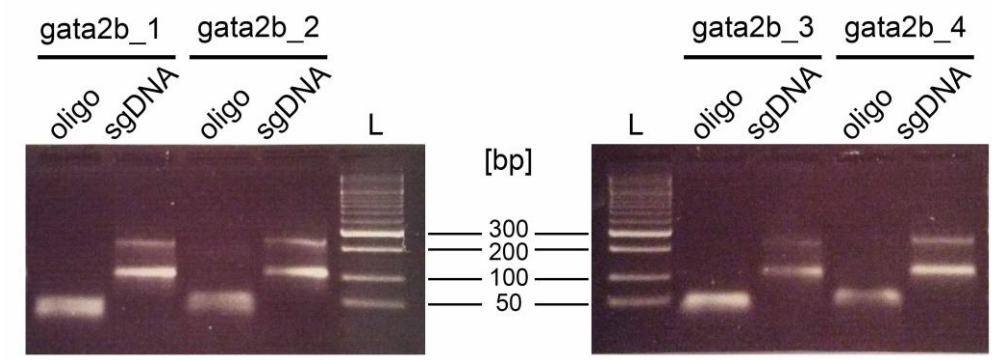

Figure 5.2 | Images of electrophoresis gels showing sgDNAs synthesized to generate sgRNAs targeting zebrafish *gata2b* gene.

Images of electrophoresis gels loaded with purified sgDNAs. The gene-specific oligonucleotide **(oligo)** and the purified sgDNA **(sgDNA)** of each sgRNA being synthesized were ran in parallel. See the text for more details. Expected sizes: all oligonucleotides, 60 bp; all sgDNAs, 120 bp. L, HypperLadder 50bp. The numbers in the column in the centre of the figure show the size in bp of relevant bands of the molecular weight marker.

The sgDNAs obtained were used as DNA template for an *in vitro* transcription reaction. The reaction was carried out using MEGAshortscript T7 transcription kit (AM1354, Ambion) following manufacturer's instructions. The reactions were incubated overnight at 37 °C. Then the DNA template were degraded by incubation with TURBO DNase for 15 minutes at 37 °C according to the manufacturer's instructions. sgRNAs obtained from the *in vitro* transcription were then purified using RNA Clean and Concentration-25 (R1017, Zymo), following the instructions of the manufacturer, with the exception that in the last step the sgRNAs were eluted in 30 µL of nuclease free water (instead of 50 µL). The sgRNAs produced were measured in a nano spectrophotometer, and the results are shown in Table 5.8.

Table 5.8 | Nano spectrophotometer measurements of sgRNAs.

sgRNA	concentration [ng/µL]	A_{260nm}/A_{280nm}	A_{260nm}/A_{230nm}
gata2b_1	1498.19	2.05	2.42
gata2b_2	2281.42	2.08	2.46
gata2b_3	379.49	2.00	2.44
gata2b_4	2364.02	2.14	2.67

The purified sgRNAs for *gata2b* gene were analysed by gel electrophoresis. For each sgRNA, 1 µL of sgRNA was loaded together with 4 µL of gel loader II (AM8546G, Ambion) into a 3% w/v agarose gel. Figure 5.3 shows an image of the electrophoresis gel, where two different bands can be distinguished for sgRNAs 1, 2, and 4. As observed in the gel electrophoresis of sgDNAs in Figure 5.2, the band near 100 bp is the most intense band, for all three sgRNAs. Consistently with the lower concentration of RNA detected by the nano spectrophotometer (see Table 5.8), the sgRNA gata2b_3 was not detected by gel electrophoresis.

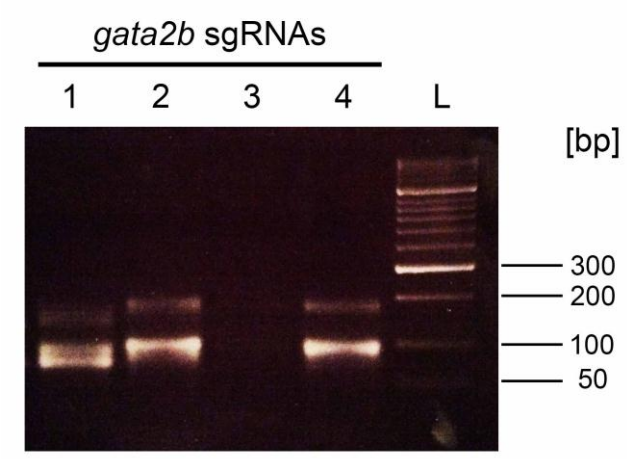

Figure 5.3 | Image of electrophoresis gel showing purified sgRNAs targeting zebrafish *gata2b* gene.

Image of an electrophoresis gel loaded with purified sgRNAs for *gata2b* gene. L, HypperLadder 50bp. The numbers in the column in the centre of the figure show the size in bp of relevant bands of the molecular weight marker.

5.2.4 Synthesis of nCas9n mRNA

nCas9n (NLS-Cas9-NLS) mRNA was synthesized from the pT3TS-nCas9n plasmid, a gift from Wenbiao Chen (Addgene plasmid #46757) (Jao et al., 2013). The full sequence of this plasmid can be found in Plasmid Sequence 9.1 and a map of the plasmid in Plasmid Map 9.1. This plasmid encodes Cas9 flanked by two nuclear localization signals under a T3 promoter in a plasmid encoding resistance to Ampicillin (Jao et al., 2013).

The pT3TS-nCas9n plasmid was transformed into TOP10 chemically competent cells using the One Shot TOP10 kit (C404010, Invitrogen) following the manufacturer's instructions. Lysogeny broth (LB) (Bertani, 1951) was inoculated with two different transformed colonies, and incubated overnight at 37 °C in a shaker. pT3TS-nCas9n plasmid was purified by miniprep, using PureYield Plasmid Miniprep System (A1222, Promega) according to manufacturer's instructions (clones 48 and 49). The plasmid DNA from clone 48 was then linearized using the restriction enzyme XbaI (R0145S, NEB). Four different 50 µL reactions were set up as described in Table 5.9:

Table 5.9 | Reaction mix for pT3TS-nCas9n linearization with XbaI enzyme.

reagent	Volume per reaction [µL]	Final concentration
10x CutSmart buffer	5	1x
XbaI enzyme	1	20 units
pT3TS-nCas9n (clone 48)	2.5 (2 µg)	40 ng/µL
nuclease free water	41.5	-

The digestion reactions were incubated for 2 hours at 37 °C and then 20 minutes at 65 °C to inactivate the restriction enzyme. The linearization was confirmed by gel electrophoresis. For each of 4 restriction digestions carried out, 2.5 µL of the reactions were loaded into a 0.8% w/v agarose gel. Figure 5.4 shows that in all 4 reaction the linearization is complete, with a single band under 8 kb (expected size, 7330 bp).

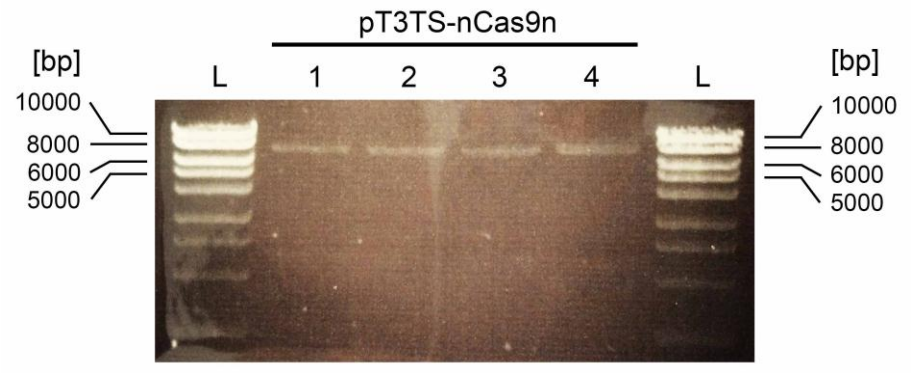

Figure 5.4 | Electrophoresis gel showing linearized pT3TS-nCas9n plasmid.

Image of an electrophoresis gel loaded with pT3TS-nCas9n plasmid digested with XbaI. Lanes 1-4 correspond to the 4 digestions carried out in parallel of pT3TS-nCas9n plasmid. L, HypperLadder 1kb. The numbers in both columns at the sides of the gel show the size in bp of relevant bands of the molecular weight marker.

All four digestions were put together and the linearized pT3TS-nCas9n plasmid was purified using QIAquick nucleotide removal kit (28304, QIAgen) following the manufacturer's instructions, and the obtained purified XbaI-digested pT3TS-nCas9n was measured in a nano spectrophotometer (see Table 5.10):

Table 5.10 | Nano spectrophotometer measurements of XbaI linearized pT3TS-nCas9n plasmid after purification.

	concentration [ng/µL]	**A_{260nm}/A_{280nm}**	**A_{260nm}/A_{230nm}**
XbaI digested pT3TS-nCas9n	161.93	1.82	2.24

Approximately 1 µg of XbaI-digested pT3TS-nCas9n was used as DNA template for an *in vitro* transcription reaction carried out using T3 mMESSAGE mMACHINE kit (AM1348, Ambion), following the manufacturer's instructions. The *in vitro* transcription reaction was incubated 2 hours at 37 °C. The removal of template DNA and the purification of nCas9n mRNA were carried out using RNA Clean and

Concentration-5 (R1015, Zymo) following the instructions of the manufacturer. In the final step, the RNA was eluted with 26 µL of nuclease free water, and the purified mRNA of nCas9n was measured in a nano spectrophotometer (see Table 5.11):

Table 5.11 | Nano spectrophotometer measurements of nCas9n mRNA.

	concentration [ng/µL]	**A_{260nm}/A_{280nm}**	**A_{260nm}/A_{230nm}**
nCas9n mRNA	386.72	2.15	2.40

5.2.5 Microinjection of *gata2b* sgRNAs and nCas9n mRNA into zebrafish embryos

Microinjections of sgRNAs targeting *gata2b* gene (see section 5.2.3) together with nCas9n mRNA (see section 5.2.4) were carried out as described in section 2.6, with changes. The details of the injection mix used for each of the four sgRNAs injected are shown in Table 5.12.

Table 5.12 | Injection mix used for each *gata2b* sgRNA.

gata2b_1 sgRNA injection mix		
reagent	**Volume [µL]**	**Final concentration [ng/µL]**
gata2b_1 sgRNA	1	299.60
nCas9n mRNA	1.36	105.19
phenol red	0.5	10% v/v
nuclease free water	2.14	-

gata2b_2 sgRNA injection mix		
reagent	**Volume [µL]**	**Final concentration [ng/µL]**
gata2b_2 sgRNA	0.5	380.17
nCas9n mRNA	0.5	64.45
phenol red	0.3	10% v/v
nuclease free water	1.7	-

gata2b_3 sgRNA injection mix		
reagent	**Volume [µL]**	**Final concentration [ng/µL]**
gata2b_3 sgRNA	2	252.99
nCas9n mRNA	0.7	90.23
phenol red	0.3	10% v/v

gata2b_4 sgRNA injection mix		
reagent	**Volume [µL]**	**Final concentration [ng/µL]**
gata2b_4 sgRNA	0.5	394.00
nCas9n mRNA	0.5	64.45
phenol red	0.3	10% v/v
nuclease free water	1.7	-

In all cases, injections were carried out directly into the blastodisc of 1-cell stage AB wild type embryos. Immediately after injection, all embryos were screened for phenol red and only positive embryos were kept. The Petri dishes were screened twice a day to remove dead embryos and non-fertilized eggs.

5.2.6 Identification of *gata2b* mutations by NGS[2]

NGS (next-generation sequencing) was used to assess the efficacy of sgRNAs injected into zebrafish embryos, to identify F0 adult fish carrying *gata2b* mutations in their germinal cells, and to determine the mutations carried by heterozygous F1 adult fish, as previously described by (Gagnon et al., 2014).

Regions of genomic DNA around the binding sites of the sgRNAs to zebrafish *gata2b* gene were amplified by PCR, and the amplicons were purified and then sequenced by a massive parallel sequencing method, using an Illumina MiSeq Next-Generation sequencer.

Primers were designed to amplify a region around the binding site of each of the four sgRNAs targeting zebrafish *gata2b* gene. As described in section 2.8, primers were designed using Primer3, to amplify a region of an optimal length of 230 bp. Figure 5.5 shows the binding sites of the MiSeq primers in the genomic sequence of *gata2b* gene. Both forward (dark green boxes) and reverse (light green boxes) primers of each amplicon are shown connected by a green line. When possible, primers were designed so the binding site of the corresponding sgRNA is in the middle of the amplicon, to increase the chances of any occurring mutation to be found by both forward and reverse reads.

[2] PCR primers and PCR conditions were designed and optimized, and then NGS was carried out by technicians in the NGS facility.

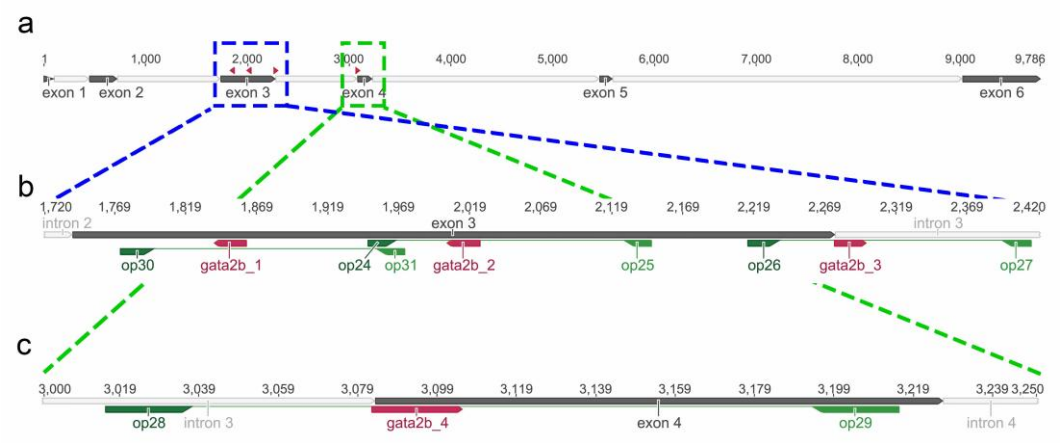

Figure 5.5 | Design of MiSeq PCR products for each sgRNA binding site.

Diagrams in **(a-c)** represent the genomic structure of zebrafish *gata2b* gene, the sites targeted by sgRNAs in Table 5.1, and the PCR products designed for MiSeq. In **(a)**, a diagram of the entire *gata2b* gene shows within boxes the two sites targeted by sgRNAs in Table 5.1, in the exons 3 and 4. The region inside the blue box, corresponding to exon 3, is shown in **(b)**, and the region in the green box, corresponding to exon 4, is shown in **(c)**. In **(b)**, the binding sites of sgRNAs gata2b_1, gata2b_2, and gata2b_3 in exon 3 are shown, together with the binding sites of the primers designed around them for MiSeq (green boxes). In **(c)**, the binding site of sgRNA gata2b_4 in exon 4 is shown flanked by the binding sites of MiSeq primers designed to amplify the region. In all diagrams, exons are depicted as dark grey boxes, introns as light grey boxes, sgRNA binding sites as red rectangles. Binding sites of forward primers are depicted as dark green boxes, and those of reverse primers are shown as light green boxes. The binding sites of forward and reverse primers of each amplicon are connected by a green line. Numbering of the sequences in **(a-c)** is relative to the first base pair of exon 1.

The Table 5.13 shows the sequences of the binding sites in *gata2b* gene of the primers designed for MiSeq.

Table 5.13 | Binding sites of primers designed for MiSeq.

sgRNA	Primer name	Binding site sequence (5' to 3')	Length	%GC	Tm
gata2b_1	op30	CCTTATCAACACTCACGGTCTTCC	24	50.0	61.2
	op31	GTTGCGTCATCGACAGGCAC	20	60.0	62.2
gata2b_2	op24	GATGCCGTGCCTGTCGATGA	20	60.0	62.9
	op25	TTGTCGTTTGCGCCAGATGC	20	55.0	62.5
gata2b_3	op26	CTCCAGAAATCTGCTCGGAAACA	23	47.8	60.9
	op27	TGCGTCTTCTCATGCTTTGCA	21	47.6	61.1
gata2b_4	op28	AGCTGTTTTCTTTACCACCCCC	22	50.0	60.8
	op29	TGGGTCTGATGAGAGGTCTGTT	22	50.0	60.5

The final primers have Illumina Nextera overhangs, that were added to the 5’ end of each sequence in Table 5.13. The sequences of both forward and reverse universal tags are shown in Table 5.14:

Table 5.14 | Sequence of universal tags for MiSeq primers.

Universal tag	Sequence (5' to 3')
Forward	TCGTCGGCAGCGTCAGATGTGTATAAGAGACAG
Reverse	GTCTCGTGGGCTCGGAGATGTGTATAAGAGACAG

The Forward and Reverse universal tag sequences shown in Table 5.14 were added to the 5’ end of forward and reverse binding sequences shown in Table 5.13. The resulting long primers with overhangs are shown in Table 5.15 with binding sites underlined and were used to amplify regions of genomic DNA to be sequenced in search for mutations induced by CRISPR.

Table 5.15 | MiSeq primer names and sequences for each *gata2b* sgRNA.

sgRNA	Primer	Sequence (5' to 3')
gata2b_1	op30	TCGTCGGCAGCGTCAGATGTGTATAAGAGACAGCCTTATCAACACTCACGGTCTTCC
	op31	GTCTCGTGGGCTCGGAGATGTGTATAAGAGACAGGTTGCGTCATCGACAGGCAC
gata2b_2	op24	TCGTCGGCAGCGTCAGATGTGTATAAGAGACAGGATGCCGTGCCTGTCGATGA
	op25	GTCTCGTGGGCTCGGAGATGTGTATAAGAGACAGTTGTCGTTTGCGCCAGATGC
gata2b_3	op26	TCGTCGGCAGCGTCAGATGTGTATAAGAGACAGCTCCAGAAATCTGCTCGGAAACA
	op27	GTCTCGTGGGCTCGGAGATGTGTATAAGAGACAGTGCGTCTTCTCATGCTTTGCA
gata2b_4	op28	TCGTCGGCAGCGTCAGATGTGTATAAGAGACAGAGCTGTTTTCTTTACCACCCCC
	op29	GTCTCGTGGGCTCGGAGATGTGTATAAGAGACAGTGGGTCTGATGAGAGGTCTGTT

The designed MiSeq primers, shown in Table 5.15, were checked for the possibility that they could form secondary structures or homodimers and heterodimers, using the web tool (http://eu.idtdna.com/calc/analyzer).

The primers shown in Table 5.15 were used to amplify the genomic regions in *gata2b* gene surrounding the binding sites of the sgRNAs designed (see diagrams in Figure 5.5). A DNA polymerase of high fidelity, 50 times higher than standard *Taq* polymerases, was used: Phusion High-Fidelity DNA polymerase (M0530S, NEB). The components and concentrations of the PCR to generate amplicons for MiSeq is shown in the Table 5.16.

Table 5.16 | Components of PCR for MiSeq.

reagent	Volume per reaction [µL]	Final concentration
5x Phusion HF buffer (B0518S, NEB)	5	1x
10 mM dNTPs	0.5	200 µM
10 µM forward primer	0.5	0.2 µM
10 µM reverse primer	0.5	0.2 µM
Phusion High-Fidelity DNA polymerase	0.25	0.5 units
genomic DNA	2	variable
nuclease free water	16.25	-

The Table 5.17 shows the cycling program used for this PCR:

Table 5.17 | Cycling conditions used in PCR for MiSeq PCR.

Phase		temperature [°C]	time [s]
initial denaturation		98	30
34 cycles	denaturation	98	10
	annealing	variable (see Table 5.18)	10
	extension	72	15
final extension		72	5 minutes

The annealing temperatures for each pair of MiSeq primers in Table 5.15 were determined by gradient PCR, and are shown in Table 5.18:

Table 5.18 | Annealing temperatures of each pair of primers for MiSeq PCR.

sgRNA	primers	Annealing temperature used
gata2b_1	op30 op31	65 °C
gata2b_2	op24 op25	68 °C
gata2b_3	op26 op27	65 °C
gata2b_4	op28 op29	64 °C

The results of the MiSeq PCRs were analysed by gel electrophoresis, to check for the presence of a single amplicon of an expected size of 267 bp. The entire volume of each MiSeq PCR was run in a 2% w/v agarose gel, and the band with the PCR product of the expected size was cut out of the gel and purified using the QIAquick gel extraction kit (28704, QIAgen) following the manufacturer's instructions. The DNA concentration of the purified PCR products was measured in a nano spectrophotometer and dilutions to 15 – 20 ng/µL were made when necessary.

The purified PCR products for MiSeq were submitted for sequencing by the UCL zebrafish sequencing consortium using MiSeq, and the results were analysed using the software Geneious, version 7.1.9 (http://www.geneious.com) (Kearse et al., 2012). Using Geneious software, the MiSeq reads from each amplicon were mapped to the wild type *gata2b* gene sequence to identify fish carrying mutations.

5.2.7 Extraction of gamete cells from adult fish

Once F0 fish reached adulthood (~ 2 months), gamete cells were extracted from them to identify those adult fish that carried mutations in their germinal cells. Then, genomic DNA was extracted from these cells as described in section 2.11.4, and used as template for MiSeq PCR (see details in section 5.2.6), and analysed using Geneious to identify those F0 fish carrying mutations in their germinal cells, that were then used as parents for a F1 generation.

In the case of female adults, one fish was anesthetized by transfer into a small breeding box with 0.08 g/L 3-aminobenzoate methanesulfonate. After a period of 1 to 2 minutes, the fish was taken from the box with anaesthesia and placed on a piece of parafilm, lying on its side. The oocytes were extracted from the fish by carefully pressing the abdomen of the fish from anterior to posterior repeated times. The eggs expelled through the cloaca were collected and placed in a PCR tube. After the procedure, the fish were put back into a tank without anaesthesia for recovery.

In the case of male adults, fish were anesthetized one by one in the same way it was done with the female fish. Once a fish was anesthetized, it was placed on a parafilm under a dissecting stereoscope, lying on its dorsal side. Then, with the end of a glass capillary, a steady but soft pressure is exerted on the area immediately posterior to the cloaca on the ventral side of the fish. The gametes enter by capillarity into the glass capillary. Once the gamete cells were collected, the fish was put back in a tank without anaesthesia for its recovery, and the gamete cells are put into a PCR tube by blowing air through the other end of the capillary with a micropipette.

After the procedure of collection of gamete cells, each fish was assigned an identifier and was put in a separate compartment of a 24-compartment tank (DC-96, R&D Aquatics).

5.2.8 Genotyping of *gata2b*^{u5008} mutant fish

The *gata2b*^{u5008} zebrafish mutant line was used in most of the experiments shown in this chapter and was one of the *gata2b* mutant lines generated by CRISPR/Cas9 technology. The *gata2b*^{u5008} mutant fish carry the mutation ENSDARG00000009094.7:g.2011_2014del: a 4 bp deletion in exon 3, causing a frameshift that encodes a premature stop codon (see section 5.3.1 for more details). The strategy developed to genotype *gata2b*^{u5008} mutant fish was a method based on PCR amplification and restriction digest of the amplicons, similar to that used to genotype *gata2a*^{um27} mutants (see section 4.2.2). The protocol starts with the amplification by PCR of a 398 bp DNA fragment of the exon 3 of *gata2b* gene containing the region of the 4 bp deletion. The PCR product was then digested with FauI enzyme, and the digestion pattern was analysed by gel electrophoresis. Wild type PCR products are cut, generating 2 fragments (289 bp and 112 bp), and mutant PCR products are not cut, as the 4 bp deletion removes the FauI restriction site, leaving one DNA fragment (395 bp).

Genomic DNA obtained from cells and gametes (section 2.11.4), embryos and larvae (section 2.11.3), or fin clips from adult fish (see section 2.11.2) was used as a template for a PCR with the primers shown in the Table 5.19:

Table 5.19 | Primers used for genotyping of *gata2b*^{u5008} mutants.

Primer name	Sequence (5' to 3')	Length	%GC	Tm
op44	TTTTTGCCAGCACGCCTTAC	20	50	60.0
op45	GGGTTGCTACGGATTGGACT	20	55	59.7

The Table 5.20 shows the components and concentrations of the PCR for *gata2b*^{u5008} genotyping. The volumes shown are calculated for one 25 µL reaction and were scaled up for large numbers of samples. Details about dNTPs, the DNA polymerase used, and its reaction buffer are available in section 2.7.

Table 5.20 | Components of PCR for *gata2b*^{u5008} genotyping.

Reagent	Volume per reaction [µL]	Final concentration
10x Standard Taq buffer	2.5	1x
10 mM dNTPs	0.5	200 µM
10 µM op44	0.5	0.2 µM
10 µM op45	0.5	0.2 µM
Standard Taq Polymerase	0.125	0.625 units
genomic DNA	2	variable
nuclease free water	18.875	-

As controls, additional samples with genomic DNA from wild type embryos as DNA template and nuclease free water instead of DNA template were used in each experiment. The PCR described above was ran under the cycling conditions described in the Table 5.21.

Table 5.21 | Cycling conditions used in PCR for *gata2b*^{u5008} genotyping.

Phase		temperature [°C]	time [s]
initial denaturation		95	30
34 cycles	denaturation	95	15
	annealing	56	30
	extension	68	30
final extension		68	5 minutes

The results from the PCR reaction were checked by electrophoresis in agarose gels. 5 µL of the PCR products were run in a 3% (w/v) agarose gel. A single 398 bp band is expected, but a double band was observed in heterozygous DNA samples, as observed during the genotyping of *gata2a*^{um27} mutants (see section 4.2.2). Given that these double bands were only observed in PCRs whose template DNA came from heterozygous *gata2b*^{u5008} fish, the formation of heterodimers

between copies of DNA amplified from wild type DNA and those copied from mutant DNA seems to be a likely explanation.

The PCR products were then digested using the restriction enzyme FauI (R0651S, NEB). The Table 5.22 shows the components and concentrations for the digestion of the PCR products with FauI enzyme:

Table 5.22 | Reaction mix for FauI digestion.

Reagent	Volume per reaction [µL]	Final concentration
10x CutSmart buffer	2	1x
FauI enzyme	0.2	2 units
PCR product	10	variable
nuclease free water	7.8	-

The FauI digestion mix was incubated 2 hours at 55 °C and 20 minutes at 65 °C for restriction enzyme inactivation. The DNA digestions were then analysed by electrophoresis in agarose gels. 10 µL of the digested DNA were ran in a 3% (w/v) agarose gel. The genotypes were read from the digestion pattern as explained in the Table 5.23.

Table 5.23 | *gata2b*^{u5008} genotypes and FauI digestion patterns.

Genotype	Number of bands	Band sizes [bp]
Wild type (+/+)	2	289 112
Heterozygote (+/u5008)	3	395 289 112
Homozygote (u5008/u5008)	1	395

5.2.9 Genotyping of *gata2b*^{delCVN} mutant fish

A further *gata2b* mutant line generated by CRISPR/Cas9 technology was used in some experiments: fish carrying the ENSDARG00000009094.7:g.3096_3104del mutation, called *gata2b*^{delCVN} for brevity. The *gata2b*^{delCVN} mutation is a 9 bp deletion in exon 4 of *gata2b* gene that encodes an in-frame deletion of cysteine 265, valine 266, and asparagine 267, p.(Cys265_Asn267del) (see section 5.3.1 for more details). In order to genotype fish carrying the *gata2b*^{delCVN} mutation, a protocol based on amplification by PCR and restriction digestion was developed, in a similar way to those develop to genotype *gata2a*^{um27} (section 4.2.2) and *gata2b*^{u5008} (section 5.2.8) mutants.

Genomic DNA obtained either from gametes (section 2.11.4), embryos and larvae (section 2.11.3), or fin clips from adult fish (see section 2.11.2) was used as template for a PCR to amplify a 430 bp region of *gata2b* gene spanning from intron 3 to intron 4 by using the primers shown in Table 5.24:

Table 5.24 | Primers used for genotyping of *gata2b*^{delCVN} mutants.

Primer name	Sequence (5' to 3')	Length	%GC	Tm
op42	ATGGCACTTGTAGAAATGACCGA	23	43.5	60.3
op43	AACTGATCATAACTGCTTGAACACAAT	27	33.3	60.0

The components and concentrations of the PCR mix for genotyping of *gata2b*^{delCVN} mutation are shown in the Table 5.25. The volumes shown are calculated for one 25 µL reaction and were scaled up for large numbers of samples. Details about dNTPs, the DNA polymerase used, and its reaction buffer are available in section 2.7.

Table 5.25 | Components of PCR for *gata2b*^{delCVN} genotyping.

reagent	Volume per reaction [µL]	Final concentration
10x Standard Taq buffer	2.5	1x
10 mM dNTPs	0.5	200 µM
10 µM op42	0.5	0.2 µM
10 µM op43	0.5	0.2 µM
Standard Taq Polymerase	0.125	0.625 units
genomic DNA	2	variable
nuclease free water	18.875	-

The cycling conditions used for the PCR reaction to genotype *gata2b*^{delCVN} mutations are shown in Table 5.26. The samples to be genotyped were ran in parallel with control tubes with wild type DNA and without DNA template.

Table 5.26 | Cycling conditions used in PCR for *gata2b*^{delCVN} genotyping.

phase		temperature [°C]	time [s]
initial denaturation		95	30
34 cycles	denaturation	95	15
	annealing	60	30
	extension	68	30
final extension		68	5 minutes

The PCR products obtained were analysed by gel electrophoresis. For each sample, 5 µL of the PCR product were run in a 3% (w/v) agarose gel. From wild type genomic DNA, the amplification of a single 430 bp band is expected; while from *gata2b*^{delCVN} DNA, a 421 bp band is expected. As observed before, in the case of the genotyping of *gata2a*^{um27} mutants, a double band was observed in heterozygous DNA samples. As discussed in the section 4.2.2, the comparison of PCR results with those of restriction digestions showed that all fish exhibiting the double bands were heterozygous *gata2b*$^{+/delCVN}$ mutants. Probably this is due to

the formation of heterodimers between copies of DNA amplified from wild type DNA and those copied from mutant *gata2b*^{delCVN} DNA. The heterodimers exhibit a different electrophoretic migration because of the mismatch between their two DNA strands.

Then the PCR products obtained were digested with the restriction enzyme Tsp509I (R0576, NEB), that cuts once the wild type sequence. The components and concentrations of the restriction digestion of the PCR products with the Tsp509I enzyme are shown in Table 5.27:

Table 5.27 | Reaction mix for Tsp509I digestion of PCR products.

reagent	Volume per reaction [µL]	Final concentration
10x NEB buffer 1	2	1x
Tsp509I enzyme	0.2	2 units
PCR product	10	variable
nuclease free water	7.8	-

The composition of the NEB buffer 1 used in the digestion with the Tsp509I restriction enzyme is shown in Table 5.28:

Table 5.28 | 1x NEB buffer 1 composition.

Reagent	Final concentration
Bis-Tris-propane-HCl	10 mM
$MgCl_2$	10 mM
1,4-dithiothreitol	1 mM
pH 7.0 (at 25 °C)	-

The digestions of PCR products with the Tsp509I restriction enzyme (see Table 5.27) were incubated for 2 hours at 65 °C. The digestion pattern of each sample was then analysed by electrophoresis in 3% w/v agarose gels. The Table 5.29 shows the digestion patterns expected for each *gata2b*^{delCVN} genotype:

Table 5.29 | *gata2b*^{delCVN} genotypes and Tsp509I digestion patterns

Genotype	Number of bands	Band sizes [bp]
Wild type (+/+)	2	265 169
Heterozygote (+/delCVN)	3	430 265 169
Homozygote (delCVN/delCVN)	1	421

5.3 Results

5.3.1 Generation of zebrafish *gata2b* mutant lines

CRISPR/Cas9 technology was used to generate stable *gata2b* mutant lines, and detailed descriptions of the method can be found in section 3. The general strategy consisted of the design and synthesis of sgRNAs targeting *gata2b* gene coding sequences, the injection of the sgRNAs in combination with Cas9 mRNA, and the screening of injected fish for *gata2b* mutations using NGS.

Four different sgRNAs were designed targeting exons 3 and 4 of the *gata2b* gene using CHOPCHOP v2 web tool (Labun et al., 2016) (see section 5.2.2 for more details about sgRNA design). sgRNAs were synthesized using a cloning-free method, based on the annealing of a gene-specific oligonucleotide to a constant oligonucleotide to make a ssDNA that is then filled-in in a T4 polymerase reaction to generate a double-stranded sgDNA. The sgDNAs generated are then used as a template for the synthesis of the final sgRNAs by *in vitro* transcription (Gagnon et al., 2014) (see section 5.2.3 for more details on sgRNA synthesis).

Wild type embryos were injected at the 1-cell stage with a mix of sgRNA and nCas9n mRNA, as described in section 5.2.5. The efficiency of each sgRNA was assessed by NGS analysis of genomic DNA extracted at 48 hpf from groups of 50 embryos injected with each sgRNA. Figure 5.6 shows graphs of the coverage of sequencing, and the percentage of identity of the reads mapped to wild type *gata2b* gene, along *gata2b* gene sequence for each of the sgRNAs injected (see the caption of Figure 5.6 for details). Graphs of percentage of identity of the reads to the *gata2b* gene show a significant decrease near the binding sites of the sgRNAs in the cases of sgRNAs gata2b_1 (Figure 5.6 a), gata2b_2 (Figure 5.6 b), and gata2b_4 (Figure 5.6 d). These results suggest that the injection of the sgRNAs gata2b_1, gata2b_2, and gata2b_4 induced high rates of indels in the embryos. In contrast, the reads obtained from embryos injected with gata2b_3 sgRNA exhibit high levels of identity to *gata2b* gene (Figure 5.6 c), suggesting low rates of indels.

Based on results shown in Figure 5.6, the embryos injected with the sgRNAs gata2b_2 and gata2b_4 were chosen to be grown until adulthood. At this point it was reasoned that embryos injected with sgRNA gata2b_2 were likely to carry mutations encoding mutant versions of Gata2b protein lacking both zinc finger

domains. And, on the other hand, it was hypothesized that the embryos injected with sgRNA gata2b_4 would allow the isolation of mutant lines encoding in-frame mutations in the N-zinc finger domain of Gata2b, which could be valuable as models of GATA2 deficiency (Greif et al., 2012).

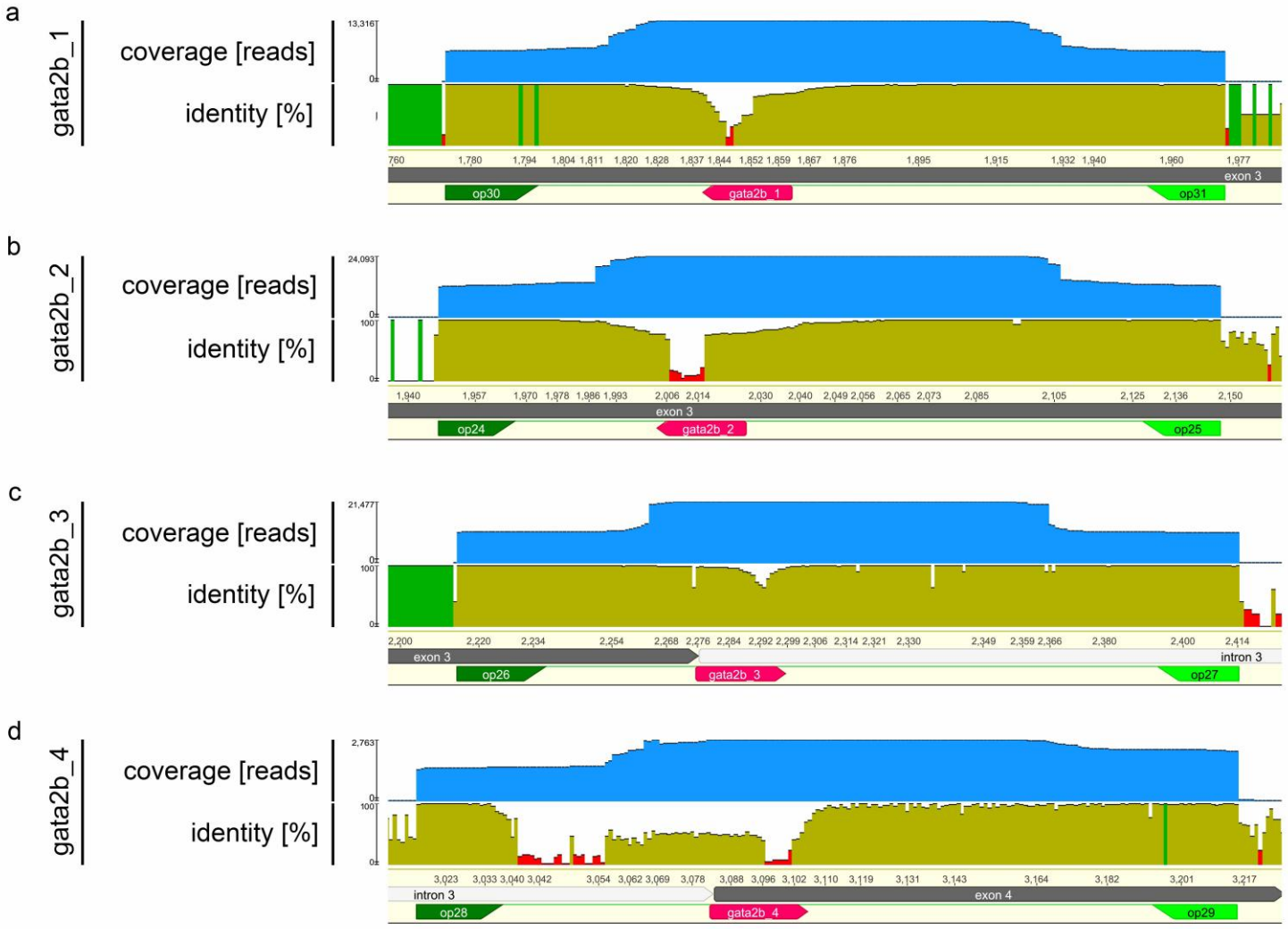
a
gata2b_1
coverage [reads]
identity [%]
13,316
0
100
0
760 1,780 1,794 1,804 1,811 1,820 1,828 1,837 1,844 1,852 1,859 1,867 1,876 1,895 1,915 1,932 1,940 1,960 1,977
exon 3
op30
gata2b_1
op31
b
gata2b_2
coverage [reads]
identity [%]
24,093
0
100
0
1,940 1,957 1,970 1,978 1,986 1,993 2,006 2,014 2,030 2,040 2,049 2,056 2,065 2,073 2,085 2,105 2,125 2,136 2,150
exon 3
op24
gata2b_2
op25
c
gata2b_3
coverage [reads]
identity [%]
21,477
0
100
0
2,200 2,220 2,234 2,254 2,268 2,276 2,284 2,292 2,299 2,306 2,314 2,321 2,330 2,349 2,359 2,366 2,380 2,400 2,414
exon 3
intron 3
op26
gata2b_3
op27
d
gata2b_4
coverage [reads]
identity [%]
2,763
0
100
0
3,023 3,033 3,040 3,042 3,054 3,062 3,069 3,078 3,088 3,096 3,102 3,110 3,119 3,131 3,143 3,164 3,182 3,201 3,217
intron 3
exon 4
op28
gata2b_4
op29

Figure 5.6 | (in previous page) Analysis of the efficiency of *gata2b* sgRNAs.

Reads obtained by NGS were mapped to wild type *gata2b* genomic sequence, and coverage of sequencing and percentage of identity of the reads were graphed along *gata2b*. Both graphs are shown over a diagram representing *gata2b* exons **(dark grey)** and introns **(light grey)** together with the binding site of each sgRNA **(red)**, and MiSeq forward **(dark green)** and reverse **(light green)** primers for each sgRNA gata2b 1 – 4 in **(a-d)**, respectively. For each sgRNA, the graph at the top shows the coverage of sequencing, in number of reads, as a blue histogram over *gata2b* sequence. The graph below shows the percentage of identity for the reads to *gata2b* sequence. Notice the significant reduction in the percentage of identity of the reads to *gata2b* sequence near the binding sites of sgRNAs 1, 2, and 4 **(a, b, and d)**. In contrast, the high percentage of identity in **(c)** shows low rate of indels induced by sgRNA gata2b_3 injection. Identity histograms are also colour coded: green, 100% identity; brown, over 30% to under 100% identity; and red, under 30% identity. The numbering of the sequences in **(a-d)** is relative to the first base pair of exon 1.

Given that F0 fish are mosaics, once they reached adulthood, F0 fish were screened for the presence of *gata2b* mutations in their germ cells. Gamete cells were extracted from each F0 fish as described in section 5.2.7, and their genomic DNA was analysed by NGS (see section 5.2.6). Only those adult F0 fish that were shown by NGS analysis to carry *gata2b* indels in more than the 20% of reads obtained from their germ cells were selected to serve as parents of the F1 generation. Selected F0 fish were then outcrossed to TL wild type fish, and F1 fish were grown until adulthood.

Once F1 fish reached adulthood, genomic DNA from fin clips was extracted and analysed by NGS, to identify the different *gata2b* mutations present in the F1 generation and to exclude those fish without *gata2b* mutations.

Analysis of NGS data with Geneious software allowed the identification of 52 adult fish carrying 13 different heterozygous mutations in the *gata2b* gene. Table 5.30

summarizes the genomic details of the mutations identified in the F1 generation. To avoid ambiguities, mutations were named following published guidelines (den Dunnen et al., 2016), by using as a reference *gata2b* Ensembl sequence ENSDARG00000009094.7. The genomic coordinates of each mutation are shown relative to chromosome 6, from version GRCz10 of the zebrafish genome. The sequences deleted or inserted are shown (5' to 3') together with their length in bp.

The *gata2b* mutations identified were predominantly deletions, and only one insertion (g.2010_2011insATGTGTCCCC, Table 5.30) and one deletion-insertion (g.3100_3101delinsGCTAC, Table 5.30) were identified. As shown previously (Gagnon et al., 2014), mutant alleles generated using CRISPR/Cas9 technology exhibited low diversity.

Table 5.30 | Genomic details of *gata2b* mutant lines generated.

mutation (ENSDARG00000009094.7 as reference)	type	genomic coordinates in chromosome 6 (5' to 3')	sequence deleted / inserted (5' to 3')	length [bp]
Mutant isolated from fish injected with sgRNA gata2b_2				
g.2006_2014del	deletion	40798484 - 40798492	ACCCCGCCC	9
g.2006_2010del	deletion	40798484 - 40798488	ACCCC	5
g.2010_2014del	deletion	40798488 - 40798492	CGCCC	5
g.2011_2014del	deletion	40798489 - 40798492	GCCC	4
g.2010_2011insATGTGTCCCC	insertion	40798488 - 40798489	ATGTGTCCCC	10
Mutant isolated from fish injected with sgRNA gata2b_4				
g.3091_3099del	deletion	40799569 - 40799577	ATGTGTAAA	9
g.3093_3100del	deletion	40799571 - 40799578	GTGTAAAT	8
g.3096_3104del	deletion	40799574 - 40799582	TAAATTGTG	9
g.3097_3103del	deletion	40799575 - 40799581	AAATTGT	7
g.3097_3100del	deletion	40799575 - 40799578	AAAT	4
g.3098_3101del	deletion	40799576 - 40799579	AATT	4
g.3100_3106del	deletion	40799578 - 40799584	TTGTGGA	7
g.3100_3101delinsGCTAC	deletion-insertion	40799578 - 40799579	TT | GCTAC	2 | 4

The mutations identified in exons 3 and 4 of *gata2b* were analysed using Geneious software to determine the protein sequences encoded by each mutant *gata2b* allele in Table 5.30. The translation of the *gata2b* transcript ENSDART00000144479.1 was used as a reference to describe each mutation at the protein level, as previously described (den Dunnen et al., 2016). In Table 5.31, the denomination of each mutation at the protein level is shown together with its type, and the predicted length of the protein encoded by each mutant allele.

In terms of the mutant proteins encoded by the mutant alleles found, the diversity of the mutations generated by CRISPR/Cas9 technology is even lower than at a genomic level (see Table 5.31), as previously suggested (Gagnon et al., 2014). Most of the mutant alleles induce a frameshift in the wild type Gata2b protein and an early stop-codon, encoding truncated proteins. Only four mutant alleles encode proteins with in-frame changes with comparable size to Gata2b. Notice that both g.3097_3100del and g.3098_3101del *gata2b* mutations encode identical mutant proteins: Gata2b:p.(Asn267ValfsTer294).

Table 5.31 | Predicted consequences at the protein level of *gata2b* mutations in Table 5.30.

mutation (ENSDARG00000009094.7 as reference)	encoded protein mutation (translated ENSDART00000144479.1 as reference)	type	predicted protein length [aa]
Mutant isolated from fish injected with sgRNA gata2b_2			
g.2006_2014del	p.(Pro171_Pro173del)	in-frame deletion	425
g.2006_2010del	p.(Thr172AlafsTer208)	frameshift	207
g.2010_2014del	p.(Pro173GlnfsTer208)	frameshift	207
g.2011_2014del	p.(Pro174LysfsTer185)	frameshift	187
g.2010_2011insATGTGTCCCC	p.(Pro174CysfsTer213)	frameshift	212
Mutant isolated from fish injected with sgRNA gata2b_4			
g.3091_3099del	p.(Glu264_Asn267delinsAsp)	deletion-insertion	425
g.3093_3100del	p.(Cys265LeufsTer284)	frameshift	283
g.3096_3104del	p.(Cys265_Asn267del)	in-frame deletion	425
g.3097_3103del	p.(Asn267GlufsTer293)	frameshift	292
g.3097_3100del	p.(Asn267ValfsTer294)	frameshift	293
g.3098_3101del	p.(Asn267ValfsTer294)	frameshift	293
g.3100_3106del	p.(Asn267LysfsTer293)	frameshift	292
g.3100_3101delinsGCTAC	p.(Asn267_Cys268delinsLysLeuArg)	deletion-insertion	429

The mutant allele ENSDARG00000009094.7:g.2011_2014del (see Table 5.30 for details) was chosen as a model of Gata2b deficiency, given that it encodes the most truncated Gata2b protein (187aa) (see Table 5.31). An additional advantage is that the ENSDARG00000009094.7:g.2011_2014del mutation deletes a restriction site for the enzyme FauI, allowing us to genotype mutant fish and larvae by PCR and posterior restriction digestion of the DNA products. The adult fish carrying the ENSDARG00000009094.7:g.2011_2014del mutation were designated with the UCL allele name *gata2b*^{u5008}.

Additionally, the mutant allele ENSDARG00000009094.7:g.3096_3104del (see Table 5.30) was also selected for further experiments, given that it encodes a mutant Gata2b protein with an in-frame deletion of 3aa in the N-terminal zinc finger domain. The 9 bp deletion in ENSDARG00000009094.7:g.3096_3104del mutants deletes the sequence encoding 3 amino acids: cysteine 265 (C), valine 266 (V), and asparagine 267 (N). These mutant fish are hereby called *gata2b*^{delCVN}.

These three amino acids are part of the N-terminal zinc finger domain, and more importantly, cysteine 265 (C) is predicted to be one of the four conserved cysteine residues coordinating a zinc ion in the C_4 zinc finger domain. Mutations in this region are frequently found in patients of GATA2 deficiency (Spinner et al., 2014). Additionally, mutations in the N-zinc finger domain of GATA2 protein are interesting, as they have been linked with biallelic mutations in *CEBPA* gene (Greif et al., 2012).

Given that homozygous *gata2a*$^{um27/um27}$ mutant embryos show lack of blood circulation in the trunk and tail (Zhu et al., 2011) and additional morphological abnormalities (as shown in Figure 4.17), all *gata2b* mutant embryos were screened for these phenotypes. In contrast to homozygous *gata2a*$^{um27/um27}$ mutant embryos, all *gata2b* mutant embryos analysed of all the mutant lines identified (see Table 5.30) showed normal blood circulation at 2 dpf and 4 dpf, and normal morphology regardless of their genotype. However, it is important to mention that in the case of the *gata2b* mutations: g.2006_2010del, g.2010_2011insATGTGTCCCC, g.3091_3099del, g.3097_3103del, g.3100_3106del, and g.3100_3101delinsGCTAC (see Table 5.30 and Table 5.31 for more details), there were only male or female fish, and therefore, no homozygous mutant embryos were obtained and only heterozygous mutant fish were analysed.

5.3.2 Myeloid development in *gata2b* mutant fish

The development of myeloid cells was analysed in *gata2b*^{u5008} and *gata2b*^{delCVN} mutant embryos and larvae using a combination of WISH, to detect the expression of known myeloid markers, and a histochemical technique, Sudan Black, that labels the primary granules of granulocytes (see section 2.3 for more details).

Primitive myeloid cells derived from the ALPM migrate over the yolk and differentiate into macrophages (Herbomel et al., 1999) and granulocytes (Le Guyader et al., 2008) that migrate to different tissues in the embryos. Myeloid cells residing in the PBI of 22 hpf *gata2b*^{u5008} mutant embryos were studied using WISH for *spi1b* and *mpx* genes. At this developmental stage, the expression of *spi1b* is decreasing, but still some labelled cells can be detected (Bennett et al., 2001; Lieschke et al., 2002). Figure 5.7 a shows a quantification of the number of *spi1b*$^{+}$ cells in the PBI of *gata2b*^{u5008} mutant embryos at 22 hpf stage. Although heterozygous *gata2b*$^{+/u5008}$ mutant embryos seem to have more variability, no statistically significant differences were found (Figure 5.7 a and Supplementary Table 9.28). In Figure 5.7 b, the number of *mpx*$^{+}$ cells in the PBI of 22 hpf embryos is shown. The quantifications show that there are no differences across genotypes in the number of labelled cells, however, data suggest that both heterozygous *gata2b*$^{+/u5008}$ and homozygous *gata2b*$^{u5008/u5008}$ mutant embryos have more variability in the number of *mpx*$^{+}$ cells in the PBI than their wild type siblings (Figure 5.7 b and Supplementary Table 9.29.

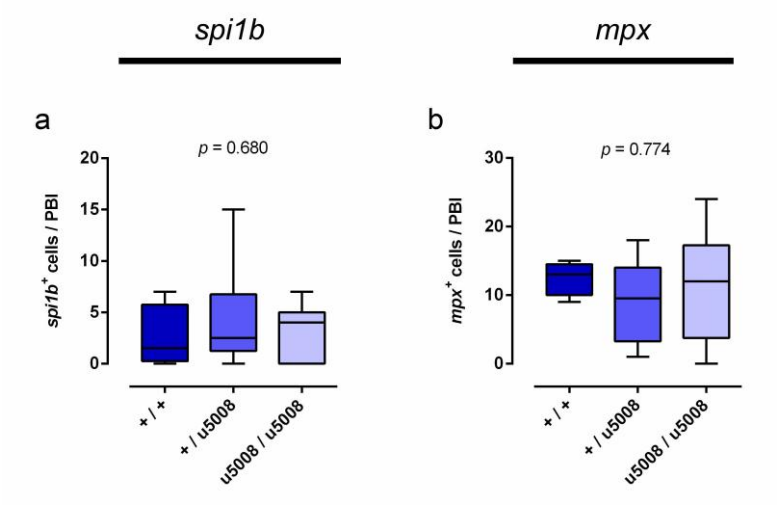

Figure 5.7 | Myeloid markers show normal numbers of primitive myeloid cells in the PBI of 22 hpf *gata2b*^{u5008} mutant embryos.

Primitive myeloid cells were labelled by *spi1b* and *mpx* WISH in 22 hpf *gata2b*^{u5008} mutant embryos, and quantifications were carried out. Quantifications of *spi1b*$^{+}$ **(a)** and *mpx*$^{+}$ **(b)** cells in the PBI of 22 hpf *gata2b*^{u5008} mutant embryos are shown. Statistical comparisons were carried out by Kruskal-Wallis test, and the *p*-values are shown in each graph. See Supplementary Table 9.28 and Supplementary Table 9.29 for more details about **(a)** and **(b)**, respectively.

Over time, the number of neutrophils in the PBI/CHT increases linearly (Renshaw et al., 2006) and *mpx*$^{+}$ neutrophils become detectable by Sudan Black staining between 33 and 35hfp (Le Guyader et al., 2008). Granulocytes of 48 hpf *gata2b*^{u5008} mutant larvae were stained with Sudan Black and the number of Sudan Black^{+} cells in the CHT was quantified (Figure 5.8 a). No significant differences in the number of granulocytes in the CHT of *gata2b*^{u5008} mutant larvae were found at this stage, suggesting that primitive granulocytes and those derived from EMPs are not affected by *gata2b*^{u5008} mutation.

At later stages, HSCs derived from the haemogenic endothelium in the ventral wall of the DA (Bertrand et al., 2010; Kissa and Herbomel, 2010) seed the CHT and give rise to a transient wave of definitive-derived granulocytes (Kissa et al., 2007; Murayama et al., 2006). To assess definitive granulopoiesis in *gata2b*^{u5008} mutant larvae, 4 dpf larvae were stained with Sudan Black and quantifications of Sudan

Black^{+} cells in the CHT were carried out (Figure 5.8 b). Quantifications in Figure 5.8 b show a dose dependent decrease in the number of Sudan Black^{+} granulocytes in the CHT of *gata2b*^{u5008} mutant larvae at 4 dpf (see Supplementary Table 9.31 for more details). These results show that Gata2b is required for definitive granulopoiesis in the CHT. Interestingly, homozygous *gata2b*$^{u5008/u5008}$ mutant larvae at 4 dpf exhibit a similar number of Sudan Black^{+} cells in the CHT (mean ± SEM: 61.36 ± 4.11) (Supplementary Table 9.31) to that found in the same group (mean ± SEM: 43.5 ± 1.119) and in wild type embryos (mean ± SEM: 51.33 ± 4.88) at 48 hpf (Supplementary Table 9.30), suggesting that granulopoiesis is severely impaired in *gata2b*$^{u5008/u5008}$ fish after the 48 hpf stage.

Additionally, a proportion of 4 dpf *gata2b*^{u5008} mutant larvae stained with Sudan Black exhibited granulocytes that were stained with very low amounts of Sudan Black. The presence of significantly lower amounts of staining, regardless of the number of Sudan Black-stained cells, was recorded and their frequency in each group is shown in Figure 5.8 c. Quantification in Figure 5.8 c suggests that larvae with weaker Sudan Black staining are more frequent among heterozygous *gata2b*$^{+/u5008}$ and homozygous *gata2b*$^{u5008/u5008}$ mutant larvae than in the wild type group. These results suggest that *gata2b*^{u5008} mutations could affect the accumulation of primary granules in the granulocytes in the CHT.

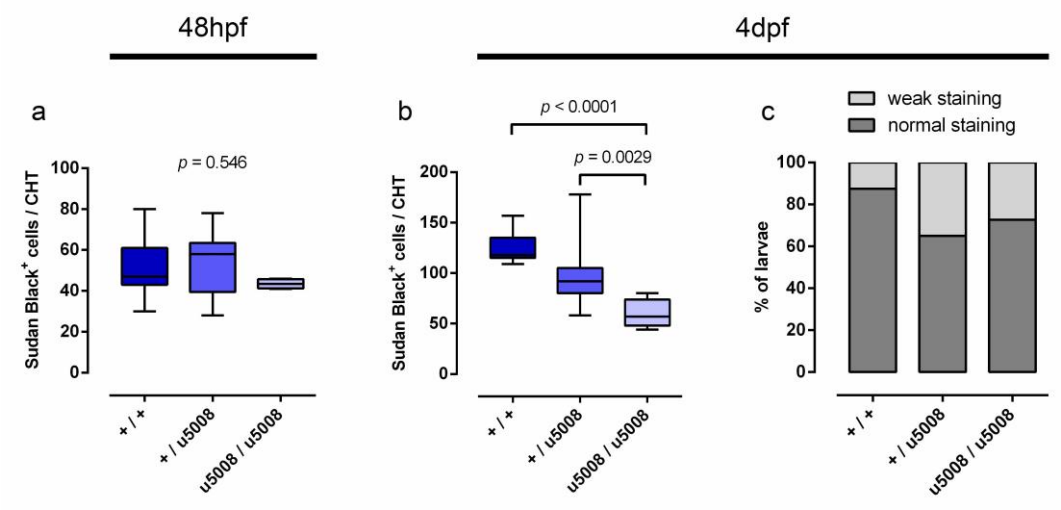

Figure 5.8 | Dose dependent decrease in the number of granulocytes in the CHT of 4 dpf *gata2b*^{u5008} mutant larvae.

Granulocytes were stained using Sudan Black in 48 hpf **(a)** and 4 dpf **(b and c)** *gata2b*^{u5008} fish. In **(a and b)**, quantifications of the number of Sudan Black^{+} cells in the CHT of 48 hpf **(a)** and 4 dpf **(b)** *gata2b*^{u5008} fish. In addition to a decreased number of Sudan Black^{+} granulocytes, some 4 dpf *gata2b*^{u5008} mutant larvae display a significantly weaker Sudan Black staining. In **(c)**, the observed frequency of this phenotype is shown for each genotype. Statistical comparisons in **(a and b)** were carried out by using Kruskal-Wallis test followed by Dunn's multiple comparisons test when appropriate. See Supplementary Table 9.30, Supplementary Table 9.31, and Supplementary Figure 9.2, for more details about **(a)**, **(b)**, and **(c)**, respectively.

Granulopoiesis was also studied in the *gata2b*^{delCVN} mutant line. As done previously with *gata2b*^{u5008} mutant fish (Figure 5.8), granulocytes in *gata2b*^{delCVN} mutant larvae were stained using Sudan Black at 48 hpf and 4 dpf stages, and quantifications were carried out. Figure 5.9 a shows the number of Sudan Black^{+} cells in the CHT of 48 hpf *gata2b*^{delCVN} mutant larvae. Statistical comparison shows that there are no significant differences among the groups, suggesting that *gata2b*^{delCVN} mutation does not affect granulopoiesis at this stage. Interestingly, larvae with significantly lower degree of staining were found among 48 hpf *gata2b*^{delCVN} mutant larvae,

similar to what was found in 4 dpf *gata2b*^{u5008} mutants. Figure 5.9 b shows the frequency of larvae with normal levels of staining (dark grey bars), regardless of the number of labelled cells, and that of larvae with weaker staining (light grey bars). Results show that the frequency of larvae with lower degree of Sudan Black staining is higher among heterozygous *gata2b*$^{+/delCVN}$ and homozygous *gata2b*$^{delCVN/delCVN}$ mutant larvae than in wild type larvae, suggesting that *gata2b*^{delCVN} mutation affects granulopoiesis at 48 hpf stage.

Definitive granulopoiesis was studied then in *gata2b*^{delCVN} larvae by staining granulocytes with Sudan Black at 4 dpf stage. The number of Sudan Black^{+} cells in the CHT of each larva was quantified and the results are shown in Figure 5.9 c. The numbers of labelled granulocytes in heterozygous *gata2b*$^{+/delCVN}$ and homozygous *gata2b*$^{delCVN/delCVN}$ mutant larvae show no significant difference from that of their wild type siblings (Figure 5.9 c), in contrast to the dose dependent decrease observed in *gata2b*^{u5008} mutants (Figure 5.8 b). These results suggest that *gata2b*^{delCVN} mutation does not affect definitive granulopoiesis.

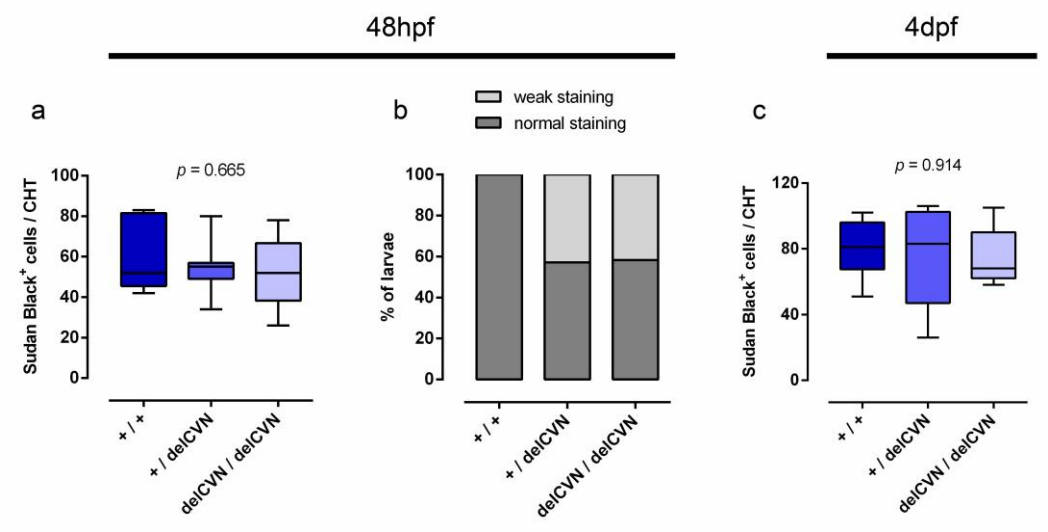

Figure 5.9 | Decreased accumulation of Sudan Black in the granulocytes of *gata2b*^{delCVN} mutants.

Granulocytes were stained using Sudan Black in 48 hpf **(a and b)** and 4 dpf **(c)** *gata2b*^{delCVN} fish. In **(a and c)**, quantifications of the number of Sudan Black^{+} cells in the CHT of 48 hpf **(a)** and 4 dpf **(c)** *gata2b*^{delCVN} fish. Despite having normal numbers of Sudan Black^{+} granulocytes, some 48 hpf *gata2b*^{delCVN} mutant larvae display a significantly weaker Sudan Black staining. In **(b)**, the observed frequency of this phenotype is shown for each genotype. Statistical comparisons in **(a and c)** were carried out by using Kruskal-Wallis, and the *p*-values are shown in each graph. See Supplementary Table 9.32 and Supplementary Table 9.33 for more details.

5.3.3 Development of myeloid cells in *gata2a*^{um27}*; gata2b*^{u5008} double mutants

Results in section 4.3 and section 5.3.2 suggest that both Gata2a and Gata2b play roles in definitive haematopoiesis. Additionally, it is possible that the similarity between the protein sequences of Gata2a and Gata2b (Butko et al., 2015) allows certain degree of functional redundancy between them. Therefore, to model human GATA2 deficiency in zebrafish, both *gata2a*^{um27} and *gata2b*^{u5008} mutations were studied together in heterozygosity. Double heterozygous fish (*gata2a*$^{+/um27}$*;*

gata2b$^{+/u5008}$), were obtained by crossing *gata2a*$^{+/um27}$ adult fish to *gata2b*$^{+/u5008}$ fish, or by outcrossing adult double heterozygous *gata2a*$^{+/um27}$*; gata2b*$^{+/u5008}$ fish to transgenic zebrafish.

Myeloid cell development was studied in double *gata2a*^{um27}*; gata2b*^{u5008} mutant fish by using the transgenic reporter line *Tg(spi1b:EGFP),* that drives the expression of EGFP to myeloid cells at early developmental stages (Hsu et al., 2004). The number of spi1b:EGFP^{+} cells in the CHT of double mutant *gata2a*^{um27}*; gata2b*^{u5008} fish was quantified at 30 hpf (Figure 5.10 a) and 48 hpf (Figure 5.10 b). At 30 hpf stage (Figure 5.10 a), statistical analysis shows that mutation in *gata2a* is a significant source of variation (*p*-value = 0.038), however, no statistically significant differences were found in pairwise comparisons (Supplementary Table 9.34). By 48 hpf (Figure 5.10 b), quantification of spi1b:EGFP^{+} cells in the CHT shows that, as found for 30 hpf fish, mutation in *gata2a* gene is a significant source of variation (*p*-value = 0.003). Pairwise comparisons show that *gata2a*$^{+/um27}$*; gata2b*$^{+/+}$ have significantly lower numbers of spi1b:EGFP^{+} cells in the CHT than wild type *gata2a*$^{+/+}$*; gata2b*$^{+/+}$ fish at 48 hpf (Figure 5.10 b, and Supplementary Table 9.35). These results suggest that at this stage Gata2a plays a role in myeloid cell development in the CHT, and that heterozygosity for the *gata2b* gene has no detectable impact on spi1b:EGFP^{+} cells in the CHT.

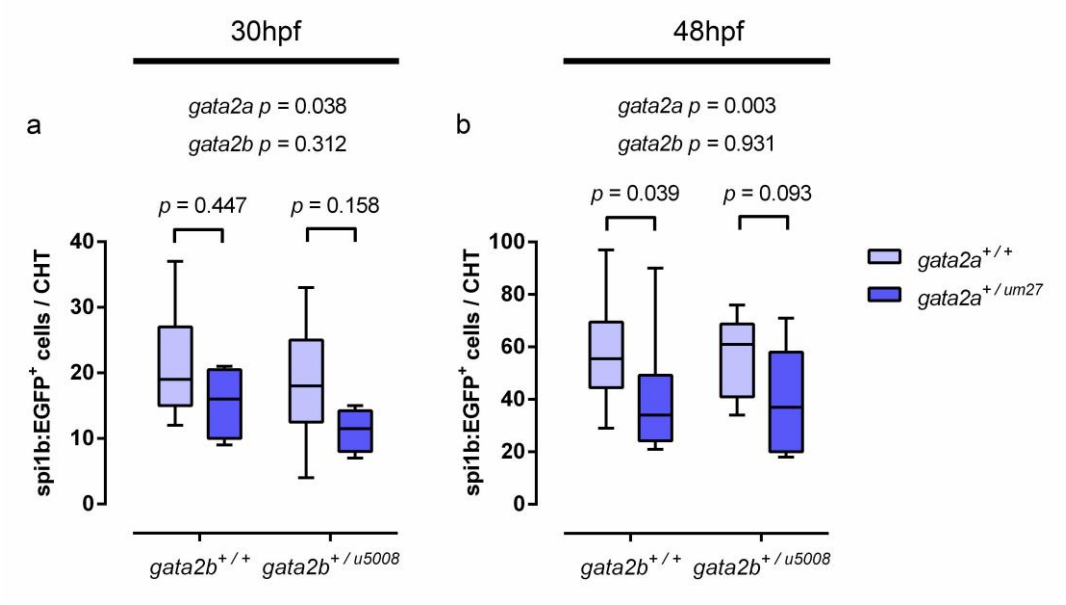

Figure 5.10 | Decreased numbers of spi1b:EGFP⁺ cells in the CHT of heterozygous *gata2a^{um27}* embryos.

Double heterozygous mutant adult fish *gata2a$^{+/um27}$; gata2b$^{+/u5008}$* were crossed to homozygous transgenic *spi1b:EGFP$^{+/+}$* adult fish and transgenic double mutant embryos were obtained. In **(a and b)**, quantifications of the number of spi1b:EGFP⁺ cells in the CHT of embryos at 30 hpf **(a)** and 48 hpf **(b)**. In both **(a and b)**, statistical comparisons were carried out by two-way ANOVA and *p*-values for each variable are shown at the top in each graph. Bonferroni's multiple comparisons tests to assess the effect of mutations in *gata2a* gene, and *p*-values for each comparison are shown in each graph. See Supplementary Table 9.34 and Supplementary Table 9.35 for more details about **(a)** and **(b)**, respectively.

The previous results (Figure 5.10) suggest that Gata2a plays a role in the development of myeloid cells present in the CHT. Closer examination shows that while by 30hpf data are not conclusive, at 48 hpf there is good evidence supporting the requirement for Gata2a, suggesting a possible role for Gata2a in myeloid cell development at later stages.

However, in *Tg(spi1b:EGFP)* fish the expression of EGFP decreases over time and labelled myeloid cells become difficult to distinguish due to the expression of EGFP in somatic muscle cells (Hsu et al., 2004). Therefore, to study the development of myeloid cells beyond 48 hpf, the transgenic reporter zebrafish line *Tg(lyz:nfsB-mCherry)* was used. In transgenic *Tg(lyz:nfsB-mCherry)* fish, the promoter of the *lyz* gene, that drives the expression in myeloid cells (Hall et al., 2007), controls the expression of *nfsB* and *mCherry* genes (see section 2.1.1 for more details).

The development of myeloid cells from 48 hpf to 4 dpf was studied using double mutant *gata2a*^{um27}*; gata2b*^{u5008} larvae carrying the transgenic reporter *Tg(lyz:nfsB-mCherry)*. The number of lyz:nfsB-mCherry^{+} cells in the CHT was quantified in *gata2a*^{um27}*; gata2b*^{u5008} at 48 hpf, 3 dpf and 4 dpf (Figure 5.11).

Quantifications carried out in 48 hpf larvae show no statistically significant differences among genotypes (Figure 5.11 a, and Supplementary Table 9.36), suggesting that heterozygosity for *gata2a*, *gata2b* or both genes does not affect lyz:nfsB-mCherry^{+} myeloid cells at this stage. Given that these results seem contradictory with the findings in Figure 5.10 b, it is interesting to notice that the numbers of spi1b:EGFP^{+} cells found in the CHT at 48 hpf (Figure 5.10 b, and Supplementary Table 9.35) are higher than those observed for lyz:nfsB-mCherry^{+} cells at the same stage (Figure 5.11 a and Supplementary Table 9.36). This difference suggests that the lyz:nfsB-mCherry^{+} cells residing in the CHT at 48 hpf are a subgroup of spi1b:EGFP^{+} cells in the same tissue, possibly neutrophils (Meijer et al., 2008). Similarly, the quantifications of lyz:nfsB-mCherry^{+} cells in the CHT of 3 dpf larvae show no significant differences (Figure 5.11 b, and Supplementary Table 9.37), suggesting that heterozygosity for *gata2a* or *gata2b* genes, or both, does not affect the numbers of lyz:nfsB-mCherry^{+} cells in the CHT at this stage.

In contrast, quantifications carried out in 4 dpf larvae (Figure 5.11 c, and Supplementary Table 9.38) suggest that mutation in *gata2b* could be a relevant source of variation (*p*-value = 0.259), and pairwise *post-hoc* comparisons show that *gata2a*$^{+/+}$*; gata2b*$^{+/u5008}$ exhibit significantly lower numbers of lyz:nfsB-mCherry^{+} cells in the CHT than those observed in wild type *gata2a*$^{+/+}$*; gata2b*$^{+/+}$ larvae (*p*-value = 0.031). These results suggest that by 4 dpf, Gata2b has a role in the development of lyz:nfsB-mCherry^{+} cells found in the CHT, in agreement with the results shown in Figure 5.8.

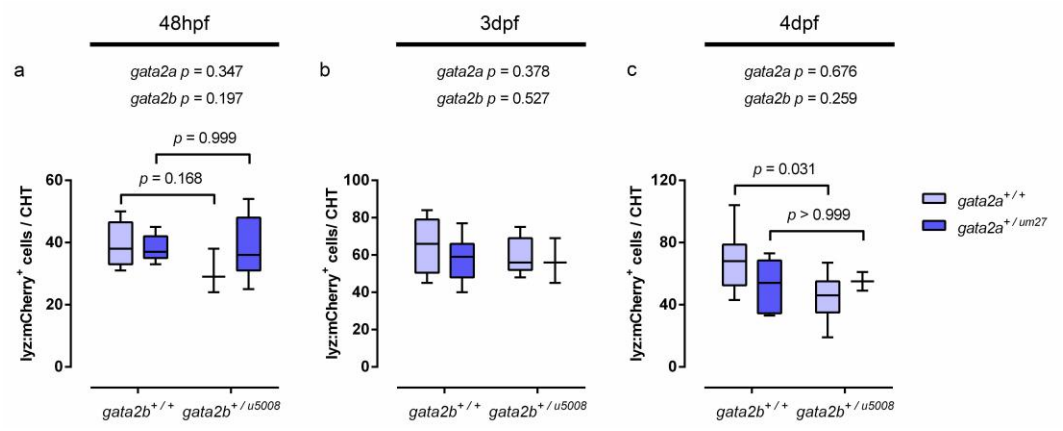

Figure 5.11 | Numbers of lyz:nfsB-mCherry^{+} cells in the CHT of *gata2a^{um27}; gata2b^{u5008}* fish at 48 hpf, 3 dpf, and 4 dpf.

Hemizygous transgenic double mutant larvae (*Tg(lyz:nfsB-mCherry)$^{+/-}$; gata2a^{um27}; gata2b^{u5008}*) were obtained by outcross of homozygous transgenic *Tg(lyz:nfsB-mCherry)* adults to double heterozygous *gata2a$^{+/um27}$; gata2b$^{+/u5008}$* adults. The number of lyz:nfsB-mCherry+ cells in the CHT was quantified at 48 hpf **(a)**, 3 dpf **(b)**, and 4 dpf **(c)**. Statistical comparisons in **(a-c)** were carried out using two-way ANOVA and the *p*-values for each source of variation are shown at the top of each graph. In the case of **(a and c)**, *post-hoc* pairwise comparisons were done using Bonferroni's multiple comparisons test, and the *p*-values are shown. See Supplementary Table 9.36, Supplementary Table 9.37 and Supplementary Table 9.38 for more details about **(a)**, **(b)**, and **(c)**, respectively.

Taken together, the results shown in Figure 5.8 and Figure 5.11 support a role for Gata2b in the development of neutrophils in the CHT. Further experiments using Sudan Black were carried out to study the effects of *gata2a* and *gata2b* deficiency on the development of granulocytes. Sudan Black staining was used to label the granulocytes in double *gata2a^{um27}; gata2b^{u5008}* mutant larvae at 48 hpf (Figure 5.12 a) and 4 dpf (Figure 5.12 b).

Quantifications of the number of Sudan Black^{+} cells in the CHT of double *gata2a*^{um27}*; gata2b*^{u5008} mutant larvae at 48 hpf, are shown in Figure 5.12 a. Analysis of variance shows strong evidence supporting *gata2a*^{um27} mutation as a source of variation ($p < 0.0001$). In keeping with the results observed in Figure 4.14 g, homozygous *gata2a*$^{um27/um27}$ mutant embryos exhibited a significant decrease in the number of Sudan Black^{+} cells in the CHT. Equivalent decreases in *gata2a*$^{um27/um27}$ homozygotes were found with independence of their genotype for *gata2b*, suggesting that Gata2b is not able to compensate for the absence of Gata2a activity. Heterozygous *gata2a*$^{+/um27}$ mutant embryos showed normal numbers of labelled granulocytes, showing that one wild type copy of Gata2a is sufficient to keep normal numbers of granulocytes at this developmental stage (see also Supplementary Table 9.39 and Supplementary Table 9.40).

In contrast, 48 hpf embryos carrying homozygous *gata2b*$^{u5008/u5008}$ mutation display normal numbers of stained granulocytes in the CHT, regardless of their genotype for *gata2a*. At this stage, heterozygosity for *gata2a*, *gata2b*, or both, had no detectable impact on the observed number of Sudan Black^{+} cells in the CHT, showing that there are no synergistic effects (Supplementary Table 9.40) that could suggest the presence of overlapping roles for Gata2a and Gata2b in primitive granulopoiesis.

In contrast, the quantification of cells labelled with Sudan Black in the CHT of 4 dpf double *gata2a*^{um27}*; gata2b*^{u5008} mutant larvae, in Figure 5.12 b, shows that the presence of *gata2b*^{u5008} mutations is a significant source of variation ($p < 0.0001$), while *gata2a*^{um27} mutation is not a relevant factor ($p = 0.656$). Importantly, *post-hoc* pairwise comparisons show that both *gata2a*$^{+/+}$*; gata2b*$^{+/u5008}$ and *gata2a*$^{+/um27}$*; gata2b*$^{+/u5008}$ have a significantly decreased number of Sudan Black^{+} cells in the CHT compared to that of both wild type *gata2a*$^{+/+}$*; gata2b*$^{+/+}$ and *gata2a*$^{+/um27}$*; gata2b*$^{+/+}$ (see Supplementary Table 9.41 for detailed statistics). In other words, heterozygous *gata2b*$^{+/u5008}$ larvae display significantly lower numbers of labelled granulocytes in the CHT when compared to wild type *gata2b*$^{+/+}$ larvae, regardless of their genotype for *gata2a.* These results suggest that Gata2b could be required for definitive granulopoiesis in the CHT, in agreement with the results shown in Figure 5.8 b. Alternatively, this could be a result of decreased numbers of HSPCs, as observed in *gata2b* morphants (Butko et al., 2015). Additionally, results in Figure 5.12 b show that heterozygous mutation in the *gata2a* gene do not affect

the numbers of granulocytes in the CHT at this stage. Furthermore, heterozygous *gata2a*$^{+/um27}$ mutation does not cooperate nor rescue the phenotype observed in heterozygous *gata2b*$^{+/u5008}$ larvae, suggesting that Gata2b's function in definitive granulopoiesis is not shared with Gata2a.

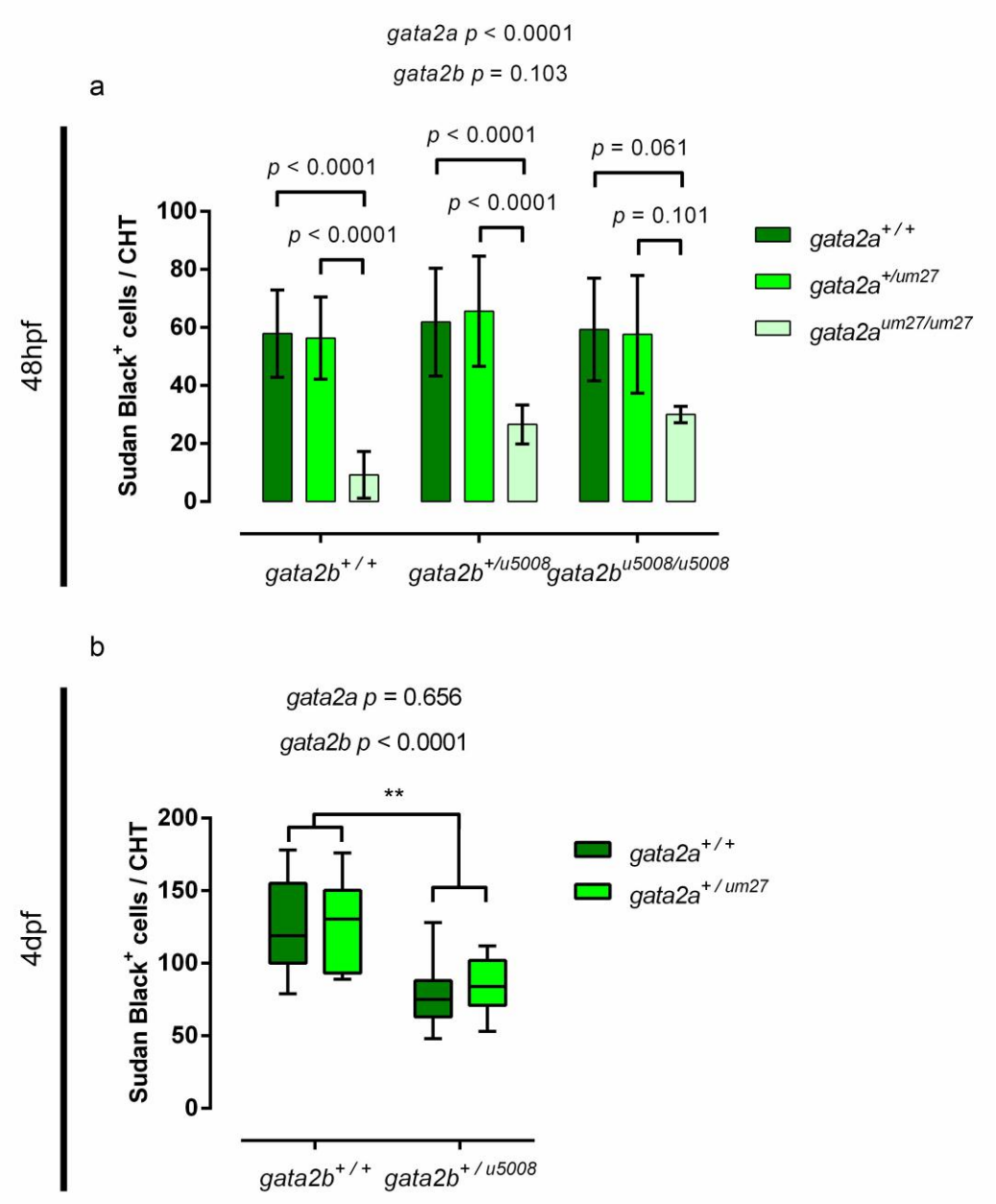

Figure 5.12 | Differential requirement for Gata2a and Gata2b in primitive and definitive granulopoiesis.

In **(a)**, double heterozygous mutant adult fish *gata2a*$^{+/um27}$*; gata2b*$^{+/u5008}$ were incrossed and embryos of all genotypes were obtained. In **(b)**, double mutant larvae *gata2a*^{um27}*; gata2b*^{u5008} were obtained by outcrossing *gata2a*$^{+/um27}$ and *gata2b*$^{+/u5008}$ heterozygous adult fish. Granulocytes were stained using Sudan Black in 48 hpf **(a)** and 4 dpf **(b).** In **(a and b)**, quantifications of the number of Sudan Black^{+} cells in the CHT of 48 hpf **(a)** and 4 dpf **(b)** larvae are shown. Statistical comparisons in **(a and b)** were carried out by using two-way ANOVA, followed by Tukey's multiple comparisons test. In **(a and b)**, the *p*-values of the effects of *gata2a* and *gata2b* calculated by two-way ANOVA are shown. In **(b)**, **, all the *p*-values of the *post-hoc* tests of the comparisons between *gata2b*$^{+/+}$ and *gata2b*$^{+/u5008}$ embryos, regardless of the *gata2a* genotype, fall in the interval $0.01 > p > 0.001$. See Supplementary Table 9.39 and Supplementary Table 9.40 for more details about **(a)**, and Supplementary Table 9.41 for details about **(b)**.

As previously found in larvae carrying the *gata2b*^{u5008} mutation (Figure 5.8 c) and the *gata2b*^{delCVN} mutation (Figure 5.9 b), Sudan Black stainings carried out in double *gata2a*^{um27}*; gata2b*^{u5008} mutant larvae at 4 dpf showed a proportion of fish with decreased levels of Sudan Black staining in their cells. The phenotype of decreased levels of Sudan Black staining was recorded in each larva analysed, and the percentage of larvae with this phenotype in each genotype is shown in Figure 5.13. In the graph of Figure 5.13, the percentage of larvae with normal levels of staining (dark grey bars) is over 90% for both wild type *gata2a*$^{+/+}$*; gata2b*$^{+/+}$ larvae (92.3%), and heterozygous *gata2a*$^{+/um27}$*; gata2b*$^{+/+}$ larvae (91.6%). In contrast, in larvae carrying the *gata2b*^{u5008} mutation, the percentages of larvae with normal levels of stainings decrease to 54.5% in heterozygous *gata2a*$^{+/+}$*; gata2b*$^{+/u5008}$ larvae, and to 70.0% in the case of double heterozygous *gata2a*$^{+/um27}$*; gata2b*$^{+/u5008}$ larvae. Given that Sudan Black staining labels granulocytes by accumulation in the primary granules of granulocytes (Sheehan and Storey, 1946), mainly neutrophils (Le Guyader et al., 2008), it could be hypothesized from these results that those granulocytes displaying low levels of Sudan Black staining

contain abnormally low levels of primary granules, which suggests that *gata2b*^{u5008} mutation affects the differentiation of definitive granulocytes.

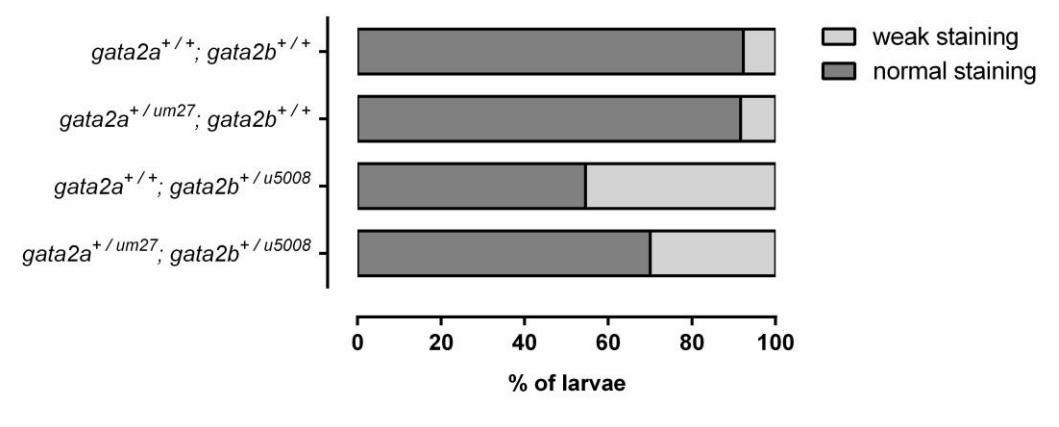

Figure 5.13 | *gata2b*$^{+/u5008}$ heterozygous larvae show increased frequency of weakly stained granulocytes.

Double heterozygous mutant adult fish *gata2a*^{um27}*; gata2b*^{u5008} were obtained by outcrossing *gata2a*$^{+/um27}$ and *gata2b*$^{+/u5008}$ heterozygous adult fish, and the larvae were stained with Sudan Black by 4 dpf to label the granulocytes. The graph shows the percentage of larvae exhibiting normal levels of Sudan Black staining **(dark grey bars)**, regardless of the number of labelled cells, and the percentage of larvae with significantly lower levels of Sudan Black staining **(light grey bars)**, for each genotype of *gata2a* and *gata2b* genes.

5.3.4 Emergence of HPSCs in *gata2a*^{um27}*; gata2b*^{u5008} double mutant embryos

Haematopoiesis during adulthood is sustained by a population HSCs, that generate all blood lineages (Traver et al., 2003). In mammals, HSCs reside in the bone marrow, while in teleost fish HSCs reside in the kidney marrow (Ma et al., 2011). However, despite these anatomical differences, in both mammals and fish HSCs are generated during embryonic development from the haemogenic

endothelium in the DA through a process known as EHT (Bertrand et al., 2010; Kissa and Herbomel, 2010).

Previous work in our group by Christopher Mahony and Dr Elspeth Payne[3] shows that both *gata2a*^{um27} and *gata2b*^{u5008} mutations induce a decrease in the number of *cmyb*$^{+}$ cells in the AGM region of 36 hpf embryos. Probably, these *cmyb*$^{+}$ cells are mostly newly generated haematopoietic progenitors, although the presence of *cmyb*$^{+}$ erythroid cells cannot be discarded. Figure 5.14 shows images of 36 hpf *gata2a*^{um27}*; gata2b*^{u5008} double mutant embryos after *cmyb* WISH. The number of *cmyb*$^{+}$ cells in the AGM of these embryos was quantified and the results are shown in Figure 5.14 f. The quantifications show that heterozygosity for *gata2a* or *gata2b* genes, or both, induces a statistically significant decrease in the number of *cmyb*$^{+}$ cells, compared to that of their wild type siblings. These results suggest a role for both *gata2a* and *gata2b* in EHT, in agreement with observations made in heterozygous *gata2a*$^{+/um27}$ mutant fish, shown in Figure 4.18, and previous reports using *gata2b* morphants (Butko et al., 2015).

[3] Data presented in Figure 5.14 were generated by Christopher Mahony and Dr Elspeth Payne at the UCL Cancer Institute, and are reproduced here with permission of the authors.

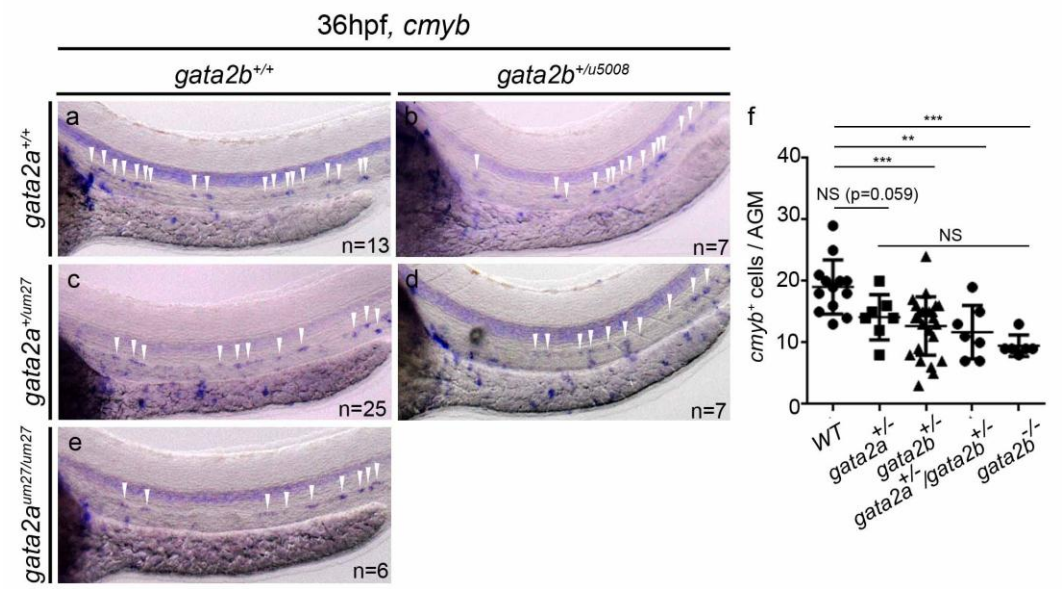

Figure 5.14 | Number of *cmyb*$^{+}$ cells in the AGM region of 36 hpf *gata2a*^{um27}; *gata2b*^{u5008} double mutant embryos.

The expression of *cmyb* was analysed by WISH in 36 hpf double mutant *gata2a*^{um27}; *gata2b*^{u5008} embryos obtained by incrossing double heterozygous *gata2a*$^{+/um27}$; *gata2b*$^{+/u5008}$ adult fish. In **(a-d)**, images of the trunk of 36 hpf mutant embryos are shown. Notice in **(a-d)** the *cmyb*$^{+}$ cells along the DA (white arrowheads). Quantification of the number of *cmyb*$^{+}$ cells in the AGM of 36 hpf double mutant *gata2a*^{um27}; *gata2b*^{u5008} embryos is shown.

The development of HSCs in double *gata2a*^{um27}; *gata2b*^{u5008} mutant larvae was studied at later developmental stages by using the transgenic reporter *Tg(itga2b:GFP).* Larvae were obtained by mating crosses of double heterozygous *gata2a*$^{+/um27}$; *gata2b*$^{+/u5008}$ adult fish with homozygous *Tg(itga2b:GFP)*$^{+/+}$ transgenic fish, so all larvae used in the experiment were hemizygous *Tg(itga2b:GFP)*$^{+/-}$ transgenics. Figure 5.15 shows the quantifications of the number of itga2b:GFP^{low} cells in the CHT of double *gata2a*^{um27}; *gata2b*^{u5008} mutant larvae at 60 hpf (Figure 5.15 a) and 4 dpf (Figure 5.15 b). Statistical comparisons show that there are no significant differences among genotypes at either developmental stages (Figure 5.15, Supplementary Table 9.42 and Supplementary Table 9.43). The normal numbers of itga2b:GFP^{low} cells observed in the CHT of *gata2a*^{um27}; *gata2b*^{u5008}

double mutant larvae suggest that heterozygosity for Gata2a or Gata2b or both does not affect HSCs after their emergence from the haemogenic endothelium of the DA.

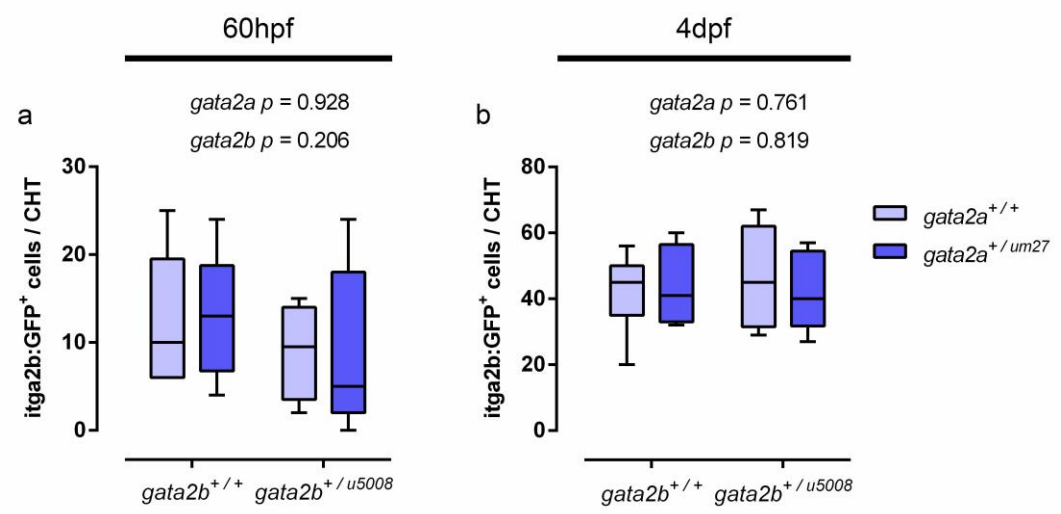

Figure 5.15 | Numbers of itga2b:GFP^{low} cells in the CHT of *gata2a^{um27}; gata2b^{u5008}* mutants.

Double heterozygous mutant adult fish *gata2a$^{+/um27}$; gata2b$^{+/u5008}$* were crossed to homozygous transgenic *Tg(itga2b:GFP)$^{+/+}$* adult fish and transgenic double mutant embryos were obtained. In **(a and b)**, quantifications of the number of itga2b:GFP^{low} cells in the CHT of 60 hpf **(a)** and 4 dpf **(b)** fish are shown. Statistical comparisons in **(a and b)** were carried out by using two-way ANOVA, and the *p*-values for the effect of each factor are shown in each graph. See Supplementary Table 9.42 and Supplementary Table 9.43 for more details about **(a)** and **(b)**, respectively.

5.4 Discussion

The Table 5.32 summarizes some of the main phenotypes of *gata2b*^{u5008} mutant fish that are shown in the section 5.3.

Table 5.32 | Summary of haematopoietic phenotype of *gata2b*^{u5008} mutants.

Lineage	Phenotype observed
HSCs	Dose dependent decrease of *cmyb*+ cells in the DA at 36 hpf. Normal *Tg(itga2b:GFP)+* cells in heterozygotes at 60 hpf and 4 dpf.
Myeloid cells	Normal *spi1b+* and *mpx+* cells in the PBI at 22 hpf. Normal Sudan Black+ cells in the CHT at 48 hpf. Dose dependent decrease of Sudan Black+ cells in the CHT at 4 dpf. Normal *Tg(lyz:nfsB-mCherry)+* cells in the CHT of heterozygotes at 48 hpf and 3 dpf. Decreased *Tg(lyz:nfsB-mCherry)+* cells in the CHT of heterozygotes at 4 dpf.

5.4.1 Gata2b is dispensable for primitive granulopoiesis

Results shown in the section 4.3.3 provide evidence to support a role for Gata2a in primitive myeloid cell development, as discussed in section 4.4.2. Additionally, analysis by WISH of myeloid markers in *gata2a*^{um27} mutant suggests that Gata2a activity is necessary for the development of caudal-derived myeloid cells other than mast cells (discussed in section 4.4.3), which have been shown to arise from EMPs in a Gata2a-dependent manner (Da'as et al., 2012; Dobson et al., 2008). In contrast with the findings made using *gata2a*^{um27} mutant fish, the results obtained in experiments using *gata2b*^{u5008} and *gata2b*^{delCVN} mutant embryos suggest that primitive myelopoiesis is not affected by *gata2b* deficiency.

The development of primitive macrophages derived from the RBI was not studied for *gata2b* mutants. However, analysis of the expression of *spi1b* and *mpx* genes in 22 hpf embryos (Figure 5.7) suggests that caudal primitive myeloid cells derived from the ICM are not affected in *gata2b* mutants. Similarly, quantifications of spi1b:EGFP^{+} cells in the CHT of transgenic embryos at 30 hpf and 48 hpf show that the numbers of myeloid cells are normal in heterozygous *gata2b*$^{+/u5008}$ embryos (Figure 5.10). It has been shown that at this developmental stage, EMPs

expressing *gata1a* and *lmo2* arise in the PBI of zebrafish embryos and generate a transient wave of haematopoiesis (Bertrand et al., 2007). Therefore, those myeloid cells found at 48 hpf in the CHT are probably a mixture of primitive cells and cells derived from EMPs, with a contribution of myeloid cells derived from the first HSCs that colonize the CHT.

Experiments carried out in 48 hpf embryos show that *gata2b*^{u5008} mutants exhibit normal numbers of granulocytes in the CHT, quantified as Sudan Black^{+} cells (Figure 5.8 a), suggesting that primitive granulopoiesis does not require Gata2b activity. It could be hypothesized that the reason why Gata2b is not required for granulopoiesis at this developmental stage is simply that it is not expressed at sufficient levels in the relevant cell lineages (Butko et al., 2015). However, observations carried out in *gata2b*^{delCVN} show that Gata2b is expressed in those cell types involved in granulopoiesis at 48 hpf. The *gata2b*^{delCVN} mutant embryos carry a 9 bp deletion that causes the in-frame deletion of 3aa in the N-terminal zinc finger of Gata2b protein, whereas the *gata2b*^{u5008} allele encodes a truncated protein prior to the zinc finger domains (see section 5.3.1 for details). At 48 hpf, *gata2b*^{delCVN} mutant embryos exhibit a phenotype of normal number of Sudan Black^{+} cells in the CHT, however, this is observed together with the presence of embryos whose granulocytes have weaker Sudan Black staining (Figure 5.9 a and b, respectively). This phenotype could be considered a neomorphic phenotype and it is important because it suggests that mutant Gata2b protein encoded by *gata2b*^{delCVN} mutant allele is active during granulopoiesis at 48 hpf. It has been shown that granules in neutrophils are produced sequentially during the maturation of neutrophils. Primary granules, which are labelled by Sudan Black (Sheehan and Storey, 1946), are the first type of granule to be formed during neutrophil's maturation process, and they are followed by secondary or specific and tertiary or gelatinase granules (Borregaard et al., 1995; Borregaard and Cowland, 1997). This process results in neutrophils that contain different types of granules with a wide range of cargoes according to their maturation stage (Theilgaard-Mönch et al., 2005). Therefore, it could be hypothesized that mutant alleles of Gata2b with aberrant function are able to disrupt differentiation of granulocytes at this stage.

5.4.2 Gata2b is required for definitive granulopoiesis

The development of definitive granulocytes produced in the CHT was studied using the transgenic reporter *Tg(lyz:nfsB-mCherry)* and the Sudan Black staining in larvae carrying mutations in *gata2b* gene and also *gata2a*. Quantifications of the number of Sudan Black^{+} cells in the CHT of 4 dpf *gata2a*^{u5008} mutant larvae (Figure 5.8 b) show a dose dependent effect of *gata2b*^{u5008} mutant allele in definitive granulopoiesis. These data strongly suggest that two copies of wild type *gata2b* gene are required for the development of normal numbers of granulocytes at this stage. Importantly, the decreased number of Sudan Black^{+} cells in the CHT of heterozygous *gata2b*$^{+/u5008}$ larvae mimics the neutropenia reported in patients carrying *GATA2* mutations (Spinner et al., 2014; Vinh et al., 2010). Similarly, an *in vitro* study reported that *GATA2*$^{-/-}$ human embryonic stem cells are not able to generate granulocytes (Huang et al., 2015). In contrast, studies in mice offer conflicting evidence about the impact of *Gata2* in granulopoiesis. Heterozygous *Gata2*$^{+/-}$ mice exhibit normal numbers of neutrophils, basophils, and eosinophils in the blood, together with many other haematopoietic lineages (Rodrigues et al., 2005), suggesting that *Gata2* haploinsufficiency has no effect on granulopoiesis. On the other hand, it has been reported that bone marrow cells from heterozygous *Gata2*$^{+/-}$ mice have a reduced granulocyte-macrophage potential *in vitro* (Rodrigues et al., 2008).

Consistent with quantifications of cells labelled with Sudan Black (Figure 5.8 b), the results from quantifications of cells expressing lyz:nfsB-mCherry show a decreased number of neutrophils in the CHT of 4 dpf heterozygous *gata2b*$^{+/u5008}$ mutant larvae (Figure 5.11 c). Quantifications carried out at earlier stages, 48 hpf and 3 dpf, show no statistically significant differences (Figure 5.11 a and b, respectively), suggesting that Gata2b haploinsufficiency affects the numbers of neutrophils derived from HSCs, but not those derived from the primitive wave of haematopoiesis and the EMPs.

Given that both Sudan Black staining and the transgenic reporter *Tg(lyz:nfsB-mCherry)* label neutrophils in their earlier stages of differentiation, it could be hypothesized that Gata2b deficiency affects an even earlier progenitor. Sudan Black is accumulated in the primary granules of neutrophils (Sheehan and Storey, 1946), which can be found already in the myeloblast stage (Amulic et al., 2012).

Similarly, the lysozyme C promoter in the transgenic reporter *Tg(lyz:nfsB-mCherry)* labels neutrophils (Hall et al., 2007). Neutrophils express lysozyme, as well as elastase and myeloperoxidase, from the myeloblast stage (Amulic et al., 2012). Therefore, the reduced number of granulocytes observed by both techniques (Figure 5.8 b, and Figure 5.11 c) show that granulopoiesis is affected at an early stage in *gata2b*^{u5008} mutants, and suggests the possibility that a defect in an earlier progenitor, even HSCs (Butko et al., 2015), could be the cause of the observed phenotypes. The role of Gata2b in HSC's emergence is discussed further in section 5.4.4.

It is interesting to point out that the use of Sudan Black to stain granulocytes uncovered the presence of two different phenotypes in *gata2b* mutant larvae: differences in number of labelled cells, and differences in the degree of staining of cells. It could be hypothesized that low accumulation of Sudan Black can lead to lower numbers of Sudan Black^{+} cells quantified. However, low numbers of Sudan Black^{+} cells without decreased levels of staining have been reported abundantly in different contexts, such as haematopoiesis and inflammation (Murayama et al., 2015; Paredes-Zúñiga et al., 2017). Conversely, analysis of 48 hpf *gata2b*^{delCVN} mutant embryos shows that decreased accumulation of Sudan Black in the cells (Figure 5.9 b) can be found concomitantly with normal numbers of Sudan Black^{+} cells (Figure 5.9 a). These results suggest that the decreased accumulation of Sudan Black in each individual cell and the decreased number of neutrophils found in *gata2b*^{u5008} mutants are independent to some extent. A similar phenotype has been reported before in the zebrafish myeloperoxidase mutant, *durif*, that has normal numbers of neutrophils, as shown by the expression of diverse markers, but whose neutrophils do not accumulate Sudan Black (Pase et al., 2012). The fact that Gata2b deficiency elicits a similar phenotype to that observed in the mutants lacking a basic component of primary granules, suggests that Gata2b has a role in the differentiation of granulocytes in addition to its role in early progenitors, discussed before.

The observed defects in accumulation of Sudan Black in the primary granules of the granulocytes of 4 dpf *gata2b*^{u5008} mutant larvae suggest that Gata2b deficiency affects the differentiation of granulocytes. Spinner and colleagues reported severe bacterial infections in 49% of GATA2 deficiency patients in addition to a high incidence of infections by nontuberculous mycobacteria (Spinner et al., 2014).

Similarly, it is interesting to mention that frequent infections have also been reported in patients with deficiency of MPO (myeloperoxidase, EC 1.11.1.7) (Cech et al., 1979; Kitahara et al., 1981; Nauseef, 1989) and ELANE (elastase, neutrophil expressed, EC 3.4.21.37) (Dale et al., 2000; Skokowa et al., 2007). Both MPO and ELANE are proteins found in the primary granules of neutrophils at early stages of maturation (Amulic et al., 2012), which makes these observations in patients very similar to the phenotype found in *gata2b* mutant fish. Neutrophils of patients with MPO and ELANE deficiency have a decreased bactericidal capacity (Kitahara et al., 1981; Skokowa et al., 2007), suggesting that it is possible that a similar phenotype could be found in the definitive neutrophils of *gata2b*^{u5008} mutant larvae.

The roles of Gata2a and Gata2b in granulopoiesis through development are compared and discussed in section 5.4.3.

5.4.3 Successive requirement of Gata2a and Gata2b during myeloid cell development

In previous sections, the roles of Gata2a (sections 4.4.2 and 4.4.3) and Gata2b (sections 5.4.1 and 5.4.2) in myeloid cell development have been discussed separately. In this section, Gata2a and Gata2b are compared based on their different participation in both primitive and definitive myelopoiesis.

In mammals, GATA2 regulates granulopoiesis by repressing SPI1 (Chou et al., 2009), which in turn has a critical role in granulocytes' development (Koschmieder et al., 2005). Similarly, both Gata2a and Gata2b are required for zebrafish granulopoiesis, as shown in sections 4.3.3, 5.3.2, and 5.3.3. However, it is important to highlight that the requirement for Gata2a and Gata2b during embryonic and larval development differ. Gata2a is required for primitive granulopoiesis, while it seems to be dispensable for definitive granulopoiesis. Conversely, data available for Gata2b strongly suggests that Gata2b is dispensable during primitive granulopoiesis, and necessary for definitive granulopoiesis. This difference suggests the possibility that while Gata2a and Gata2b proteins carry out similar functions in granulocytes' progenitors, but the divergence of *gata2a* and *gata2b* expression patterns has temporally segregated them.

Current data suggests that Gata2a is required in myeloid cell development, during the primitive wave of haematopoiesis and also in the development of myeloid cells from EMPs (Bertrand et al., 2007). Results shown in section 4.3.3, using *gata2a*^{um27} mutant embryos, suggest that Gata2a is necessary for the development of primitive macrophages, as discussed in section 4.4.2. In contrast, experiments carried out using *gata2b* morphants (Butko et al., 2015), suggest that the development of primitive macrophages does not require Gata2b. However, it should be noticed that Butko and colleagues do not report quantifications of primitive macrophages (Butko et al., 2015), so the possibility of a subtle phenotype elicited by *gata2b* morpholino cannot be ruled out.

Myeloid cell development in caudal tissues is also affected in *gata2a*^{um27} mutant embryos (see section 4.3.3). As discussed in section 4.4.3, Gata2a has previously been shown to be necessary for the development of mast cells (Dobson et al., 2008) from the EMPs in the PBI and CHT (Da'as et al., 2012). Additionally, other types of granulocytes are affected by Gata2a deficiency in *gata2a*^{um27} mutant embryos. By 22 hpf, *gata2a*^{um27} mutant embryos exhibit a dose-dependent decrease in the number of *cebpα*$^{+}$ cells in the PBI, as shown in Figure 4.9.

The requirement of Gata2a and Gata2b for the development of neutrophils in zebrafish is particularly interesting, as the current evidence supports both the presence of conserved and divergent roles for them. Both Gata2a and Gata2b are required for the development of normal numbers of neutrophils, however, while Gata2a is required early in development, Gata2b is required for definitive haematopoiesis.

The critical role of Gata2a in the development of neutrophils from the primitive wave of haematopoiesis and EMPS is clearly exemplified by two results. Expression analysis of *mpx* gene showed that 32 hpf homozygous *gata2a*$^{um27/um27}$ mutant larvae have severely decreased numbers of neutrophils (see Figure 4.13). Similarly, quantifications of Sudan Black-stained cells in the CHT of *gata2a*^{um27} mutant embryos shows similar results by 48 hpf (see Figure 4.14). In contrast, Gata2b activity is dispensable for neutrophils' development at this stage. By 22 hpf, *gata2b*^{u5008} mutants show normal numbers of *mpx*$^{+}$ cells in the PBI (see Figure 5.7), and quantifications of granulocytes labelled with Sudan Black at 48 hpf also show normal development of neutrophils in all *gata2b* mutants (see Figure 5.8 and Figure 5.9).

Quantification of spi1b:EGFP^{+} cells in 30 hpf *gata2a*^{um27} mutant embryos expressing a transgenic reporter (see Figure 5.10) suggest that the effects of Gata2a deficiency on neutrophils' development could start earlier than 32 hpf. Consistently, the effect of *gata2a*^{um27} mutation on a population of *cebpα*$^{+}$ cells in the PBI of 22 hpf (see Figure 4.9), suggests that Gata2a acts on an early myeloid progenitor, resulting in wide effects on the granulocytes.

Further quantifications of Sudan Black^{+} cells in the CHT of double mutant *gata2a*^{um27}*; gata2b*^{u5008} embryos by 48 hpf (see Figure 5.12 a) shows that homozygous *gata2a*$^{um27/um27}$ mutant embryos displayed significantly decreased numbers of labelled neutrophils, regardless of the presence of *gata2b*^{u5008} mutations. No evidence of synergy between *gata2a*^{um27} and *gata2b*^{u5008} mutations was found. This is an important point, given that homozygous *gata2a*$^{um27/um27}$ mutations do not completely abolish the development of neutrophils in 48 hpf embryos (see Figure 4.14 and Figure 5.12 a), which could have been explained by a redundant transcriptional activity of Gata2b at that stage. However, this explanation is not supported by the observation that double homozygous *gata2a*$^{um27/um27}$*; gata2b*$^{u5008/u5008}$ embryos do not exhibit a stronger phenotype than *gata2a*$^{um27/um27}$*; gata2b*$^{+/u5008}$ or *gata2a*$^{um27/um27}$*; gata2b*$^{+/+}$ mutant embryos (see Figure 5.12 a).

Although data suggest that Gata2b is dispensable for the development of neutrophils from the primitive wave of haematopoiesis and from EMPs, the current results strongly suggest that Gata2b is critical for the development of definitive neutrophils. Sudan Black stainings carried out at 4 dpf show decreased numbers of labelled neutrophils in the CHT of *gata2b*^{u5008} larvae (see Figure 5.8 b) and also defects in the appearance of the primary granules (see Figure 5.8 c), which could be indicative of a defective differentiation. Further experiments combining *gata2a*^{um27} and *gata2b*^{u5008} mutations with the *Tg(lyz:nfsB-mCherry)* transgenic reporter line confirm the role of Gata2b in neutrophils' development at this stage, and show no effects on the number of labelled neutrophils of 4 dpf *gata2a*$^{+/um27}$ mutant larvae (see Figure 5.11 c). Similarly, quantifications of Sudan Black^{+} cells in the CHT of double mutant *gata2a*^{um27}*; gata2b*^{u5008} larvae at 4 dpf show that heterozygosity for *gata2b*$^{+/u5008}$ induces a significant reduction in the number of neutrophils regardless of *gata2a* genotype (see Figure 5.12 b). As mentioned before, the lack of synergy between *gata2a*^{um27} and *gata2b*^{u5008} mutations strongly

suggests that Gata2a and Gata2b do not have redundant functions in the development of neutrophils. In a different context, this is consistent with the failure of *gata2a* mRNA to rescue the lack of HSCs observed in *gata2b* morphants reported previously (Butko et al., 2015).

It could be hypothesised that although Gata2a and Gata2b have similar functions during granulopoiesis, the requirement for Gata2a seems to be restricted to primitive haematopoiesis and the myeloid cells derived from EMPs, while Gata2b is dispensable for primitive granulopoiesis, it is critical for definitive haematopoiesis.

5.4.4 Emergence of HSCs requires both Gata2b and Gata2a

GATA2 has been shown to be critical for both the emergence and survival of HSCs in mice (de Pater et al., 2013). Studies carried out *in vitro* with human cells have also found that GATA2 is required for EHT (Huang et al., 2015). In zebrafish, experiments carried out with *gata2b* morphants showed that the emergence of HSCs from the ventral wall of the DA through EHT requires Gata2b activity (Butko et al., 2015). Butko and colleagues reported that the vasculature develops normally in *gata2b* morphants, as the vascular and arterial markers *kdrl* and *efnb2a* are normally expressed (Butko et al., 2015). Consistent with this, no defects in blood circulation were observed in any of the *gata2b* mutant zebrafish lines generated by CRISPR/Cas9.

Results in Figure 5.14 show that both Gata2a and Gata2b are required for the emergence of HSCs, labelled as *cmyb*$^{+}$ cells, from the ventral wall of the DA. In the case of Gata2b, these results are consistent with results reported in *gata2b* morphants (Butko et al., 2015). Quantifications carried out at later stages in *Tg(itga2b:GFP)* transgenic fish suggest that heterozygous *gata2a*$^{+/um27}$ mutant larvae have a decreased number of HSCs in the CHT at 52 hpf, compared to that of their wild type siblings. However, by 72 hpf stage, no statistically significant difference is observed (Figure 4.18 h). In contrast with the results obtained by WISH analysis of *cmyb* expression, shown in Figure 5.14, quantifications carried out in fish expressing the *Tg(itga2b:GFP)* transgenic reporter have the

disadvantage that, in addition to HSCs, thrombocytes and their progenitors also express GFP (Lin et al., 2005).

The fact that some of homozygous *gata2a*$^{um27/um27}$ mutant larvae develop HSCs (see Figure 4.19) suggests the possibility that Gata2a is dispensable for the emergence of HSCs, or that the lack of Gata2a is rescued by another redundant mechanism, possibly Gata2b. However, *gata2a* mRNA injection is not able to rescue the production of HSCs in *gata2b* morphants (Butko et al., 2015), showing that Gata2b is indispensable for HSCs' emergence.

The recent findings reported by Tian and colleagues regarding the origin of the first lymphocytes observed in the thymi of zebrafish larvae (Tian et al., 2017) make it necessary to reinterpret the evidence found in *gata2b* morphants, about the role of Gata2b in early lymphopoiesis (Butko et al., 2015). It has been shown that all lymphocytes found in the thymi of 4 dpf arise from progenitors that emerge from the DA in a HSC-independent manner (Tian et al., 2017). The severe decrease in the expression of *rag1* gene observed in 4 dpf *gata2b* morphants (Butko et al., 2015) suggests that Gata2b is required for the emergence of these lymphoid progenitors from the DA, in a very similar way to *gata2a*^{um27} mutant embryos (see sections 4.3.6 and 4.4.6). Therefore, it could be hypothesized that Gata2a and Gata2b share a role in the emergence of lymphoid progenitors from endothelial cells in the DA.

5.4.5 Subfunctionalization of Gata2a and Gata2b

The evolution of teleost fish has been shaped by an event of whole genome duplication (Glasauer and Neuhauss, 2014) that occurred at the base of the teleost fish lineage (Amores et al., 1998; Postlethwait et al., 1998). Subfunctionalization, initially called duplication-degeneration complementation model (Force et al., 1999), is only one of the models that explain the retention of additional copies of genes produced by duplication events (Glasauer and Neuhauss, 2014). After two genes have been produced by duplication of a common ancestor, mutations and random genetic drift can lead to the loss of one of the duplicated genes, inactivation of one of the genes, or the loss of individual regulatory elements. The term subfunctionalization is used to describe those duplicated genes that have lost

functions and domains of expression through mutations, but together recapitulate the functions and expression of the ancestral gene (Force et al., 1999). Although the loss of one paralogue has been shown to be the most common fate after gene duplication (Jaillon et al., 2004; Woods et al., 2005), as observed in the GATA family of transcription factors (Gillis et al., 2009), subfunctionalization has also been reported in zebrafish (Fleisch et al., 2008; Renninger et al., 2011).

Based on differences in the expression patterns and functions of Gata2a and Gata2b, Butko and her colleagues proposed that Gata2a and Gata2b have undergone subfunctionalization (Butko et al., 2015). Considering the severe vasculature defects found in homozygous *gata2a*$^{um27/um27}$ mutant embryos (Zhu et al., 2011), and the critical role of Gata2b in the emergence of HSCs, Butko and her colleagues conclude that "Gata2a and Gata2b appear to additively fulfil the endothelial roles of GATA2, suggesting that duplication of the gata2 locus has led to an evolutionary separation of its endothelial and hematopoietic functions" (Butko et al., 2015).

Current data supports Butko and colleagues' view in terms of the endothelial functions of GATA2 in zebrafish. While Gata2b seems to be dispensable for the development of vasculature in both morphants (Butko et al., 2015) and mutants, there is abundant evidence showing the requirement for Gata2a in vascular morphogenesis and also in endothelial identity (Umamahesan, 2014; Zhu et al., 2011). An interesting example of the role of Gata2a in endothelial identity is the development of the first T lymphocytes from the DA in *gata2a*^{um27} mutant larvae (Figure 4.21). Analysis of the expression of *lck* gene in 4 dpf *gata2a*^{um27} mutant larvae, in Figure 4.21, shows that heterozygous *gata2a*$^{+/um27}$ mutant larvae have a wide range of phenotypes, ranging from normal expression to significantly decreased. It has been shown that T lymphocytes found in both thymi at this developmental stage arise from endothelial cells in the DA independently from HSCs (Tian et al., 2017).

However, the clean separation of endothelial and haematopoietic functions between Gata2a and Gata2b, respectively, that has been previously proposed (Butko et al., 2015), is refuted by data gathered about developmental haematopoiesis in *gata2a*^{um27} mutant fish (see sections 4.3.3, 4.3.4, and 4.3.6). The evidence supporting a role for Gata2a in primitive haematopoiesis is discussed in detail in sections 4.4.2 and 4.4.3. Results suggest an important role for Gata2a

in the myeloid cell development during the primitive wave of haematopoiesis and also in the myelopoiesis from EMPs. Expression analysis suggests that the differentiation of primitive macrophages in the yolk sac requires Gata2a. Additionally, there is evidence to suggest that Gata2a is critical for granulopoiesis in early development. Gata2a has been shown to be critical for mast cell production from EMPs (Da'as et al., 2012; Dobson et al., 2008). Additionally, results in section 4.3.3 show that Gata2a is necessary for the development of normal numbers of neutrophils, and possibly other cell types, in the PBI, which is discussed in detail in sections 4.4.3 and 5.4.3. Therefore, it is important to stress that the functions of Gata2a are not restricted to its role in the morphogenesis of the vasculature, and that both Gata2a and Gata2b carry out haematopoietic functions. Furthermore, as discussed in section 5.4.3, current data suggests that Gata2a carries out haematopoietic functions during the primitive wave of haematopoiesis (see sections 4.3.3 and 4.4.2), in mast cells' development from EMPs (Da'as et al., 2012; Dobson et al., 2008), in granulopoiesis (see sections 4.3.3 and 5.4.3), and in the generation of lymphocytes from the DA (see sections 4.3.6 and 4.4.6); while Gata2b is involved in the emergence and survival of HSCs, and also in definitive granulopoiesis.

6 Modelling MDS with loss of 5q using *rps14* mutants

6.1 Introduction

6.1.1 Rps14 deficiency in zebrafish morphants

MDS with del(5q) was modelled in zebrafish using knockdown of *rps14* with morpholinos. Payne and her colleagues (2012) injected *rps14* morpholinos in zebrafish embryos and achieved haploinsufficient levels of Rps14 protein in the morphants. The *rps14* morphant embryos, and also *rps19* morphants, displayed a severe phenotype with morphological abnormalities, such as reduced body length and eye diameter, together with severe anaemia, demonstrated by a striking decrease in the haemoglobinization of erythroid cells (Payne et al., 2012). Later work showed an increase in the mRNA levels of *tp53* in both *rps14* and *rps19* morphants. This is consistent with the previous observations in murine models, where haploinsufficiency for *Rps14* leads to p53 activation (Barlow et al., 2010; Schneider et al., 2016).

Evidence from different models suggests that haploinsufficiency for Rps14 disrupts ribosome assembly and induces p53 activation (reviewed in Komrokji et al., 2013). Payne and her colleagues (2012) hypothesized that activation of mRNA translation would rescue the phenotype observed in *rps14* morphants. After treatment with L-leucine, both *rps19* and *rps14* morphants exhibit partial rescue of their morphological defects and anaemic phenotype (Payne et al., 2012). Further work showed that L-leucine effect is independent of p53 (Narla et al., 2014). Additionally, the injection of *rps14* morpholino into a *Tp53* mutant genetic background does not rescue the phenotype of *rps14* morphants (Narla et al., 2014), in contrast to the partial recovery observed in murine models (Barlow et al., 2010; Schneider et al., 2016).

6.1.2 Effect of proinflammatory signalling through Toll-like receptors

Activation of mRNA translation by exposure to L-leucine, has been shown to induce a partial rescue of the phenotypes of *rps14* morphant embryos (Payne et al., 2012). The significant improvements observed in the morphology and haemoglobinization of *rps14* morphant embryos after treatment with L-leucine, served as well as a probe of principle for a screen of small molecules on these morphants (Jung, 2013). The screen takes advantage of the use of morpholinos, and the phenotype of the morphants. The use of morpholinos allows to obtain hundreds of morphants after one session of injection, without the need for further genotyping of embryos. On the other hand, the presence of a consistent morphological phenotype in the morphants allowed the running of a primary screen where the morphants exposed to each compound were screened under a dissecting microscope for rescue of their morphological defects (Jung, 2013).

Using this strategy, imiquimod (1-(2-methylpropyl)imidazo[4,5-c]quinolin-4-amine)) was identified as a molecule capable of inducing a partial rescue of the morphological defects and anaemic phenotype exhibited by *rps14* morphants (Jung, 2013). Imiquimod is a synthetic agonist of both TLR7 and TLR8 (Hemmi et al., 2002; Jurk et al., 2002). The effects of imiquimod treatment on *rps14* morphants suggest that TLR signalling pathways play a role in del(5q) pathogenesis. In this chapter the effect of TLR signalling modulation by imiquimod is shown in *rps14* mutant fish, and evidence for a role for TLR7 activation in erythroid cell development is presented.

6.1.3 Aims of the experiments described in this chapter

1. To define the phenotype of *rps14* haploinsufficiency in the developmental haematopoiesis in zebrafish.
2. To study the effects of TLR7 and TLR8 pathway modulation in erythroid development.

6.2 Methods

6.2.1 Fish husbandry

The zebrafish line carrying a mutation in *rps14* gene[4] (ENSDARG00000036629.5) used in the experiments presented in chapter 6 was generated in research group of Dr Elspeth Payne by using TALENs. TALENs were designed to target exon 2 of the zebrafish *rps14* gene using the online tool Zifit targeter (http://zifit.partners.org/ZiFiT). Assembly of TALENs[5] was carried out using fast ligation-based assembly solid phase high-throughput (FLASH), as described previously (Reyon et al., 2013). Synthesis of TALEN mRNAs was carried out by *in vitro* transcription using mMESSAGE mMACHINE T7 kit (AM1344, Ambion). TALEN mRNAs were injected into 1-cell stage embryos, and F0 founders were identified by isolation of gamete cells and NGS, in a similar way to that described for *gata2b* mutant fish in sections 5.2.7 and 5.2.6, respectively.

One mutant zebrafish line was isolated, carrying a complex deletion-insertion in the *rps14* gene, g.26_38delinsGA, encoding a mutant protein with a frameshift in amino acid residue 9, p.(Lys9ArgfsTer19). This mutant *rps14* allele is herein named E8fs for the sake of simplicity.

6.2.2 Genotyping of *rps14*^{E8fs} mutant fish

The genotyping of *rps14*^{E8fs} mutants was carried out in a different way to that used for *gata2a*^{um27} (see section 4.2.2) and *gata2b*^{u5008} (see section 5.2.8), by using only amplification by PCR and analysis by gel electrophoresis. The *rps14*^{E8fs} mutants carry an 11 bp deletion in the first coding exon of *rps14* gene (see section 6.2.1 for details). To identify the *rps14*^{E8fs} mutant alleles in the samples, a standard PCR reaction was carried out using primers flanking the region of *rps14* gene with the deletion (shown in Table 6.1).

[4] The *rps14* zebrafish mutant line used in the experiments presented in this chapter was generated in Dr Elspeth Payne's research group and is not part of this doctoral work.

[5] TALENs used to generate the *rps14* zebrafish mutant line were synthetized by Leonardo E. Valdivia and Karin Tuschl.

Table 6.1 | Primers used for *rps14*^{E8fs} genotyping.

Primer name	Sequence (5' to 3')	Length	%GC	Tm
rps14 gdna for	TGTTCTGACTGTTGACTGTGTGTT	24	41.7	60.8
rps14_rev151	GGTGTCGTTGAAGGATGCGA	20	55.0	60.7

The Table 6.2 shows the components and concentrations of the PCR used for *rps14*^{E8fs} genotyping. The volumes shown are calculated for one 25 µL reaction and were scaled up for large numbers of samples. Details about dNTPs, the DNA polymerase used, and its reaction buffer are available in section 2.7.

Table 6.2 | Components and concentrations of PCR for *rps14*^{E8fs} genotyping.

Reagent	Volume per reaction [µL]	Final concentration
10x Standard Taq buffer	2.5	1x
10 mM dNTPs	1	400 µM
10 µM rps14 gdna for	1	0.4 µM
10 µM rps14_rev151	1	0.4 µM
Standard Taq Polymerase	2	1 unit
genomic DNA	5	variable
nuclease free water	12.5	-

The genomic DNA of cells, embryos, or fin clips from adults was used as a template for the PCR shown in Table 6.2 with the primers shown in Table 6.1. The cycling conditions for this PCR are detailed in the Table 6.3.

Table 6.3 | Cycling conditions used in PCR for *rps14*^{E8fs} genotyping

Phase		temperature [°C]	time [s]
initial denaturation		95	30
34 cycles	denaturation	95	15
	annealing	56	30
	extension	68	30
final extension		68	5 minutes

The PCR products were then visualized by electrophoresis in agarose / metaphor gels (1.75% w/v agarose, 1.75% w/v metaphor). Metaphor agarose was used in combination with agarose to achieve resolution of the PCR products expected: 151 bp from the wild type *rps14* allele, and 140 bp from the mutant *rps14*^{E8fs} allele. The genotypes were read from the PCR products in the gels as explained in the Table 6.4:

Table 6.4 | Band patterns expected for each *rps14*^{E8fs} genotype.

Genotype	Number of bands	Band sizes [bp]
Wild type (+/+)	1	151
Heterozygote (+/E8fs)	2	151 140
Homozygote (E8fs/E8fs)	1	140

6.2.3 Quantification of circulating thrombocytes and heart rate

In order to quantify the number of circulating thrombocytes in *rps14*^{E8fs} mutant larvae, a similar method to that previously used for neutrophils (Paredes-Zúñiga et al., 2017; Walters et al., 2010) was used. Transgenic fish carrying the *Tg(itga2b:GFP)* transgene were used, in which thrombocytes expressing high levels of GFP can be observed in the blood circulation from 3 dpf (Lin et al., 2005).

Similarly to the method used to measure neutrophils in the blood circulation (Walters et al., 2010), instead of measuring the total number of thrombocytes in the blood stream at a given time point, the number of thrombocytes passing through a point of the dorsal aorta during a given period of time was quantified.

Given that anaesthesia is expected to alter the number of circulating blood cells, all larvae were anesthetized in the same way, and data acquisition was carried out under controlled conditions, as previously described (Paredes-Zúñiga et al., 2017). Heart rates were also measured for each larva as an internal control. Each larva was anesthetized by exposure to 0.08 g/L 3-aminobenzoate methanesulfonate in E3 for 1 minute, and then a real-time movie of the blood circulation in the dorsal aorta over the end of the extension of the yolk was acquired in the GFP channel during the following 2 minutes using a Leica M205 FA stereoscope. This was followed by the acquisition of another real-time movie, in bright field of the heart of the larva. Then the larva was put in a 48-well plate for *rps14*^{E8fs} genotyping (see section 6.2.2). This procedure was repeated with each larva in the experiments shown in Figure 6.7.

The number of itga2b:GFP^{high} cells circulating through the dorsal aorta during the 2 minutes-long movies was quantified from the movies acquired, and the results are shown as [itga2b:GFP^{+}/minutes]. Similarly, heart rates were quantified from the movies acquired of fish's hearts.

6.2.4 Rps14 and Gata1a knockdown with morpholinos

Morpholinos targeting zebrafish *rps14* and *gata1a* genes were used in the knockdown experiments shown in section 6.3.2, as described previously (Narla et al., 2014; Payne et al., 2012). For knockdown of Rps14, a morpholino targeting the boundary between exon 2 and intron 2 of *rps14* was used (see Table 6.5). The morpholino used to knockdown Gata1a targets the 5' UTR of *gata1a* (see Table 6.5). In both cases, Gene-Tools standard control was injected as a negative control. The standard control morpholino targets a mutant variant of human haemoglobin subunit beta (*HBB*) gene sequence found in the pre-mRNA of *HBB* in the reticulocytes of thalassaemic humans, without predicted targets in the zebrafish transcriptome (see Table 6.5). In this way, all the embryos used in the

experiment have been microinjected with a morpholino, and the toxic effects are present in all the fish, allowing to make comparisons among groups (Heasman, 2002).

Morpholinos for *rps14, gata1a,* and the standard control were injected into 1-cell stage embryos as described in section 2.6. The amounts depicted in Table 6.5 were injected together with 10% v/v Phenol red, to allow the identification of those embryos successfully injected.

Table 6.5 | Morpholino sequences and doses injected.

gene targeted	type	Sequence (5' to 3')	amount [ng]
rps14	exon 2 - intron 2	CAGGTTTTCAGGATACATACTTGCC	0.8
gata1	5' UTR	CTGCAAGTGTAGGTATTGAAGATGTC	4
standard control	(details in text)	CCTCTTACCTCAGTTACAATTTATA	0.8

6.2.5 Anatomical and fluorescence measurements

Anatomical measurements in experiments from Figure 6.9 and Figure 6.10 were carried out using Fiji version v1.49u software (Schindelin et al., 2012). For measurements of body length, whole mount bright field images of each larva were acquired with a Leica M205 FA fluorescent dissecting stereoscope equipped with a Leica DFC 365 FX camera. Then Fiji software was used to measure the length of each larva by drawing a segmented line going from the most anterior part of the jaw to the beginning of the notochord, and following the notochord until the tip of the tail. Similarly, the diameter of the left eye of each larva was measured as the length of a straight line crossing the eye diametrically along the dorso-ventral axis.

In the case of measurements of intensity of fluorescence in Figure 6.10, images of the CHT of each *Tg(gata1a:dsRed)* transgenic larva in both the dsRed and bright field channels were acquired using the identical settings. Using the bright field pictures, a polygon surrounding the CHT of each larva was drawn with Fiji

software, and the intensity of fluorescence within the polygon was measured in dsRed channel. The area of the polygon was measured too in each case, to be used as an internal control.

6.2.6 Exposure of fish to TLR agonists

Pharmacological modulation of Toll-like receptors (TLR) was carried out by immersion of embryos from 24 hpf for variable times of incubation. Imiquimod (CAY14956, Cayman), an agonist of both TLR7 and TLR8 receptors (Hemmi et al., 2002; Jurk et al., 2002); gardiquimod (SML0877, Sigma), a TLR7 agonist (Zhu et al., 2008); and motolimod, a TLR8 agonist (Lu et al., 2012), were diluted in DMSO (dimethyl sulfoxide) to a stock concentration of 10 mM.

For experiments, the stock solutions of all agonists were diluted in E3 medium at the concentrations indicated for each experiment. Groups of embryos were treated with maximum equivalent concentration of DMSO as negative control in each experiment.

6.2.7 Exposure of fish to cold stress during embryonic development

For experiments in Figure 6.12, cold stress was induced in *rps14*^{E8fs} mutant embryos by exposure to 22 °C during early development. The embryos were allowed to grow at 28 °C during the earliest phases of development, gastrulation and the beginning of somitogenesis, to obtain low mortality and a maximum number of embryos without gross morphological abnormalities. By 6 ss (12 hpf) the embryos were placed in an incubator at 22 °C, and kept until they reached prim-22 developmental stage (36 hpf).

6.2.8 Induction of haemolytic stress

For experiments involving haemolytic stress in sections 6.3.3 and 6.3.4. Haemolytic stress was induced by exposure of embryos to phenylhydrazine (PHZ), under conditions described previously (Lenard et al., 2016; Shafizadeh et al., 2004). Embryos were incubated in 1 µg/mL PHZ from 24 hpf to 48 hpf. For

recovery, PHZ was washed with E3 three times, and embryos were incubated in E3 for recovery for the time periods indicated in each experiment.

6.2.9 Flow cytometry of zebrafish larvae

For flow cytometry experiments shown in Figure 6.14 c and d, individual larvae were placed in 3mL of cooled 1% FBS (foetal bovine serum) PBS in MACS tubes (130-093-237, Miltenyi Biotec) and kept on ice. Positive and negative control tubes were included with fish carrying the transgenic reporter and fish without fluorescence, respectively. Fish were then dissociated on a gentleMACS Octo dissociator (130-095-937, Miltenyi Biotec). The content of the MACS tubes was transferred to a flow tube with strainer (352235, Corning), and centrifuged at 400rcf for 5 minutes at 4 °C. The supernatant was discarded, and the remining volume was resuspended in a total volume of 339 µL of DPBS (14190-169, Sigma-Aldrich) with 1% FBS. Then 10 µL of flow Check Fluorospheres (6605359, Beckman Coulter) and 1 µL of 10% Hoechst (33342, Invitrogen) dilution were added to each tube. Flow cytometry of the samples was carried out in a LSRFortessa X20 cell analyser machine (LSRFORTESSA X-20, BD Biosciences) and results were analysed using FlowJo Version 10 (FlowJo).

6.3 Results

6.3.1 Developmental haematopoiesis in *rps14*^{E8fs} mutant fish

Haemoglobinization of erythroid cells was studied in *rp14*^{E8fs} mutant fish by using *o*-dianisidine staining, which is described in detail in section 2.4. Figure 6.1 shows images of representative *rps14*^{E8fs} mutant fish stained with *o*-dianisidine at 48 hpf (Figure 6.1 a-c') and at 4 dpf (Figure 6.1 d-f'). A ventral view of the head of a 48 hpf wild type embryo, in Figure 6.1 a, and a lateral view of the trunk, in Figure 6.1 a', show the normal pattern of haemoglobinization observed at this developmental stage. Most of erythroid cells containing haemoglobin locate in the heart (Figure 6.1 a), and along the DA and CV (Figure 6.1 a'). The heterozygous *rps14*$^{+/E8fs}$ mutant embryos display a normal pattern of haemoglobinization (Figure 6.1 b and b'), indistinguishable from that of wild type embryos (Figure 6.1 a and a'). In contrast with heterozygotes, homozygous *rps14*$^{E8fs/E8fs}$ mutant embryos show a severe decrease in the degree of *o*-dianisidine staining, suggesting an also reduced number of erythrocytes (Figure 6.1 c and c'). Haemoglobinization in *rps14*$^{E8fs/E8fs}$ embryos is decreased throughout the body, but not completely abolished (see labelled cells over the yolk in Figure 6.1 c). Detectable levels of erythrocytes stained with *o*-dianisidine were found in all the homozygous *rps14*$^{E8fs/E8fs}$ mutant embryos analysed.

Staining with *o*-dianisidine were also carried out in 4 dpf *rps14*^{E8fs} mutant larvae to assess the haemoglobinization of erythroid cells once definitive haematopoiesis has already started. Figure 6.1 shows images of representative *rps14*^{E8fs} mutant larvae stained with *o*-dianisidine at 4 dpf. Ventral view of the head of wild type *rps14*$^{+/+}$ larvae displays abundant labelled erythrocytes in the heart, PHS, both primitive internal carotid arteries (PICA), and other vessels (Figure 6.1 d). In contrast, erythroid cells stained with *o*-dianisidine are far less abundant in the tail. Scattered labelled cells are seen along the DLAV, the DA, and mostly along the CV (Figure 6.1 d'). As found with 48 hpf embryos, at 4 dpf heterozygous *rps14*$^{+/E8fs}$ mutant larvae display a similar pattern of haemoglobinization (Figure 6.1 e and e') to that observed in wild type larvae (Figure 6.1 d and d'). In the case of 4 dpf homozygous *rps14*$^{E8fs/E8fs}$ mutant larvae, the developmental delay and the decrease in *o*-dianisidine staining are even more severe than what was found in 48 hpf embryos. However, haemoglobinization is not abolished in *rps14*$^{E8fs/E8fs}$

homozygotes. Labelled erythroid cells can be observed in the heart, PHS (Figure 6.1 f), and along the CV (Figure 6.1 f'), showing that erythroid differentiation can proceed in spite of the Rps14 deficiency.

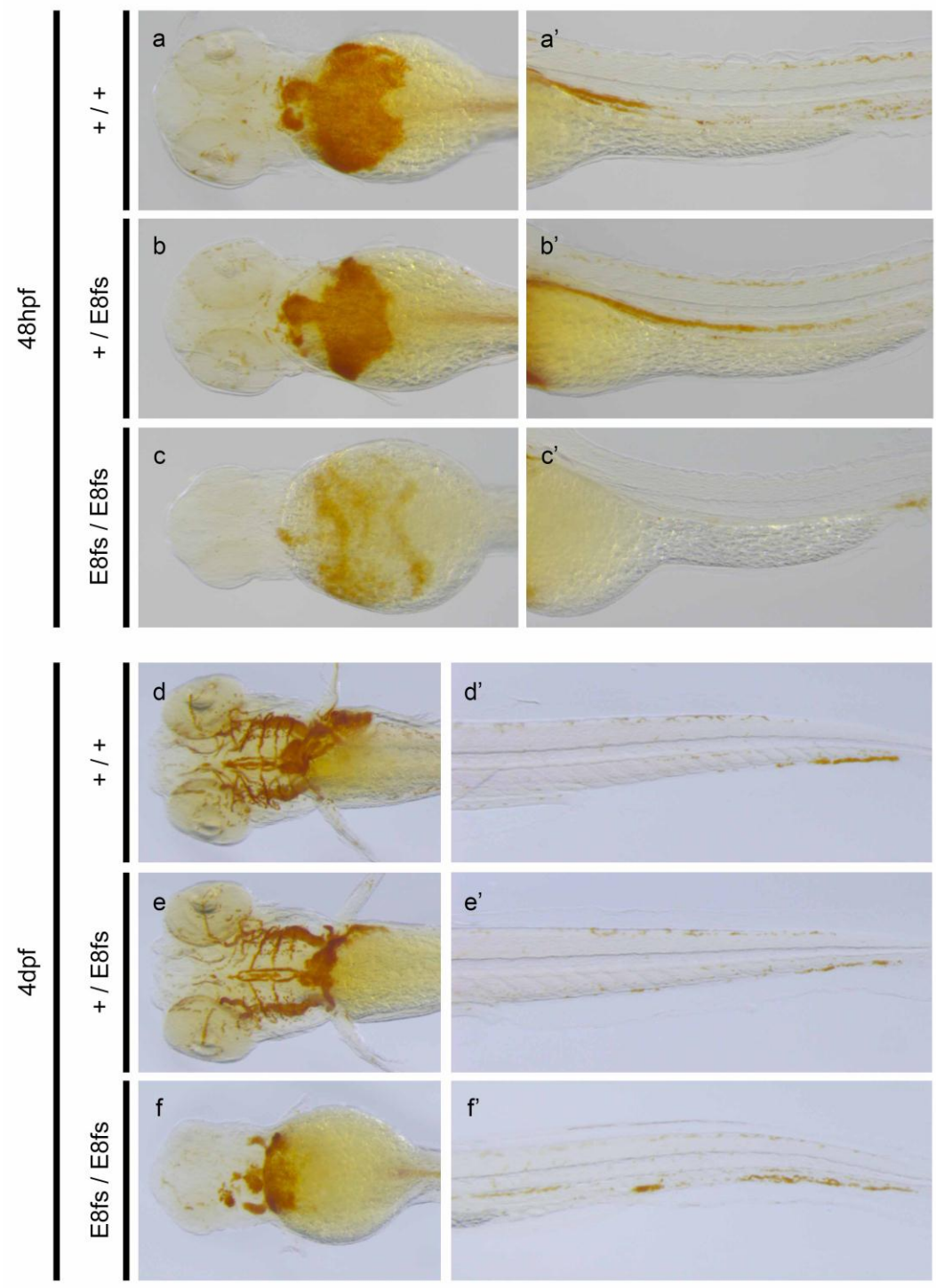

Figure 6.1 | Haemoglobinization of erythroid cells in *rsp14^{E8fs}* mutant fish.

O-dianisidine staining was used to label haemoglobin in the erythroid cells of 48 hpf **(a-c and a'-c')** and 4 dpf **(d-f and d'-f')** *rps14^{E8fs}* mutant fish. Images of wild type **(a, a', d, and d')**, heterozygous *rps14$^{+/E8fs}$* **(b, b', e, and e')**, and homozygous *rps14$^{E8fs/E8fs}$* mutant **(c, c', f, and**

f') larvae are shown. **(a-f)** Ventral views of the heads of larvae. **(a'-f')** Lateral views of the trunk and tails of larvae. All images show anterior to the left.

The development of granulocytes in *rps14*^{E8fs} mutant embryos by Sudan Black staining, which accumulates in their primary granules (Sheehan and Storey, 1946). Mutant embryos were stained at 48 hpf with Sudan Black, as described in section 2.3, and quantifications together with imaging were carried out. Figure 6.2 a-c show images of the tails of representative *rps14*^{E8fs} mutant embryos stained with Sudan Black at 48 hpf. In the wild type *rps14*$^{+/+}$ embryos, most of the labelled granulocytes reside in the CHT, and a few of them can be found along the dorsal ridge and the myoseptum (Figure 6.2 a), as previously described (Le Guyader et al., 2008). As observed before in the haemoglobinization of erythroid cells (Figure 6.1), heterozygous *rps14*$^{+/E8fs}$ mutant embryos show a similar pattern of Sudan Black staining (Figure 6.2 b). In contrast, homozygous *rps14*$^{E8fs/E8fs}$ mutant embryos exhibit severely decreased number of labelled granulocytes (Figure 6.2 c). These results suggest that Rps14 has a role in primitive granulopoiesis.

The number of granulocytes stained with Sudan Black was quantified in the CHT of 48 hpf *rps14*^{E8fs} mutant embryos (Figure 6.2 d). The results show a dose-dependent decrease in the number of labelled granulocytes, which suggest a role for Rps14 in granulopoiesis (Supplementary Table 9.44). However, labelled granulocytes were observed in all homozygous *rps14*$^{E8fs/E8fs}$ mutant embryos analysed, showing that the development of granulocytes can proceed to the formation of primary granules in embryos lacking wild type Rps14.

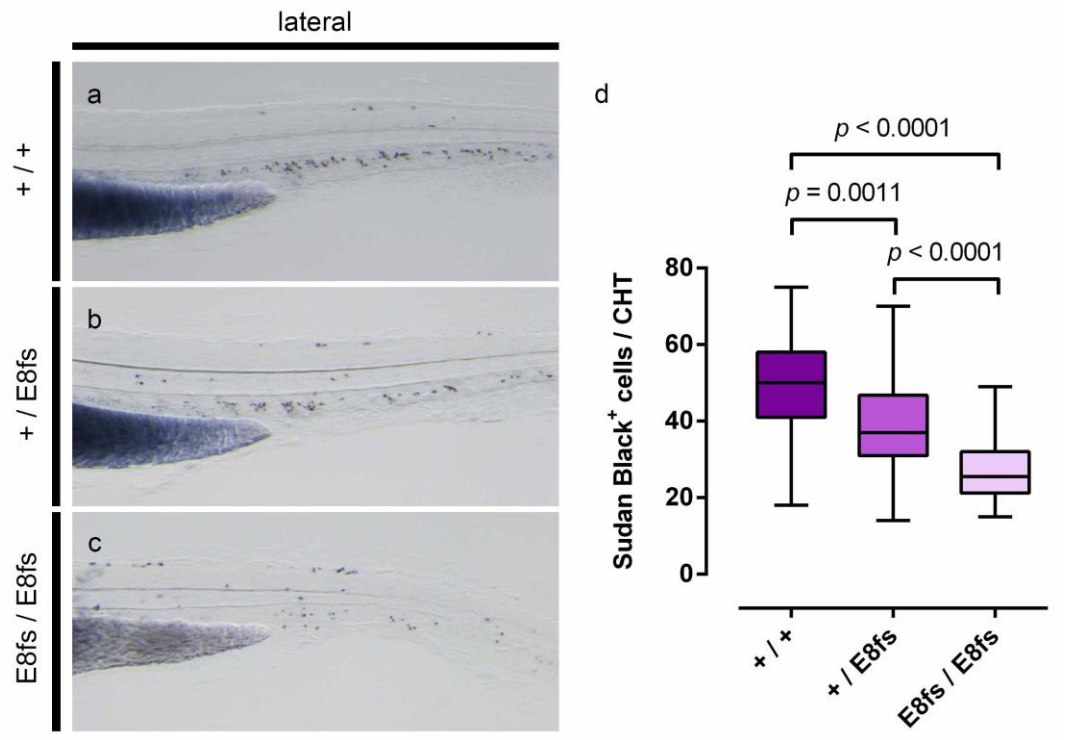

Figure 6.2 | Dose dependent decrease in the number of Sudan Black$^+$ granulocytes in the CHT of 48 hpf *rps14^{E8fs}* embryos.

Sudan Black was used to label the granulocytes of 48 hpf *rps14^{E8fs}* mutant embryos. **(a-c)** Lateral views of the trunk and tails of representative wild type **(a)**, heterozygous **(b)**, and homozygous mutant **(c)** embryos stained with Sudan Black are shown. All images show anterior to the left. **(d)** Quantification of Sudan Black$^+$ granulocytes in the CHT of 48 hpf *rps14^{E8fs}* embryos. Statistical comparison was carried out by one-way ANOVA ($p < 0.0001$) followed by Tukey's multiple comparisons test (individual *p*-values shown in the graph). See Supplementary Table 9.44 for more details.

Given that the results in Figure 6.2 show a dose-dependent decrease in the number of Sudan Black$^+$ cells in the CHT, that suggests that Rps14 has a role in primitive granulopoiesis, further experiments were carried out at later developmental stages to determine whether definitive granulopoiesis also requires Rps14. Granulocytes were stained using Sudan Black in 4 dpf *rps14^{E8fs}* mutant larvae, quantifications of labelled cells in the CHT were carried out and images

acquired. Figure 6.3 a-c show images of the tails of representative larvae stained with Sudan Black are shown. Sudan Black is accumulated in the primary granules of granulocytes (Sheehan and Storey, 1946), which in wild type larvae reside in the CHT, while low numbers of granulocytes can also be found along the dorsal ridge (Le Guyader et al., 2008). The images of wild type *rps14*$^{+/+}$ and heterozygous *rps14*$^{+/E8fs}$ mutant larvae show normal distribution of granulocytes in the CHT in apparently normal numbers (Figure 6.3 a and b, respectively). In a similar way as found in 48 hpf embryos in Figure 6.2 c, the number of labelled granulocytes in the CHT of 4 dpf homozygous *rps14*$^{E8fs/E8fs}$ mutant larvae is severely decreased (Figure 6.3 c).

The number of Sudan Black^{+} cells in the CHT of 4 dpf *rps14*^{E8fs} mutant larvae was quantified, and the results are depicted in Figure 6.3 d. Statistical analysis shows that there is a dose-dependent decrease in the number of labelled granulocytes in the CHT of 4 dpf larvae (Supplementary Table 9.45), in close agreement with was observed in 48 hpf embryos (Figure 6.2 and Supplementary Table 9.44). It should be noticed that in heterozygous *rps14*^{E8fs} mutant larvae, the numbers of labelled granulocytes found in the CHT increase from 48 hpf (38.75 ± 1.761, Supplementary Table 9.44) to 4 dpf (124.5 ± 7.9, Supplementary Table 9.45); while the number of Sudan Black^{+} cells in the CHT of homozygous *rps14*$^{E8fs/E8fs}$ mutant fish remains constant from 48 hpf (26.54 ± 1.494, Supplementary Table 9.44) to 4 dpf (28.39 ± 1.840, Supplementary Table 9.45). These results suggest that Rps14 deficiency in *rps14*$^{E8fs/E8fs}$ homozygotes causes a major disruption in the definitive granulopoiesis. It is also important to mention that heterozygous *rps14*$^{+/E8fs}$ mutant larvae display lower numbers of Sudan Black^{+} cells in the CHT than their wild type siblings, showing that Rps14 haploinsufficiency affects definitive granulopoiesis.

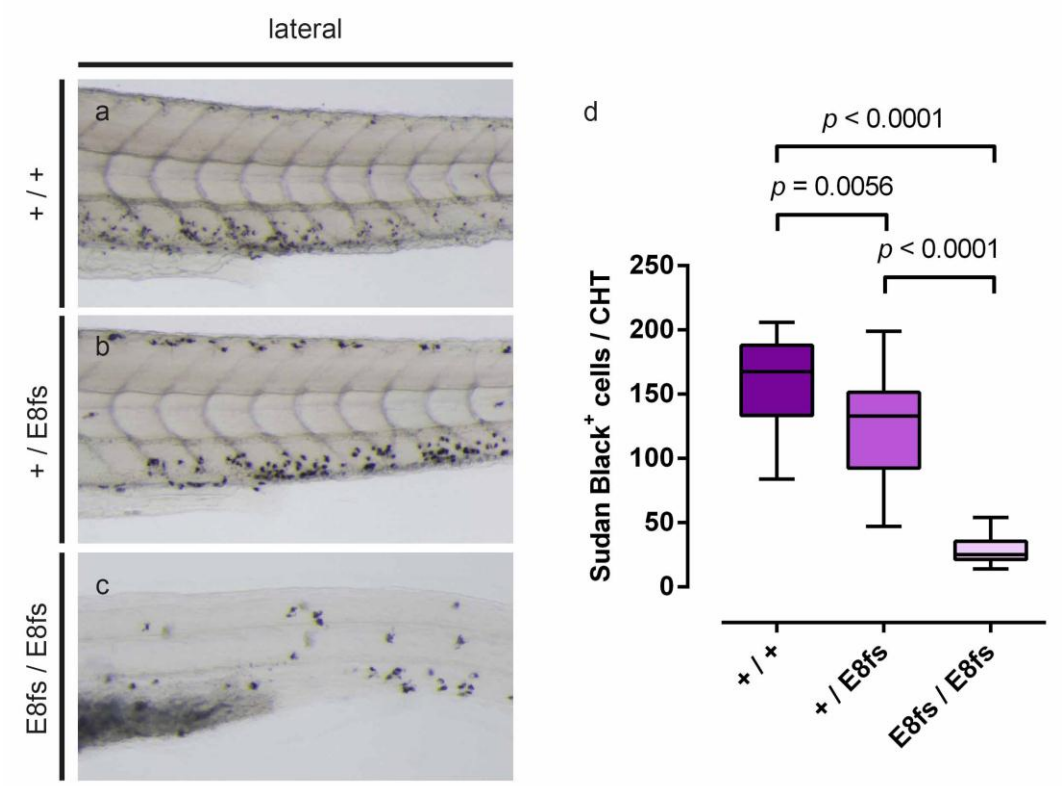

Figure 6.3 | Dose dependent decrease of the number of Sudan Black$^+$ granulocytes in the CHT of 4 dpf *rps14*^{E8fs} mutant larvae.

Granulocytes of 4 dpf *rps14*^{E8fs} mutant larvae were labelled with Sudan Black staining. In **(a-c)**, lateral views of the trunk and tails of representative wild type **(a)**, heterozygous **(b)**, and homozygous mutant **(c)** larvae are shown with anterior to the left. **(d)** Quantification of Sudan Black$^+$ granulocytes in the CHT of 4 dpf *rps14*^{E8fs} larvae. Statistical comparison was carried out by one-way ANOVA (p < 0.0001) followed by Tukey's multiple comparisons test (individual p-values shown in the graph). See Supplementary Table 9.45 for more details.

Given that results in Figure 6.3 show a decrease in the number of Sudan Black$^+$ granulocytes in 4 dpf *rps14*^{E8fs} mutant larvae, additional experiments were carried out to study definitive granulopoiesis at a later developmental stage. In zebrafish, after a transient period of definitive granulopoiesis carried out in the CHT (Murayama et al., 2006), haematopoietic progenitors colonize the kidney (Bertrand

et al., 2008), where Sudan Black^{+} definitive granulocytes can be seen as soon as 7 dpf and granulopoiesis occurs until adulthood (Le Guyader et al., 2008). By 8 dpf, *rps14*^{E8fs} mutant larvae were stained with Sudan Black, as described in section 2.3, and then imaged under a stereoscope (described in section 2.12). Figure 6.4 a and b, shows lateral views of the anterior part of a wild type *rps14*$^{+/+}$ larvae stained with Sudan Black at 8 dpf. The area of the kidney is inside the white rectangle in Figure 6.4 a. Figure 6.4 b shows the area of the kidney at higher magnification, where several Sudan Black^{+} granulocytes are clustered together. A very similar pattern was observed in heterozygous *rps14*$^{+/E8fs}$ mutant larvae, depicted in Figure 6.4 c and d, suggesting that granulopoiesis is normal in heterozygotes by 8 dpf. The close clustering of the labelled cells in the kidney made it impossible to carry out reliable quantifications of the cells (see Figure 6.4 b and d), and therefore, subtle differences in number of granulocytes in the kidney could not be detected with the same precision as done previously in the CHT of 4 dpf larvae (Figure 6.3 d). No images of homozygous *rps14*$^{E8fs/E8fs}$ mutant larvae are shown because all homozygous larvae die before reaching 8 dpf.

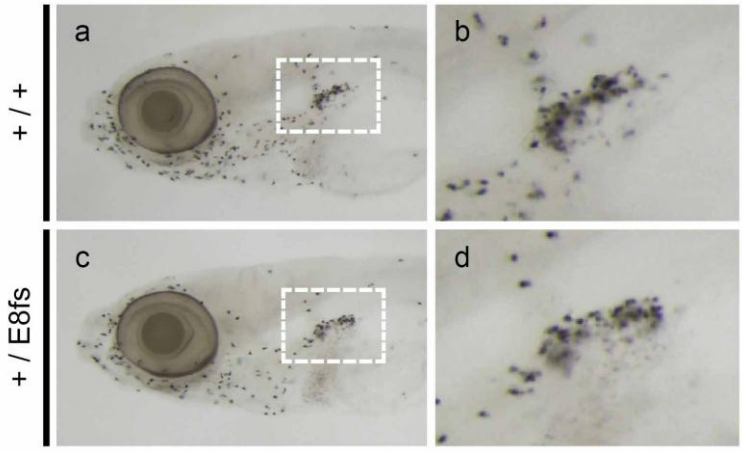

Figure 6.4 | Normal definitive granulopoiesis in the kidney of *rps14*^{E8fs} mutant larvae at 8 dpf.

Sudan Black staining was used to label the granulocytes of *rps14*^{E8fs} mutant fish at 8 dpf. In **(a and c)**, lateral views of the heads of representative wild type **(a)**, heterozygous *rps14*$^{+/E8fs}$ **(c)** fish are shown. The dashed lines in **(a and c)** encircle the area of the kidney,

showed at higher magnification in **(b and d)**, respectively. All images show anterior to the left.

The decreased number of Sudan Black^{+} granulocytes found in the CHT of both heterozygous and homozygous *rps14*^{E8fs} mutant larvae at 4 dpf (see Figure 6.3) suggests that definitive haematopoiesis is affected by *rps14*^{E8fs} mutation. It could be hypothesized that the observed decrease in the number of definitive granulocytes is caused by defective HSCs in the CHT. Compound double transgenic *rps14*^{E8fs} mutant larvae expressing both *Tg(lyz:nfsB-mCherry)* and *Tg(itga2b:GFP)* transgenes were obtained by outcross to assess both HSC and granulopoiesis in the same fish, and both quantifications of labelled cells in the CHT and imaging were carried out in 3 dpf larvae. Figure 6.5 shows images of both heterozygous *rps14*$^{+/E8fs}$ larvae (Figure 6.5 a'-d') and their wild type *rps14*$^{+/+}$ siblings (Figure 6.5 a-d) at 3 dpf. Heterozygote larvae exhibit normal morphology (Figure 6.5 a'), and its myeloid cells (Figure 6.5 c'), as well as its HSCs and other itga2b:GFP^{low} progenitors (Figure 6.5 b') reside in the CHT in apparently normal numbers, when compared to a wild type larva (Figure 6.5 a-d).

Quantifications of the cells labelled with fluorophores by both reporter lines were carried out in these larvae (Figure 6.5 e and f). Figure 6.5 e shows the normalized number of itga2b:GFP^{low} cells observed in the CHT of 3 dpf *rps14*^{E8fs} mutant larvae expressing the *Tg(itga2b:GFP)* transgenic reporter. Although the statistical comparison between groups shows no evidence of a significant difference between heterozygous *rps14*$^{+/E8fs}$ mutant larvae and their wild type siblings (p = 0.170, Supplementary Table 9.46), it is important to notice the wide range of variability of the data in the heterozygous group suggests that heterozygosity for *rps14* gene could affect the number of HSCs in a fraction of the heterozygous larvae.

Similarly, the number of lyz:nfsB-mCherry^{+} cells was quantified in the CHT of 3 dpf *rps14*^{E8fs} mutant larvae, and the results show that there is no significant difference between heterozygous larvae and their wild type siblings (p = 0.821, Supplementary Table 9.47). Previous reports using transgenic lines with the same promoter used in *Tg(lyz:nfsB-mCherry)* transgenic fish, suggest that lyz:nfsB-mCherry^{+} cells at this developmental stage are mainly neutrophils (Hall et al., 2007). In the same way, it has been suggested that Sudan Black staining labels

preferentially neutrophils in zebrafish larvae (Le Guyader et al., 2008). Therefore, it was reasoned that both experiments shown in Figure 6.3 and Figure 6.5 were comparing the numbers of neutrophils between groups, and that heterozygous *rps14*^{E8fs} mutant larvae have normal numbers of neutrophils in the CHT by 3 dpf, but by 4 dpf, their number is significantly decreased, compared to that of their wild type siblings. The fact that a difference in the number of neutrophils in the CHT between heterozygotes and wild type larvae seems to arise between 3 dpf and 4 dpf suggests that this is due to a defect in the number or function of HSCs.

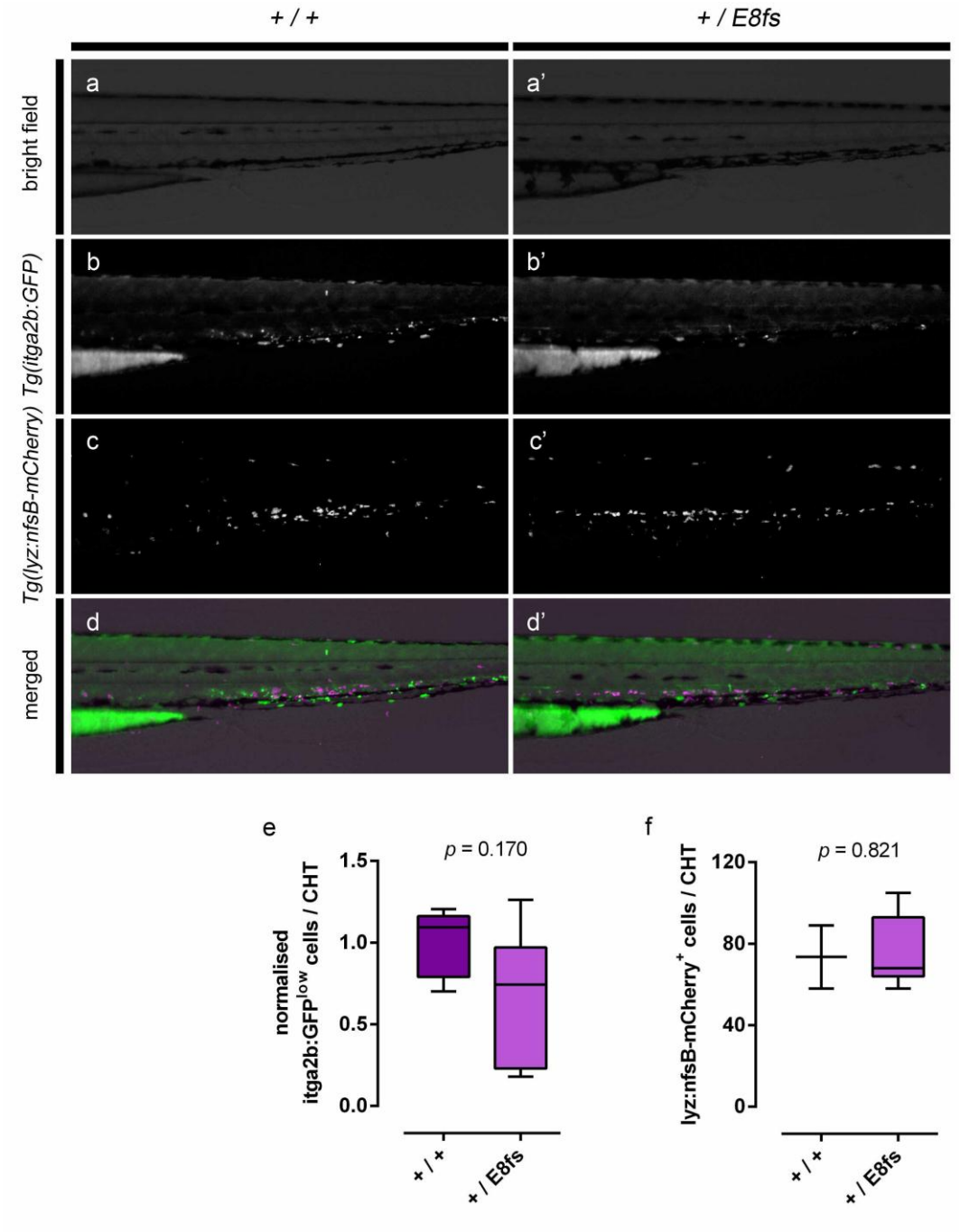

Figure 6.5 | Imaging and quantifications of itga2b:GFP^{low} and lyz:nfsB-mCherry^{+} cells in the CHT of 3 dpf *rps14^{E8fs}* mutant larvae.

Compound double transgenic *Tg(itga2b:GFP); Tg(lyz:nfsB-mCherry); rps14^{E8fs}* mutant fish were obtained by outcrossing homozygous *Tg(lyz:nfsB-mCherry)$^{+/+}$* adult fish to *Tg(itga2b:GFP)$^{+/-}$; rps14$^{+/E8fs}$* adult fish. In **(a-d and a'-d')**, lateral views of the tails of 3 dpf representative wild type **(a-d)** and heterozygous *rps14$^{+/E8fs}$* mutant

(a'-d') larvae are shown. Images of bright field **(a and a')**, GFP **(b and b')**, and mCherry **(c and c')** channels are shown along with images of all three channels merged **(d and d')**. All images show anterior to the left. In **(e and f)**, quantifications of itga2b:GFP^{low} **(e)** and lyz:nfsB-mCherry^{+} **(f)** cells in the CHT of 3 dpf *rps14*^{E8fs} mutant larvae are shown. Statistical comparisons in both **(e and f)** were carried out by Mann Whitney test (*p*-values shown). See Supplementary Table 9.46 and Supplementary Table 9.47 for more details about **(e)** and **(f)**, respectively.

Imaging and quantifications of HSCs and other haematopoietic progenitors expressing itga2b:GFP were carried out in 4 dpf *rps14*^{E8fs} mutant larvae carrying the *Tg(itga2b:GFP)* transgene. Figure 6.6 a-c' show lateral images of the trunk and tail of 4 dpf *rps14*^{E8fs} mutant larvae expressing the *Tg(itga2b:GFP)* transgene. As mentioned before, heterozygous larvae exhibit a normal morphology, and their itga2b:GFP^{low} cells reside in the CHT (Figure 6.6 b and b'), in the same way as observed in their wild type siblings (Figure 6.6 a and a'). In contrast, homozygous *rps14*$^{E8fs/E8fs}$ mutant larvae exhibit a severe delay in development at this stage, with cardiac oedema, antero-posterior axis ventrally curved, among other defects (Figure 6.6 c). Figure 6.6 c' shows that itga2b:GFP^{low} cells are almost absent in the CHT, and irregular patches of fluorescence can be seen in the skin, which are likely to be auto-fluorescence observed in necrotic tissues in zebrafish embryos.

The number of itag2b:GFP^{low} cells in the CHT of 4 dpf *rps14*^{E8fs} mutant embryos was quantified under a fluorescence stereoscope, and the results are shown in Figure 6.6 d as the number of itag2b:GFP^{low} cells normalized to that of the wild type group. The statistical analysis shows that there is a dose-dependent decrease in the number of itga2b:GFP^{low} cells in the CHT of *rps14*^{E8fs} mutant larvae (Figure 6.6 d and Supplementary Table 9.48), showing that Rps14 haploinsufficiency affects the number of HSCs and haematopoietic progenitors found in the CHT of larvae.

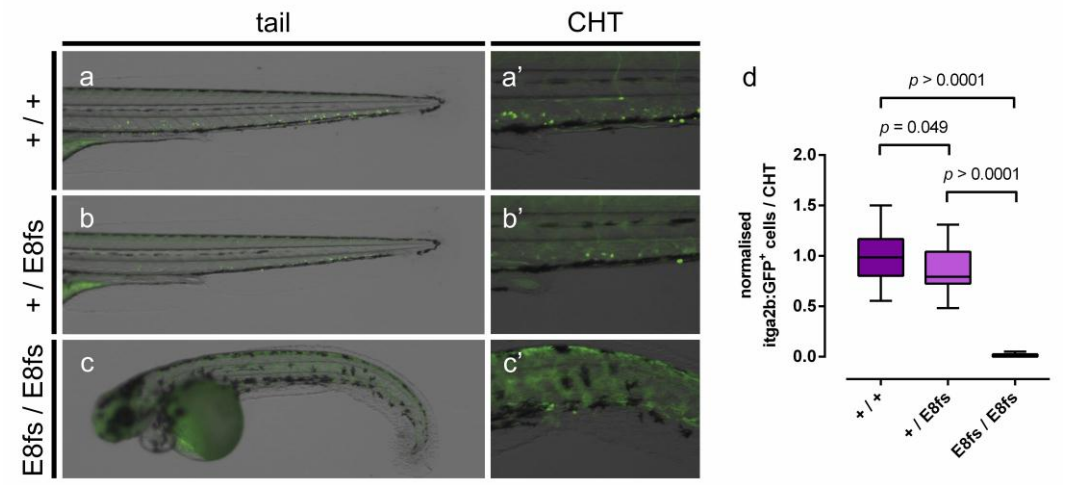

Figure 6.6 | Dose dependent decrease in the number of itga2b:GFP^{low} cells in the CHT of 4 dpf *rps14^{E8fs}* mutant larvae.

Transgenic *Tg(itga2b:GFP); rps14^{E8fs}* mutant adult fish were cross to heterozygous *rps14$^{+/E8fs}$* adult fish to obtain hemizygous *Tg(itga2b:GFP)$^{+/-}$; rps14^{E8fs}* mutant embryos. **(a-c and a'-c')** show lateral views of the tails **(a-c)** and part of the CHT **(a'-c')** of wild type **(a and a')**, heterozygous *rps14$^{+/E8fs}$* **(b and b')**, and homozygous *rps14$^{E8fs/E8fs}$* mutant **(c and c')** larvae at 4 dpf. Images of bright field and GFP channels are shown merged, with anterior to the left **(a-c and a'-c')**. In **(d)**, quantification of itga2b:GFP^{low} cells in the CHT of 4 dpf *rps14^{E8fs}* mutant larvae is shown. Statistical comparison in **(d)** was carried out by one-way ANOVA ($p < 0.0001$) followed by Tukey's multiple comparisons test (p-values for each comparison shown). See Supplementary Table 9.48 for more details.

The quantifications of itga2b:GFP^{low} cells in the CHT of 4 dpf *rps14^{E8fs}* mutant larvae shown in Figure 6.6 d suggest that other haematopoietic lineages could be affected by the decrease in the number of HSCs and other progenitors observed in heterozygotes and homozygous *rps14$^{E8fs/E8fs}$* mutant larvae. Therefore, the number of circulating thrombocytes was measured using the *Tg(itga2b:GFP)* transgenic reporter line, where circulating thrombocytes express high levels of GFP (Lin et al., 2005). This methodology is described in detail in section 6.2.3, and it is based on previous reports (Paredes-Zúñiga et al., 2017; Walters et al., 2010).

Measurements of the heart rate were also carried out in each case as internal controls, see section 6.2.3 for details.

Figure 6.7 shows the quantification of the number of circulating itga2b:GFP^{high} thrombocytes per minute in 3 dpf (Figure 6.7 a) and 4 dpf (Figure 6.7 c) *rps14*^{E8fs} mutant larvae, along with measurements of their respective heart rates (Figure 6.7 b and d, respectively) as internal controls. Results suggest that heterozygous *rps14*$^{+/E8fs}$ mutant larvae show an increasing number of circulating thrombocytes, however, statistical analysis of the data show that there is no statistically significant difference between both groups (Supplementary Table 9.49 and Supplementary Table 9.51).

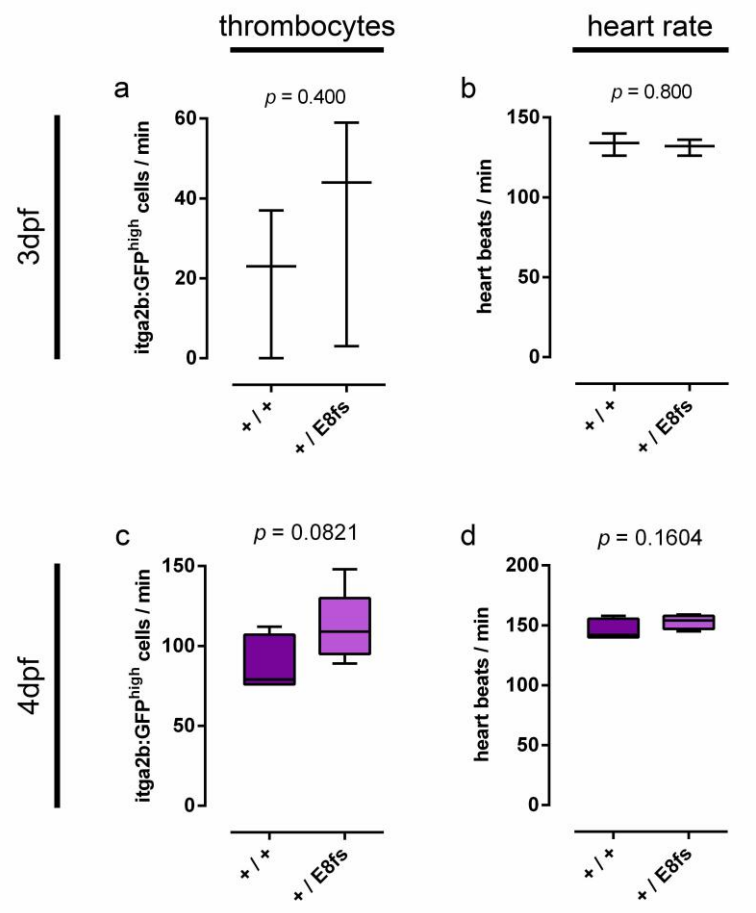

Figure 6.7 | Quantifications of circulating thrombocytes and heart rate in *rps14*^{E8fs} mutant larvae at 3 dpf and 4 dpf.

Transgenic *Tg(itga2b:GFP); rps14*^{E8fs} mutant larvae were obtained by outcross. Circulating GFP^{high} thrombocytes **(a and c)** and heart rates **(b and d)** were quantified as described in section 6.2.3 in *rps14*^{E8fs} mutant larvae at 3 dpf **(a and b)** and 4 dpf **(c and d)**. All statistical comparisons were carried out by Mann Whitney test (*p*-values shown). See Supplementary Table 9.49, Supplementary Table 9.50, Supplementary Table 9.51, and Supplementary Table 9.52 for more details about **(a-d)**, respectively.

6.3.2 Exposure to an agonist of TLR7 and TLR8, imiquimod, alleviates anaemia in *rps14* and *gata1a* morphants

The experiments in this section, and those in section 6.3.4, explore the effects of pharmacological modulation of TLR pathways on the haematopoietic cells of *rps14* morphants and mutants. Previous work carried out in our laboratory by Youngrock Jung[6] as part of his master thesis, found that imiquimod, an agonist of TLR7 and TLR8 (Hemmi et al., 2002; Jurk et al., 2002), partially rescues the phenotype of *rps14* morphant embryos (Jung, 2013). In his work, a library of 720 compounds (Microsource Discovery Systems) were tested in 3 successive screens for their potential to rescue the phenotypes of *rps14* morphants (Jung, 2013), previously reported (Payne et al., 2012). Figure 6.8 a shows a diagram explaining the successive screens carried out on *rps14* morphant larvae. The design is based on successive rounds of screen, where only the compounds found as positives from the previous round are tested again in the next one. Additionally, on each round the phenotypes screened are more specific, in order to decrease the total number of compounds to be tested in an efficient way. For example, the first screen takes advantage of the severe developmetal delay of *rps14* morphants (Payne et al., 2012).The *rps14* morphant larvae exposed to two different doses of each tested compound were examined under a dissecting microscope at 2, 3, and 4 dpf by two independent researchers. The phenotypes of the morphant larvae were scored according to the level of improvement in their morphological development and numbers of circulating cells. The compounds found as positives in this primary screen were then tested again in a secondary screen where *rps14* morphant larvae were stained with *o*-dianisidine and then scored for their degree of haemoglobinization. In this way, compounds improving overall development without rescuing the anaemic phenotype of *rps14* morphants were excluded. Finally, the positives were tested again in a tertiary screen where a series of different concentrations (5, 20, 50, and 100 µM) of each compound were assess for their potential to rescue the defects in haemoglobinization, body length and eye diameter, found in *rps14* morphant fish (Jung, 2013).

[6] Data represented in Figure 6.8 are part of Youngrock Jung MSc's work, carried out under the supervision of Dr Elspeth Payne at the UCL Cancer Institute, and are reproduced here with permission of the authors.

The drug screen carried out in *rps14* morphants, explained in Figure 6.8 a, led to the identification of imiquimod, an agonist of both TLR7 and TLR8 (Hemmi et al., 2002; Jurk et al., 2002), as a positive (Jung, 2013). Imiquimod exposure from 24 hpf was found to partially rescue the body length and eye diameter defects observed in *rps14* morphants during larval development (Jung, 2013). Importantly, exposure to 20 µM imiquimod from 24 hpf to 4 dpf was shown to partially rescue the severe defects in haemoglobinization in the erythroid cells of *rps14* morphants (Figure 6.8 b-i) (Jung, 2013), in a similar way to the previously reported effects of L-leucine in fish (Narla et al., 2014; Payne et al., 2012), which was used as a positive control. Comparison of ventral views of uninjected (Figure 6.8 b) and *rps14* morphant (Figure 6.8 c) larvae treated with DMSO shows the severe developmental delay of the morphants: smaller head, smaller eyes, and almost complete absence of erythroid cells with haemoglobin detectable by *o*-dianisidine staining. Those morphant larvae exposed to 20 µM imiquimod (Figure 6.8 d) show a significant increase in the size of their heads, bigger eyes, and considerable haemoglobinization of erythroid cells in the heart, PHS, and other minor blood vessels (Jung, 2013). These results suggest that agonists of either TLR7 or TLR8, or both, were capable of inducing a significant improvement in the erythroid development of *rps14* morphants.

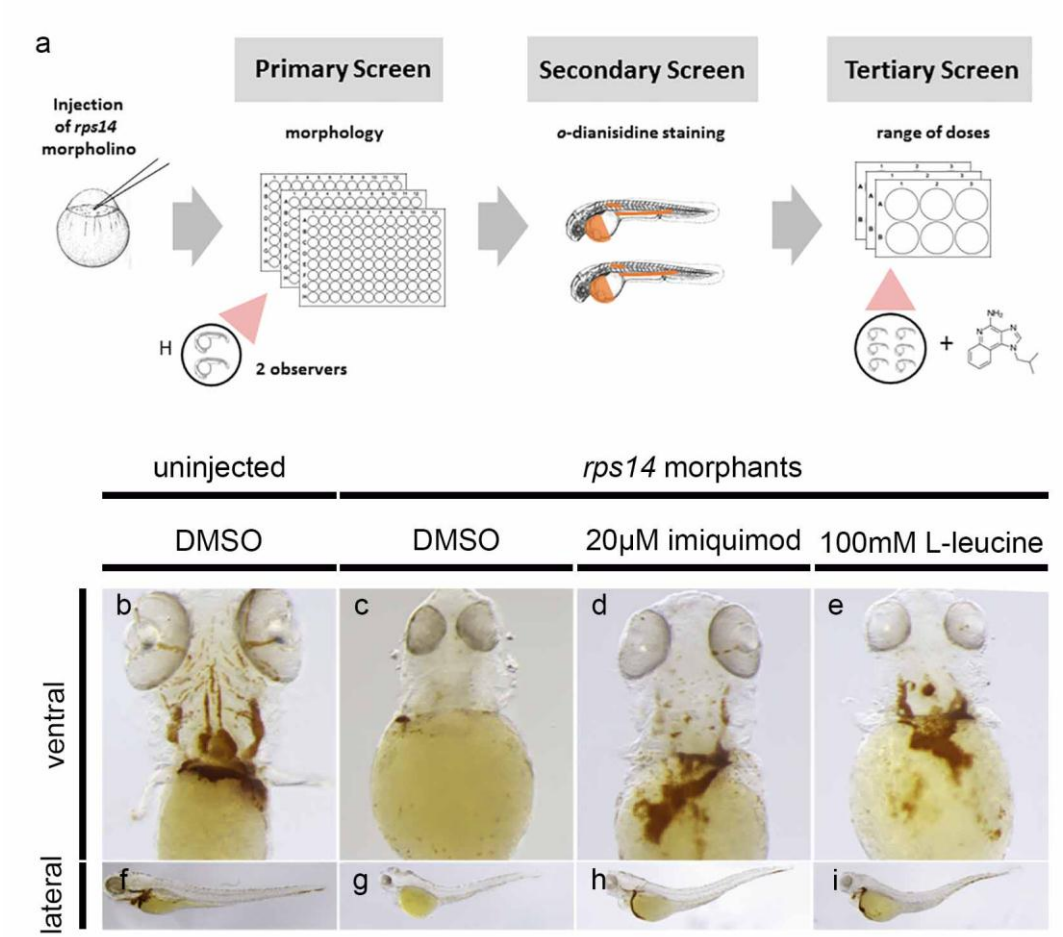

Figure 6.8 | Design of drug screen and rescue of haemoglobinization of *rps14* morphants by imiquimod exposure.

Image in **(a)** shows a diagram representing the design of the three successive screens used to find the potential of imiquimod to rescue the phenotype of *rps14* morphants. The images in **(b-i)** show ventral **(b-e)** and lateral **(f-i)** views of *o*-dianisidine stainings of 4 dpf *rps14* morphants **(c-e and g-i)** and uninjected controls **(b and f)** treated with 0.2% v/v DMSO **(b-c and f-g)**, 20 µM imiquimod **(d and h)**, and 100 mM L-leucine **(e and i)**. **(b-e)** ventral views showing anterior to the top. **(f-i)** lateral views showing anterior to the left. Image in **(a)** was created based on previous work (Jung, 2013), and images in **(b-i)** are were adapted from Youngrock Jung's work (Jung, 2013) modified by Dr Elspeth Payne (unpublished data).

Further experiments were carried out replicating results previously shown (Jung, 2013). Interestingly, exposure to even lower doses of imiquimod (5 µM) is sufficient to induce a moderate rescue of the body length of *rps14* morphant larvae by 4 dpf. Figure 6.9 shows measurements of body length and eye diameter carried out at 2 dpf and 4 dpf in *rps14* and control morphants treated from 24 hpf with 0.05% v/v DMSO, 5 µM imiquimod, or 5 µM gardiquimod. Given that imiquimod is an agonist of both TLR7 and TLR8 (Hemmi et al., 2002; Jurk et al., 2002), gardiquimod, an agonist of TLR7 (Zhu et al., 2008), was included in the experiments.

By 2 dpf, no comparisons show any statistically significant difference, other than weak evidence supporting that *rps14* morphants treated with 5 µM gardiquimod could have decreased body length ($p = 0.071$, Figure 6.9 a, Supplementary Table 9.54). Consistent with this, statistical comparisons of the body length measurements of 4 dpf larvae show that exposure to 5 µM gardiquimod has a significant effect, inducing a decrease in the body length of both control ($p < 0.0001$) and *rps14* ($p < 0.0001$) morphant larvae (Figure 6.9 c, and Supplementary Table 9.58). In contrast, exposure to 5 µM imiquimod induced a moderate but statistically significant increase in the body length of *rps14* morphants ($p = 0.020$), while no significant change was observed in the control morphants ($p = 0.183$, Figure 6.9 c, Supplementary Table 9.58). It is important to notice that the rescue of body length of *rps14* morphants reported previously after exposure to 20 µM imiquimod (Jung, 2013), is in Figure 6.9 c detectable at a 4 times lower concentration, 5 µM imiquimod.

Figure 6.9 d shows the measurements of the eye diameter of morphants at 4 dpf. While control morphants show a small, but statistically significant, decrease in their eye diameter induced by treatment with 5 µM imiquimod ($p = 0.055$) or 5 µM gardiquimod ($p = 0.0048$); *rps14* morphants were not affected by imiquimod ($p = 0.102$) or gardiquimod ($p = 0.440$) exposure (Figure 6.9 d, and Supplementary Table 9.60). However, all *rps14* morphants show lower average eye diameter compared to all control morphants, regardless of the compounds with which they were exposed (Figure 6.9 d, and Supplementary Table 9.59).

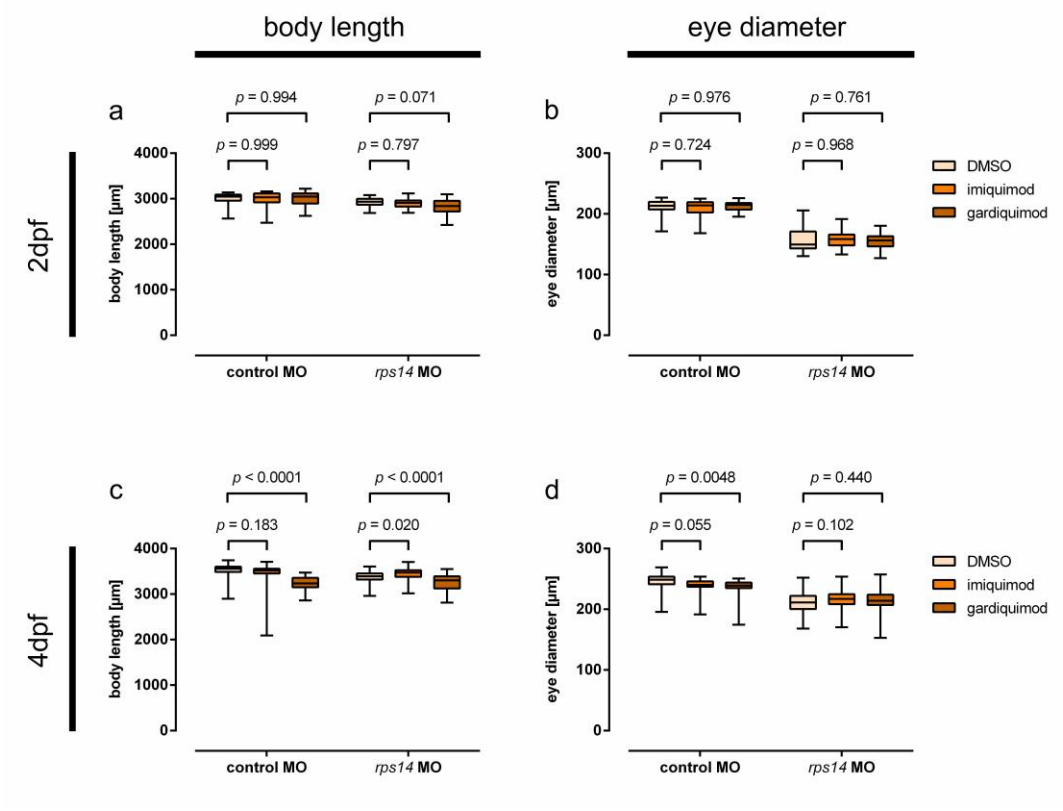

Figure 6.9 | Measurements of body length and eye diameter in *rps14* morphants treated with 5 µM imiquimod and 5 µM gardiquimod.

Embryos injected with *rps14* and control morpholinos were treated with 0.05% v/v DMSO (light orange), 5 µM imiquimod (orange), or 5 µM gardiquimod (dark orange) from 24 hpf. Measurements of body length **(a and c)** and eye diameter **(b and d)** were carried out at 2 dpf **(a and b)** and 4 dpf **(c and d)** as described in section 6.2.5. Statistical comparisons in **(a-d)** were carried out by using two-way ANOVA, and the *p*-values for the effect of each factor can be found in their respective Supplementary Tables. Two-way ANOVA analysis was followed by Dunnett's multiple comparisons test to DMSO controls, and the *p*-values for each comparison made are shown in each graph. See Supplementary Table 9.53 to Supplementary Table 9.60, for more details about **(a)**, **(b)**, **(c)**, and **(d)**, respectively.

The findings showing that TLR7 and TLR8 modulation by imiquimod exposure was able to partially rescue the anaemia and other phenotypes observed in *rps14*

morphants (Jung, 2013), raise the question on whether the observed effects of TLR pathway modulation on erythroid cell development are restricted to those cases where anaemia is induced by deficiency in a ribosomal protein. In order to test this, the effects of imiquimod exposure were studied in *gata1a* morphants, whose erythroid development is severely impeded (Galloway et al., 2005).

Control and *gata1a* morpholinos were injected into 1-cell stage transgenic *Tg(gata1a:dsRed)* embryos that were then treated with 0.05% v/v DMSO or 5 µM imiquimod from 24 hpf to 4 dpf. At 4 dpf, fluorescence images were acquired of the CHT of all larvae, and representative images of each group are shown in Figure 6.10 a-d. In the transgenic *Tg(gata1a:dsRed)* reporter line, erythroid cells express dsRed, together with a minor degree of expression in other cells type (Traver et al., 2003). By 4 dpf, most $dsRed^+$ erythroid cells are observed in the blood circulation, and a few cells remain stationary in the CHT, as can be observed in both control morphants treated with DMSO (Figure 6.10 a) and imiquimod (Figure 6.10 c). In contrast, *gata1a* morpholino induces accumulation of $dsRed^+$ cells in the CHT (Figure 6.10 b), as the expression of erythroid genes that depend on Gata1a activity is disrupted (Galloway et al., 2005). The accumulation of $dsRed^+$ erythroid progenitors in the CHT of *gata1a* morphants, observed in Figure 6.10 b, provides an opportunity to indirectly quantify the effect of imiquimod exposure on these cells. Using Fiji software, see section 6.2.5 for methodological details, the intensity of fluorescence within the CHT was measured in each larva, and the results are shown in Figure 6.10 e. In the case of the larvae injected with the control morpholino, no effects of imiquimod exposure are observed in the CHT ($p > 0.999$, Supplementary Table 9.61), probably because erythroid cells differentiate and enter the blood circulation, making it impossible to detect any change by observing the CHT. In contrast, in those larvae injected with *gata1a* morpholino, $dsRed^+$ cells do not exit the CHT. Comparison of *gata1a* morphants treated with 0.05% v/v DMSO and 5 µM imiquimod shows an accumulation of $dsRed^+$ cells in the CHT that can be observed as a significant increase in the dsRed fluorescence of the CHT of *gata1a* morphants exposed to imiquimod ($p = 0.0016$, Figure 6.10 e, Supplementary Table 9.61). The areas of the CHT of all larvae analysed were also measured and compared as an internal control, but no significant differences were found among the groups (Figure 6.10 f, Supplementary Table 9.62). These results suggest that modulation of TLR7 and TLR8 by imiquimod exposure improves erythroid cell development, although it cannot rescue the defects in erythroid

differentiation found in *gata1a* morphants. It is also important to mention that imiquimod's effects are not restricted to the deficiency of ribosomal proteins, suggesting that TLR pathways could play a role in developmental haematopoiesis.

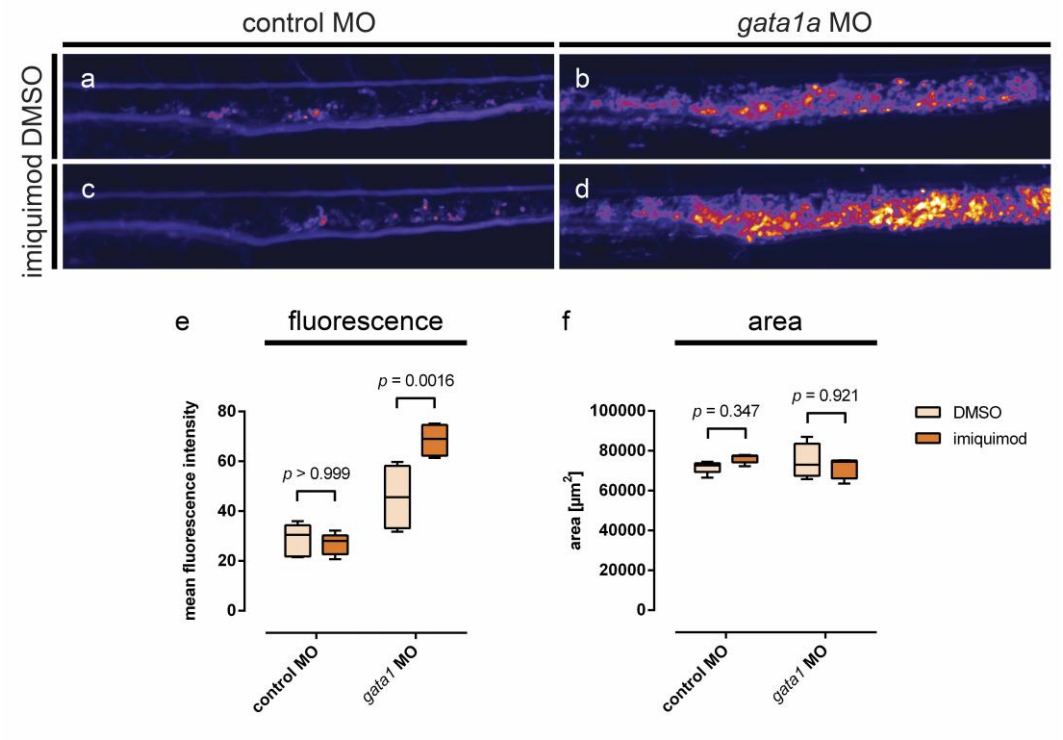

Figure 6.10 | Imiquimod treatment increases erythroid development in *gata1a* morphants.

Homozygous transgenic *Tg(gata1a:dsRed)*$^{+/+}$ embryos injected with *gata1a* morpholino were exposed to 5 µM imiquimod or 0.05% v/v DMSO from 24 hpf to 4 dpf. In **(a-d)**, fluorescence images of the CHT of representative larvae are shown pseudo-coloured according to fluorescence intensity using Fiji software (see section 2.12 for details). All images in **(a-d)** show anterior to the left. The intensity of dsRed fluorescence was measured using Fiji software in the CHT of each larva and the results are shown in **(e)**. In **(f)**, the areas of the CHT of each larva were also measured as an internal control for data in **(e)**. The methodology used for the measurements shown in **(e)** and **(f)** is described in detail in section 6.2.5. Statistical comparisons in **(e and f)** were carried out by using two-way ANOVA, and the *p*-values

for the effect of each factor are shown in each graph. In the case of data shown in **(e)**, two-way ANOVA analysis was followed by Bonferroni's multiple comparisons test, and the *p*-values for each comparison made are shown in the graph. See Supplementary Table 9.61 and Supplementary Table 9.62 for more details about **(e)** and **(f)**, respectively.

Further experiments were carried out to study other cell types that could be affected by the pharmacological modulation of TLR7 and TLR8 with imiquimod. Previous reports had found that exposure to imiquimod is able to induce a partial rescue of the haemoglobinization of erythroid cells of *rps14* morphants by 4 dpf (Jung, 2013). It was hypothesized that imiquimod treatment affects the number of HSCs by modulating either TLR7, TLR8, or both. To test this hypothesis, *rps14*^{E8fs} mutant fish carrying the *Tg(itga2b:GFP)* transgenic reporter were treated with 5 µM imiquimod, 0.05% v/v DMSO, or E3 from 24 hpf to 4 dpf. The *Tg(itga2b:GFP)* transgene drives the expression of high levels of GFP in thrombocytes, while HSCs and other haematopoietic progenitors in the CHT express low levels of GFP (Lin et al., 2005). The number of itga2b:GFP^{low} cells over the AGM area and in the CHT of each larva was quantified. The results, in Figure 6.11 a and b, show no statistically significant difference among the groups receiving different treatments (Figure 6.11 a and b, Supplementary Table 9.63, and Supplementary Table 9.64).

The effect of TLR7 and TLR8 modulation on granulocytes of *rps14*^{E8fs} mutant larvae by treatment with imiquimod were also studied. Wild type and heterozygous *rps14*$^{+/E8fs}$ mutant larvae were treated with 5 µM imiquimod, 0.05% v/v DMSO, or E3 from 24 hpf to 4 dpf, and granulocytes were stained using Sudan Black staining (as described in section 2.3). Sudan Black^{+} granulocytes were quantified in the CHT of each larva, and the results are shown in Figure 6.11 c. Statistical analysis shows no significant differences among all groups (Supplementary Table 9.65), suggesting that exposure to imiquimod, and therefore modulation of TLR7 and TLR8, has no impact on the number of granulocytes found at this stage.

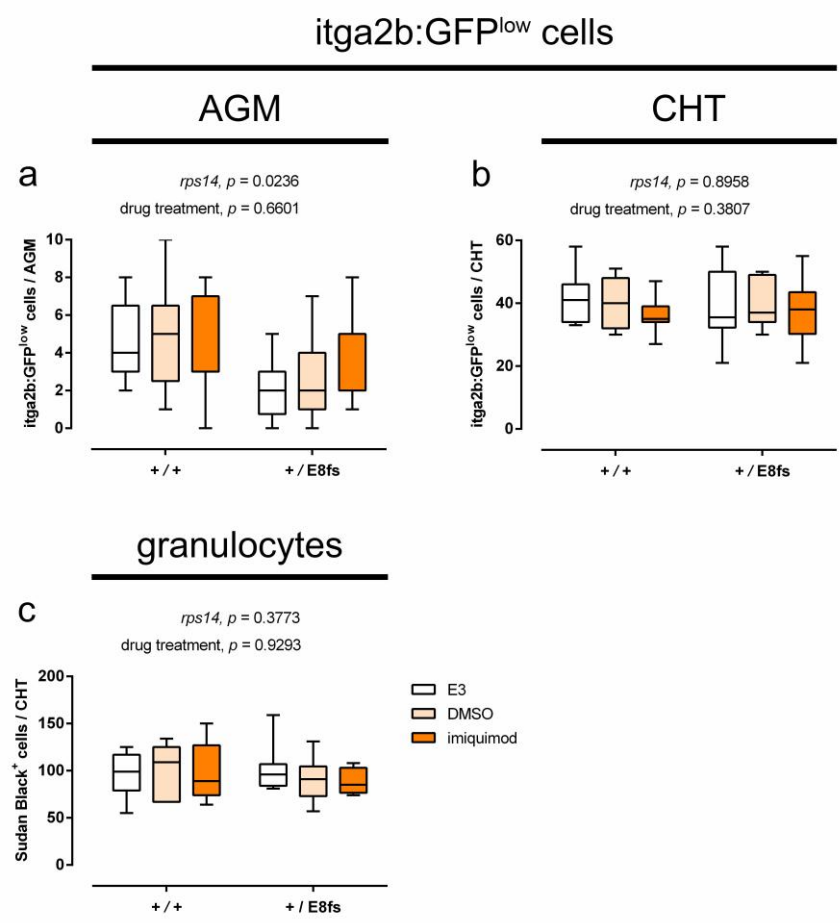

Figure 6.11 | Quantifications of itga2b:GFP^{low} and Sudan Black^{+} cells in the CHT of 4dfp *rps14^{E8fs}* mutant larvae exposed to imiquimod.

Graphs in **(a and b)**, show quantifications carried out in transgenic *rps14^{E8fs}* mutant larvae expressing *Tg(itga2b:GFP)*, and the graph in **(c)** shows quantifications carried out on *rps14^{E8fs}* mutant larvae stained with Sudan Black. All fish in (a, b, and c) were treated with E3 (white bars), 0.05% v/v DMSO (light orange bars), and 5 µM imiquimod (orange bars) from 24 hpf to 4 dpf. In (a and b), at 4 dpf itga2b^{low} cells were quantified along the AGM, shown in **(a)**, and in the CHT, shown in **(b)**. In **(c)**, granulocytes labelled by Sudan Black were quantified in the CHT of each larva at 4 dpf. Statistical comparisons in **(a, b, and c)** were carried out by using two-way ANOVA, and the *p*-values for the effect of each factor are shown in each graph. See Supplementary Table 9.63, Supplementary Table

9.64, and Supplementary Table 9.65, for more details about **(a)**, **(b)** and **(c)**, respectively.

6.3.3 Heterozygous *rps14*$^{+/E8fs}$ mutants exhibit anaemia when exposed to cold and haemolytic stress

The results in Figure 6.1 show that heterozygous *rps14*$^{+/E8fs}$ fish display normal levels of haemoglobinization of erythroid cells at 48 hpf and 4 dpf, which strongly suggests that *rps14*$^{+/E8fs}$ heterozygosity does not induce anaemia in the zebrafish. However, during previous work carried out by Dr Elspeth Payne, it was observed that *rps14* mutant larvae raised at 24 °C from the 18 ss to 2 dpf, show delayed cardiac development (Dr Elspeth Payne, unpublished data). This observation led to the hypothesis that *rps14*^{E8fs} mutation could increase the sensitivity of developmental haematopoiesis to stress. To test this hypothesis, *rps14*^{E8fs} mutant embryos were raised at 22 °C from the 6 ss (12 hpf) to prim-22 stage (36 hpf) and stained with *o*-dianisidine, as described in section 2.4. Figure 6.12 a and b shows ventral views of representative wild type (a), and heterozygous *rps14*$^{+/E8fs}$ mutant larvae stained with *o*-dianisidine at prim-22 stage. Wild type embryos, in Figure 6.12 a, exhibit haemoglobinization of erythroid cells over the yolk sac and in the heart, while heterozygous *rps14*^{E8fs} mutant embryos, in Figure 6.12 b, show extremely reduced levels of haemoglobinization. All embryos were also scored according to their degree of haemoglobinization, and the proportion of embryos displaying normal levels of haemoglobinization (as that of the embryo shown in Figure 6.12 a), and an anaemic phenotype (as that of the embryo shown in Figure 6.12 b), were compared between wild type and heterozygous *rps14*$^{+/E8fs}$ mutant embryos (Figure 6.12 c). It is important to notice that both normal and anaemic phenotypes are found among wild type and heterozygous embryos, however, the penetrance of the anaemic phenotype is severely increased within the group of heterozygous *rps14*$^{+/E8fs}$ mutant embryos (Figure 6.12 c). Close examination of those embryos with severe anaemia shows that they have *o*-dianisidine^{+} cells (Figure 6.12 b), demonstrating that the haemoglobinization is not abolished in these cases, but delayed. The higher penetrance of anaemia observed among heterozygotes suggests that erythroid cell development in heterozygous *rps14*$^{+/E8fs}$ mutant embryos is more sensitive to cold stress than in wild type *rps14*$^{+/+}$ embryos.

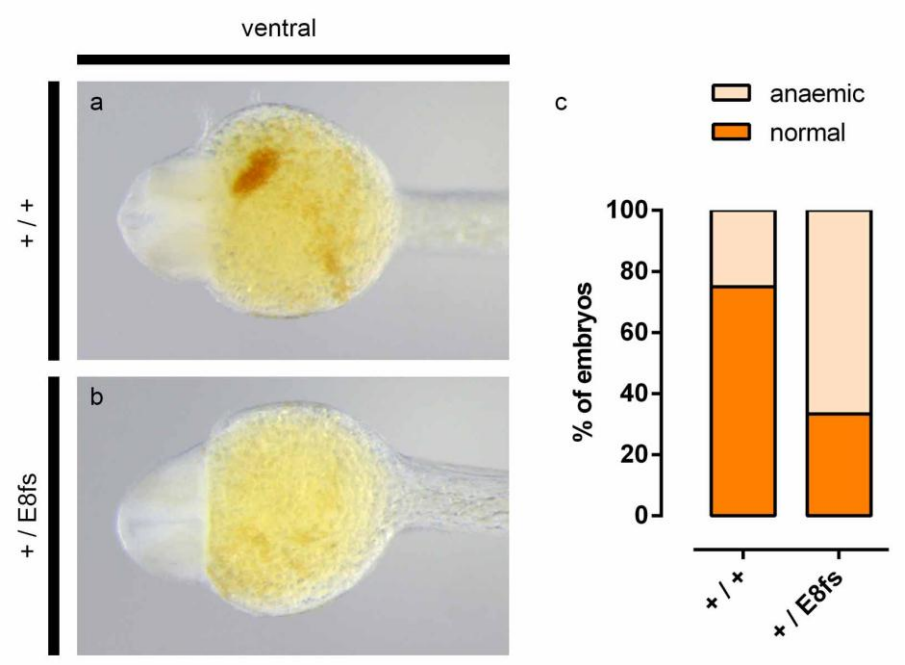

Figure 6.12 | Erythropoiesis in heterozygous *rps14*$^{+/E8fs}$ embryos is more sensitive to cold stress than in wild type embryos.

The effect of cold stress during early development on haemoglobinization of erythrocytes was studied in heterozygous *rps14*$^{+/E8fs}$ mutant embryos compared to their wild type siblings. Embryos were raised at 22 °C from 6 ss stage (12 hpf) to prim-22 (36 hpf) and stained with *o*-dianisidine. In **(a and b)**, ventral views of representative wild type **(a)**, and heterozygous *rps14*^{E8fs} mutant **(b)** embryos at prim-22 stage are shown with anterior to the left. In **(c)**, the percentage of embryos displaying anaemic (light orange) or normal (dark orange) phenotype is shown for each genotype. Notice the increased proportion of embryos with anaemic phenotype in the group of *rp14*^{E8fs} heterozygotes.

Results in Figure 6.12 show that in response to cold stress, a significant proportion of heterozygous *rps14*$^{+/E8fs}$ mutant embryos exhibit an anaemic phenotype that suggests that developmental haematopoiesis is more delayed under stress conditions in heterozygotes than in wild type embryos. Therefore, it was hypothesized that heterozygous *rps14*$^{+/E8fs}$ mutant fish exhibit poorer recovery of erythroid cells after haemolytic stress. As described in section 6.2.8, haemolytic

stress was induced by treatment with 1 µg/mL PHZ from 24 hpf to 48 hpf, which is sufficient to induce death of erythroid cells (Lenard et al., 2016). At 48 hpf, PHZ was washed away and replaced by E3, and larvae were allowed to recover until 6 dpf. Larvae were stained with *o*-dianisidine at 6 dpf and all fish were imaged. Figure 6.13 a and a' shows haemoglobinization after recovery from haemolytic stress in wild type *rps14*$^{+/+}$ larvae. Erythroid cells labelled with *o*-dianisidine are observed in the heart, PHS, and other blood vessels (Figure 6.13 a and a'). In contrast, heterozygous *rps14*$^{+/E8fs}$ mutant larvae show a reduced degree of haemoglobinization (Figure 6.13 b and b') in comparison with their wild type siblings (Figure 6.13 a and a'). Larvae were scored according to their haemoglobinization phenotype as normal or anaemic and the proportion of each phenotype is graphed for each genotype in Figure 6.13 c. Most wild type larvae (89%) exhibit a normal phenotype, while only 11% show anaemia. In contrast, 59% of heterozygous *rps14*$^{+/E8fs}$ mutant larvae displayed anaemia (Figure 6.13 c). Statistical comparison shows that the penetrance of the anaemic phenotype is significantly higher in heterozygous *rps14*$^{+/E8fs}$ mutant larvae than in their wild type siblings (p = 0.0009, Fisher's exact test). These results suggest that erythroid cell development in *rps14*$^{+/E8fs}$ haploinsufficient larvae has a decreased performance, which manifests as an increased penetrance of anaemic phenotypes under stress conditions.

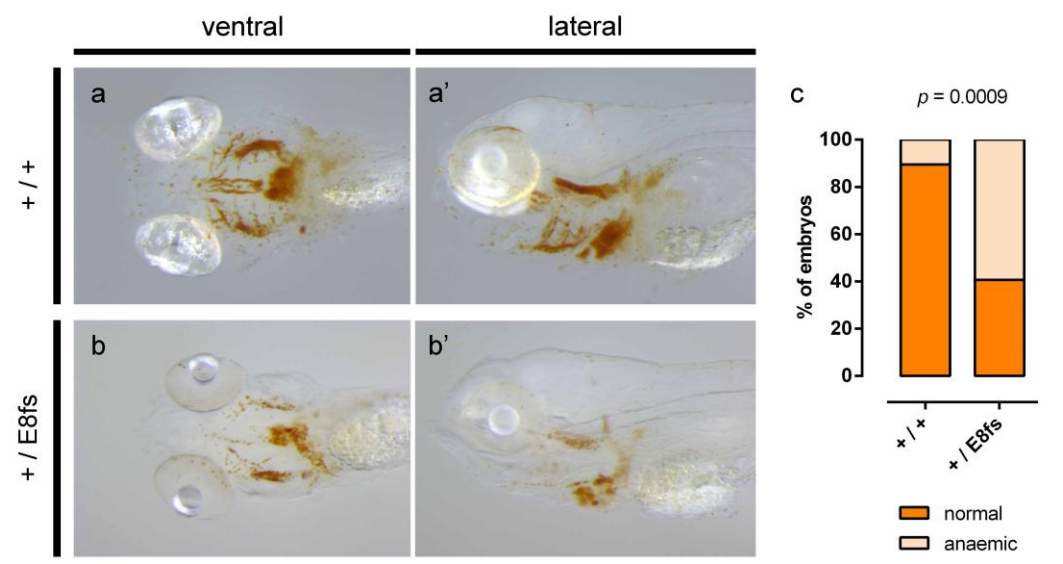

Figure 6.13 | Heterozygous *rps14*$^{+/E8fs}$ larvae exhibit poorer recovery after haemolytic stress than wild type larvae.

Haemolytic stress was induced in *rps14*^{E8fs} mutant embryos from 24 hpf to 48 hpf by exposure to 1 µg/mL PHZ (see section 6.2.8 for details). At 48 hpf, PHZ was washed away and fish were allowed to recover until 6 dpf. At 6 dpf, larvae were stained with *o*-dianisidine and imaging was carried out. Images in **(a-b')** show ventral **(a and b)**, and lateral **(a' and b')** views of wild type *rps14*$^{+/+}$ **(a and a')** and heterozygous *rps14*$^{+/E8fs}$ **(b and b')** larvae with anterior to the left. In **(c)**, the percentage of embryos displaying anaemic (light orange) or normal (dark orange) phenotype is shown for each genotype. Statistical comparison between genotypes was carried out by Fisher's exact test and the *p*-value is shown in the graph.

Further experiments were carried out to characterize the recovery of erythroid cells after chemically induced-haemolytic stress in *rps14*$^{+/E8fs}$ heterozygotes. Transgenic *rps14*^{E8fs} mutant fish expressing the *Tg(gata1a:dsRed)* transgene, that drives the expression of dsRed to erythroid cells (Traver et al., 2003), were used for fluorescence imaging and flow cytometry analysis after recovery from haemolytic stress. As described for experiments in Figure 6.13, haemolytic stress was induced by incubation in 1 µg/mL PHZ from 24 hpf to 48 hpf, PHZ was replaced by E3 at 48 hpf, and fish recover in E3 (see section 6.2.9 for details). Figure 6.14 a and a'

show lateral views of the tails of *Tg(gata1a:dsRed)* transgenic wild type larvae at 6 dpf. Erythroid cells expressing dsRed can be found circulating in the DA, CV, Se, and residing in the CHT. Imaging of 6 dpf heterozygous *rps14*$^{+/E8fs}$ larvae shows a similar distribution of gata1a:dsRed^{+} cells (Figure 6.14 b and b'), however, some of the heterozygotes display an apparently reduced number of labelled cells in the CHT (compare Figure 6.14 a and b). Therefore, quantifications of gata1a:dsRed^{+} cells in *rps14*^{E8fs} mutants were carried out by flow cytometry analysis. Quantifications in 3 dpf larvae, depicted in Figure 6.14 c, show that heterozygous *rps14*$^{+/E8fs}$ larvae have decreased numbers of gata1a:dsRed^{+} cells compared to their wild type siblings (p = 0.048, Supplementary Table 9.66). Similarly, quantifications carried out in 6 dpf larvae (Figure 6.14 d) also show a decrease in gata1a:dsRed^{+} cells in heterozygotes in comparison to wild type *rps14*$^{+/+}$ larvae (p = 0.004, Supplementary Table 9.67). These results, in agreement with data on haemoglobinization shown in Figure 6.13, suggest that *rps14* haploinsufficiency affects haematopoiesis, making the haematopoietic compartment more susceptible under stress conditions.

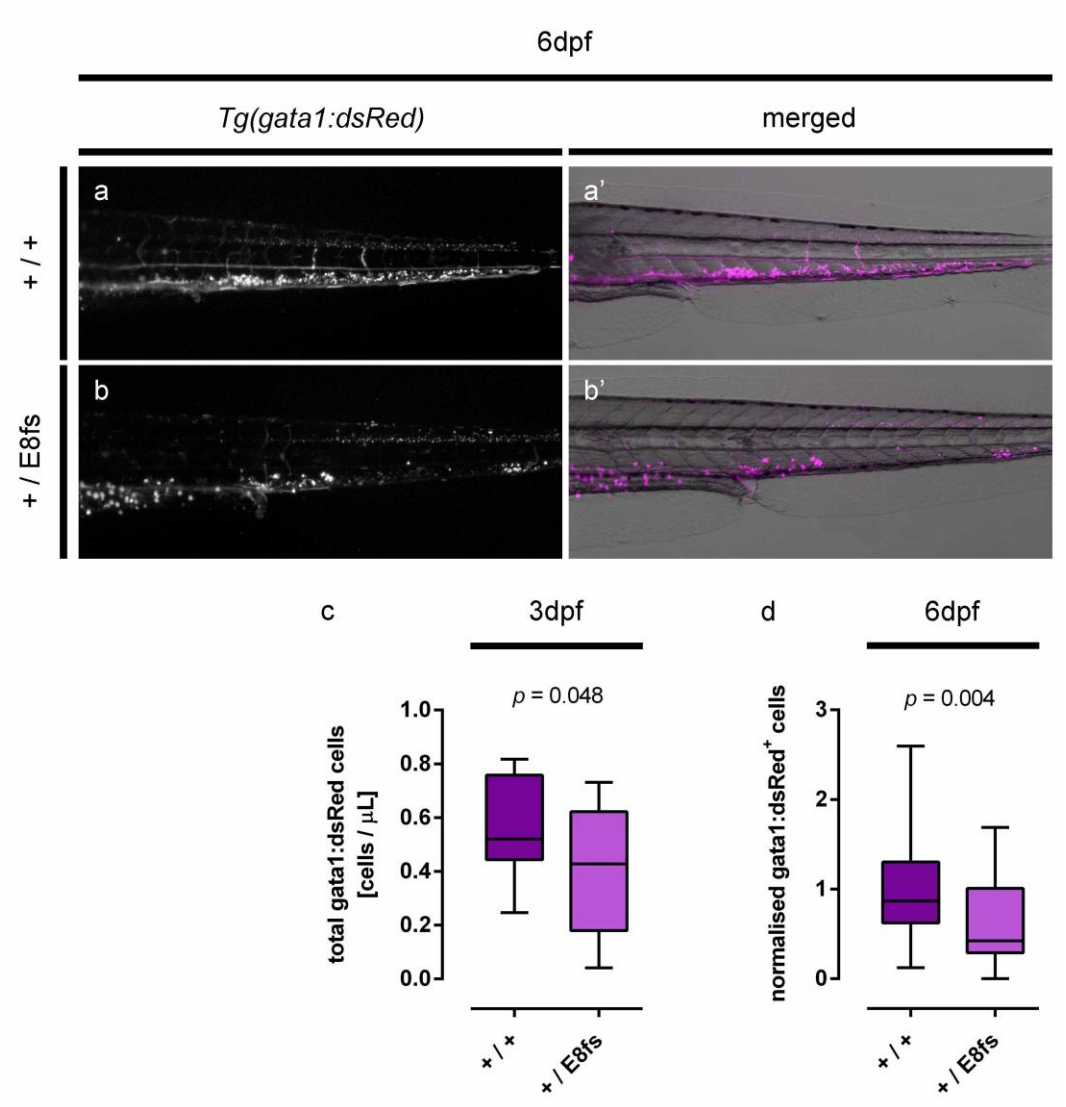

Figure 6.14 | Imaging and quantification of gata1a:dsRed⁺ cells in *rps14*^{E8fs} mutants during recovery after haemolytic stress.

Haemolytic stress was induced in *rps14*^{E8fs} mutant embryos carrying the transgenic reporter *Tg(gata1a:dsRed)*, by exposure to 1 µg/mL PHZ from 24 hpf to 48 hpf (see section 6.2.8 for details). At 48 hpf, PHZ was washed away and fish were allowed to recover until 3 dpf **(c)**, or 6 dpf **(a-b', and d)**. In **(a-b')**, fluorescence images of the tails of wild type **(a and a')** and heterozygous *rps14*$^{+/E8fs}$ **(b and b')** larvae at 6 dpf are shown with anterior to the left. In **(a and b)**, dsRed channel is shown in greyscale, and in **(a' and b')** bright field and dsRed channels, in magenta, are shown merged. In **(c and d)**, gata1a:dsRed⁺ cells were quantified in individual larvae by flow

cytometry analysis at 3 dpf **(c)**, and 6 dpf **(d)**. Statistical comparison in **(c)** was carried out by unpaired t test, and in the case of **(d)**, by Mann Whitney test. See Supplementary Table 9.66, and Supplementary Table 9.67, for more details about **(c)**, and **(d)**, respectively.

6.3.4 Pharmacological activation of TLR7 partially rescues delayed haemoglobinization after chemically induced haemolytic stress

Previous work in the laboratory of Dr Elspeth Payne identified imiquimod through a drug screen carried out on *rps14* morphants (Jung, 2013). Imiquimod is an agonist of both TLR7 and TLR8 (Hemmi et al., 2002; Jurk et al., 2002), and exposure to it during embryonic and larval development was shown to partially rescue the anaemic phenotype of *rps14* morphants (Jung, 2013). Treatment with imiquimod also caused moderate rescue of body length and eye diameter in *rps14* morphant larvae (Jung, 2013), showing that its effects were not restricted to haematopoietic cells.

Experiments carried out in heterozygous *rps14*$^{+/E8fs}$ mutant larvae show that haemolytic stress elicits a significant increase in the penetrance of anaemia among heterozygotes (Figure 6.13 and Figure 6.14). This phenotype was used as a model to study the effect of pharmacological modulation of TLR7 and TLR8, by inducing haemolytic stress by exposure to PHZ in combination with treatment with agonists of both TLR7 and TLR8.

The effects of imiquimod on *rps14*^{E8fs} mutant larvae were further studied by exposure to different concentrations of imiquimod during recovery after haemolytic stress. As described before for experiments in Figure 6.13 and Figure 6.14, haemolytic stress was induced by exposure of embryos to 1 µg/mL PHZ from 24 hpf to 48 hpf (see section 6.2.8 for more details). Then larvae were allowed to recover until 6 dpf in different concentrations of imiquimod (from 1 µM to 100 µM) or 1% v/v DMSO (see section 6.2.6 for more details). At 6 dpf, larvae were stained with *o*-dianisidine and imaging was carried out. Figure 6.15 a-e' shows ventral views of 6 dpf wild type (a-e) and heterozygous *rps14*$^{+/E8fs}$ mutant (a'-e') larvae treated with increasing concentrations of imiquimod. All larvae were scored

according to their haemoglobinization phenotype as normal or anaemic, and the percentage of larvae displaying each phenotype was graphed for each genotype under each treatment in Figure 6.15 f. In the case of the control group, larvae were allowed to recover in 1% v/v DMSO after treatment with PHZ, the results in Figure 6.15 f are similar to those shown previously in Figure 6.13 c. Figure 6.15 f shows that 77.3% of wild type larvae exhibit normal haemoglobinization (see Figure 6.15 a), while 26.7% of them show anaemia. In the case of heterozygous *rps14*$^{+/E8fs}$ mutant larvae, this proportion is inverted, with only 22.2% displaying normal haemoglobinization, and 77.8% of heterozygotes showing anaemia (Figure 6.15 a'). In heterozygotes exposed to 1 µM imiquimod the proportion of larvae displaying anaemia is also high (88.9%, Figure 6.15 b and b'), which descends to 60.0% within heterozygous *rps14*$^{+/E8fs}$ larvae treated with 5 µM imiquimod (Figure 6.15 c and c'). In contrast, the penetrance of the anaemic phenotype among heterozygotes exposed to 20 µM imiquimod is only 22.2%, similar to that found among wild type larvae under the same treatment (26.7%, Figure 6.15 d and d'). These results suggest that activation of TLR7, TLR8 or both induces a rescue in the haemoglobinization of heterozygous *rps14*$^{+/E8fs}$ larvae. Notice also that higher concentrations of imiquimod seem to induce higher rates of anaemia and morphological abnormalities (see Figure 6.15 e, e', and f).

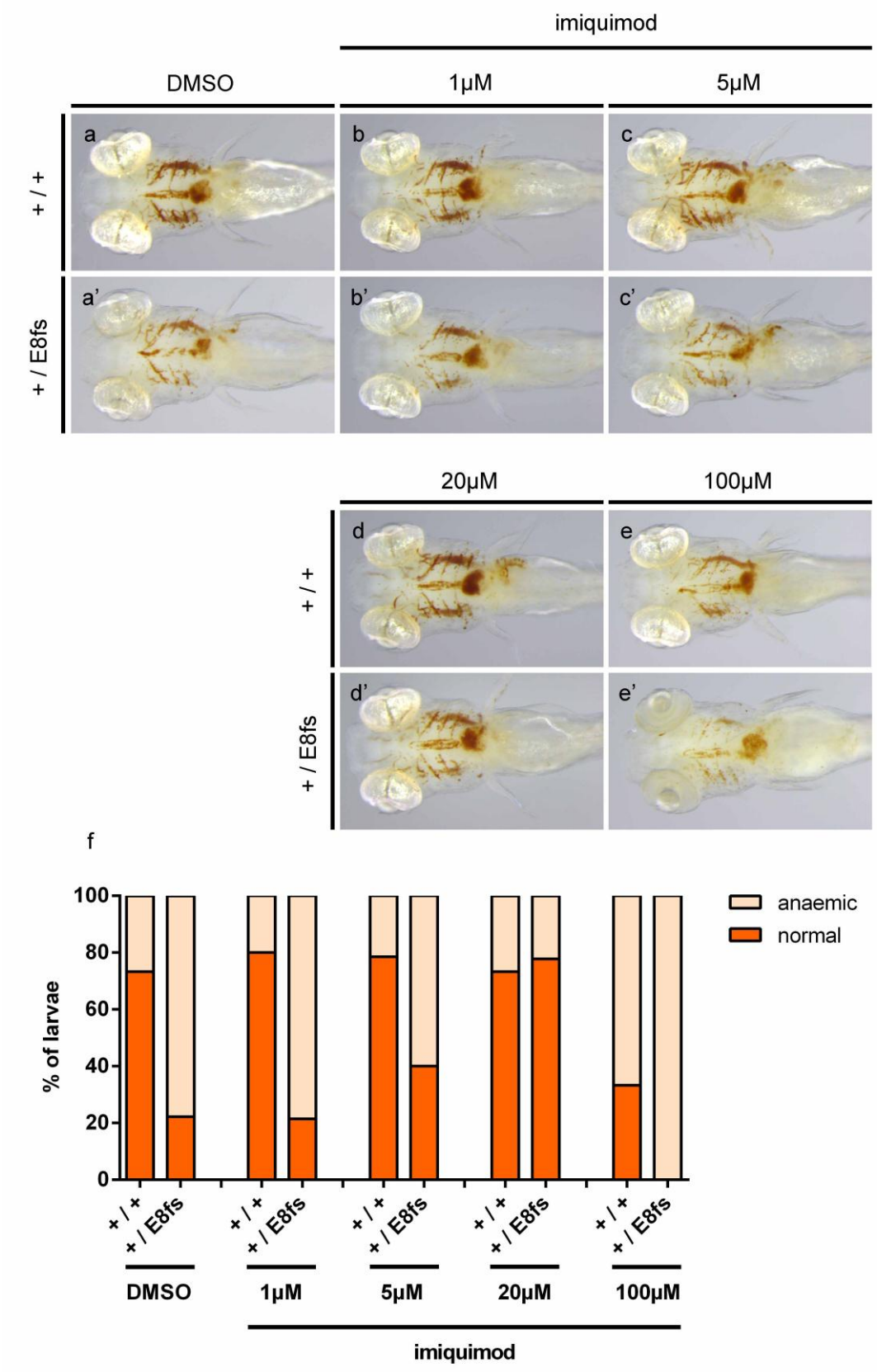
imiquimod
DMSO
1μM
5μM
a
b
c
+ / +
a'
b'
c'
+ / E8fs
20μM
100μM
d
e
+ / +
d'
e'
+ / E8fs
f
100
80
60
40
20
0
% of larvae
anaemic
normal
+ / +
+ / E8fs
DMSO
1μM
5μM
20μM
100μM
imiquimod

Figure 6.15 | (in previous page) Imiquimod treatment improves recovery of *rps14*$^{+/E8fs}$ mutant larvae after haemolytic stress.

Effect of imiquimod on haemoglobinization during recovery after haemolytic stress. Haemolytic stress was induced by exposure of *rps14*^{E8fs} mutant fish to 1 µg/mL PHZ from 24 hpf to 48 hpf. Fish were allowed to recover until 6 dpf in the presence of different concentrations of imiquimod or DMSO. Larvae were stained with *o*-dianisidine at 6 dpf and imaged to assess their degree of haemoglobinization. In **(a-e')**, ventral views of *o*-dianisidine stainings of 6 dpf larvae are shown with anterior to the left. Representative wild type **(a-e)** and heterozygous *rps14*$^{+/E8fs}$ mutant **(a'-e')** larvae are shown for each treatment: 1% v/v DMSO **(a and a')**, 1 µM imiquimod **(b and b')**, 5 µM imiquimod **(c and c')**, 20 µM imiquimod **(d and d')**, and 100 µM imiquimod **(e and e')**. In **(f)**, the percentage of larvae with normal (dark orange) or anaemic (light orange) phenotype is graphed for each genotype under each different treatment.

Further experiments were carried out with more specific agonists, to determine whether the rescue observed after imiquimod treatment in both *rps14* morphants (Jung, 2013) and mutants (Figure 6.15), is caused by modulation of TLR7, TLR8, or both. Two different compounds, gardiquimod and motolimod, agonists of TLR7 and TLR8, respectively, were used in similar experiments to that carried out with imiquimod (in Figure 6.15).

Gardiquimod, a TLR7 agonist (Zhu et al., 2008), was used in recovery experiments after haemolytic stress. As done with imiquimod in the experiment of Figure 6.15, fish were incubated in different concentrations of gardiquimod from 48 hpf to 6 dpf after haemolytic stress was induced by exposure to 1 µg/mL PHZ (see sections 6.2.6 and 6.2.8, for more details). At 6 dpf, larvae were stained with *o*-dianisidine, as described in section 2.4, and then imaged to be scored according to their haemoglobinization phenotype. Figure 6.16 a-e' shows ventral views of *o*-dianisidine stainings of representative larvae of each genotype for each treatment, and in Figure 6.16 f, the percentage of larvae with normal (dark orange bars) and anaemic (light orange bars) phenotype are graphed for each genotype within each

drug treatment. In the group control treated with DMSO, 64.5% of wild type larvae showed normal haemoglobinization, while anaemia was observed in 35.5% of them. In contrast, anaemic phenotype has a high penetrance among heterozygous *rps14*$^{+/E8fs}$ mutant larvae (70.6%, Figure 6.16 a and a'), as previously observed (Figure 6.13 and Figure 6.15). Treatment with increasing concentrations of gardiquimod during the recovery phase led to a progressive decrease of the penetrance of the anaemic phenotype among heterozygotes (Figure 6.16 f). Among heterozygous *rps14*$^{+/E8fs}$ mutant larvae exposed to 1 µM gardiquimod, anaemia was observed in 66.7% of fish (Figure 6.16 b and b'); treatment with 5 µM gardiquimod led to 50.0% of anaemic heterozygous larvae (Figure 6.16 c and c'); and in those heterozygous fish exposed to 20 µM gardiquimod, the penetrance of the anaemic phenotype is only 37.5% (Figure 6.16 d and d'), comparable to that observed among wild type larvae under the same treatment (31.3%) and among wild type larvae treated with DMSO (35.5%). Treatment with higher concentrations of gardiquimod, 100 µM in Figure 6.16, led to an increase in the penetrance of anaemia among heterozygous *rps14*$^{+/E8fs}$ mutant larvae (Figure 6.16 e and e'). These results suggest that exposure to the TLR7 agonist, gardiquimod, is sufficient to induce a rescue in the haemoglobinization of heterozygous *rps14*$^{+/E8fs}$ mutant larvae.

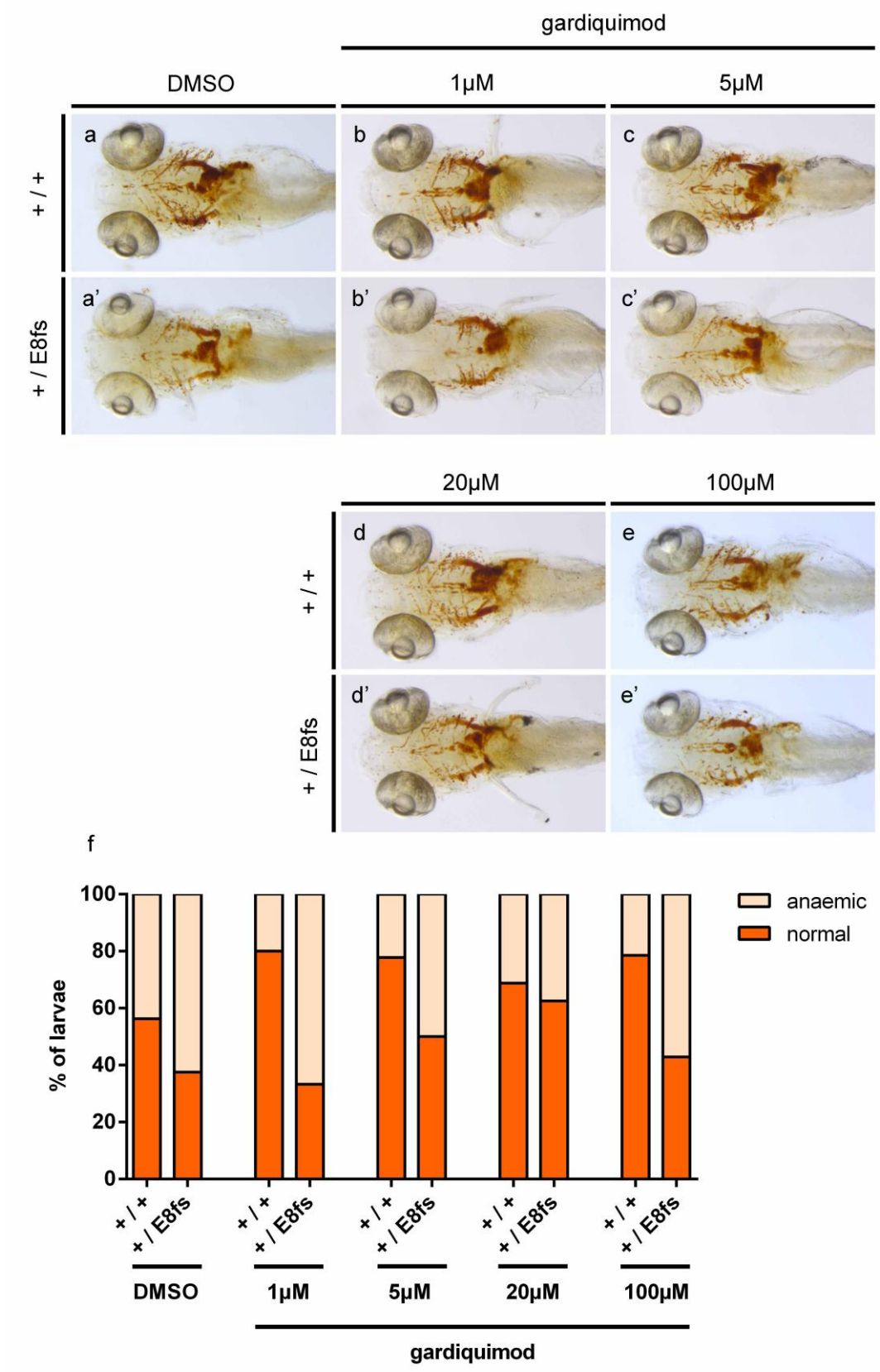
gardiquimod
DMSO
1μM
5μM
a
b
c
+ / +
a'
b'
c'
+ / E8fs
20μM
100μM
d
e
+ / +
d'
e'
+ / E8fs
f
anaemic
normal
% of larvae
100
80
60
40
20
0
+ / +
+ / E8fs
DMSO
1μM
5μM
20μM
100μM
gardiquimod

Figure 6.16 | (in previous page) Exposure to TLR7 agonist, gardiquimod, improves recovery after haemolytic stress in *rps14*^{E8fs} mutant larvae.

Effect of gardiquimod on haemoglobinization during recovery after haemolytic stress. Haemolytic stress was induced by exposure of *rps14*^{E8fs} mutant fish to 1 µg/mL PHZ from 24 hpf to 48 hpf. Fish were allowed to recover until 6 dpf in the presence of increasing concentrations of gardiquimod or DMSO. At 6 dpf larvae were stained with *o*-dianisidine and imaged to assess their degree of haemoglobinization. In **(a-e')**, ventral views of *o*-dianisidine stainings of 6 dpf larvae are shown with anterior to the left. Representative wild type **(a-e)** and heterozygous *rps14*$^{+/E8fs}$ mutant **(a'-e')** larvae are shown for each treatment: 1% v/v DMSO **(a and a')**, 1 µM gardiquimod **(b and b')**, 5 µM gardiquimod **(c and c')**, 20 µM gardiquimod **(d and d')**, and 100 µM gardiquimod **(e and e')**. In **(f)**, the percentage of larvae with normal (dark orange) or anaemic (light orange) phenotype is graphed for each genotype under each different treatment.

Although results in Figure 6.16 show that pharmacological modulation of TLR7 with the agonist gardiquimod induces a rescue in the haemoglobinization of heterozygous *rps14*$^{+/E8fs}$ mutant larvae, this does not rule out the possibility that modulation of TLR8 could elicit a similar effect. Therefore, similar experiments were carried out where *rps14*^{E8fs} mutant larvae were incubated in different concentrations of motolimod, a TLR8 agonist (Lu et al., 2012), during the recovery phase after haemolytic stress. Incubation with 1 µg/mL PHZ from 24 hpf to 48 hpf was used to induce haemolytic stress (see section 6.2.8 for more details), as done before. At 48 hpf, PHZ was replaced by 1% v/v DMSO, or increasing concentrations of motolimod (0.1, 1, 10, and 100 µM; see section 6.2.6 for more details), and the larvae were allowed to recover until 6 dpf. *O*-dianisidine stainings were carried out at 6 dpf, and all larvae were imaged for later assessment of their haemoglobinization phenotype. Figure 6.17 a-e' shows ventral views of representative larvae stained with *o*-dianisidine for each genotype under each drug treatment. The percentage of larvae displaying normal haemoglobinization (dark

orange bars) and anaemic phenotype (light orange bars) is shown for each genotype under each drug treatment in Figure 6.17 f. Among fish exposed to DMSO during the phase of recovery, 62.5% of wild type larvae exhibit normal haemoglobinization (Figure 6.17 a), while only 37.5% show anaemia. In contrast, only 9.1% of heterozygotes have normal haemoglobinization, and 90.1% display anaemic phenotype (Figure 6.17 a'), as shown in Figure 6.13. Treatment with increasing concentrations of motolimod during the recovery phase led to variable increases of the percentage of heterozygous *rps14*$^{+/E8fs}$ larvae with normal haemoglobinization (Figure 6.17 f). Among heterozygotes treated with 0.1 µM motolimod, 75% of larvae show anaemic phenotype (Figure 6.17 b'), 80% of those treated with 1 µM motolimod (Figure 6.17 c'). In the group exposed to 10 µM motolimod, half of heterozygotes show anaemia (Figure 6.17 d'), and 53% of heterozygotes treated with 100 µM (Figure 6.17 e'). In contrast to what was observed in the results shown in Figure 6.15 and Figure 6.16, exposure to increasing concentrations of motolimod produced a progressive increment in the percentage of wild type larvae exhibiting normal haemoglobinization (Figure 6.17 f), from 50.0% in wild type larvae treated with 0.1 µM motolimod, to 100% of those treated with 100 µM motolimod. These results show a significant effect of TLR8 modulation increasing the haemoglobinization of wild type larvae after haemolytic stress. However, the effect of motolimod treatment on the haemoglobinization phenotype of heterozygous *rps14*$^{+/E8fs}$ mutant larvae is milder than that observed among wild type fish.

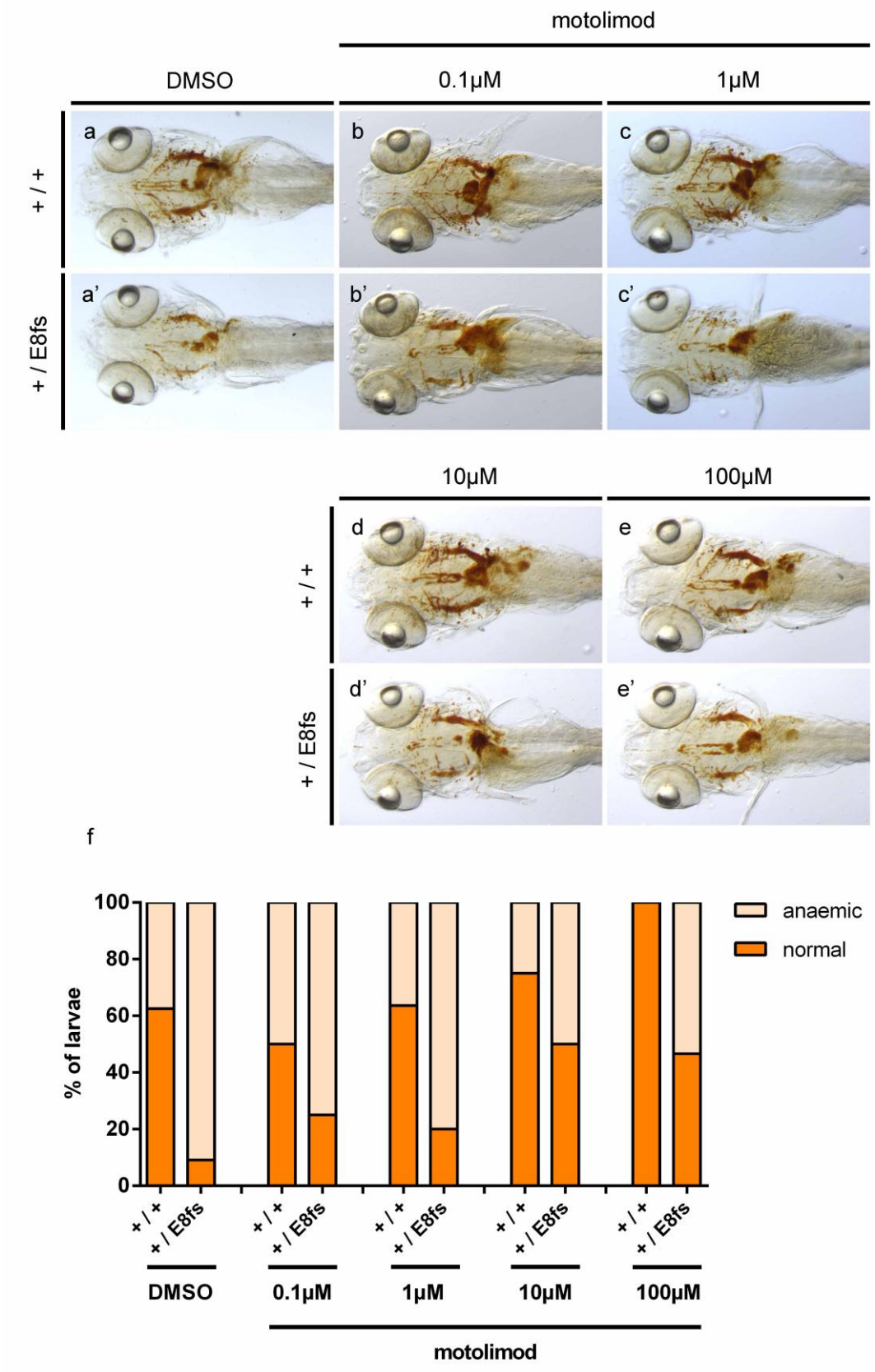
motolimod
DMSO
0.1μM
1μM
a
b
c
+ / +
a'
b'
c'
+ / E8fs
10μM
100μM
d
e
+ / +
d'
e'
+ / E8fs
f
100
80
60
40
20
0
% of larvae
anaemic
normal
+ / +
+ / E8fs
DMSO
0.1μM
1μM
10μM
100μM
motolimod

Figure 6.17 | (in previous page) Haemoglobinization after haemolytic stress in *rps14*^{E8fs} mutant larvae treated with the TLR8 agonist, motolimod.

Effect of motolimod on haemoglobinization during recovery after haemolytic stress. Haemolytic stress was induced by exposure of *rps14*^{E8fs} mutant fish to 1 µg/mL PHZ from 24 hpf to 48 hpf. Fish were allowed to recover until 6 dpf in the presence of increasing concentrations of motolimod or DMSO. At 6 dpf, larvae were stained with *o*-dianisidine and imaged to assess their degree of haemoglobinization. In **(a-e')**, ventral views of *o*-dianisidine stainings of 6 dpf larvae are shown with anterior to the left. Representative wild type **(a-e)** and heterozygous *rps14*$^{+/E8fs}$ mutant **(a'-e')** larvae are shown for each treatment: 1% v/v DMSO **(a and a')**, 0.1 µM motolimod **(b and b')**, 1 µM motolimod **(c and c')**, 10 µM motolimod **(d and d')**, and 100 µM motolimod **(e and e')**. In **(f)**, the percentage of larvae with normal (dark orange) or anaemic (light orange) phenotype is graphed for each genotype under each different treatment.

6.4 Discussion

The Table 6.6 summarizes the main haematopoietic phenotypes found in *rps14*^{E8fs} mutants.

Table 6.6 | Summary of the haematopoietic phenotype of *rps14*^{E8fs} mutants.

Lineage	Phenotype observed
HSCs	Dose dependent decrease of *Tg(itga2b:GFP)+* cells in the CHT at 4 dpf.
Erythroid cells	Decreased *o*-dianisidine staining in homozygotes at 48 hpf. Decreased *o*-dianisidine staining in homozygotes at 4 dpf. Decreased *o*-dianisidine staining in 36 hpf heterozygotes raised at 22 °C. Decreased *o*-dianisidine staining in 6 dpf heterozygotes recovering from chemically induced haemolysis. Decreased *Tg(gata1a:dsRed)+* cells in 6 dpf heterozygotes recovering from chemically induced haemolysis.
Myeloid cells	Dose dependent decrease of Sudan Black+ cells in the CHT at 48 hpf. Dose dependent decrease of Sudan Black+ cells in the CHT at 4 dpf.

6.4.1 Primitive haematopoiesis requires normal levels of Rps14

Although primitive haematopoiesis was not studied in detail, experiments carried out in *rps14*^{E8fs} mutant embryos suggest that *rps14* deficiency affects the haematopoietic cells derived from the primitive wave of haematopoiesis or from EMPs. The phenotype of homozygous *rps14*$^{E8fs/E8fs}$ mutant embryos suggests that Rps14 is required in multiple processes. Homozygous mutant fish exhibit a severedevelopmental delay detectable at 48 hpf (Figure 6.1 c and c'), and morphological abnormalities, such as shorter body length, smaller eyes, ventral curvature of the tail (Figure 6.2 c and Figure 6.6 c), and cardiac oedema (Figure 6.6 c), as reported previously in *rps14* morphants (Jung, 2013). Additionally, homozygous *rps14*$^{E8fs/E8fs}$ mutation is lethal, and *rps14*$^{E8fs/E8fs}$ larvae do not survive beyond 5 dpf. These morphological abnormalities and the developmental delay make it necessary to use wild type controls at equivalent developmental stages, not necessarily the same chronological age, to draw conclusions from the phenotypes observed in their haematopoietic cells. This restriction is particularly

important when comparing numbers of cells. However, it is important to notice that the production of both *o*-dianisidine^{+} erythroid cells and Sudan Black^{+} granulocytes is not completely abolished in homozygous *rps14*$^{E8fs/E8fs}$ mutant embryos (Figure 6.1 c and c', and Figure 6.2 c and d). These results suggest that Rps14 is dispensable for the production of erythrocytes and granulocytes at this stage. However, there is robust evidence showing that *rps14* deficiency induces a decrease in the number of *o*-dianisidine^{+} erythroid cells and Sudan Black^{+} granulocytes.

In contrast to homozygous mutants, heterozygous *rps14*$^{+/E8fs}$ mutant embryos display normal development without detectable morphological defects, making their phenotypes directly comparable with their wild type siblings. *O*-dianisidine stainings on 48 hpf *rps14*^{E8fs} mutant embryos, in Figure 6.1, show no detectable differences in the haemoglobinization of heterozygous *rps14*$^{+/E8fs}$ embryos and their wild type siblings. Although these results suggest that heterozygosity for *rps14* does not affect development of erythroid cells from the primitive wave of haematopoiesis and EMPs, cold stress experiments (Figure 6.12) suggest otherwise. By prim-22 stage (36 hpf), heterozygous *rps14*$^{+/E8fs}$ mutant larvae exposed to cold stress show a high penetrance of anaemia (66.7%), compared to that observed among wild type embryos (25.0%, Figure 6.12). Given that at this developmental stage EMPs are already present in the PBI (Bertrand et al., 2007), the anaemic phenotype observed in heterozygotes under cold stress suggests that *rps14* haploinsufficiency disrupts the development of erythroid cells from the primitive wave of haematopoiesis and from EMPs.

Additionally, quantifications of erythroid cells by flow cytometry on 3 dpf *rps14*^{E8fs} mutant larvae after haemolytic stress also suggest that *rps14* haploinsufficiency affects EMPs. Haemolytic stress was induced by treatment with PHZ from 24 hpf to 48 hpf, which induces the death of the vast majority of erythroid cells present at this stage (Lenard et al., 2016; Shafizadeh et al., 2004). The work of Lenard and colleagues with PHZ (Lenard et al., 2016), suggests that the erythroid cells observed at 3 dpf come from both EMPs (Bertrand et al., 2007) and from the first HSCs that colonize the CHT (Murayama et al., 2006). Results in Figure 6.14 c show that heterozygous *rps14*$^{+/E8fs}$ mutant larvae have a reduced number of erythroid gata1a:dsRed^{+} cells compared to their wild type siblings. This suggests that *rps14* haploinsufficiency could affect the production of erythroid cells from

EMPs. However, it is also possible that these results are explained by a disruption in HSCs, given that quantifications carried out at a later stage (4 dpf) show a dose dependent reduction in the number of itga2b:GFP^{low} HSCs in the CHT (Figure 6.6).

Quantifications of granulocytes stained with Sudan Black in 48 hpf *rps14*^{E8fs} mutant embryos shows a dose dependent decrease in the number of labelled granulocytes in the CHT of both heterozygous and homozygous *rps14*$^{E8fs/E8fs}$ mutant larvae (Figure 6.2). Different reports suggest that the granulocytes found in the CHT of 48 hpf embryos are most likely a mixture of granulocytes derived from EMPs, neutrophils derived from the primitive wave of haematopoiesis, and possibly some granulocytes derived from the first HSCs that colonize the CHT. It has been shown that the first cells showing detectable accumulation of Sudan Black are observed at 33 hpf (Le Guyader et al., 2008), consistently with results obtained using the transgenic *TgBAC(mpx:GFP)i114* reporter, where the first GFP^{+} neutrophils are found by 30 hpf, and their number increases linearly during the next two days (Renshaw et al., 2006). EMPs expressing *lmo2* and *gata1a* have been found in the PBI at this stage (30 hpf) (Bertrand et al., 2007), suggesting that an important proportion of granulocytes in the CHT labelled by Sudan Black by 48 hpf are derived from EMPs. Therefore, it could be hypothesized that *rps14* haploinsufficiency could affect the function, or number, of EMPs, given that the production of both erythroid and myeloid cells is decreased.

6.4.2 Defective definitive haematopoiesis in *rps14*$^{+/E8fs}$ heterozygotes

Once definitive haematopoiesis starts, myeloid, erythroid and lymphoid cells are produced ultimately by HSCs (Ciau-Uitz et al., 2014). HSCs emerge from the ventral wall of the DA (Bertrand et al., 2010; Kissa and Herbomel, 2010), enter the blood circulation through the CV, and colonize the CHT where definitive haematopoiesis occurs transiently (Murayama et al., 2006). At later stages, HSCs from the CHT colonize the kidney (Bertrand et al., 2008) and thymi (Hess and Boehm, 2012; Kissa et al., 2007), where definitive haematopoiesis carries on until adulthood.

HSCs have a central role in definitive haematopoiesis, and the results in Figure 6.6 show a dose dependent decrease in the number of itga2b:GFP^{low} HSCs in the CHT

of 4 dpf *rps14*^{E8fs} mutant larvae. The difference observed between heterozygous *rps14*$^{+/E8fs}$ mutant larvae and their wild type siblings is moderate, but statistically significant (p = 0.049, Figure 6.6 d). The cause of the observed decrease in the number of HSCs in the CHT was not determined, but there are some possible hypotheses that could explain this phenotype.

Possible hypotheses could be based on a defect in the processes involved in the emergence of HSCs from the DA. Abnormal EHT, release of new HSCs from the endothelium, homing to the CHT, or proliferation of HSCs in the CHT could explain the lower numbers observed in heterozygotes. It is relevant to mention quantifications of itga2b:GFP^{low} cells carried out by flow cytometry in the kidney marrows of adult *rps14*^{E8fs} mutant fish at 5 months (Dr Elspeth Payne, unpublished data). In 5 months adult fish, the kidney marrows of heterozygotes show significantly higher numbers of itga2b:GFP^{low} progenitor cells compared to those found in wild type fish (Dr Elspeth Payne, unpublished data). Interestingly, no other haematopoietic lineages were found to be affected in the kidney marrow of heterozygotes. These results combined show that the generation of HSCs in the kidney marrow of heterozygous *rps14*$^{+/E8fs}$ mutant fish is not defective.

The effect of *rps14* haploinsufficiency on HSCs probably has a complex explanation, given that flow cytometry analysis of kidney marrows of adult *rps14*^{E8fs} mutant fish at 12 months show a significant decrease of the number of progenitors in heterozygotes, accompanied by significant decreases in erythroid, myeloid, and lymphoid cells (Dr Elspeth Payne, unpublished data). The observed signs of marrow failure and dysplasia in all haematopoietic lineages suggest that haematopoietic progenitors in heterozygotes undergo increased cycling, as reported previously in a conditional *Rps14* knockout murine model (Schneider et al., 2016).

In addition to the decrease in the number of itga2b:GFP^{low} HSCs in the CHT of heterozygous *rps14*$^{+/E8fs}$ larvae at 4 dpf (Figure 6.6), there is evidence that suggests an increment in the number of circulating thrombocytes at the same stage (Figure 6.7). This is consistent with the thrombocytosis observed in patients with del(5q) MDS (Brusamolino et al., 1988) and suggests the possibility of a role for RPS14 in thrombocytosis in del(5q) patients. Thrombocytosis has also been reported previously in a murine model with knockdown of two microRNAs (miRNAs): Mir145 and Mir146a (Starczynowski et al., 2010). Similar results have

been reported in *in vitro* studies on human cells after Mir145 knockdown (Kumar et al., 2011).

Erythroid development in heterozygous *rps14*$^{+/E8fs}$ mutant larvae was studied in normal conditions and also under haemolytic stress. Using a histochemical technique, *o*-dianisidine staining, the haemoglobinization of erythroid cells was studied in *rps14*^{E8fs} mutant fish. By 4 dpf, heterozygous *rps14*$^{+/E8fs}$ mutant larvae show normal levels of haemoglobinization, with no detectable differences from their wild type siblings (Figure 6.1). However, quantification by flow cytometry of dsRed^{+} erythroid cells in 4 dpf transgenic *Tg(gata1a:dsRed)* larvae carrying *rps14*^{E8fs} mutations shows a dose dependent decrease (Dr Elspeth Payne, unpublished data). This moderate decrease in the number of erythroid cells found in heterozygotes differs from the severe anaemia reported in *rps14* morphants (Jung, 2013; Payne et al., 2012), whose phenotype is very similar to that of homozygous *rps14*$^{E8fs/E8fs}$ mutant fish (Figure 6.1). These results suggest that the actual levels of expression in *rps14* morphant fish used in previous reports (Jung, 2013; Payne et al., 2012) were below the level of expression observed in heterozygotes, however, genetic compensation in heterozygous *rps14*$^{+/E8fs}$ mutant fish cannot be ruled out (El-Brolosy and Stainier, 2017; Rossi et al., 2015).

Exposure of heterozygous *rps14*$^{+/E8fs}$ mutant fish to two different forms of stress induced in both cases a severe increase in the penetrance of a phenotype of low haemoglobinization of erythroid cells (Figure 6.12 and Figure 6.13). In the case of haemolytic stress, the use of PHZ to induce the death of all erythroid cells between 24 hpf and 48 hpf, provided an opportunity to study the recovery of erythroid cells in the absence of a significant proportion of those erythroid cells produced during the primitive wave of haematopoiesis (Figure 6.13). By 48 hpf, when the recovery period starts, the first HSCs have already colonized the CHT (Murayama et al., 2006), and the EMPs expressing *lmo2* and *gata1a* are not found after 72 hpf (Bertrand et al., 2007). This suggests that the majority of the *o*-dianisidine^{+} erythroid cells observed by 6 dpf are derived from HSCs, with a contribution of cells derived from EMPs. The observed increase in the penetrance of anaemic phenotype among heterozygotes after haemolytic stress (Figure 6.13) shows that *rps14* haploinsufficiency affects the development of erythroid cells from the definitive wave of haematopoiesis.

The number of granulocytes in the CHT at 4 dpf larvae show a dose dependent decrease in *rps14*^{E8fs} larvae (Figure 6.3). Granulocytes found in the CHT of 4 dpf larvae derive from HSCs, EMPs, and the primitive wave of haematopoiesis. Results of quantifications in *rps14*^{E8fs} embryos at 48 hpf show that there is an effect of *rps14* deficiency at this stage (discussed in section 6.4.1), however, close examination of the data suggests that the effect of *rps14*^{E8fs} heterozygosity on granulopoiesis in 48 hpf embryos (Supplementary Table 9.44) is not sufficient to explain the decrease observed in the granulocytes of 4 dpf heterozygotes (Supplementary Table 9.45). Then, it can be hypothesized that *rps14* haploinsufficiency also has an effect on definitive granulopoiesis in the CHT.

6.4.3 A role for TLR7 in regulation of developmental haematopoiesis

A drug screen carried out in *rps14* morphant identified imiquimod, an agonist of TLR7 and TLR8 (Hemmi et al., 2002; Jurk et al., 2002), that is able to induce a partial rescue of the haemoglobinization in *rps14* morphants, together with moderate improvements in other morphological abnormalities (Jung, 2013).

Given that heterozygous *rps14*$^{+/E8fs}$ mutant fish do not show a severe anaemic phenotype (Figure 6.1) comparable to that found in *rps14* morphants (Payne et al., 2012), the rescue experiments with imiquimod carried out previously (Jung, 2013) could not be performed with *rps14*^{E8fs} mutants. As an example, Figure 6.11 shows quantifications of HSCs and granulocytes in *rps14*^{E8fs} mutant larvae exposed to imiquimod, however, no evidence of significant changes elicited by imiquimod was found.

Haemolytic stress, induced by treatment with PHZ as described previously (Lenard et al., 2016; Shafizadeh et al., 2004), allowed to uncover a latent anaemic phenotype in heterozygous *rps14*$^{+/E8fs}$ mutant larvae (Figure 6.13 and Figure 6.14), and importantly, it also provided a model of a phenotype that could be rescued by pharmacological modulation of pathways of interest. Previous work had identified that the modulation of TLR7, TLR8 or both by exposure to imiquimod was able to induce a rescue of the haemoglobinization in *rps14* morphants (see Figure 6.8, adapted from Jung, 2013). Therefore, imiquimod treatment was used during the recovery phase of larvae after haemolytic stress to validate previous findings, now

in a heterozygous mutant model of *rps14* deficiency. The results show that imiquimod treatment can decrease the prevalence of anaemia among the heterozygotes, to levels comparable to those observed among the wild type larvae (Figure 6.15). The confirmation of the previous results obtained using *rps14* morphants (Jung, 2013), through experiments with heterozygous *rps14*$^{+/E8fs}$ mutant fish, suggests that despite the discussed differences between morphants and mutants, the underlying molecular mechanisms for imiquimod's action are conversed in these experimental models.

Similar experiments of recovery of haemolytic stress in the presence of agonists of TLR7 (Figure 6.16) and TLR8 (Figure 6.17) were carried out to study the role both receptors in the development of erythroid cells. Recovery after haemolytic stress in the presence of the TLR7 agonist, gardiquimod (Zhu et al., 2008), induced a dose dependent increase in the penetrance of normal haemoglobinization among heterozygotes (Figure 6.16). These results suggest that pharmacological activation of TLR7 is sufficient to induce a rescue in the haemoglobinization levels of heterozygous *rps14*$^{+/E8fs}$ larvae.

Interestingly, exposure to gardiquimod did not induce detectable changes in the haemoglobinization of wild type larvae, suggesting that TLR7 modulation has an impact on erythroid development only among heterozygotes. In contrast, treatment with the TLR8 agonist, motolimod (Lu et al., 2012), induces a dose dependent increase in the percentage of wild type larvae exhibiting normal haemoglobinization after haemolytic stress (Figure 6.17). These results suggest that the development of erythroid cells can be regulated by TLR8 signalling in wild type fish. Both *tlr7* and *tlr8b* (previously known as TLR8.1) are expressed throughout embryonic development since 12 hpf (Jault et al., 2004) and in adults (Meijer et al., 2004).

It could be hypothesized that TLR7 modulation by imiquimod and gardiquimod has an effect in the number of HSCs or other haematopoietic progenitors. For this reason, flow cytometry experiments were carried out on transgenic *Tg(itag2b:GFP) rps14*^{E8fs} mutants exposed to imiquimod after haemolytic stress, to determine whether imiquimod treatment induces a change in the number of itag2b:GFP^{low} cells. However, the quantifications of itag2b:GFP^{low} cells in individual larvae were not reproducible, possibly due to the low number of cells present in each fish.

It is important to highlight that there is evidence that suggests that the effects of imiquimod exposure on erythroid development are not restricted to the rescue of deficiencies in ribosomal proteins, as that found in *rps14*^{E8fs} mutant fish. Treatment of *gata1a* morphant embryos with imiquimod induced an increase in the number of *Tg(gata1a:dsRed)*$^{+}$ cells (Figure 6.10). Additionally, analysis of erythroid cells of *gata1a* morphant embryos after cytospin shows a partial rescue of the differentiation of erythroid cells in the group morphants treated with imiquimod (Dr Elspeth Payne, unpublished data). These results show that exposure to imiquimod can partially rescue anaemia in *gata1a* morphant embryos. The fact that pharmacological modulation of TLR signalling with imiquimod can alleviate anaemia in these different models suggests the possibility that TLR7 or TLR8, or both, have a role in regulating erythroid cell development.

7 Conclusion

7.1 Towards a zebrafish model of TEL-AML1 leukaemia

7.1.1 *Tg(ZβA:hTEL-AML1-EGFP)* transgenic fish as a model of t(12;21)(p13;q22) chromosomal translocation in humans

The study of developmental haematopoiesis in *Tg(ZβA:hTEL-AML1-EGFP)* transgenic embryos showed that the expression of the human TEL-AML1 fusion protein is sufficient to induce a transient increase in the number of granulocytes in the CHT of fish. Importantly, this shows that hTEL-AML1 fusion protein is active in zebrafish, highlighting the high degree of conservation between zebrafish and humans. The conservation of the molecular mechanisms that direct haematopoiesis, as well as that of the molecular components involved are crucial, as they could allow the use of zebrafish for large chemical screenings to find potential molecules capable of modulating hTEL-AML1 activity. Perhaps the simplest design would allow the identification of molecules that inhibit the activity of hTEL-AML1. However, it is interesting to note that if the hypothesis of addiction to hTEL-AML1 is correct, then hTEL-AML1 activity would be required for the maintenance of the cells, and its inhibition would affect the viability of those cells expressing hTEL-AML1.

Additionally, there are reasons to think that the restricted effects of hTEL-AML1 expression in *Tg(ZβA:hTEL-AML1-EGFP)* transgenic fish could be caused by the restricted expression of the transgene (see Figure 3.1). Comparison of transgenic animal models expressing TEL-AML1 fusion protein shows that lymphoid promoters, including those of *rag2* and *IGH* genes, fail to induce leukaemia both in zebrafish and mice (Andreasson et al., 2001; Sabaawy et al., 2006). Murine models where TEL-AML1 expression is controlled by the endogenous *TEL* gene promoter have reported alterations in the haematopoietic compartment, and develop leukaemia when combined with other genetic lesions (Schindler et al., 2009; van der Weyden et al., 2011).

Transgenic *ZBA-EGFP-TA* fish have been shown to develop overt leukaemia with low penetrance during adulthood (Sabaawy et al., 2006). In both the *ZBA-EGFP-TA* (Sabaawy et al., 2006) and *Tg(ZβA:GFP-hTEL-AML1)* transgenic fish, the

human TEL-AML1 fusion protein is fused to GFP, and the expression of the whole DNA construct is controlled by a fragment of the promoter of the zebrafish *β-actin* gene (Higashijima et al., 1997; Sabaawy et al., 2006). Although the zebrafish *β-actin* gene promoter is thought to direct expression to all lineages, it has been reported that it drives expression mainly to skin cells (Higashijima et al., 1997; Traver et al., 2003) but at low levels in haematopoietic cells (Mosimann et al., 2011). These reports are consistent with the results shown in Figure 3.1, and they could explain the low penetrance of leukaemia in *ZBA-EGFP-TA* transgenic fish (Sabaawy et al., 2006).

It is important to mention another aspect of the design of animal models that carry a transgene to express human TEL-AML1 fusion protein. The t(12;21)(p13;q22) chromosomal translocation fuses part of the coding sequence of one copy of the *TEL* gene to one of the copies of the *AML1* gene (Romana et al., 1995). As a result, the resulting *TEL-AML1* fusion gene is expressed under the control of the promoter of *TEL* gene, and the cell that has undergone the chromosomal translocation is left with only one remaining wild type copy of the *TEL* gene (Zelent et al., 2004). Two murine models have been developed that express human TEL-AML1 under the control of the endogenous *TEL* gene promoter, this means that the transgene carrying *TEL-AML1* sequence is inserted in one of the endogenous copies of the *TEL* gene, disrupting it (Schindler et al., 2009; van der Weyden et al., 2011). Consistent with this, both studies report embryonic lethality in the homozygous transgenic mice (Schindler et al., 2009; van der Weyden et al., 2011), in agreement with what has been shown for homozygous *TEL* knockout mice (Wang et al., 1997). The function of the wild type copies of the *TEL* has critical importance in the development of a model for leukaemia, because the loss of the non-translocated copy of *TEL* gene is one of the most frequent secondary genetic alterations found in *TEL-AML1*-positive patients (Attarbaschi et al., 2004).

7.1.2 Further development of transgenic fish to model TEL-AML1 leukaemias

The genome editing technologies currently available allow the generation of zebrafish models of TEL-AML1 leukemia of higher complexity than an insertion of a transgene in a random site of the genome. Such complexity could overcome

many of the defects of the current transgenic models, making it possible for the new research models to represent more accurately the genomic consequences of the t(12;21)(p13;q22) chromosomal translocation. Additionally, such models could incorporate tools that will help to address many additional aspects of the development and molecular causes of the disease. An interesting example is the hypothesis of TEL-AML1 addiction, according to which leukaemic cells become dependent on the expression of TEL-AML1 (Mangolini et al., 2013; Teitell and Pandolfi, 2009). A simple approach to test this hypothesis would be to develop a transgenic model where the expression of hTEL-AML1 can be stopped at a given time. A possible design for a zebrafish model of TEL-AML1 is represented schematically in Figure 7.1. In the proposed model, the expression of the hTEL-AML1 fusion protein is achieved by the targeted insertion of a DNA cassette downstream of the promoter of the endogenous zebrafish *tel* gene (Figure 7.1 a). This DNA cassette would allow the hTEL-AML1 chimeric protein and EGFP to be expressed as two different peptides, separated by the P2A peptide from porcine teschovirus-1. The two proteins are produced separated in a stoichiometric fashion because the peptide bond between the last two amino acids of P2A peptide fails to form (Provost et al., 2007; Weber and Köster, 2013). This strategy, already proven in zebrafish (Provost et al., 2007), would allow imaging of cells expressing hTEL-AML1 by fluorescent microscopy, avoiding the interference of EGFP in hTEL-AML1 activity. In the proposed model, the *EGFP-P2A-hTEL-AML1* sequence is flanked by *loxP* sites, in this way it can be used in combination with transgenic fish expressing Cre to generate a switchable model. The *Tg(ubi:cre^{ERt2})* transgenic fish (Mosimann et al., 2011) is shown in the Figure 7.1 b as an example of one application of this strategy. In the resulting compound transgenic fish (Figure 7.1 c), the ubiquitously expressed Cre^{ERt2} recombinase will be activated by the addition of 4-OH (4-hydroxytamoxifen) to the media. Cre^{ERt2} recombinase would elicit the excision of the *EGFP-P2A-hTEL-AML1* fragment, leaving the sequences encoding mKOκ (monomeric Kusabira orange kappa) fluorescent protein next to the *tel* gene promoter. The excision of the transgene encoding hTEL-AML1 would be visible by the loss of EGFP expression, and those cells that carried out Cre-mediated recombination would still be visible by the expression of mKOκ, also controlled by the *tel* gene promoter. In this way this transgenic model would allow removal of the transgene encoding hTEL-AML1 fusion, to identify those cells that

have lost hTEL-AML1 encoding gene, and to track those cells after the excision using fluorescence microscopy (Figure 7.1 c).

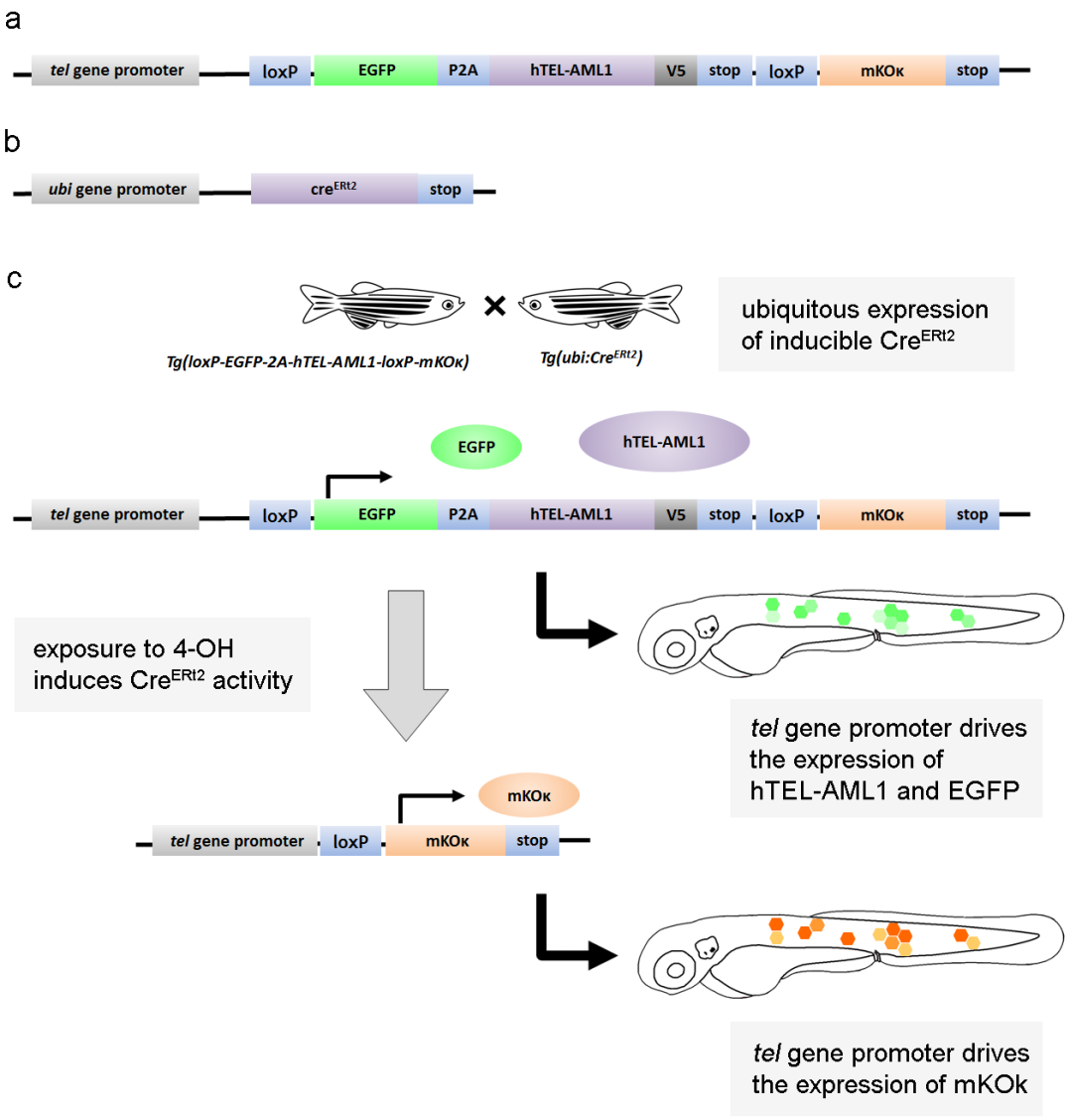

Figure 7.1 | Design of a switchable zebrafish model of TEL-AML1 leukaemia.

(a) Schematic representation of a hypothetic zebrafish model of TEL-AML1 leukaemia. A DNA construct encoding EGFP and hTEL-AML1 proteins has been inserted downstream the promoter of the *tel* zebrafish gene leaving the expression of the transgene under the control of *tel* gene promoter. *EGFP-P2A-hTEL-AML1* sequence is flanked by *loxP* sites and followed by the gene encoding mKOκ

protein. **(b)** Diagram of the DNA construct inserted in a transgenic line expressing an inducible Cre (Mosimann et al., 2011) (Cre^{ERt2}) where a fragment of the zebrafish *ubiquitin B* gene promoter drives the expression Cre^{ERt2}. **(c)** Diagram of the hypothetical cross of the transgenic lines described in **(a)** and **(b)**: the compound transgenic embryos express both EGFP and hTEL-AML1 in the domain of expression of zebrafish *tel* gene, and parallelly, the inactive Cre^{ERt2} protein is expressed ubiquitously. Once double transgenic embryos are exposed to 4-OH, Cre^{ERt2} activity is induced and the sequence of *EGFP-P2A-hTEL-AML1* is excised, stopping the expression of EGFP and hTEL-AML1, and leaving the expression of mKOκ under de control of *tel* promoter. DNA constructs are not depicted proportionally to the actual length of their sequences. Diagram in **(b)** was modified from Mosimann et al., 2011.

The insertion of the sequence encoding hTEL-AML1 and the fluorophores in the first exons of the zebrafish *tel* gene has two objectives. As already mentioned, in this way the expression of hTEL-AML1 fusion protein is controlled by the *tel* gene promoter, as in the t(12;21)(p13;q22) chromosomal translocation (Zelent et al., 2004). Additionally, a homozygous fish for this transgenic insertion would have at the same time an insertional deletion of both wild type endogenous copies of the *tel* gene. Given the fact that TEL-AML1 patients with loss of the nontranslocated copy of *TEL*, one of the most recurrent deletions found in TEL-AML1 leukemia, have a worse prognosis than those without it (Attarbaschi et al., 2004), the insertional deletion of the zebrafish *tel* gene is expected to increase the penetrance of overt leukaemia. Importantly, zebrafish lines carrying insertional deletions of the *tel* gene without the hTEL-AML1 expression could be obtained by Cre^{ERt2}-mediated excision of hTEL-AML1 gene (Figure 7.1 c), to be used as experimental controls for the effect of hTEL-AML1 expression. This design will also allow studying the effect of different levels of expression of hTEL-AML1 by the generation of transgenic lines carrying different numbers of copies of the hTEL-AML1 fusion gene. Finally, transplantation experiments of cells from this transgenic model to wild type recipients would allow the study of the effects of hTEL-AML1, $tel^{-/-}$ cells in a wild type $tel^{+/+}$ cellular environment that does not express hTEL-AML1.

Another interesting possibility is the development of zebrafish lines that allow the study of the clonality of leukaemias induced by hTEL-AML1 expression. The Brainbow (Weber and Köster, 2013) system could be used in a similar strategy to that presented in Figure 7.1. In the proposed model (Figure 7.2), Cre protein is expressed together with hTEL-AML1 under the control of the endogenous zebrafish *tel* gene (Figure 7.2 a), as described in Figure 7.1 a. This fish line could be outcrossed to a fish carrying a Brainbow DNA construct. As an example, Figure 7.2 b shows a diagram representing the transgenic insertion in the *Tg(ubi:Zebrabow-S)a132* transgenic zebrafish line (Pan et al., 2013). Compound transgenic fish (Figure 7.2 c) would carry out Cre-mediated recombination in those cells expressing Cre and hTEL-AML1, making them express different combinations of fluorescent proteins. Fish could be monitored by fluorescence microscopy over time to define whether leukaemic cells are derived from a single clone or from a large number of different clones. Notice that fish expressing hTEL-AML1 and Cre could also be used in combination with other transgenic lines, like *Tg(–3.5ubi:loxP-EGFP-loxP-mCherry)* (Mosimann et al., 2011), also known as *ubi:Switch*, making it possible to label permanently all those cells derived from cells that once expressed hTEL-AML1. Additionally, in the model presented in Figure 7.2 a, the *Cre-P2A-hTEL-AML1* sequence is flanked by *frt* sites and followed by the *mKate2* gene (Shcherbo et al., 2009), to allow the excision of *Cre-P2A-hTEL-AML1* sequence when combined with fish expressing flippase (Weber and Köster, 2013), in a similar way to what is described in Figure 7.1.

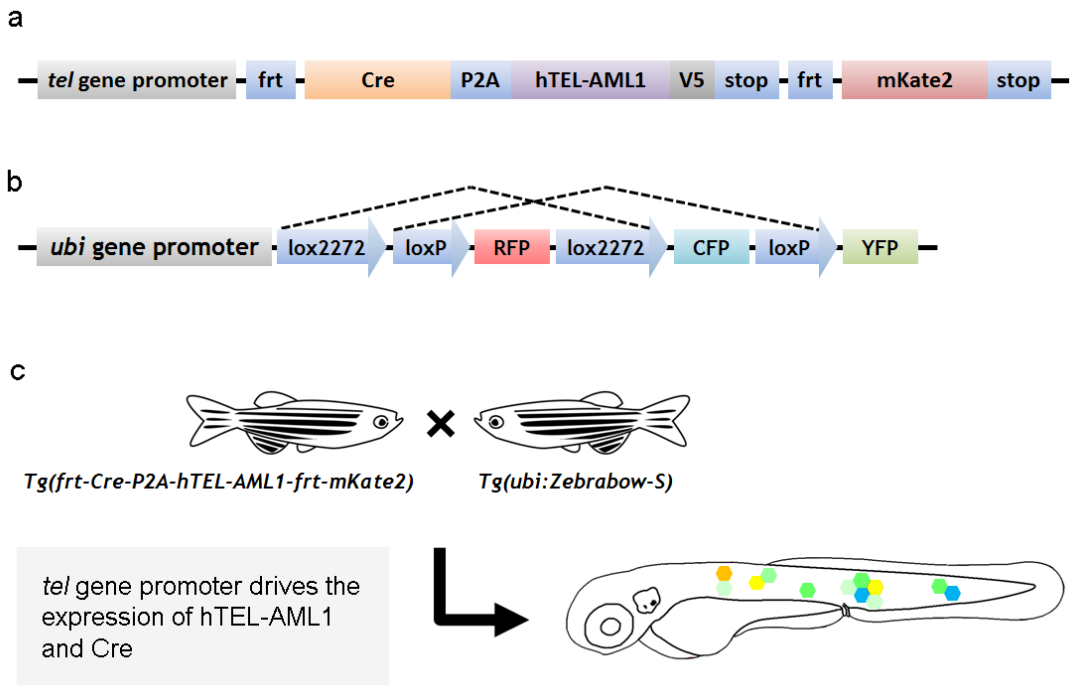

Figure 7.2 | Design of a zebrafish model to study the clonality of TEL-AML1 leukaemia.

(a) Schematic representation of a hypothetic zebrafish model of TEL-AML1 leukaemia to study clonality. Through a transgenic insertion in the endogenous *tel* locus, the sequences encoding Cre and hTEL-AML1 proteins are located under the control of the promoter of zebrafish *tel* gene. The *Cre-P2A-hTEL-AML1* DNA sequence is flanked by *frt* sites, and followed by the gene encoding the far-red protein, mKate2 (Shcherbo et al., 2009). **(b)** Schematic representation of the Brainbow construct present in the transgenic line *Tg(ubi:Zebrabow-S)a132* (Pan et al., 2013). Dashed lines indicate the Cre-mediated recombination between compatible *lox* sites. **(c)** Diagram of the hypothetical cross of the transgenic lines described in **(a)** and **(b)**: the compound transgenic embryos express both Cre and hTEL-AML1 in the domain of expression of zebrafish *tel* gene, and RFP is expressed ubiquitously. In the domain of expression of *tel* gene Cre randomly recombines the rainbow construct **(b**, dashed lines) generating cells expressing different combinations of fluorophores. RFP expression in cells that do not undergo recombination is omitted for the sake of simplicity. DNA

constructs are not depicted proportionally to the actual length of their sequences. Diagram in **(b)** was modified from Pan et al., 2013. RFP, red fluorescent protein; CFP, cyan fluorescent protein; YFP, yellow fluorescent protein.

7.2 Future studies on GATA2 deficiency using zebrafish

7.2.1 Phenotype – genotype correlation in GATA2 deficiency

It has been suggested that the extremely diverse manifestations of GATA2 deficiency found in patients could be explained by the different mutations that have been identified (Spinner et al., 2014). Spinner and colleagues (2014), analysed a cohort of patients with *GATA2* mutations, and only found statistical correlation in the case of lymphedema, which is found only in patients with null or regulatory mutations, while it was not observed in patients with missense mutations in the *GATA2* gene.

Genome editing technologies, such as CRISPR/Cas9 and TALEN, allow the generation of multiple mutant alleles in different sites of the genome, providing an effective method to study the functions of each domain of Gata2a and Gata2b, as well as the phenotypic consequences of different mutations. Throughout this work, GATA2 deficiency was modelled by using heterozygous *gata2a* and *gata2b* mutant fish. However, the results presented are almost entirely based on experiments carried out using mutants encoding truncated proteins without zinc finger domains. This kind of mutation represents only a fraction of the spectrum of mutations found in patients (Dickinson et al., 2011; Hahn et al., 2011; Hsu et al., 2011; Ostergaard et al., 2011). Further development of new zebrafish lines carrying different mutations in the *gata2a* and *gata2b* genes, would allow important questions to be considered about the function of each domain of Gata2a and Gata2b, that could be critical to our understanding of the symptoms found in patients. The additional use of NGS together with genome editing technologies allows the screening in each generation for those fish carrying relevant mutant alleles. This makes it feasible to generate mutant zebrafish lines carrying mutations that closely resemble those found in patients. Although the conservation at the level of genomic DNA sequence can represent a problem to identify an equivalent in certain regions of the zebrafish genes, the regions with more clinical relevance are those encoding zinc finger domains (Spinner et al., 2014; Wlodarski et al., 2016).

7.2.2 Towards a model of somatic *GATA2* mutations

The combination of CRISPR/Cas9 technology and NGS opens another interesting possibility to model GATA2 deficiency in zebrafish. Given that the components of CRISPR/Cas9 technology can be genetically encoded, several research groups have been working on the development of strategies to induce conditional mutants by inducing the expression of both sgRNA and Cas9 protein in a tissue and time-controlled manner (Henninger et al., 2017; Putri and Chen, 2018; Simone et al., 2018). Using this technique with appropriate promoters, it would be possible to express sgRNAs targeting *gata2a* or *gata2b* genes together with Cas9 protein in small numbers of HSCs or progenitor cells. Embryonic and larval development could be skipped and the expression of the CRISPR/Cas9 components could be induced in juvenile animals or adults. This method would allow animals with small numbers of *gata2a* or *gata2b* mutant cells to be obtained in a wild type genetic background, as found in patients who carry acquired mutations (Greif et al., 2012; Spinner et al., 2014). The relevant cell populations could also be isolated, and the frequency and type of mutations could be assessed using NGS.

Another exciting possibility is to study the effect of acquired somatic mutations in a genetic background of germinal mutation. In the case of GATA2 deficiency, patients with germinal mutations in *GATA2* gene have been found to carry also somatic mutations in other loci, such as *ASXL1* (Additional sex combs-like 1 gene), *RUNX1*, *SETBP1* (SET binding protein 1), *IKZF1* (IKAROS family zinc finger 1) and *CRLF2* (cytokine receptor like factor 2) (Fisher et al., 2017). Experimental approaches with animal models would allow the assessment of the presence of synergistic effects between the pre-existent germinal mutations and the newly acquired somatic mutations. Additionally, it would be possible to interrogate whether haematopoiesis is more sensitive to somatic mutations when they arise in certain cellular compartments, by inducing the expression of CRISPR/Cas9 components in different cell types during development.

An interesting example is presented by those patients carrying germinal *GATA2* mutations together with acquired heterozygous mutations in *ASXL1* gene (Bödör et al., 2012; West et al., 2014). The zebrafish model of *GATA2* germinal mutation developed in chapters 4 and 5 could be combined with current genome-editing

technologies to target the zebrafish *ASXL1* orthologue and induce somatic mutations in a *gata2a; gata2b* heterozygous mutant genetic background.

Preliminary work in this direction was carried out, using a simple approach to generate mosaic *asxl1* mutations in double heterozygous *gata2a*$^{+/um27}$*; gata2b*$^{+/u5008}$ mutant background (data not shown)[7]. Most somatic mutations in the *ASXL1* gene found in patients are concentrated in exon 12 (Gelsi-Boyer et al., 2012), although other mutations have been reported in other exons (Abdel-Wahab et al., 2011). The most frequent mutation, c.1934dupG, leads to the frameshift p. Gly646TrpfsX12, and represents more than 50% of all mutations in *ASXL1* (Gelsi-Boyer et al., 2012). Mutations in *ASXL1* are found in MDS, myeloproliferative neoplasms, chronic myelomonocytic leukaemia, and AML. ASXL1 interacts with polycomb repressive complex 2 (PRC2), and its loss has been shown to result in the loss of gene repression by PRC2, which contributes to myeloid transformation (Abdel-Wahab et al., 2012).

The protein sequences encoded by the human *ASXL1* gene (ENSG00000171456) and its zebrafish ortholog, the *asxl1* (ENSDARG00000036956), were aligned and the zebrafish gene region equivalent to the human to that encoding human ASXL1 Gly646 was identified. Small guide RNAs targeting this region of zebrafish *asxl1* gene were designed and synthesised in the same way as described for *gata2b* sgRNAs in sections 5.2.2 and 5.2.3. The efficiency of the sgRNAs synthesised was assessed by NGS, using MiSeq, of embryos injected at 1-cell stage with the guides. One of the guides induced a rate of mutation of 40% and was then injected into 1-cell stage embryos obtained form an outcross between transgenic adult fish and double heterozygous *gata2a*$^{+/um27}$*; gata2b*$^{+/u5008}$ mutant adult fish. Quantifications of different haematopoietic cells by fluorescence microscopy was carried out from 48 hpf to 4 dpf. By 4 dpf, larvae were used for histochemical staining of granulocytes, by Sudan Black, and after quantification of labelled cells the genomic DNA of each larvae was extracted to be used for genotyping purposes. Mutations in both *gata2a* and *gata2b* genes were identified by PCR and restriction digestion as described in the sections 4.2.2 and 5.2.8, and *asxl1* mutations were identified by NGS, with MiSeq using a very similar strategy to that

[7] The work on mosaic *asxl1* mutations in heterozygous *gata2a* and *gata2b* mutant fish was carried out by Jasmine Rowell and Oscar Peña in the laboratory of Dr Elspeth Payne in the UCL Cancer Institute.

described to identify *gata2b* mutants (see section 5.2.6). Although no significant effects of somatic *asxl1* mutations were found from 48 hpf to 4 dpf, this work served as a proof of principle for the combined use of stable mutant lines, mosaic mutants obtained by CRISPR, and NGS.

The combination of these techniques to model haematological diseases with the current lineage tracing tools existing for haematopoietic cells (Henninger et al., 2017), makes zebrafish a powerful model for the study malignancies with altered clonality. Additionally, possible synergistic effects of secondary acquired mutations could be studied. A report by Avagyan and her colleagues (2017) shows the use of a similar strategy, where heterozygous *gata2b* mutant fish were injected with sgRNAs targeting *asxl1* gene, generating mosaic *asxl1* mutants in a heterozygous *gata2b* mutant background. Additionally, Avagyan and her colleagues used the optimized Zebrabow techniques (Henninger et al., 2017) to track the haematopoietic lineages. No perturbations in the haematopoietic compartments were found during embryonic and larval development. In contrast, lineage tracing in juveniles shows that somatic mutations increase the penetrance and severity of myelocytopenias found in *gata2b* heterozygous fish (Avagyan et al., 2017).

These results show that, conversely, this strategy could be applied to the study of haematological disorders where acquired *GATA2* mutations are found in patients with mutant background (Greif et al., 2012).

7.3 Concluding remarks

This work presents the development and characterization of zebrafish models for haematopoietic diseases with underlying genetic lesions. The availability of technologies for genome editing, such as CRISPR/Cas9 and TALEN, combined with classic transgenesis tools in zebrafish make it possible to develop fish lines that simulate genetic lesions found in human disorders. These technologies, together with NGS sequencing, allow the screening and identification of specific mutant alleles or transgenic insertions among a large pool of genetically modified animals, speeding up the generation of zebrafish lines with specific genetic lesions.

In this work, a transgenic zebrafish line was used as a model of B-cell leukaemias with TEL-AML1 fusion expression; CRISPR/Cas9 technology was used to generate *gata2b* zebrafish mutant lines to model GATA2 deficiency in combination with existing *gata2a*^{um27} mutant line (Zhu et al., 2011); and an *rps14* mutant line, previously generated using TALENs (Dr Elspeth Payne, unpublished data), was used as a model of MDS with del(5q). Primitive and definitive haematopoiesis were studied in these models of haematopoietic diseases to find the earliest defects in developmental haematopoiesis.

A vast amount of literature shows that despite anatomical differences, the molecular mechanisms that direct many biological processes are highly conserved between zebrafish and human. High conservation makes zebrafish an outstanding model for vertebrate biology. Mechanisms and processes discovered using zebrafish as a model have been proven to be relevant to the understanding of human biology and diseases (Tobin et al., 2010; Walters et al., 2010). Additionally, the small size of zebrafish embryos, their availability in large numbers, and low cost of maintenance, make zebrafish an ideal animal model for screening of mutants and drugs. As shown by previous work in this laboratory, a chemical screen on *rps14* morphants led to the discovery of the role of TLR signalling in the development of erythroid cells (Jung, 2013). These findings were replicated in zebrafish *rps14* mutants, and more importantly, in cells derived from patients (Dr Elspeth Payne, unpublished data), highlighting the potential of zebrafish developmental biology as a tool to investigate human diseases.

8 References

Abdel-Wahab, O., Adli, M., LaFave, L.M., Gao, J., Hricik, T., Shih, A.H., Pandey, S., Patel, J.P., Chung, Y.R., Koche, R., Perna, F., Zhao, X., Taylor, J.E., Park, C.Y., Carroll, M., Melnick, A., Nimer, S.D., Jaffe, J.D., Aifantis, I., Bernstein, B.E., Levine, R.L., 2012. ASXL1 Mutations Promote Myeloid Transformation through Loss of PRC2-Mediated Gene Repression. Cancer Cell 22, 180–193.

Abdel-Wahab, O., Pardanani, A., Patel, J., Wadleigh, M., Lasho, T., Heguy, A., Beran, M., Gilliland, D.G., Levine, R.L., Tefferi, A., 2011. Concomitant analysis of EZH2 and ASXL1 mutations in myelofibrosis, chronic myelomonocytic leukemia and blast-phase myeloproliferative neoplasms. Leukemia 25, 1200–1202.

Amores, A., Force, A., Yan, Y.L., Joly, L., Amemiya, C., Fritz, A., Ho, R.K., Langeland, J., Prince, V., Wang, Y.L., Westerfield, M., Ekker, M., Postlethwait, J.H., 1998. Zebrafish hox clusters and vertebrate genome evolution. Science 282, 1711–4.

Amulic, B., Cazalet, C., Hayes, G.L., Metzler, K.D., Zychlinsky, A., 2012. Neutrophil Function: From Mechanisms to Disease. Annu. Rev. Immunol. 30, 459–489.

Andreasson, P., Schwaller, J., Anastasiadou, E., Aster, J., Gilliland, D.G., 2001. The expression of ETV6/CBFA2 (TEL/AML1) is not sufficient for the transformation of hematopoietic cell lines in vitro or the induction of hematologic disease in vivo. Cancer Genet. Cytogenet. 130, 93–104.

Andrzejczuk, L.A., Banerjee, S., England, S.J., Voufo, C., Kamara, K., Lewis, K.E., 2018. Tal1, Gata2a, and Gata3 have distinct functions in the development of V2b and cerebrospinal fluid-contacting KA spinal neurons. Front. Neurosci. 12, 1–24.

Arinobu, Y., Iwasaki, H., Gurish, M.F., Mizuno, S., Shigematsu, H., Ozawa, H., Tenen, D.G., Austen, K.F., Akashi, K., 2005. Developmental checkpoints of the basophil/mast cell lineages in adult murine hematopoiesis. Proc. Natl. Acad. Sci. U. S. A. 102, 18105–10.

Asnagli, H., Afkarian, M., Murphy, K.M., 2002. Cutting Edge: Identification of an Alternative GATA-3 Promoter Directing Tissue-Specific Gene Expression in Mouse and Human. J. Immunol. 168, 4268–4271.

Attarbaschi, A., Mann, G., König, M., Dworzak, M.N., Trebo, M.M., Mühlegger, N., Gadner, H., Haas, O.A., 2004. Incidence and relevance of secondary chromosome abnormalities in childhood TEL/AML1 + acute lymphoblastic leukemia: An interphase FISH analysis. Leukemia 18, 1611–1616.

Avagyan, S., Mannherz, W., Zon, L., 2017. Visualizing Clonal Hematopoiesis Associated with gata2 Deficiency in Zebrafish Using Color-Barcoding, in: Blood. p. 130:4237.

Balla, K.M., Lugo-Villarino, G., Spitsbergen, J.M., Stachura, D.L., Hu, Y., Bañuelos, K., Romo-Fewell, O., Aroian, R. V., Traver, D., 2010. Eosinophils in the zebrafish: Prospective isolation, characterization, and eosinophilia induction by helminth determinants. Blood 116, 3944–3954.

Barlow, J.L., Drynan, L.F., Hewett, D.R., Holmes, L.R., Lorenzo-Abalde, S., Lane, A.L., Jolin, H.E., Pannell, R., Middleton, A.J., Wong, S.H., Warren, A.J., Wainscoat, J.S., Boultwood, J., McKenzie, A.N.J., 2010. A p53-dependent mechanism underlies macrocytic anemia in a mouse model of human 5q-syndrome. Nat. Med. 16, 59–66.

Bennett, C.M., Kanki, J.P., Rhodes, J., Liu, T.X., Paw, B.H., Kieran, M.W., Langenau, D.M., Delahaye-Brown, a, Zon, L.I., Fleming, M.D., Look, a T., 2001. Myelopoiesis in the zebrafish, Danio rerio. Blood 98, 643–651.

Bernardin, F., Yang, Y., Cleaves, R., Zahurak, M., Cheng, L., Civin, C.I., Friedman, A.D., 2002. TEL-AML1, expressed from t(12;21) in human acute lymphocytic leukemia, induces acute leukemia in mice. Cancer Res. 62, 3904–8.

Bertani, G., 1951. Studies on Lysogenesis I. The mode of phageliberation by lysogenic eschericia coli. J. Bacteriol. 62, 293–300.

Bertrand, J.Y., Chi, N.C., Santoso, B., Teng, S., Stainier, D.Y.R., Traver, D., 2010. Haematopoietic stem cells derive directly from aortic endothelium during development. Nature 464, 108–111.

Bertrand, J.Y., Kim, A.D., Teng, S., Traver, D., 2008. CD41+ cmyb+ precursors colonize the zebrafish pronephros by a novel migration route to initiate adult hematopoiesis. Development 135, 1853–1862.

Bertrand, J.Y.Y., Kim, A.D.D., Violette, E.P.P., Stachura, D.L.L., Cisson, J.L.L., Traver, D., 2007. Definitive hematopoiesis initiates through a committed erythromyeloid progenitor in the zebrafish embryo. Development 134, 4147–4156.

Bigley, V., Haniffa, M., Doulatov, S., Wang, X.-N., Dickinson, R., McGovern, N., Jardine, L., Pagan, S., Dimmick, I., Chua, I., Wallis, J., Lordan, J., Morgan, C., Kumararatne, D.S., Doffinger, R., van der Burg, M., van Dongen, J., Cant, A., Dick, J.E., Hambleton, S., Collin, M., 2011. The human syndrome of dendritic cell, monocyte, B and NK lymphoid deficiency. J. Exp. Med. 208, 227–234.

Bödör, C., Renneville, A., Smith, M., Charazac, A., Iqbal, S., Étancelin, P., Cavenagh, J., Barnett, M.J., Kramarzová, K., Krishnan, B., Matolcsy, A., Preudhomme, C., Fitzgibbon, J., Owen, C., 2012. Germ-line GATA2 p.THR354MET mutation in familial myelodysplastic syndrome with acquired monosomy 7 and ASXL1 mutation demonstrating rapid onset and poor survival. Haematologica 97, 890–894.

Böiers, C., Carrelha, J., Lutteropp, M., Luc, S., Green, J.C.A., Azzoni, E., Woll, P.S., Mead, A.J., Hultquist, A., Swiers, G., Perdiguero, E.G., Macaulay, I.C., Melchiori, L., Luis, T.C., Kharazi, S., Bouriez-Jones, T., Deng, Q., Pontén, A., Atkinson, D., Jensen, C.T., Sitnicka, E., Geissmann, F., Godin, I., Sandberg, R., de Bruijn, M.F.T.R., Jacobsen, S.E.W., 2013. Lymphomyeloid Contribution of an Immune-Restricted Progenitor Emerging Prior to Definitive Hematopoietic Stem Cells. Cell Stem Cell 13, 535–548.

Böiers, C., Richardson, S.E., Laycock, E., Zriwil, A., Turati, V.A., Brown, J., Wray, J.P., Wang, D., James, C., Herrero, J., Sitnicka, E., Karlsson, S., Smith, A.J.H., Jacobsen, S.E.W., Enver, T., 2018. A Human IPS Model Implicates Embryonic B-Myeloid Fate Restriction as Developmental Susceptibility to B Acute Lymphoblastic Leukemia-Associated ETV6-RUNX1. Dev. Cell 44, 362-377.e7.

Borregaard, N., Cowland, J.B., 1997. Granules of the human neutrophilic polymorphonuclear leukocyte. Blood 89, 3503–21.

Borregaard, N., Sehested, M., Nielsen, B.S., Sengeløv, H., Kjeldsen, L., 1995. Biosynthesis of granule proteins in normal human bone marrow cells. Gelatinase is a marker of terminal neutrophil differentiation. Blood 85, 812–7.

Boultwood, J., Fidler, C., Lewis, S., Kelly, S., Sheridan, H., Littlewood, T.J., Buckle, V.J., Wainscoat, J.S., 1994. Molecular Mapping of Uncharacteristically Small 5q Deletions in Two Patients with the 5q- Syndrome: Delineation of the Critical Region on 5q and Identification of a 5q- Breakpoint. Genomics 19, 425–432.

Boultwood, J., Fidler, C., Strickson, A.J., Watkins, F., Gama, S., Kearney, L., Tosi, S., Kasprzyk, A., Cheng, J.F., Jaju, R.J., Wainscoat, J.S., 2002. Narrowing and genomic annotation of the commonly deleted region of the 5q- syndrome. Blood 99, 4638–4641.

Brown, L.A., Rodaway, A.R.F., Schilling, T.F., Jowett, T., Ingham, P.W., Patient, R.K., Sharrocks, A.D., 2000. Insights into early vasculogenesis revealed by expression of the ETS-domain transcription factor Fli-1 in wild-type and mutant zebrafish embryos. Mech. Dev. 90, 237–252.

Brusamolino, E., Orlandi, E., Morra, E., Bernasconi, P., Pagnucco, G., Colombo, A., Lazzarino, M., Bernasconi, C., 1988. Hematologic and clinical features of patients with chromosome 5 monosomy or deletion (5q). Med. Pediatr. Oncol. 16, 88–94.

Butko, E., Distel, M., Pouget, C., Weijts, B., Kobayashi, I., Ng, K., Mosimann, C., Poulain, F.E., McPherson, A., Ni, C.-W., Stachura, D.L., Del Cid, N., Espin-Palazon, R., Lawson, N.D., Dorsky, R., Clements, W.K., Traver, D., 2015. Gata2b is a restricted early regulator of hemogenic endothelium in the zebrafish embryo. Development 142, 1050–1061.

Carroll, K.J., North, T.E., 2014. Oceans of opportunity: Exploring vertebrate hematopoiesis in zebrafish. Exp. Hematol. 42, 684–696.

Cech, P., Stalder, H., Widmann, J.J., Rohner, A., Miescher, P.A., 1979. Leukocyte myeloperoxidase deficiency and diabetes mellitus associated with Candida albicans liver abscess. Am. J. Med. 66, 149–53.

Charron, F., Nemer, M., 1999. GATA transcription factors and cardiac development. Semin. Cell Dev. Biol. 10, 85–91.

Choi, J., Dong, L., Ahn, J., Dao, D., Hammerschmidt, M., Chen, J.N., 2007. FoxH1 negatively modulates flk1 gene expression and vascular formation in zebrafish. Dev. Biol. 304, 735–744.

Chou, S.T., Khandros, E., Bailey, L.C., Nichols, K.E., Vakoc, C.R., Yao, Y., Huang, Z., Crispino, J.D., Hardison, R.C., Blobel, G. a, Weiss, M.J., 2009. Graded repression of PU.1/Sfpi1 gene transcription by GATA factors regulates hematopoietic cell fate. Blood 114, 983–94.

Ciau-Uitz, A., Monteiro, R., Kirmizitas, A., Patient, R., 2014. Developmental hematopoiesis: Ontogeny, genetic programming and conservation. Exp. Hematol. 42, 669–683.

Cooper, S., Guo, H., Friedman, A.D., 2015. The +37 kb Cebpa enhancer is critical for Cebpa myeloid gene expression and contains functional sites that bind SCL, GATA2, C/EBPα, PU.1, and additional Ets factors. PLoS One 10, 1–18.

Craven, S.E., French, D., Ye, W., De Sauvage, F., Rosenthal, A., 2005. Loss of Hspa9b in zebrafish recapitulates the ineffective hematopoiesis of the myelodysplastic syndrome. Blood 105, 3528–3534.

Da'as, S.I., Coombs, A.J., Balci, T.B., Grondin, C.A., Ferrando, A.A., Berman, J.N., 2012. The zebrafish reveals dependence of the mast cell lineage on Notch signaling in vivo. Blood 119, 3585–3594.

Dai, Y., Zhu, L., Huang, Z., Zhou, M., Jin, W., Liu, W., Xu, M., Yu, T., Zhang, Y., Wen, Z., Liao, W., Zhang, W., 2016. Cebpα is essential for the embryonic myeloid progenitor and neutrophil maintenance in zebrafish. J. Genet. Genomics 43, 593–600.

Dale, D.C., Person, R.E., Bolyard, a a, Aprikyan, a G., Bos, C., Bonilla, M. a, Boxer, L. a, Kannourakis, G., Zeidler, C., Welte, K., Benson, K.F., Horwitz, M., 2000. Mutations in the gene encoding neutrophil elastase in congenital and cyclic neutropenia. Blood 96, 2317–22.

Dana, S., Wasmuth, J.J., 1982. Linkage of theleuS, emtB, andchr genes on chromosome 5 in humans and expression of human genes encoding protein synthetic components in human-Chinese hamster hybrids. Somatic Cell Genet. 8, 245–264.

Danilova, N., Steiner, L. a A., 2002. B cells develop in the zebrafish pancreas. Proc. Natl. Acad. Sci. 99, 13711–13716.

De Braekeleer, E., Douet-Guilbert, N., Morel, F., Le Bris, M.J., Basinko, A., De Braekeleer, M., 2012. ETV6 fusion genes in hematological malignancies: A review. Leuk. Res. 36, 945–961.

de Pater, E., Kaimakis, P., Vink, C.S., Yokomizo, T., Yamada-Inagawa, T., van der Linden, R., Kartalaei, P.S., Camper, S.A., Speck, N., Dzierzak, E., 2013. Gata2 is required for HSC generation and survival. J. Exp. Med. 210, 2843–50.

Dekker, R.J., Van Soest, S., Fontijn, R.D., Salamanca, S., De Groot, P.G., VanBavel, E., Pannekoek, H., Horrevoets, A.J.G., 2002. Prolonged fluid shear stress induces a distinct set of endothelial cell genes, most specifically lung Krüppel-like factor (KLF2). Blood 100, 1689–1698.

den Dunnen, J.T., Dalgleish, R., Maglott, D.R., Hart, R.K., Greenblatt, M.S., McGowan-Jordan, J., Roux, A.-F., Smith, T., Antonarakis, S.E., Taschner, P.E.M., 2016. HGVS Recommendations for the Description of Sequence Variants: 2016 Update. Hum. Mutat. 37, 564–569.

Detrich, H.W., Kieran, M.W., Chan, F.Y., Barone, L.M., Yee, K., Rundstadler, J.A., Pratt, S., Ransom, D., Zon, L.I., 1995. Intraembryonic hematopoietic cell migration during vertebrate development. Proc. Natl. Acad. Sci. U. S. A. 92, 10713–7.

Diakos, C., Krapf, G., Gerner, C., Inthal, A., Lemberger, C., Ban, J., Dohnal, A.M., Panzer-Gruemayer, E.R., 2007. RNAi-mediated silencing of TEL/AML1 reveals a heat-shock protein- and survivin-dependent mechanism for survival. Blood 109, 2607–2610.

Dickinson, R.E., Griffin, H., Bigley, V., Reynard, L.N., Hussain, R., Haniffa, M., Lakey, J.H., Rahman, T., Wang, X.N., McGovern, N., Pagan, S., Cookson, S., McDonald, D., Chua, I., Wallis, J., Cant, A., Wright, M., Keavney, B., Chinnery, P.F., Loughlin, J., Hambleton, S., Santibanez-Koref, M., Collin, M., 2011. Exome sequencing identifies GATA-2 mutation as the cause of dendritic cell, monocyte, B and NK lymphoid deficiency. Blood 118, 2656–2658.

Ding, L.-W., Ikezoe, T., Tan, K.-T., Mori, M., Mayakonda, A., Chien, W., Lin, D.-C., Jiang, Y.-Y., Lill, M., Yang, H., Sun, Q.-Y., Koeffler, H.P., 2017. Mutational profiling of a MonoMAC syndrome family with GATA2 deficiency. Leukemia 31, 244–245.

Dobson, J.T., Seibert, J., Teh, E.M., Da, S., Fraser, R.B., Paw, B.H., Lin, T., Berman, J.N., 2008. Carboxypeptidase A5 identifies a novel mast cell lineage in the zebrafish providing new insight into mast cell fate determination. Blood 112, 2969–2972.

Douet-Guilbert, N., De Braekeleer, E., Basinko, A., Herry, A., Gueganic, N., Bovo, C., Trillet, K., Dos Santos, A., Le Bris, M.J., Morel, F., Eveillard, J.R., Berthou, C., De Braekeleer, M., 2012. Molecular characterization of deletions of the long arm of chromosome 5 (del(5q)) in 94 MDS/AML patients. Leukemia 26, 1695–1697.

Ebert, B.L., Pretz, J., Bosco, J., Chang, C.Y., Tamayo, P., Galili, N., Raza, A., Root, D.E., Attar, E., Ellis, S.R., Golub, T.R., 2008. Identification of RPS14 as a 5q- syndrome gene by RNA interference screen. Nature 451, 335–339.

El-Brolosy, M.A., Stainier, D.Y.R., 2017. Genetic compensation: A phenomenon in search of mechanisms. PLoS Genet. 13, 1–17.

Emberger, J.M., Navarro, M., Dejean, M., Izarn, P., 1979. [Deaf-mutism, lymphedema of the lower limbs and hematological abnormalities (acute leukemia, cytopenia) with autosomal dominant transmission]. J. Genet. Hum. 27, 237–45.

Eppig, J., 2007. Mouse Strain and Genetic NomenclatureAn Abbreviated Guide, in: The Mouse in Biomedical Research. Elsevier, pp. 79–98.

Espín-Palazón, R., Stachura, D.L., Campbell, C.A., García-Moreno, D., Del Cid, N., Kim, A.D., Candel, S., Meseguer, J., Mulero, V., Traver, D., 2014. Proinflammatory signaling regulates hematopoietic stem cell emergence. Cell 159, 1070–1085.

Ferreira-Cerca, S., Hurt, E., 2009. Cell biology: Arrest by ribosome. Nature 459, 46–7.

Fischer, M., Schwieger, M., Horn, S., Niebuhr, B., Ford, A., Roscher, S., Bergholz, U., Greaves, M., Löhler, J., Stocking, C., 2005. Defining the oncogenic function of the TEL/AML1 (ETV6/RUNX1) fusion protein in a mouse model. Oncogene 24, 7579–7591.

Fisher, K.E., Hsu, A.P., Williams, C.L., Sayeed, H., Merritt, B.Y., Elghetany, M.T., Holland, S.M., Bertuch, A.A., Gramatges, M.M., 2017. Somatic mutations in children with *GATA2* -associated myelodysplastic syndrome who lack other features of GATA2 deficiency. Blood Adv. 1, 443–448.

Fleisch, V.C., Schonthaler, H.B., von Lintig, J., Neuhauss, S.C.F., 2008. Subfunctionalization of a Retinoid-Binding Protein Provides Evidence for Two Parallel Visual Cycles in the Cone-Dominant Zebrafish Retina. J. Neurosci. 28, 8208–8216.

Force, A., Lynch, M., Pickett, F.B., Amores, A., Yan, Y.L., Postlethwait, J., 1999. Preservation of duplicate genes by complementary, degenerative mutations. Genetics 151, 1531–45.

Fujiwara, Y., Chang, A.N., Williams, A.M., Orkin, S.H., 2004. Functional overlap of GATA-1 and GATA-2 in primitive hematopoietic development. Blood 103, 583–585.

Fuka, G., Kantner, H.P., Grausenburger, R., Inthal, A., Bauer, E., Krapf, G., Kaindl, U., Kauer, M., Dworzak, M.N., Stoiber, D., Haas, O.A., Panzer-Grümayer, R., 2012. Silencing of ETV6/RUNX1 abrogates PI3K/AKT/mTOR signaling and impairs reconstitution of leukemia in xenografts. Leukemia 26, 927–933.

Fuka, G., Kauer, M., Kofler, R., Haas, O.A., Panzer-Grümayer, R., 2011. The Leukemia-Specific Fusion Gene ETV6/RUNX1 Perturbs Distinct Key Biological Functions Primarily by Gene Repression. PLoS One 6, e26348.

Gagnon, J.A., Valen, E., Thyme, S.B., Huang, P., Ahkmetova, L., Pauli, A., Montague, T.G., Zimmerman, S., Richter, C., Schier, A.F., 2014. Efficient mutagenesis by Cas9 protein-mediated oligonucleotide insertion and large-scale assessment of single-guide RNAs. PLoS One 9, 5–12.

Galloway, J.L., Wingert, R.A., Thisse, C., Thisse, B., Zon, L.I., 2005. Loss of Gata1 but not Gata2 converts erythropoiesis to myelopoiesis in zebrafish embryos. Dev. Cell 8, 109–116.

Gau, P., Curtright, A., Condon, L., Raible, D.W., Dhaka, A., 2017. An ancient neurotrophin receptor code; a single Runx/Cbfβ complex determines somatosensory neuron fate specification in zebrafish. PLoS Genet. 13, 1–30.

Gelsi-Boyer, V., Brecqueville, M., Devillier, R., Murati, A., Mozziconacci, M.J., Birnbaum, D., 2012. Mutations in ASXL1 are associated with poor prognosis across the spectrum of malignant myeloid diseases. J. Hematol. Oncol. 5, 1–6.

Gering, M., Yamada, Y., Rabbitts, T.H., Patient, R.K., 2003. Lmo2 and Scl/Tal1 convert non-axial mesoderm into haemangioblasts which differentiate into endothelial cells in the absence of Gata1. Development 130, 6187–99.

Ghazavi, F., Lammens, T., Van Roy, N., Poppe, B., Speleman, F., Benoit, Y., Van Vlierberghe, P., De Moerloose, B., 2015. Molecular basis and clinical significance of genetic aberrations in B-cell precursor acute lymphoblastic leukemia. Exp. Hematol. 43, 640–653.

Gillis, W.Q., St John, J., Bowerman, B., Schneider, S.Q., 2009. Whole genome duplications and expansion of the vertebrate GATA transcription factor gene family. BMC Evol. Biol. 9, 207.

Glasauer, S.M.K., Neuhauss, S.C.F., 2014. Whole-genome duplication in teleost fishes and its evolutionary consequences. Mol. Genet. Genomics 289, 1045–60.

Golub, T.R.R., Barker, G.F.F., Lovett, M., Gilliland, D.G.G., 1994. Fusion of PDGF receptor β to a novel ets-like gene, tel, in chronic myelomonocytic leukemia with t(5;12) chromosomal translocation. Cell 77, 307–316.

Greaves, M., 2009. Darwin and evolutionary tales in leukemia. The Ham-Wasserman Lecture. Hematol. Am. Soc. Hematol. Educ. Progr. 2009, 3–12.

Greaves, M.F., Wiemels, J., 2003. Origins of chromosome translocations in childhood leukaemia. Nat. Rev. Cancer 3, 639–649.

Greif, P.A., Dufour, A., Konstandin, N.P., Ksienzyk, B., Zellmeier, E., Tizazu, B., Sturm, J., Benthaus, T., Herold, T., Yaghmaie, M., Dorge, P., Hopfner, K.-P., Hauser, A., Graf, A., Krebs, S., Blum, H., Kakadia, P.M., Schneider, S., Hoster, E., Schneider, F., Stanulla, M., Braess, J., Sauerland, M.C., Berdel, W.E., Buchner, T., Woermann, B.J., Hiddemann, W., Spiekermann, K., Bohlander, S.K., 2012. GATA2 zinc finger 1 mutations associated with biallelic CEBPA mutations define a unique genetic entity of acute myeloid leukemia. Blood 120, 395–403.

Hahn, C.N., Chong, C.-E., Carmichael, C.L., Wilkins, E.J., Brautigan, P.J., Li, X.-C., Babic, M., Lin, M., Carmagnac, A., Lee, Y.K., Kok, C.H., Gagliardi, L., Friend, K.L., Ekert, P.G., Butcher, C.M., Brown, A.L., Lewis, I.D., To, L.B., Timms, A.E., Storek, J., Moore, S., Altree, M., Escher, R., Bardy, P.G., Suthers, G.K., D'Andrea, R.J., Horwitz, M.S., Scott, H.S., 2011. Heritable GATA2 mutations associated with familial myelodysplastic syndrome and acute myeloid leukemia. Nat. Genet. 43, 1012–1017.

Hall, C., Flores, M., Storm, T., Crosier, K., Crosier, P., 2007. The zebrafish lysozyme C promoter drives myeloid-specific expression in transgenic fish. BMC Dev. Biol. 7, 1–17.

He, Q., Zhang, C., Wang, L., Zhang, P., Ma, D., Lv, J., Liu, F., 2015. In flammatory signaling regulates hematopoietic stem and progenitor cell emergence in vertebrates. Blood 125, 1098–1106.

Heasman, J., 2002. Morpholino Oligos: Making Sense of Antisense? Dev. Biol. 243, 209–214.

Hemmi, H., Kaisho, T., Takeuchi, O., Sato, S., Sanjo, H., Hoshino, K., Horiuchi, T., Tomizawa, H., Takeda, K., Akira, S., 2002. Small anti-viral compounds activate immune cells via the TLR7 MyD88–dependent signaling pathway. Nat. Immunol. 3, 196–200.

Henninger, J., Santoso, B., Hans, S., Durand, E., Moore, J., Mosimann, C., Brand, M., Traver, D., Zon, L., 2017. Clonal fate mapping quantifies the number of haematopoietic stem cells that arise during development. Nat. Cell Biol. 19, 17–27.

Herbomel, P., Thisse, B., Thisse, C., 2001. Zebrafish early macrophages colonize cephalic mesenchyme and developing brain, retina, and epidermis through a M-CSF receptor-dependent invasive process. Dev. Biol. 238, 274–288.

Herbomel, P., Thisse, B., Thisse, C., 1999. Ontogeny and behaviour of early macrophages in the zebrafish embryo. Development 126, 3735–45.

Hess, I., Boehm, T., 2012. Intravital Imaging of Thymopoiesis Reveals Dynamic Lympho-Epithelial Interactions. Immunity 36, 298–309.

Higashijima, S. ichi, Okamoto, H., Ueno, N., Hotta, Y., Eguchi, G., 1997. High-frequency generation of transgenic zebrafish which reliably express GFP in whole muscles or the whole body by using promoters of zebrafish origin. Dev. Biol. 192, 289–299.

Hsu, A.P., Sampaio, E.P., Khan, J., Calvo, K.R., Lemieux, J.E., Patel, S.Y., Frucht, D.M., Vinh, D.C., Auth, R.D., Freeman, A.F., Olivier, K.N., Uzel, G., Zerbe, C.S., Spalding, C., Pittaluga, S., Raffeld, M., Kuhns, D.B., Ding, L., Paulson, M.L., Marciano, B.E., Gea-Banacloche, J.C., Orange, J.S., Cuellar-Rodriguez, J., Hickstein, D.D., Holland, S.M., 2011. Mutations in GATA2 are associated with the autosomal dominant and sporadic monocytopenia and mycobacterial infection (MonoMAC) syndrome. Blood 118, 2653–2655.

Hsu, K., Traver, D., Kutok, J.L., Hagen, A., Liu, T.X., Paw, B.H., Rhodes, J., Berman, J.N., Zon, L.I., Kanki, J.P., Look, A.T., 2004. The pu.1 promoter drives myeloid gene expression in zebrafish. Blood 104, 1291–1297.

Huang, H., Li, Y., Liu, B., 2016. Transcriptional regulation of mast cell and basophil lineage commitment. Semin. Immunopathol. 38, 539–548.

Huang, K., Du, J., Ma, N., Liu, J., Wu, P., Dong, X., Meng, M., Wang, W., Chen, X., Shi, X., Chen, Q., Yang, Z., Chen, S., Zhang, J., Li, Y., Li, W., Zheng, Y., Cai, J., Li, P., Sun, X., Wang, J., Pei, D., Pan, G., 2015. GATA2(-/-) human ESCs undergo attenuated endothelial to hematopoietic transition and

thereafter granulocyte commitment. Cell Regen. (London, England) 4, 4.

Huddleson, J.P., Ahmad, N., Srinivasan, S., Lingrel, J.B., 2005. Induction of KLF2 by fluid shear stress requires a novel promoter element activated by a phosphatidylinositol 3-kinase-dependent chromatin-remodeling pathway. J. Biol. Chem. 280, 23371–23379.

Ichikawa, M., Yoshimi, A., Nakagawa, M., Nishimoto, N., Watanabe-Okochi, N., Kurokawa, M., 2013. A role for RUNX1 in hematopoiesis and myeloid leukemia. Int. J. Hematol. 97, 726–734.

Isogai, S., Horiguchi, M., Weinstein, B.M., 2001. The vascular anatomy of the developing zebrafish: An atlas of embryonic and early larval development. Dev. Biol. 230, 278–301.

Ito, E., Toki, T., Ishihara, H., Ohtani, H., Gu, L., Yokoyama, M., Douglas Engel, J., Yamamoto, M., 1993. Erythroid transcription factor GATA-1 is abundantly transcribed in mouse testis. Nature 362, 466–468.

Jackson, T.A., Taylor, H.E., Sharma, D., Desiderio, S., Danoff, S.K., 2005. Vascular Endothelial Growth Factor Receptor-2. J. Biol. Chem. 280, 29856–29863.

Jaffe, N., Reaman, G.H., Smith, F.O., 2011. Childhood Leukemia, The American journal of medical technology, Pediatric Oncology. Springer Berlin Heidelberg, Berlin, Heidelberg.

Jaillon, O., Aury, J.-M., Brunet, F., Petit, J.-L., Stange-Thomann, N., Mauceli, E., Bouneau, L., Fischer, C., Ozouf-Costaz, C., Bernot, A., Nicaud, S., Jaffe, D., Fisher, S., Lutfalla, G., Dossat, C., Segurens, B., Dasilva, C., Salanoubat, M., Levy, M., Boudet, N., Castellano, S., Anthouard, V., Jubin, C., Castelli, V., Katinka, M., Vacherie, B., Biémont, C., Skalli, Z., Cattolico, L., Poulain, J., de Berardinis, V., Cruaud, C., Duprat, S., Brottier, P., Coutanceau, J.-P., Gouzy, J., Parra, G., Lardier, G., Chapple, C., McKernan, K.J., McEwan, P., Bosak, S., Kellis, M., Volff, J.-N., Guigó, R., Zody, M.C., Mesirov, J., Lindblad-Toh, K., Birren, B., Nusbaum, C., Kahn, D., Robinson-Rechavi, M., Laudet, V., Schachter, V., Quétier, F., Saurin, W., Scarpelli, C., Wincker, P., Lander, E.S., Weissenbach, J., Roest Crollius, H., 2004. Genome duplication in the teleost fish Tetraodon nigroviridis reveals the early vertebrate proto-karyotype.

Nature 431, 946–957.

Jaju, R.J., Boultwood, J., Oliver, F.J., Kostrzewa, M., Fidler, C., Parker, N., McPherson, J.D., Morris, S.W., Müller, U., Wainscoat, J.S., Kearney, L., 1998. Molecular cytogenetic delineation of the critical deleted region in the 5q- syndrome. Genes Chromosom. Cancer 22, 251–256.

Jao, L.-E., Wente, S.R., Chen, W., 2013. Efficient multiplex biallelic zebrafish genome editing using a CRISPR nuclease system. Proc. Natl. Acad. Sci. 110, 13904–13909.

Jault, C., Pichon, L., Chluba, J., 2004. Toll-like receptor gene family and TIR-domain adapters in Danio rerio. Mol. Immunol. 40, 759–771.

Jing, C. Bin, Chen, Y., Dong, M., Peng, X.L., Jia, X.E., Gao, L., Ma, K., Deng, M., Liu, T.X., Zon, L.I., Zhu, J., Zhou, Yi, Zhou, Yong, 2013. Phospholipase C gamma-1 is required for granulocyte maturation in zebrafish. Dev. Biol. 374, 24–31.

Jones, K.M., Sarić, N., Russell, J.P., Andoniadou, C.L., Scambler, P.J., Basson, M.A., 2015. CHD7 maintains neural stem cell quiescence and prevents premature stem cell depletion in the adult hippocampus. Stem Cells 33, 196–210.

Jung, Y., 2013. Small Molecule Screening for Modifiers of Anaemia in Ribosomal Protein (RP) -haploinsufficient Zebrafish : New Therapeutic Aspect of Imiquimod. University College London.

Jurk, M., Heil, F., Vollmer, J., Schetter, C., Krieg, A.M., Wagner, H., Lipford, G., Bauer, S., 2002. Human TLR7 or TLR8 independently confer responsiveness to the antiviral compound R-848. Nat. Immunol. 3, 499–499.

Kalev-Zylinska, M.L., Horsfield, J.A., Flores, M.V.C., Postlethwait, J.H., Vitas, M.R., Baas, A.M., Crosier, P.S., Crosier, K.E., 2002. Runx1 is required for zebrafish blood and vessel development and expression of a human RUNX1-CBF2T1 transgene advances a model for studies of leukemogenesis. Development 129, 2015–30.

Kazenwadel, J., Betterman, K.L., Chong, C.E., Stokes, P.H., Lee, Y.K., Secker, G.A., Agalarov, Y., Demir, C.S., Lawrence, D.M., Sutton, D.L., Tabruyn, S.P., Miura, N., Salminen, M., Petrova, T. V., Matthews, J.M., Hahn, C.N., Scott, H.S., Harvey, N.L., 2015. GATA2 is required for lymphatic vessel valve development and maintenance. J. Clin. Invest. 125, 2879–2994.

Kearse, M., Moir, R., Wilson, A., Stones-Havas, S., Cheung, M., Sturrock, S., Buxton, S., Cooper, A., Markowitz, S., Duran, C., Thierer, T., Ashton, B., Meintjes, P., Drummond, A., 2012. Geneious Basic: An integrated and extendable desktop software platform for the organization and analysis of sequence data. Bioinformatics 28, 1647–1649.

Kell, M.J., Riccio, R.E., Baumgartner, E.A., Compton, Z.J., Pecorin, P.J., Mitchell, T.A., Topczewski, J., LeClair, E.E., 2018. Targeted deletion of the zebrafish actin-bundling protein L-plastin (lcp1). PLoS One 13, 1–23.

Kimmel, C.B., Ballard, W.W., Kimmel, S.R., Ullmann, B., Schilling, T.F., 1995. Stages of embryonic development of the zebrafish. Dev. Dyn. 203, 253–310.

Kissa, K., Herbomel, P., 2010. Blood stem cells emerge from aortic endothelium by a novel type of cell transition. Nature 464, 112–115.

Kissa, K., Murayama, E., Zapata, A., Cortes, A., Perret, E., Machu, C., Herbomel, P., 2007. Live imaging of emerging hematopoietic stem cells and early thymus colonization. Blood 111, 1147–1156.

Kitahara, M., Eyre, H.J., Simonian, Y., Atkin, C.L., Hasstedt, S.J., 1981. Hereditary myeloperoxidase deficiency. Blood 57, 888–93.

Ko, L.J., Engel, J.D., 1993. DNA-binding specificities of the GATA transcription factor family. Mol. Cell. Biol. 13, 4011–4022.

Kok, F.O., Shin, M., Ni, C.W., Gupta, A., Grosse, A.S., vanImpel, A., Kirchmaier, B.C., Peterson-Maduro, J., Kourkoulis, G., Male, I., DeSantis, D.F., Sheppard-Tindell, S., Ebarasi, L., Betsholtz, C., Schulte-Merker, S., Wolfe, S.A., Lawson, N.D., 2015. Reverse genetic screening reveals poor correlation between morpholino-induced and mutant phenotypes in zebrafish. Dev. Cell 32, 97–108.

Komrokji, R.S., Padron, E., Ebert, B.L., List, A.F., 2013. Deletion 5q MDS: Molecular and therapeutic implications. Best Pract. Res. Clin. Haematol. 26, 365–375.

Koschmieder, S., Rosenbauer, F., Steidl, U., Owens, B.M., Tenen, D.G., 2005. Role of transcription factors C/EBPalpha and PU.1 in normal hematopoiesis and leukemia. Int. J. Hematol. 81, 368–77.

Kumar, M.S., Narla, A., Nonami, A., Mullally, A., Dimitrova, N., Ball, B., McAuley, J.R., Poveromo, L., Kutok, J.L., Galili, N., Raza, A., Attar, E., Gilliland, D.G., Jacks, T., Ebert, B.L., 2011. Coordinate loss of a microRNA and protein-coding gene cooperate in the pathogenesis of 5q- syndrome. Blood 118, 4666–4673.

Kwan, K.M., Fujimoto, E., Grabher, C., Mangum, B.D., Hardy, M.E., Campbell, D.S., Parant, J.M., Yost, H.J., Kanki, J.P., Chien, C. Bin, 2007. The Tol2kit: A multisite gateway-based construction Kit for Tol2 transposon transgenesis constructs. Dev. Dyn. 236, 3088–3099.

Kwan, W., Cortes, M., Frost, I., Esain, V., Theodore, L.N., Liu, S.Y., Budrow, N., Goessling, W., North, T.E., 2016. The Central Nervous System Regulates Embryonic HSPC Production via Stress-Responsive Glucocorticoid Receptor Signaling. Cell Stem Cell 19, 370–382.

Labun, K., Montague, T.G., Gagnon, J.A., Thyme, S.B., Valen, E., 2016. CHOPCHOP v2: a web tool for the next generation of CRISPR genome engineering. Nucleic Acids Res. 44, W272–W276.

Langenau, D.M., Ferrando, A.A., Traver, D., Kutok, J.L., Hezel, J.-P.D., Kanki, J.P., Zon, L.I., Look, A.T., Trede, N.S., 2004. In vivo tracking of T cell development, ablation, and engraftment in transgenic zebrafish. Proc. Natl. Acad. Sci. 101, 7369–7374.

Le Beau, M.M., Espinosa, R., Davis, E.M., Eisenbart, J.D., Larson, R.A., Green, E.D., 1996. Cytogenetic and molecular delineation of a region of chromosome 7 commonly deleted in malignant myeloid diseases. Blood 88, 1930–5.

Le Guyader, D., Redd, M.J., Colucci-Guyon, E., Murayama, E., Kissa, K., Briolat, V., Mordelet, E., Zapata, A., Shinomiya, H., Herbomel, P., 2008. Origins and unconventional behavior of neutrophils in developing zebrafish. Blood 111, 132–141.

Lenard, A., Alghisi, E., Daff, H., Donzelli, M., McGinnis, C., Lengerke, C., 2016. Using zebrafish to model erythroid lineage toxicity and regeneration. Haematologica 101, e164–e167.

Li, Y., Esain, V., Teng, L., Xu, J., Kwan, W., Frost, I.M., Yzaguirre, A.D., Cai, X., Cortes, M., Maijenburg, M.W., Tober, J., Dzierzak, E., Orkin, S.H., Tan, K., North, T.E., Speck, N.A., 2014. Inflammatory signaling regulates embryonic hematopoietic stem and progenitor cell production. Genes Dev. 28, 2597–2612.

Lieschke, G.J., Oates, A.C., Paw, B.H., Thompson, M.A., Hall, N.E., Ward, A.C., Ho, R.K., Zon, L.I., Layton, J.E., 2002. Zebrafish SPI-1 (PU.1) marks a site of myeloid development independent of primitive erythropoiesis: Implications for axial patterning. Dev. Biol. 246, 274–295.

Lieschke, G.J.J., Oates, A.C., Crowhurst, M.O., Ward, A.C., Layton, J.E., 2001. Morphologic and functional characterization of granulocytes and macrophages in embryonic and adult zebrafish. Blood 98, 3087–3096.

Lim, K.C., Hosoya, T., Brandt, W., Ku, C.J., Hosoya-Ohmura, S., Camper, S.A., Yamamoto, M., Engel, J.D., 2012. Conditional Gata2 inactivation results in HSC loss and lymphatic mispatterning. J. Clin. Invest. 122, 3705–3717.

Lin, H.F., Traver, D., Zhu, H., Dooley, K., Paw, B.H., Zon, L.I., Handin, R.I., 2005. Analysis of thrombocyte development in CD41-GFP transgenic zebrafish. Blood 106, 3803–3810.

Ling, K.-W., Ottersbach, K., van Hamburg, J.P., Oziemlak, A., Tsai, F.-Y., Orkin, S.H., Ploemacher, R., Hendriks, R.W., Dzierzak, E., 2004. GATA-2 Plays Two Functionally Distinct Roles during the Ontogeny of Hematopoietic Stem Cells. J. Exp. Med. 200, 871–882.

Liu, J., Jiang, J., Wang, Z., He, Y., Zhang, Q., 2016. Origin and evolution of GATA2a and GATA2b in teleosts: insights from tongue sole, Cynoglossus semilaevis. PeerJ 4, e1790.

Liu, T.X., Becker, M.W., Jelinek, J., Wu, W.-S., Deng, M., Mikhalkevich, N., Hsu, K., Bloomfield, C.D., Stone, R.M., DeAngelo, D.J., Galinsky, I.A., Issa, J.-P., Clarke, M.F., Look, A.T., 2007. Chromosome 5q deletion and epigenetic suppression of the gene encoding α-catenin (CTNNA1) in myeloid cell transformation. Nat. Med. 13, 78–83.

Long, Q., Meng, a, Wang, H., Jessen, J.R., Farrell, M.J., Lin, S., 1997. GATA-1 expression pattern can be recapitulated in living transgenic zebrafish using GFP reporter gene. Development 124, 4105–4111.

Lowry, J.A., Atchley, W.R., 2000. Molecular evolution of the GATA family of transcription factors: Conservation within the DNA-binding domain. J. Mol. Evol. 50, 103–115.

Lu, H., Dietsch, G.N., Matthews, M.-A.H., Yang, Y., Ghanekar, S., Inokuma, M., Suni, M., Maino, V.C., Henderson, K.E., Howbert, J.J., Disis, M.L., Hershberg, R.M., 2012. VTX-2337 Is a Novel TLR8 Agonist That Activates NK Cells and Augments ADCC. Clin. Cancer Res. 18, 499–509.

Luis, T.C., Luc, S., Mizukami, T., Boukarabila, H., Thongjuea, S., Woll, P.S., Azzoni, E., Giustacchini, A., Lutteropp, M., Bouriez-Jones, T., Vaidya, H., Mead, A.J., Atkinson, D., Böiers, C., Carrelha, J., MacAulay, I.C., Patient, R., Geissmann, F., Nerlov, C., Sandberg, R., De Bruijn, M.F.T.R., Blackburn, C.C., Godin, I., Jacobsen, S.E.W., 2016. Initial seeding of the embryonic thymus by immune-restricted lympho-myeloid progenitors. Nat. Immunol. 17, 1424–1435.

Lyons, S.E., Shue, B.C., Lei, L., Oates, A.C., Zon, L.I., Liu, P.P., 2001. Molecular cloning, genetic mapping, and expression analysis of four zebrafish c/ebp genes. Gene 281, 43–51.

Ma, D., Wei, Y., Liu, F., 2013. Regulatory mechanisms of thymus and T cell development. Dev. Comp. Immunol. 39, 91–102.

Ma, D., Zhang, J., Lin, H. -f., Italiano, J., Handin, R.I., 2011. The identification and characterization of zebrafish hematopoietic stem cells. Blood 118, 289–297.

Mammoto, A., Connor, K.M., Mammoto, T., Yung, C.W., Huh, D., Aderman, C.M., Mostoslavsky, G., Smith, L.E.H., Ingber, D.E., 2009. A mechanosensitive transcriptional mechanism that controls angiogenesis. Nature 457, 1103–1108.

Mammoto, A., Huang, S., Ingber, D.E., 2007. Filamin links cell shape and cytoskeletal structure to Rho regulation by controlling accumulation of p190RhoGAP in lipid rafts. J. Cell Sci. 120, 456–467.

Mangolini, M., De Boer, J., Walf-Vorderwülbecke, V., Pieters, R., Den Boer, M.L., Williams, O., 2013. STAT3 mediates oncogenic addiction to TEL-AML1 in t(12;21) acute lymphoblastic leukemia. Blood 122, 542–549.

McGowan, K.A., Li, J.Z., Park, C.Y., Beaudry, V., Tabor, H.K., Sabnis, A.J., Zhang, W., Fuchs, H., De Angelis, M.H., Myers, R.M., Attardi, L.D., Barsh, G.S., 2008. Ribosomal mutations cause p53-mediated dark skin and pleiotropic effects. Nat. Genet. 40, 963–970.

Meijer, A.H., Gabby Krens, S.F., Medina Rodriguez, I.A., He, S., Bitter, W., Snaar-Jagalska, B.E., Spaink, H.P., 2004. Expression analysis of the Toll-like receptor and TIR domain adaptor families of zebrafish. Mol. Immunol. 40, 773–783.

Meijer, A.H., van der Sar, A.M., Cunha, C., Lamers, G.E.M., Laplante, M.A., Kikuta, H., Bitter, W., Becker, T.S., Spaink, H.P., 2008. Identification and real-time imaging of a myc-expressing neutrophil population involved in inflammation and mycobacterial granuloma formation in zebrafish. Dev. Comp. Immunol. 32, 36–49.

Minami, T., Murakami, T., Horiuchi, K., Miura, M., Noguchi, T., Miyazaki, J., Hamakubo, T., Aird, W.C., Kodama, T., 2004. Interaction between hex and GATA transcription factors in vascular endothelial cells inhibits flk-1/KDR-mediated vascular endothelial growth factor signaling. J. Biol. Chem. 279, 20626–35.

Minami, T., Rosenberg, R.D., Aird, W.C., 2001. Transforming Growth Factor-β 1 -mediated Inhibition of the flk-1/KDR Gene Is Mediated by a 5′-Untranslated Region Palindromic GATA Site. J. Biol. Chem. 276, 5395–5402.

Minegishi, N., Ohta, J., Suwabe, N., Nakauchi, H., Ishihara, H., Hayashi, N., Yamamoto, M., 1998. Alternative Promoters Regulate Transcription of the Mouse GATA-2 Gene. J. Biol. Chem. 273, 3625–3634.

Minegishi, N., Suzuki, N., Yokomizo, T., Pan, X., Fujimoto, T., Takahashi, S., Hara, T., Miyajima, A., Nishikawa, S.-I., Yamamoto, M., 2003. Expression and domain-specific function of GATA-2 during differentiation of the hematopoietic precursor cells in midgestation mouse embryos. Blood 102, 896–905.

Miyoshi, H., Shimizu, K., Kozu, T., Maseki, N., Kaneko, Y., Ohki, M., 1991. t(8;21) breakpoints on chromosome 21 in acute myeloid leukemia are clustered within a limited region of a single gene, AML1. Proc. Natl. Acad. Sci. U. S. A. 88, 10431–4.

Molkentin, J.D., 2000. The Zinc Finger-containing Transcription Factors GATA-4, -5, and -6. J. Biol. Chem. 275, 38949–38952.

Momand, J., Zambetti, G.P., Olson, D.C., George, D., Levine, A.J., 1992. The mdm-2 oncogene product forms a complex with the p53 protein and inhibits p53-mediated transactivation. Cell 69, 1237–1245.

Morrow, M., Horton, S., Kioussis, D., Brady, H.J.M., Williams, O., 2004. TEL-AML1 promotes development of specific hematopoietic lineages consistent with preleukemic activity. Blood 103, 3890–3896.

Mosimann, C., Kaufman, C.K.K., Li, P., Pugach, E.K.K., Tamplin, O.J.J., Zon, L.I.I., 2011. Ubiquitous transgene expression and Cre-based recombination driven by the ubiquitin promoter in zebrafish. Development 138, 169–177.

Murayama, E., Kissa, K., Zapata, A., Mordelet, E., Briolat, V., Lin, H.F., Handin, R.I., Herbomel, P., 2006. Tracing Hematopoietic Precursor Migration to Successive Hematopoietic Organs during Zebrafish Development. Immunity 25, 963–975.

Murayama, E., Sarris, M., Redd, M., Le Guyader, D., Vivier, C., Horsley, W., Trede, N., Herbomel, P., 2015. NACA deficiency reveals the crucial role of somite-derived stromal cells in haematopoietic niche formation. Nat. Commun. 6, 8375.

Nakamichi, N.N., Kao, F.-T., Wasmuth, J., Roufa, D.J., 1986. Ribosomal protein gene sequences map to human chromosomes 5, 8, and 17. Somat. Cell Mol. Genet. 12, 225–236.

Narla, A., Ebert, B.L., 2010. Ribosomopathies: human disorders of ribosome dysfunction. Blood 115, 3196–205.

Narla, A., Payne, E.M., Abayasekara, N., Hurst, S.N., Raiser, D.M., Look, A.T., Berliner, N., Ebert, B.L., Khanna-Gupta, A., 2014. L-Leucine improves the anaemia in models of Diamond Blackfan anaemia and the 5q- syndrome in a TP53-independent way. Br. J. Haematol. 167, 524–528.

Nauseef, W.M., 1989. Aberrant restriction endonuclease digests of DNA from subjects with hereditary myeloperoxidase deficiency. Blood 73, 290–5.

Neave, B., Rodaway, A., Wilson, S.W., Patient, R., Holder, N., 1995. Expression of zebrafish GATA 3 (gta3) during gastrulation and neurulation suggests a role in the specification of cell fate. Mech. Dev. 51, 169–182.

Nicoli, S., Standley, C., Walker, P., Hurlstone, A., Fogarty, K.E., Lawson, N.D., 2010. MicroRNA-mediated integration of haemodynamics and Vegf signalling during angiogenesis. Nature 464, 1196–1200.

North, T.E., Goessling, W., Peeters, M., Li, P., Ceol, C., Lord, A.M., Weber, G.J., Harris, J., Cutting, C.C., Huang, P., Dzierzak, E., Zon, L.I., 2009. Hematopoietic Stem Cell Development Is Dependent on Blood Flow. Cell 137, 736–748.

Novodvorsky, P., Watson, O., Gray, C., Wilkinson, R.N., Reeve, S., Smythe, C., Beniston, R., Plant, K., Maguire, R., M. K. Rothman, A., Elworthy, S., van Eeden, F.J.M., Chico, T.J.A., 2015. klf2ash317 Mutant Zebrafish Do Not Recapitulate Morpholino-Induced Vascular and Haematopoietic Phenotypes. PLoS One 10, e0141611.

Nüsslein-Volhard, C., Dahm, R., 2002. Zebrafish: A Practical Approach. Oxford University Press; 1 edition (November 21, 2002).

Orkin, S.H., 1995. Transcription factors and hematopoietic development. J. Biol. Chem. 270, 4955–8.

Ostergaard, P., Simpson, M.A., Connell, F.C., Steward, C.G., Brice, G., Woollard, W.J., Dafou, D., Kilo, T., Smithson, S., Lunt, P., Murday, V.A., Hodgson, S., Keenan, R., Pilz, D.T., Martinez-Corral, I., Makinen, T., Mortimer, P.S., Jeffery, S., Trembath, R.C., Mansour, S., 2011. Mutations in GATA2 cause primary lymphedema associated with a predisposition to acute myeloid leukemia (Emberger syndrome). Nat. Genet. 43, 929–931.

Page, D.M., Wittamer, V., Bertrand, J.Y., Lewis, K.L., Pratt, D.N., Delgado, N., Schale, S.E., McGue, C., Jacobsen, B.H., Doty, A., Pao, Y., Yang, H., Chi, N.C., Magor, B.G., Traver, D., 2013. An evolutionarily conserved program of B-cell development and activation in zebrafish. Blood 122, e1–e11.

Pan, X., Minegishi, N., Harigae, H., Yamagiwa, H., Minegishi, M., Akine, Y., Yamamoto, M., 2000. Identification of Human GATA-2 Gene Distal IS Exon and Its Expression in Hematopoietic Stem Cell Fractions. J. Biochem. 127, 105–112.

Pan, Y.A., Freundlich, T., Weissman, T.A., Schoppik, D., Wang, X.C., Zimmerman, S., Ciruna, B., Sanes, J.R., Lichtman, J.W., Schier, A.F., 2013. Zebrabow: multispectral cell labeling for cell tracing and lineage analysis in zebrafish. Development 140, 2835–2846.

Paredes-Zúñiga, S., Morales, R.A., Muñoz-Sánchez, S., Muñoz-Montecinos, C., Parada, M., Tapia, K., Rubilar, C., Allende, M.L., Peña, O.A., 2017. CXCL12a/CXCR4b acts to retain neutrophils in caudal hematopoietic tissue and to antagonize recruitment to an injury site in the zebrafish larva. Immunogenetics 69, 341–349.

Parmar, K.M., Larman, H.B., Dai, G., Zhang, Y., Wang, E.T., Moorthy, S.N., Kratz, J.R., Lin, Z., Jain, M.K., Gimbrone, M.A., García-Cardeña, G., 2006. Integration of flow-dependent endothelial phenotypes by Kruppel-like factor 2. J. Clin. Invest. 116, 49–58.

Pase, L., Layton, J.E., Kloosterman, W.P., Carradice, D., Waterhouse, P.M., Lieschke, G.J., 2009. miR-451 regulates zebrafish erythroid maturation in vivo via its target gata2. Blood 113, 1794–1804.

Pase, L., Layton, J.E., Wittmann, C., Ellett, F., Nowell, C.J., Reyes-Aldasoro, C.C., Varma, S., Rogers, K.L., Hall, C.J., Keightley, M.C., Crosier, P.S., Grabher, C., Heath, J.K., Renshaw, S.A., Lieschke, G.J., 2012. Neutrophil-delivered myeloperoxidase dampens the hydrogen peroxide burst after tissue wounding in zebrafish. Curr. Biol. 22, 1818–24.

Patterson, L.J., Gering, M., Eckfeldt, C.E., Green, A.R., Verfaillie, C.M., Ekker, S.C., Patient, R., 2007. The transcription factors Scl and Lmo2 act together during development of the hemangioblast in zebrafish. Blood 109, 2389–2398.

Payne, E.M., Virgilio, M., Narla, A., Sun, H., Levine, M., Paw, B.H., Berliner, N., Look, A.T., Ebert, B.L., Khanna-Gupta, A., 2012. L-leucine improves the anemia and developmental defects associated with Diamond-Blackfan anemia and del(5q) MDS by activating the mTOR pathway. Blood 120, 2214–2224.

Postlethwait, J.H., Yan, Y.L., Gates, M.A., Horne, S., Amores, A., Brownlie, A., Donovan, A., Egan, E.S., Force, A., Gong, Z., Goutel, C., Fritz, A., Kelsh, R., Knapik, E., Liao, E., Paw, B., Ransom, D., Singer, A., Thomson, M., Abduljabbar, T.S., Yelick, P., Beier, D., Joly, J.S., Larhammar, D., Rosa, F., Westerfield, M., Zon, L.I., Johnson, S.L., Talbot, W.S., 1998. Vertebrate genome evolution and the zebrafish gene map. Nat. Genet. 18, 345–349.

Provost, E., Rhee, J., Leach, S.D., 2007. Viral 2A peptides allow expression of multiple proteins from a single ORF in transgenic zebrafish embryos. Genesis 45, 625–9.

Putri, R.R., Chen, L., 2018. Spatiotemporal control of zebrafish (Danio rerio) gene expression using a light-activated CRISPR activation system. Gene 677, 273–279.

Qi, X., Hong, J., Chaves, L., Zhuang, Y., Chen, Y., Wang, D., Chabon, J., Graham, B., Ohmori, K., Li, Y., Huang, H., 2013. Antagonistic Regulation by the Transcription Factors C/EBPα and MITF Specifies Basophil and Mast Cell

Fates. Immunity 39, 97–110.

Quiroz, Y., Lopez, M., Mavropoulos, A., Motte, P., Martial, J. a, Hammerschmidt, M., Muller, M., 2012. The HMG-box transcription factor Sox4b is required for pituitary expression of gata2a and specification of thyrotrope and gonadotrope cells in zebrafish. Mol. Endocrinol. 26, 1014–27.

Renninger, S.L., Gesemann, M., Neuhauss, S.C.F., 2011. Cone arrestin confers cone vision of high temporal resolution in zebrafish larvae. Eur. J. Neurosci. 33, 658–667.

Renshaw, S.A., Loynes, C.A., Trushell, D.M.I., Elworthy, S., Ingham, P.W., Whyte, M.K.B., 2006. A transgenic zebrafish model of neutrophilic inflammation. Blood 108, 3976–8.

Reyon, D., Maeder, M.L., Khayter, C., Tsai, S.Q., Foley, J.E., Sander, J.D., Joung, J.K., 2013. Engineering Customized TALE Nucleases (TALENs) and TALE Transcription Factors by Fast Ligation-Based Automatable Solid-Phase High-Throughput (FLASH) Assembly, in: Current Protocols in Molecular Biology. John Wiley & Sons, Inc., Hoboken, NJ, USA, pp. 1–18.

Rhoads, D.D., Dixit, A., Roufa, D.J., 1986. Primary structure of human ribosomal protein S14 and the gene that encodes it. Mol. Cell. Biol. 6, 2774–2783.

Rodrigues, N.P., Boyd, A.S., Fugazza, C., May, G.E., Guo, Y., Tipping, A.J., Scadden, D.T., Vyas, P., Enver, T., 2008. GATA-2 regulates granulocyte-macrophage progenitor cell function. Blood 112, 4862–4873.

Rodrigues, N.P., Janzen, V., Forkert, R., Dombkowski, D.M., Boyd, A.S., Orkin, S.H., Enver, T., Vyas, P., Scadden, D.T., 2005. Haploinsufficiency of GATA-2 perturbs adult hematopoietic stem-cell homeostasis. Blood 106, 477–484.

Romana, S.P., Le Coniat, M., Poirel, H., Marynen, P., Bernard, O., Berger, R., 1996. Deletion of the short arm of chromosome 12 is a secondary event in acute lymphoblastic leukemia with t(12;21). Leukemia 10, 167–70.

Romana, S.P., Poirel, H., Leconiat, M., Flexor, M. a, Mauchauffé, M., Jonveaux, P., Macintyre, E. a, Berger, R., Bernard, O. a, 1995. High frequency of t(12;21) in childhood B-lineage acute lymphoblastic leukemia. Blood 86, 4263–4269.

Rompaey, L. Van, Potter, M., Adams, C., Grosveld, G., 2000. Tel induces a G1 arrest and suppresses Ras-induced transformation. Oncogene 19, 5244–50.

Rossi, A., Kontarakis, Z., Gerri, C., Nolte, H., Hölper, S., Krüger, M., Stainier, D.Y.R., 2015. Genetic compensation induced by deleterious mutations but not gene knockdowns. Nature 524, 230–233.

Sabaawy, H.E., Azuma, M., Embree, L.J., Tsai, H.-J., Starost, M.F., Hickstein, D.D., 2006. TEL-AML1 transgenic zebrafish model of precursor B cell acute lymphoblastic leukemia. Proc. Natl. Acad. Sci. U. S. A. 103, 15166–71.

Sawamiphak, S., Kontarakis, Z., Stainier, D.Y.R.Y.R., 2014. Interferon Gamma Signaling Positively Regulates Hematopoietic Stem Cell Emergence. Dev. Cell 31, 640–653.

Schindelin, J., Arganda-Carreras, I., Frise, E., Kaynig, V., Longair, M., Pietzsch, T., Preibisch, S., Rueden, C., Saalfeld, S., Schmid, B., Tinevez, J.-Y., White, D.J., Hartenstein, V., Eliceiri, K., Tomancak, P., Cardona, A., 2012. Fiji: an open-source platform for biological-image analysis. Nat. Methods 9, 676–682.

Schindler, J.W., Van Buren, D., Foudi, A., Krejci, O., Qin, J., Orkin, S.H., Hock, H., 2009. TEL-AML1 Corrupts Hematopoietic Stem Cells to Persist in the Bone Marrow and Initiate Leukemia. Cell Stem Cell 5, 43–53.

Schneider, R.K., Schenone, M., Ferreira, M.V., Kramann, R., Joyce, C.E., Hartigan, C., Beier, F., Brümmendorf, T.H., Germing, U., Platzbecker, U., Büsche, G., Knüchel, R., Chen, M.C., Waters, C.S., Chen, E., Chu, L.P., Novina, C.D., Lindsley, R.C., Carr, S.A., Ebert, B.L., 2016. Rps14 haploinsufficiency causes a block in erythroid differentiation mediated by S100A8 and S100A9. Nat. Med. 22, 288–297.

Shafizadeh, E., Peterson, R.T., Lin, S., 2004. Induction of reversible hemolytic anemia in living zebrafish using a novel small molecule. Comp. Biochem. Physiol. - C Toxicol. Pharmacol. 138, 245–249.

Shcherbo, D., Murphy, C.S., Ermakova, G.V., Solovieva, E.A., Chepurnykh, T.V., Shcheglov, A.S., Verkhusha, V.V., Pletnev, V.Z., Hazelwood, K.L., Roche, P.M., Lukyanov, S., Zaraisky, A.G., Davidson, M.W., Chudakov, D.M., 2009. Far-red fluorescent tags for protein imaging in living tissues. Biochem. J. 418,

567–574.

Sheehan, H.L., Storey, G.W., 1946. An improved method of staining leucocyte granules with Sudan black B. J. Pathol. Bacteriol. 59, 336.

Simon, M.C., 1995. Gotta have GATA. Nat. Genet. 11, 9–11.

Simone, B.W., Martínez-Gálvez, G., WareJoncas, Z., Ekker, S.C., 2018. Fishing for understanding: Unlocking the zebrafish gene editor's toolbox. Methods 150, 3–10.

Skokowa, J., Germeshausen, M., Zeidler, C., Welte, K., 2007. Severe congenital neutropenia: inheritance and pathophysiology. Curr. Opin. Hematol. 14, 22–8.

Spinner, M.A., Sanchez, L.A., Hsu, A.P., Shaw, P.A., Zerbe, C.S., Calvo, K.R., Arthur, D.C., Gu, W., Gould, C.M., Brewer, C.C., Cowen, E.W., Freeman, A.F., Olivier, K.N., Uzel, G., Zelazny, A.M., Daub, J.R., Spalding, C.D., Claypool, R.J., Giri, N.K., Alter, B.P., Mace, E.M., Orange, J.S., Cuellar-Rodriguez, J., Hickstein, D.D., Holland, S.M., 2014. GATA2 deficiency: A protean disorder of hematopoiesis, lymphatics, and immunity. Blood 123, 809–821.

Starczynowski, D.T., Kuchenbauer, F., Argiropoulos, B., Sung, S., Morin, R., Muranyi, A., Hirst, M., Hogge, D., Marra, M., Wells, R.A., Buckstein, R., Lam, W., Humphries, R.K., Karsan, A., 2010. Identification of miR-145 and miR-146a as mediators of the 5q-syndrome phenotype. Nat. Med. 16, 49–58.

Su, F., Juarez, M. a, Cooke, C.L., Lapointe, L., Shavit, J. a, Yamaoka, J.S., Lyons, S.E., 2007. Differential regulation of primitive myelopoiesis in the zebrafish by Spi-1/Pu.1 and C/ebp1. Zebrafish 4, 187–99.

Swaminathan, S., Klemm, L., Park, E., Papaemmanuil, E., Ford, A., Kweon, S.M., Trageser, D., Hasselfeld, B., Henke, N., Mooster, J., Geng, H., Schwarz, K., Kogan, S.C., Casellas, R., Schatz, D.G., Lieber, M.R., Greaves, M.F., Müschen, M., 2015. Mechanisms of clonal evolution in childhood acute lymphoblastic leukemia. Nat. Immunol. 16, 766–774.

Tehranchi, R., Woll, P.S., Anderson, K., Buza-Vidas, N., Mizukami, T., Mead, A.J., Astrand-Grundström, I., Strömbeck, B., Horvat, A., Ferry, H., Dhanda, R.S., Hast, R., Rydén, T., Vyas, P., Göhring, G., Schlegelberger, B., Johansson, B., Hellström-Lindberg, E., List, A., Nilsson, L., Jacobsen, S.E.W., 2010. Persistent malignant stem cells in del(5q) myelodysplasia in remission. N. Engl. J. Med. 363, 1025–1037.

Teitell, M.A., Pandolfi, P.P., 2009. Molecular Genetics of Acute Lymphoblastic Leukemia. Annu. Rev. Pathol. Mech. Dis. 4, 175–198.

Theilgaard-Mönch, K., Jacobsen, L.C., Borup, R., Rasmussen, T., Bjerregaard, M.D., Nielsen, F.C., Cowland, J.B., Borregaard, N., 2005. The transcriptional program of terminal granulocytic differentiation. Blood 105, 1785–96.

Thisse, B., Pflumio, S., Fürthauer, M., Loppin, B., Heyer, V., Degrave, A., Woehl, R., Lux, A., Steffan, T., Charbonnier, X.Q., Thisse, C., 2001. Expression of the zebrafish genome during embryogenesis (NIH R01 RR15402). ZFIN Direct Data Submiss.

Tian, Y., Xu, J., Feng, S., He, S., Zhao, S., Zhu, L., Jin, W., Dai, Y., Luo, L., Qu, J.Y., Wen, Z., 2017. The first wave of T lymphopoiesis in zebrafish arises from aorta endothelium independent of hematopoietic stem cells. J. Exp. Med. 214, 3347–3360.

Ting, C.-N., Olson, M.C., Barton, K.P., Leiden, J.M., 1996. Transcription factor GATA-3 is required for development of the T-cell lineage. Nature 384, 474–478.

Tobin, D.M., Vary, J.C., Ray, J.P., Walsh, G.S., Dunstan, S.J., Bang, N.D., Hagge, D.A., Khadge, S., King, M.C., Hawn, T.R., Moens, C.B., Ramakrishnan, L., 2010. The lta4h Locus Modulates Susceptibility to Mycobacterial Infection in Zebrafish and Humans. Cell 140, 717–730.

Todd, E.M., Deady, L.E., Morley, S.C., 2011. The Actin-Bundling Protein L-Plastin Is Essential for Marginal Zone B Cell Development. J. Immunol. 187, 3015–3025.

Trainor, C.D., Omichinski, J.G., Vandergon, T.L., Gronenborn, a M., Clore, G.M., Felsenfeld, G., 1996. A palindromic regulatory site within vertebrate GATA-1 promoters requires both zinc fingers of the GATA-1 DNA-binding domain for high-affinity interaction. Mol. Cell. Biol. 16, 2238–47.

Traver, D., Paw, B.H., Poss, K.D., Penberthy, W.T., Lin, S., Zon, L.I., 2003. Transplantation and in vivo imaging of multilineage engraftment in zebrafish bloodless mutants. Nat. Immunol. 4, 1238–1246.

Tsai, F.-Y., Keller, G., Kuo, F.C., Weiss, M., Chen, J., Rosenblatt, M., Alt, F.W., Orkin, S.H., 1994. An early haematopoietic defect in mice lacking the transcription factor GATA-2. Nature 371, 221–226.

Tsai, F.Y., Orkin, S.H., 1997. Transcription factor GATA-2 is required for proliferation/survival of early hematopoietic cells and mast cell formation, but not for erythroid and myeloid terminal differentiation. Blood 89, 3636–43.

Tsuzuki, S., Seto, M., Greaves, M., Enver, T., 2004. Modeling first-hit functions of the t(12;21) TEL-AML1 translocation in mice. Proc. Natl. Acad. Sci. 101, 8443–8448.

Umamahesan, C., 2014. Defining the role of gata2 in developmental haematopoiesis. University College London.

Uphoff, C.C., MacLeod, R.A., Denkmann, S.A., Golub, T.R., Borkhardt, A., Janssen, J.W., Drexler, H.G., 1997. Occurrence of TEL-AML1 fusion resulting from (12;21) translocation in human early B-lineage leukemia cell lines. Leukemia 11, 441–7.

Van Den Berghe, H., Cassiman, J.J., David, G., Fryns, J.P., Michaux, J.L., Sokal, G., 1974. Distinct haematological disorder with deletion of long arm of No.5 chromosome. Nature 251, 437–438.

van der Weyden, L., Giotopoulos, G., Rust, A.G., Matheson, L.S., van Delft, F.W., Kong, J., Corcoran, A.E., Greaves, M.F., Mullighan, C.G., Huntly, B.J., Adams, D.J., 2011. Modeling the evolution of ETV6-RUNX1-induced B-cell precursor acute lymphoblastic leukemia in mice. Blood 118, 1041–1051.

Vicente, C., Conchillo, A., García-Sánchez, M.A., Odero, M.D., 2012. The role of the GATA2 transcription factor in normal and malignant hematopoiesis. Crit.

Rev. Oncol. Hematol. 82, 1–17.

Viger, R.S., Guittot, S.M., Anttonen, M., Wilson, D.B., Heikinheimo, M., 2008. Role of the GATA Family of Transcription Factors in Endocrine Development, Function, and Disease. Mol. Endocrinol. 22, 781–798.

Vinh, D.C., Patel, S.Y., Uzel, G., Anderson, V.L., Freeman, A.F., Olivier, K.N., Spalding, C., Hughes, S., Pittaluga, S., Raffeld, M., Sorbara, L.R., Elloumi, H.Z., Kuhns, D.B., Turner, M.L., Cowen, E.W., Fink, D., Long-Priel, D., Hsu, A.P., Ding, L., Paulson, M.L., Whitney, A.R., Sampaio, E.P., Frucht, D.M., DeLeo, F.R., Holland, S.M., 2010. Autosomal dominant and sporadic monocytopenia with susceptibility to mycobacteria, fungi, papillomaviruses, and myelodysplasia. Blood 115, 1519–1529.

Vogeli, K.M., Jin, S.W., Martin, G.R., Stainier, D.Y.R., 2006. A common progenitor for haematopoietic and endothelial lineages in the zebrafish gastrula. Nature 443, 337–339.

Wain, H.M., Bruford, E.A., Lovering, R.C., Lush, M.J., Wright, M.W., Povey, S., 2002. Guidelines for Human Gene Nomenclature. Genomics 79, 464–470.

Walters, K.B., Green, J.M., Surfus, J.C., Yoo, S.K., Huttenlocher, A., 2010. Live imaging of neutrophil motility in a zebrafish model of WHIM syndrome. Blood 116, 2803–2811.

Wang, C., Morley, S.C., Donermeyer, D., Peng, I., Lee, W.P., Devoss, J., Danilenko, D.M., Lin, Z., Zhang, J., Zhou, J., Allen, P.M., Brown, E.J., 2010. Actin-Bundling Protein L-Plastin Regulates T Cell Activation. J. Immunol. 185, 7487–7497.

Wang, L., Zhang, P., Wei, Y., Gao, Y., Patient, R., Liu, F., 2011. A blood flow-dependent klf2a-NO signaling cascade is required for stabilization of hematopoietic stem cell programming in zebrafish embryos. Blood 118, 4102–4110.

Wang, L.C.C., Kuo, F., Fujiwara, Y., Gilliland, D.G.G., Golub, T.R.T.R.T.R.T.R., Orkin, S.H.S.H.S.H.S.H., 1997. Yolk sac angiogenic defect and intra-embryonic apoptosis in mice lacking the Ets-related factor TEL. EMBO J. 16, 4374–4383.

Wang, X., Robertson, A.L.L., Li, J., Chai, R.J.J., Haishan, W., Sadiku, P., Ogryzko, N.V. V., Everett, M., Yoganathan, K., Luo, H.R.R., Renshaw, S.A.A., Ingham, P.W.W., 2014. Inhibitors of neutrophil recruitment identified using transgenic zebrafish to screen a natural product library. Dis. Model. Mech. 7, 163–169.

Warga, R.M., Kane, D.A., Ho, R.K., 2009. Fate Mapping Embryonic Blood in Zebrafish: Multi- and Unipotential Lineages Are Segregated at Gastrulation. Dev. Cell 16, 744–755.

Weber, T., Köster, R., 2013. Genetic tools for multicolor imaging in zebrafish larvae. Methods 62, 279–291.

West, R.R., Hsu, A.P., Holland, S.M., Cuellar-Rodriguez, J., Hickstein, D.D., 2014. Acquired ASXL1 mutations are common in patients with inherited GATA2 mutations and correlate with myeloid transformation. Haematologica 99, 276–81.

Westerfield, M., 2000. The Zebrafish Book: A Guide for the Laboratory Use of Zebrafish (Danio rerio). University of Oregon Press, Eugene, OR.

White, R.M., Sessa, A., Burke, C., Bowman, T., LeBlanc, J., Ceol, C., Bourque, C., Dovey, M., Goessling, W., Burns, C.E., Zon, L.I., 2008. Transparent adult zebrafish as a tool for in vivo transplantation analysis. Cell Stem Cell 2, 183–9.

Wiemels, J.L., Cazzaniga, G., Daniotti, M., Eden, O.B., Addison, G.M., Masera, G., Saha, V., Biondi, A., Greaves, M.F., 1999. Prenatal origin of acute lymphoblastic leukaemia in children. Lancet 354, 1499–1503.

Willett, C.E., Kawasaki, H., Amemiya, C.T., Lin, S., Steiner, L.A., 2001. Ikaros expression as a marker for lymphoid progenitors during zebrafish development. Dev. Dyn. 222, 694–698.

Wlodarski, M.W., Hirabayashi, S., Pastor, V., Stary, J., Hasle, H., Masetti, R., Dworzak, M., Schmugge, M., van den Heuvel-Eibrink, M., Ussowicz, M., De Moerloose, B., Catala, A., Smith, O.P., Sedlacek, P., Lankester, A.C., Zecca, M., Bordon, V., Matthes-Martin, S., Abrahamsson, J., Kuhl, J.S., Sykora, K.-W., Albert, M.H., Przychodzien, B., Maciejewski, J.P., Schwarz, S., Gohring, G., Schlegelberger, B., Cseh, A., Noellke, P., Yoshimi, A., Locatelli, F.,

Baumann, I., Strahm, B., Niemeyer, C.M., 2016. Prevalence, clinical characteristics, and prognosis of GATA2-related myelodysplastic syndromes in children and adolescents. Blood 127, 1387–1397.

Woods, I.G., Wilson, C., Friedlander, B., Chang, P., Reyes, D.K., Nix, R., Kelly, P.D., Chu, F., Postlethwait, J.H., Talbot, W.S., 2005. The zebrafish gene map defines ancestral vertebrate chromosomes. Genome Res. 15, 1307–14.

Zaliova, M., Madzo, J., Cario, G., Trka, J., 2011. Revealing the role of TEL/AML1 for leukemic cell survival by RNAi-mediated silencing. Leukemia 25, 313–320.

Zelent, A., Greaves, M., Enver, T., 2004. Role of the TEL-AML1 fusion gene in the molecular pathogenesis of childhood acute lymphoblastic leukaemia. Oncogene 23, 4275–4283.

Zhang, D.E., Zhang, P., Wang, N.D., Hetherington, C.J., Darlington, G.J., Tenen, D.G., 1997. Absence of granulocyte colony-stimulating factor signaling and neutrophil development in CCAAT enhancer binding protein alpha-deficient mice. Proc. Natl. Acad. Sci. U. S. A. 94, 569–74.

Zhao, N., Stoffel, a, Wang, P.W., Eisenbart, J.D., Espinosa, R., Larson, R. a, Le Beau, M.M., 1997. Molecular delineation of the smallest commonly deleted region of chromosome 5 in malignant myeloid diseases to 1-1.5 Mb and preparation of a PAC-based physical map. Proc. Natl. Acad. Sci. U. S. A. 94, 6948–53.

Zhu, C., Smith, T., McNulty, J., Rayla, A.L., Lakshmanan, A., Siekmann, A.F., Buffardi, M., Meng, X., Shin, J., Padmanabhan, A., Cifuentes, D., Giraldez, A.J., Look, A.T., Epstein, J.A., Lawson, N.D., Wolfe, S.A., 2011. Evaluation and application of modularly assembled zinc-finger nucleases in zebrafish. Development 138, 4555–64.

Zhu, J., Lai, K., Brownile, R., Babiuk, L.A., Mutwiri, G.K., 2008. Porcine TLR8 and TLR7 are both activated by a selective TLR7 ligand, imiquimod. Mol. Immunol. 45, 3238–3243.

9 Supplementary Data

9.1 Supplementary Figures

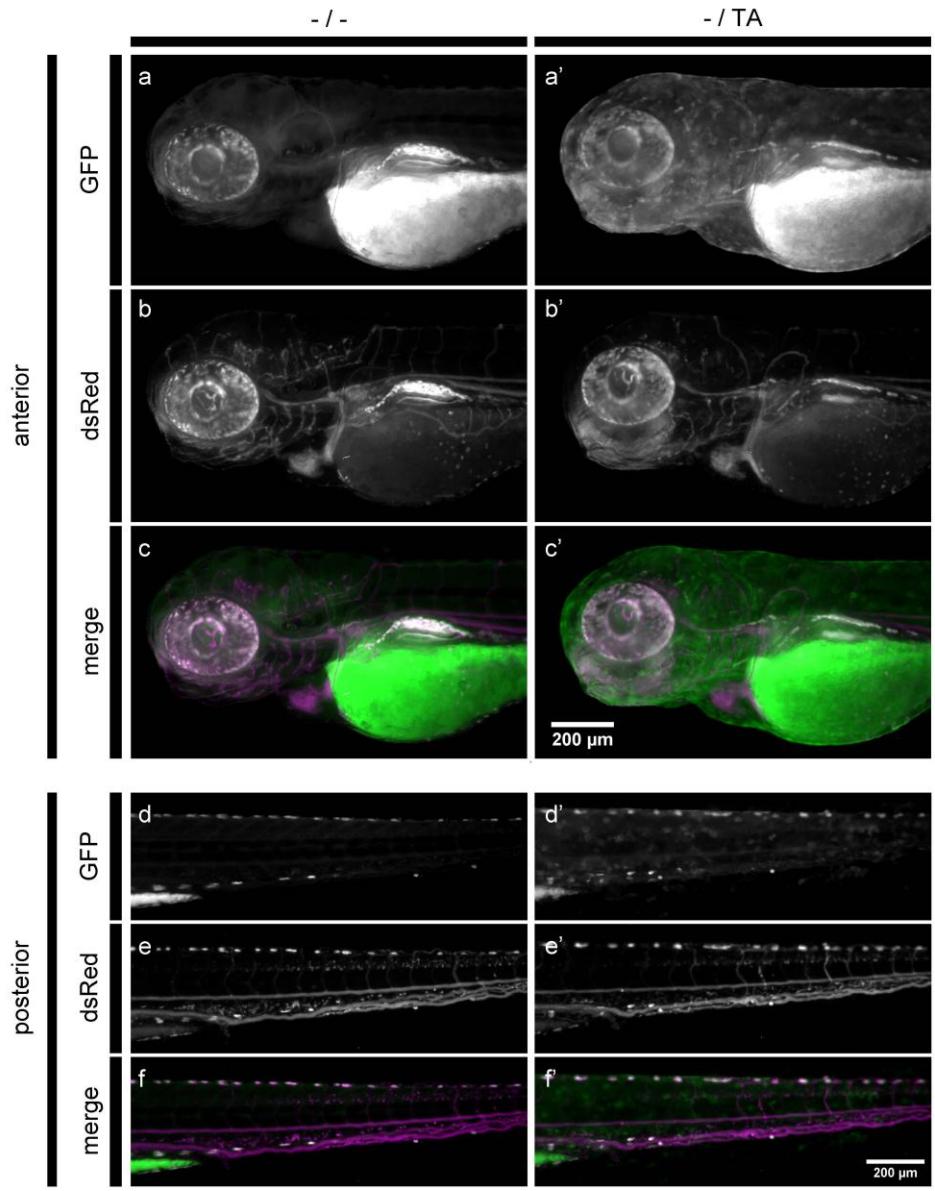

Supplementary Figure 9.1 | Erythroid cells in *Tg(ZβA:GFP-hTEL-AML1)*$^{+/-}$ fish at 72 hpf.

The transgenic reporter line *Tg(gata1a:dsRed)* was used to label erythroid cells in *Tg(ZβA:GFP-hTEL-AML1)* fish at 72 hpf. Anterior **(a-c and a'-c')** and posterior **(d-f and d'-f')** images were acquired of both wild type **(a-f)** and *Tg(ZβA:GFP-hTEL-AML1)*$^{+/-}$ **(a'-f')** larvae.

GFP **(a-a' and d-d')** and dsRed **(b-b' and e-e')** channels are shown together with images of both channels merged **(c-c' and f-f')**. Scale bars: **(a-c and a'-c')**, 200 µm; **(d-f and d'-f')**, 200 µm.

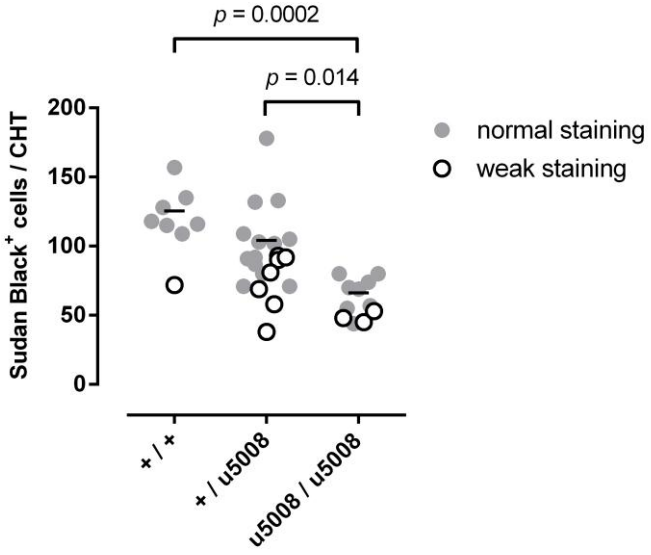

Supplementary Figure 9.2 | Analysis of data presented in Figure 5.8 b and c.

The data presented in Figure 5.8 b and c from 4 dpf *gata2b*^{u5008} mutant larvae are shown combined for further analysis. Each circle represents a measurement of the number of Sudan Black^{+} cells in the CHT carried out in a different larva. **Filled grey circles** correspond to larvae with normal Sudan Black accumulation, while those larvae with weak Sudan Black staining are shown as **open circles**. Notice that the number of labelled granulocytes of all larvae exhibiting low accumulation of Sudan Black is in the bottom half of the distribution for that genotype. Data were analysed again excluding larvae with low accumulation of Sudan Black (open circles). Statistical comparisons among larvae with normal Sudan Black staining (filled grey circles) were carried out by Kruskal-Wallis test (p = 0.0002) followed by Dunn's multiple comparisons test and p-values for each comparison are shown in the graph. The mean of the group of larvae with normal Sudan Black staining is shown as a horizontal black line for each genotype.

9.2 Supplementary Tables

This section contains Supplementary Tables that add descriptive and inferential statistics for quantitative data presented in previous chapters.

Supplementary Table 9.1 | Statistics of data shown in Figure 3.7 d.

Descriptive statistics		
Genotype	**- / -**	**- / TA**
Number of values	10	9
Mean	53	57.44
Standard Deviation	5.077	9.002
Standard Error of Mean	1.606	3.001
Lower 95% CI of mean	49.37	50.53
Upper 95% CI of mean	56.63	64.36

D'Agostino & Pearson omnibus normality test		
p-value	0.6462	0.3365

Inferential statistics		
Unpaired t test		
	p-value	0.197

Supplementary Table 9.2 | Statistics of data shown in Figure 3.9 a.

Descriptive statistics		
Genotype	**- / -**	**- / TA**
Number of values	19	22
Mean	1.737	2.227
Standard Deviation	1.408	2.022
Standard Error of Mean	0.323	0.4311
Lower 95% CI of mean	1.058	1.331
Upper 95% CI of mean	2.415	3.124

D'Agostino & Pearson omnibus normality test		
p-value	0.414	0.127

Inferential statistics		
Unpaired t test		
	p-value	0.3805

Supplementary Table 9.3 | Statistics of data shown in Figure 3.9 b.

Descriptive statistics		
Genotype	**- / -**	**- / TA**
Number of values	19	21
Mean	56.79	71.19
Standard Deviation	17.69	18.46
Standard Error of Mean	4.058	4.028
Lower 95% CI of mean	48.26	62.79
Upper 95% CI of mean	65.32	79.59

D'Agostino & Pearson omnibus normality test		
p-value	0.0975	0.2671

Inferential statistics		
Unpaired t test		
	p-value	0.0163
Difference between means		14.40 ± 5.730
95% confidence interval of the difference		2.801 to 26.00

Supplementary Table 9.4 | Statistics of data shown in Figure 3.9 c.

Descriptive statistics		
Genotype	**- / -**	**- / TA**
Number of values	38	52
Mean	102.5	121.4
Standard Deviation	23.15	34.01
Standard Error of Mean	3.755	4.717
Lower 95% CI of mean	94.87	112
Upper 95% CI of mean	110.1	130.9

D'Agostino & Pearson omnibus normality test		
p-value	0.9564	0.9379

Inferential statistics	
Unpaired t test	
p-value	0.0038
Difference between means	18.97 ± 6.387
95% confidence interval of the difference	6.276 to 31.66

Supplementary Table 9.5 | Statistics of data shown in Figure 3.9 d.

Descriptive statistics		
Genotype	**- / -**	**- / TA**
Number of values	27	19
Mean	116.9	121.3
Standard Deviation	28.45	19.67
Standard Error of Mean	5.476	4.513
Lower 95% CI of mean	105.6	111.8
Upper 95% CI of mean	128.1	130.8

D'Agostino & Pearson omnibus normality test		
p-value	0.805	0.7442

Inferential statistics	
Unpaired t test	
p-value	0.5577

Supplementary Table 9.6 | Statistics of data shown in Figure 3.9 e.

Descriptive statistics		
Genotype	**- / -**	**- / TA**
Number of values	24	17
Mean	184.6	170.9
Standard Deviation	35.64	33.99
Standard Error of Mean	7.275	8.245
Lower 95% CI of mean	169.6	153.4
Upper 95% CI of mean	199.7	188.4

D'Agostino & Pearson omnibus normality test		
p-value	0.7376	0.1854

Inferential statistics		
Unpaired t test		
	p-value	0.2226

Supplementary Table 9.7 | Statistics of data shown in Figure 4.6 d.

Descriptive statistics			
Genotype	**+ / +**	**+ / um27**	**um27 / um27**
Number of values	15	15	9
Mean	86.07	84.33	80.11
Standard Deviation	24.19	28.26	17.95
Standard Error of Mean	6.246	7.298	5.985
Lower 95% CI of mean	72.67	68.68	66.31
Upper 95% CI of mean	99.46	99.99	93.91

D'Agostino & Pearson omnibus normality test			
p-value	0.265	0.5533	0.6026

Inferential statistics		
Kruskal-Wallis test		
	p-value	0.848

Supplementary Table 9.8 | Statistics of data shown in Figure 4.7 g.

Descriptive statistics			
Genotype	**+ / +**	**+ / um27**	**um27 / um27**
Number of values	3	12	3
Mean	191.3	171.2	186.7
Standard Deviation	11.02	29.24	15.31
Standard Error of Mean	6.36	8.44	8.838
Lower 95% CI of mean	164	152.6	148.6
Upper 95% CI of mean	218.7	189.7	224.7

Inferential statistics	
Kruskal-Wallis test	
p-value	0.374

Supplementary Table 9.9 | Statistics of data shown in Figure 4.7 h.

Descriptive statistics			
Genotype	**+ / +**	**+ / um27**	**um27 / um27**
Number of values	3	12	3
Mean	170	152.6	163
Standard Deviation	14.42	30.89	19.67
Standard Error of Mean	8.327	8.916	11.36
Lower 95% CI of mean	134.2	133	114.1
Upper 95% CI of mean	205.8	172.2	211.9

Inferential statistics	
Kruskal-Wallis test	
p-value	0.582

Supplementary Table 9.10 | Statistics of data shown in Figure 4.7 i.

Descriptive statistics			
Genotype	**+ / +**	**+ / um27**	**um27 / um27**
Number of values	3	12	3
Mean	13.67	10.83	17.33
Standard Deviation	2.517	4.687	4.163
Standard Error of Mean	1.453	1.353	2.404
Lower 95% CI of mean	7.415	7.855	6.991
Upper 95% CI of mean	19.92	13.81	27.68

Inferential statistics	
Kruskal-Wallis test	
p-value	0.157

Supplementary Table 9.11 | Statistics of data shown in Figure 4.7 j.

Descriptive statistics			
Genotype	**+ / +**	**+ / um27**	**um27 / um27**
Number of values	3	12	3
Mean	7.667	7.75	6.333
Standard Deviation	6.351	8.487	2.082
Standard Error of Mean	3.667	2.45	1.202
Lower 95% CI of mean	-8.11	2.358	1.162
Upper 95% CI of mean	23.44	13.14	11.5

Inferential statistics	
Kruskal-Wallis test	
p-value	0.874

Supplementary Table 9.12 | Statistics of data shown in Figure 4.8 d.

Descriptive statistics			
Genotype	**+ / +**	**+ / um27**	**um27 / um27**
Number of values	7	10	7
Mean	27.86	30.5	15.43
Standard Deviation	9.529	8.196	6.294
Standard Error of Mean	3.602	2.592	2.379
Lower 95% CI of mean	19.04	24.64	9.607
Upper 95% CI of mean	36.67	36.36	21.25

Inferential statistics	
Kruskal-Wallis test	
p-value	0.012

Dunn's multiple comparisons test		
Groups compared		Adjusted *p*-value
+ / +	+ / um27	> 0.9999
+ / +	um27 / um27	0.060
+ / um27	um27 / um27	0.015

Supplementary Table 9.13 | Statistics of data shown in Figure 4.8 e.

Descriptive statistics			
Genotype	**+ / +**	**+ / um27**	**um27 / um27**
Number of values	7	10	7
Mean	19.43	19.3	16.14
Standard Deviation	5.35	6.684	3.891
Standard Error of Mean	2.022	2.114	1.471
Lower 95% CI of mean	14.48	14.52	12.54
Upper 95% CI of mean	24.38	24.08	19.74

Inferential statistics	
Kruskal-Wallis test	
p-value	0.342

Supplementary Table 9.14 | Statistics of data shown in Figure 4.9 d.

Descriptive statistics			
Genotype	**+ / +**	**+ / um27**	**um27 / um27**
Number of values	9	14	13
Mean	9.222	6.857	3.769
Standard Deviation	3.032	2.983	1.641
Standard Error of Mean	1.011	0.7974	0.4551
Lower 95% CI of mean	6.891	5.135	2.778
Upper 95% CI of mean	11.55	8.58	4.761

D'Agostino & Pearson omnibus normality test			
p-value	0.2882	0.6351	0.4653

Inferential statistics		
One-way ANOVA		
	p-value	0.0001

Tukey's multiple comparisons test		
Groups compared		Adjusted *p*-value
+ / +	+ / um27	0.098
+ / +	um27 / um27	< 0.0001
+ / um27	um27 / um27	0.011

Supplementary Table 9.15 | Statistics of data shown in Figure 4.11 d.

Descriptive statistics

Genotype	+ / +	+ / um27	um27 / um27
Number of values	2	5	3
Mean	90	105.4	88.33
Standard Deviation	22.63	18.8	27.65
Standard Error of Mean	16	8.406	15.96
Lower 95% CI of mean	-113.3	82.06	19.66
Upper 95% CI of mean	293.3	128.7	157

Inferential statistics

Kruskal-Wallis test

p-value	0.504

Dunn's multiple comparisons test

Groups compared		Adjusted *p*-value
+ / +	+ / um27	0.624
+ / +	um27 / um27	> 0.9999
+ / um27	um27 / um27	0.215

Supplementary Table 9.16 | Statistics of data shown in Figure 4.12 a.

Descriptive statistics

Genotype	+ / +	+ / um27	um27 / um27
Number of values	4	13	2
Mean	117.5	152.2	41
Standard Deviation	37.81	39.91	24.04
Standard Error of Mean	18.91	11.07	17
Lower 95% CI of mean	57.33	128	-175
Upper 95% CI of mean	177.7	176.3	257

Inferential statistics

Kruskal-Wallis test

p-value	0.018

Dunn's multiple comparisons test

Groups compared		Adjusted *p*-value
+ / +	+ / um27	0.611
+ / +	um27 / um27	0.572
+ / um27	um27 / um27	0.043

Supplementary Table 9.17 | Statistics of data shown in Figure 4.12 b.

Descriptive statistics

Genotype	+ / +	+ / um27	um27 / um27
Number of values	4	13	2
Mean	107	132.2	39
Standard Deviation	35.06	35	25.46
Standard Error of Mean	17.53	9.706	18
Lower 95% CI of mean	51.21	111.1	-189.7
Upper 95% CI of mean	162.8	153.4	267.7

Inferential statistics

Kruskal-Wallis test

p-value	0.030

Dunn's multiple comparisons test

Groups compared		Adjusted *p*-value
+ / +	+ / um27	> 0.9999
+ / +	um27 / um27	0.431
+ / um27	um27 / um27	0.050

Supplementary Table 9.18 | Statistics of data shown in Figure 4.12 c.

Descriptive statistics

Genotype	+ / +	+ / um27	um27 / um27
Number of values	4	13	2
Mean	8	11.62	1.5
Standard Deviation	8.756	5.98	2.121
Standard Error of Mean	4.378	1.658	1.5
Lower 95% CI of mean	-5.933	8.002	-17.56
Upper 95% CI of mean	21.93	15.23	20.56

Inferential statistics

Kruskal-Wallis test

p-value	0.015

Dunn's multiple comparisons test

Groups compared		Adjusted *p*-value
+ / +	+ / um27	0.361
+ / +	um27 / um27	0.877
+ / um27	um27 / um27	0.053

Supplementary Table 9.19 | Statistics of data shown in Figure 4.12 d.

Descriptive statistics			
Genotype	**+ / +**	**+ / um27**	**um27 / um27**
Number of values	4	13	2
Mean	2.5	8.308	0.5
Standard Deviation	2.38	7.51	0.7071
Standard Error of Mean	1.19	2.083	0.5
Lower 95% CI of mean	-1.288	3.77	-5.853
Upper 95% CI of mean	6.288	12.85	6.853

Inferential statistics	
Kruskal-Wallis test	
p-value	0.122

Dunn's multiple comparisons test		
Groups compared		Adjusted *p*-value
+ / +	+ / um27	0.624
+ / +	um27 / um27	> 0.9999
+ / um27	um27 / um27	0.215

Supplementary Table 9.20 | Statistics of data shown in Figure 4.13 a.

Descriptive statistics			
Genotype	**+ / +**	**+ / um27**	**um27 / um27**
Number of values	10	9	5
Mean	55.4	60.78	55.8
Standard Deviation	9.913	12.32	12.13
Standard Error of Mean	3.135	4.105	5.426
Lower 95% CI of mean	48.31	51.31	40.74
Upper 95% CI of mean	62.49	70.25	70.86

Inferential statistics	
Kruskal-Wallis test	
p-value	0.595

Supplementary Table 9.21 | Statistics of data shown in Figure 4.13 b.

Descriptive statistics			
Genotype	**+ / +**	**+ / um27**	**um27 / um27**
Number of values	10	9	5
Mean	35.12	37.94	51.27
Standard Deviation	10.13	14.48	12.42
Standard Error of Mean	3.204	4.828	5.555
Lower 95% CI of mean	27.87	26.81	35.84
Upper 95% CI of mean	42.37	49.08	66.69

Inferential statistics	
Kruskal-Wallis test	
p-value	0.084

Dunn's multiple comparisons test		
Groups compared		Adjusted *p*-value
+ / +	+ / um27	> 0.9999
+ / +	um27 / um27	0.085
+ / um27	um27 / um27	0.251

Supplementary Table 9.22 | Statistics of data shown in Figure 4.13 c.

Descriptive statistics			
Genotype	**+ / +**	**+ / um27**	**um27 / um27**
Number of values	11	18	3
Mean	3.182	2.722	2.333
Standard Deviation	2.926	1.809	1.528
Standard Error of Mean	0.8823	0.4263	0.8819
Lower 95% CI of mean	1.216	1.823	-1.461
Upper 95% CI of mean	5.148	3.622	6.128

Inferential statistics	
Kruskal-Wallis test	
p-value	0.926

Supplementary Table 9.23 | Statistics of data shown in Figure 4.13 d.

Descriptive statistics			
Genotype	**+ / +**	**+ / um27**	**um27 / um27**
Number of values	20	27	8
Mean	15.35	16.67	2.5
Standard Deviation	5.363	5.798	2.07
Standard Error of Mean	1.199	1.116	0.7319
Lower 95% CI of mean	12.84	14.37	0.7693
Upper 95% CI of mean	17.86	18.96	4.231

D'Agostino & Pearson omnibus normality test			
p-value	0.6771	0.8934	0.929

Inferential statistics		
One-way ANOVA		
	p-value	< 0.0001

Tukey's multiple comparisons test		
Groups compared		Adjusted *p*-value
+ / +	+ / um27	0.677
+ / +	um27 / um27	< 0.0001
+ / um27	um27 / um27	< 0.0001

Supplementary Table 9.24 | Statistics of data shown in Figure 4.14 g.

Descriptive statistics			
Genotype	**+ / +**	**+ / um27**	**um27 / um27**
Number of values	22	40	24
Mean	44.23	48.18	9.042
Standard Deviation	11.49	11.35	6.497
Standard Error of Mean	2.449	1.794	1.326
Lower 95% CI of mean	39.13	44.55	6.298
Upper 95% CI of mean	49.32	51.8	11.79

D'Agostino & Pearson omnibus normality test			
p-value	0.4751	0.9555	0.0129

Inferential statistics		
Kruskal-Wallis test		
	p-value	< 0.0001

Dunn's multiple comparisons test		
Groups compared		Adjusted *p*-value
+ / +	+ / um27	> 0.9999
+ / +	um27 / um27	< 0.0001
+ / um27	um27 / um27	< 0.0001

Supplementary Table 9.25 | Statistics of data shown in Figure 4.16 j.

Descriptive statistics

Genotype	+ / +	+ / um27	um27 / um27
Number of values	3	11	4
Mean	7.667	7.818	2.5
Standard Deviation	0.5774	0.9816	0.5774
Standard Error of Mean	0.3333	0.296	0.2887
Lower 95% CI of mean	6.232	7.159	1.581
Upper 95% CI of mean	9.101	8.478	3.419

Inferential statistics

Kruskal-Wallis test	
p-value	0.002

Dunn's multiple comparisons test		
Groups compared		Adjusted *p*-value
+ / +	+ / um27	> 0.9999
+ / +	um27 / um27	0.107
+ / um27	um27 / um27	0.008

Supplementary Table 9.26 | Statistics of data shown in Figure 4.18 g.

Descriptive statistics

Time point	**28 hpf**		**52 hpf**		**72 hpf**	
Genotype	**+ / +**	**+/um27**	**+ / +**	**+/um27**	**+ / +**	**+/um27**
Number of values	3	6	3	6	3	6
Mean	14.33	9.67	72.00	73.67	78.67	77.67
Standard Deviation	5.13	3.56	9.54	17.28	5.13	13.29
Standard Error of Mean	2.96	1.45	5.51	7.06	2.96	5.43

Inferential statistics

Repeated measures two-way ANOVA

Source of Variation	% of total variation	*p*-value
Interaction	0.1459	0.7637
Time	77.9900	< 0.0001
Genotype	0.0385	0.8398
Subjects (matching)	6.1230	0.0274

Bonferroni's multiple comparisons test

Time point	Adjusted *p*-value
28	> 0.9999
52	> 0.9999
72	> 0.9999

Supplementary Table 9.27 | Statistics of data shown in Figure 4.18 h.

Descriptive statistics

Time point	**52 hpf**		**72 hpf**	
Genotype	**+ / +**	**+ / um27**	**+ / +**	**+ / um27**
Number of values	3	6	3	6
Mean	13.00	4.83	32.67	27.50
Standard Deviation	6.56	2.04	2.52	5.68
Standard Error of Mean	3.79	0.83	1.45	2.32

Inferential statistics

Repeated measures two-way ANOVA		
Source of Variation	% of total variation	*p*-value
Interaction	0.3488	0.4887
Time	69.45	< 0.0001
Genotype	6.89	0.0280
Subjects (matching)	6.317	0.3403

Bonferroni's multiple comparisons test	
Time point	Adjusted *p*-value
52	0.0438
72	0.2504

Supplementary Table 9.28 | Statistics of data shown in Figure 5.7 a.

Descriptive statistics

Genotype	**+ / +**	**+ / u5008**	**u5008 / u5008**
Number of values	4	16	7
Mean	2.5	4.438	3.143
Standard Deviation	3.109	4.589	2.61
Standard Error of Mean	1.555	1.147	0.9863
Lower 95% CI of mean	-2.447	1.992	0.7294
Upper 95% CI of mean	7.447	6.883	5.556

Inferential statistics

Kruskal-Wallis test	
p-value	0.681

Supplementary Table 9.29 | Statistics of data shown in Figure 5.7 b.

Descriptive statistics			
Genotype	**+ / +**	**+ / u5008**	**u5008 / u5008**
Number of values	4	8	10
Mean	12.5	9.375	11
Standard Deviation	2.517	5.999	7.972
Standard Error of Mean	1.258	2.121	2.521
Lower 95% CI of mean	8.495	4.36	5.297
Upper 95% CI of mean	16.5	14.39	16.7

Inferential statistics	
Kruskal-Wallis test	
p-value	0.774

Supplementary Table 9.30 | Statistics of data shown in Figure 5.8 a.

Descriptive statistics			
Genotype	**+ / +**	**+ / u5008**	**u5008 / u5008**
Number of values	9	17	4
Mean	51.33	52.24	43.5
Standard Deviation	14.66	14.65	2.38
Standard Error of Mean	4.888	3.554	1.19
Lower 95% CI of mean	40.06	44.7	39.71
Upper 95% CI of mean	62.6	59.77	47.29

Inferential statistics	
Kruskal-Wallis test	
p-value	0.546

Supplementary Table 9.31 | Statistics of data shown in Figure 5.8 b.

Descriptive statistics			
Genotype	**+ / +**	**+ / u5008**	**u5008 / u5008**
Number of values	7	19	11
Mean	125.4	96.68	61.36
Standard Deviation	16.42	27.69	13.65
Standard Error of Mean	6.206	6.353	4.117
Lower 95% CI of mean	110.2	83.34	52.19
Upper 95% CI of mean	140.6	110	70.54

Inferential statistics	
Kruskal-Wallis test	
p-value	< 0.0001

Dunn's multiple comparisons test		
Groups compared		Adjusted *p*-value
+ / +	+ / u5008	0.087
+ / +	u5008 / u5008	< 0.0001
+ / u5008	u5008 / u5008	0.003

Supplementary Table 9.32 | Statistics of data shown in Figure 5.9 a.

Descriptive statistics			
Genotype	**+ / +**	**+ /delCVN**	**delCVN/delCVN**
Number of values	5	7	12
Mean	61.2	54.29	52
Standard Deviation	18.91	13.71	17.61
Standard Error of Mean	8.458	5.181	5.084
Lower 95% CI of mean	37.72	41.61	40.81
Upper 95% CI of mean	84.68	66.96	63.19

Inferential statistics	
Kruskal-Wallis test	
p-value	0.655

Supplementary Table 9.33 | Statistics of data shown in Figure 5.9 b.

Descriptive statistics			
Genotype	**+ / +**	**+ /delCVN**	**delCVN/delCVN**
Number of values	6	13	5
Mean	80.33	73.85	74.4
Standard Deviation	17.74	27.59	18.15
Standard Error of Mean	7.242	7.651	8.115
Lower 95% CI of mean	61.72	57.18	51.87
Upper 95% CI of mean	98.95	90.52	96.93

Inferential statistics	
Kruskal-Wallis test	
p-value	0.915

Supplementary Table 9.34 | Statistics of data shown in Figure 5.10 a.

Descriptive statistics				
***gata2a* genotype**	**+ / +**		**+ / um27**	
***gata2b* genotype**	**+ / +**	**+ / u5008**	**+ / +**	**+ / u5008**
Number of values	15	17	4	4
Mean	20.80	18.88	15.50	11.25
Standard Deviation	7.63	8.45	5.51	3.30
Standard Error of Mean	1.97	2.05	2.75	1.65

Inferential statistics		
Two-way ANOVA		
Source of Variation	% of total variation	*p*-value
Interaction	0.3609	0.7005
gata2a	11.09	0.0383
gata2b	2.523	0.312

Bonferroni's multiple comparisons test	
gata2a$^{+/+}$ - *gata2a*$^{+/um27}$	Adjusted *p*-value
gata2b$^{+/+}$	0.4471
gata2b$^{+/u5008}$	0.1586

Supplementary Table 9.35 | Statistics of data shown in Figure 5.10 b.

Descriptive statistics

***gata2a* genotype**	**+ / +**		**+ / um27**	
***gata2b* genotype**	**+ / +**	**+ / u5008**	**+ / +**	**+ / u5008**
Number of values	10	8	14	15
Mean	58.40	57.88	39.21	40.73
Standard Deviation	20.73	15.44	20.76	18.07
Standard Error of Mean	6.56	5.46	5.55	4.66

Inferential statistics

Two-way ANOVA

Source of Variation	% of total variation	*p*-value
Interaction	0.05933	0.86
gata2a	18.74	0.0029
gata2b	0.01403	0.9316

Bonferroni's multiple comparisons test

$gata2a^{+/+}$ - $gata2a^{+/um27}$	Adjusted *p*-value
$gata2b^{+/+}$	0.0392
$gata2b^{+/u5008}$	0.0933

Supplementary Table 9.36 | Statistics of data shown in Figure 5.11 a.

Descriptive statistics				
***gata2a* genotype**	**+ / +**		**+ / um27**	
***gata2b* genotype**	**+ / +**	**+ / u5008**	**+ / +**	**+ / u5008**
Number of values	9	3	5	7
Mean	39.56	30.33	38.20	38.29
Standard Deviation	7.09	7.09	4.38	10.09
Standard Error of Mean	2.36	4.10	1.96	3.82

Inferential statistics		
Two-way ANOVA		
Source of Variation	% of total variation	*p*-value
Interaction	7.925	0.1892
gata2a	3.981	0.3469
gata2b	7.636	0.1971

Bonferroni's multiple comparisons test	
gata2b$^{+/+}$ - *gata2b*$^{+/u5008}$	Adjusted *p*-value
gata2a$^{+/+}$	0.1686
gata2a$^{+/um27}$	0.9998

Supplementary Table 9.37 | Statistics of data shown in Figure 5.11 b.

Descriptive statistics

***gata2a* genotype**	**+ / +**		**+ / um27**	
***gata2b* genotype**	**+ / +**	**+ / u5008**	**+ / +**	**+ / u5008**
Number of values	8	5	7	3
Mean	65.38	59.60	58.14	56.67
Standard Deviation	14.38	10.11	11.99	12.01
Standard Error of Mean	5.08	4.52	4.53	6.94

Inferential statistics

Two-way ANOVA		
Source of Variation	% of total variation	*p*-value
Interaction	0.7024	0.7069
gata2a	3.928	0.3781
gata2b	1.998	0.5274

Supplementary Table 9.38 | Statistics of data shown in Figure 5.11 c.

Descriptive statistics

***gata2a* genotype**	**+ / +**		**+ / um27**	
***gata2b* genotype**	**+ / +**	**+ / u5008**	**+ / +**	**+ / u5008**
Number of values	8	5	7	3
Mean	65.38	59.60	58.14	56.67
Standard Deviation	14.38	10.11	11.99	12.01
Standard Error of Mean	5.08	4.52	4.53	6.94

Inferential statistics

Two-way ANOVA		
Source of Variation	% of total variation	*p*-value
Interaction	0.7024	0.7069
gata2a	3.928	0.3781
gata2b	1.998	0.5274

Bonferroni's multiple comparisons test	
gata2b$^{+/+}$ - *gata2b*$^{+/u5008}$	Adjusted *p*-value
gata2a$^{+/+}$	0.0317
gata2a$^{+/um27}$	> 0.9999

Supplementary Table 9.39 | Descriptive statistics of data from Figure 5.12 a.

Descriptive statistics

***gata2a* genotype**	**+ / +**			**+ / um27**			**um27 / um27**		
***gata2b* genotype**	**+ / +**	**+ / u5008**	**u5008 / u5008**	**+ / +**	**+ / u5008**	**u5008 / u5008**	**+ / +**	**+ / u5008**	**u5008 / u5008**
Number of values	26	33	9	17	22	6	11	5	2
Mean	57.88	61.88	59.33	56.35	65.59	57.67	9.18	26.60	30.00
Standard Deviation	15.06	18.57	17.68	14.17	19.00	20.27	8.06	6.69	2.83
Standard Error of Mean	2.95	3.23	5.90	3.44	4.05	8.28	2.43	2.99	2.00

Supplementary Table 9.40 | Inferential statistics of data from Figure 5.12 a.

Inferential statistics

Two-way ANOVA		
Source of Variation	% of total variation	*p*-value
Interaction	1.761	0.4589
gata2a	37.17	< 0.0001
gata2b	2.228	0.1036

Tukey's multiple comparisons test	
gata2b$^{+/+}$	Adjusted *p*-value
gata2a$^{+/+}$ - *gata2a*$^{+/um27}$	0.952
gata2a$^{+/+}$ - *gata2a*$^{um27/um27}$	< 0.0001
gata2a$^{+/um27}$ - *gata2a*$^{um27/um27}$	< 0.0001

gata2b$^{+/u5008}$	Adjusted *p*-value
gata2a$^{+/+}$ - *gata2a*$^{+/um27}$	0.6908
gata2a$^{+/+}$ - *gata2a*$^{um27/um27}$	< 0.0001
gata2a$^{+/um27}$ - *gata2a*$^{um27/um27}$	< 0.0001

gata2b$^{u5008/u5008}$	Adjusted *p*-value
gata2a$^{+/+}$ - *gata2a*$^{+/um27}$	0.9799
gata2a$^{+/+}$ - *gata2a*$^{um27/um27}$	0.0617
gata2a$^{+/um27}$ - *gata2a*$^{um27/um27}$	0.1017

Supplementary Table 9.41 | Statistics of data shown in Figure 5.12 b.

Descriptive statistics				
***gata2a* genotype**	**+ / +**		**+ / um27**	
***gata2b* genotype**	**+ / +**	**+ / u5008**	**+ / +**	**+ / u5008**
Number of values	13	11	12	10
Mean	124.62	77.91	124.50	85.00
Standard Deviation	30.95	21.90	29.68	18.17
Standard Error of Mean	8.58	6.60	8.57	5.75

Inferential statistics		
Two-way ANOVA		
Source of Variation	% of total variation	*p*-value
Interaction	0.2923	0.6456
gata2a	0.2739	0.6562
gata2b	41.84	< 0.0001

Bonferroni's multiple comparisons test	
gata2b$^{+/+}$ - *gata2b*$^{+/u5008}$	Adjusted *p*-value
gata2a$^{+/+}$	0.0002
gata2a$^{+/um27}$	0.0021

Supplementary Table 9.42 | Statistics of data shown in Figure 5.15 a.

Descriptive statistics

***gata2a* genotype**	**+ / +**		**+ / um27**	
***gata2b* genotype**	**+ / +**	**+ / u5008**	**+ / +**	**+ / u5008**
Number of values	5	4	8	7
Mean	12.20	9.00	13.50	8.29
Standard Deviation	7.89	5.48	6.85	9.03
Standard Error of Mean	3.53	2.74	2.42	3.41

Inferential statistics

Two-way ANOVA		
Source of Variation	% of total variation	*p*-value
Interaction	0.4412	0.7578
gata2a	0.03731	0.9285
gata2b	7.699	0.2063

Supplementary Table 9.43 | Statistics of data shown in Figure 5.15 b.

Descriptive statistics				
***gata2a* genotype**	**+ / +**		**+ / um27**	
***gata2b* genotype**	**+ / +**	**+ / u5008**	**+ / +**	**+ / u5008**
Number of values	7	5	4	8
Mean	42.29	46.40	43.50	41.88
Standard Deviation	11.91	15.77	12.48	11.37
Standard Error of Mean	4.50	7.05	6.24	4.02

Inferential statistics		
Two-way ANOVA		
Source of Variation	% of total variation	*p*-value
Interaction	1.395	0.5992
gata2a	0.4641	0.7612
gata2b	0.2624	0.8192

Supplementary Table 9.44 | Statistics of data shown in Figure 6.2 d.

Descriptive statistics			
Genotype	**+ / +**	**+ / E8fs**	**E8fs / E8fs**
Number of values	24	40	28
Mean	49.33	38.75	26.54
Standard Deviation	13.99	11.14	7.904
Standard Error of Mean	2.856	1.761	1.494
Lower 95% CI of mean	43.42	35.19	23.47
Upper 95% CI of mean	55.24	42.31	29.6

D'Agostino & Pearson omnibus normality test			
p-value	0.8465	0.0672	0.0846

Inferential statistics		
One-way ANOVA test		
	p-value	< 0.0001

Tukey's multiple comparisons test		
Groups compared		Adjusted *p*-value
+ / +	+ / E8fs	0.0011
+ / +	E8fs / E8fs	< 0.0001
+ / E8fs	E8fs / E8fs	< 0.0001

Supplementary Table 9.45 | Statistics of data shown in Figure 6.3 d.

Descriptive statistics			
Genotype	**+ / +**	**+ / E8fs**	**E8fs / E8fs**
Number of values	10	25	33
Mean	159	124.5	28.39
Standard Deviation	37.12	39.5	10.57
Standard Error of Mean	11.74	7.9	1.84
Lower 95% CI of mean	132.4	108.2	24.65
Upper 95% CI of mean	185.6	140.8	32.14

D'Agostino & Pearson omnibus normality test			
p-value	0.3995	0.5273	0.2402

Inferential statistics		
One-way ANOVA test		
	p-value	< 0.0001

Tukey's multiple comparisons test		
Groups compared		Adjusted *p*-value
+ / +	+ / E8fs	0.0056
+ / +	E8fs / E8fs	< 0.0001
+ / E8fs	E8fs / E8fs	< 0.0001

Supplementary Table 9.46 | Statistics of data shown in Figure 6.5 e.

Descriptive statistics		
Genotype	**+ / +**	**+ / E8fs**
Number of values	5	8
Mean	1	0.666
Standard Deviation	0.2057	0.4071
Standard Error of Mean	0.09199	0.1439
Lower 95% CI of mean	0.7446	0.3256
Upper 95% CI of mean	1.255	1.006

Inferential statistics		
Mann Whitney test		
	p-value	0.171

Supplementary Table 9.47 | Statistics of data shown in Figure 6.5 f.

Descriptive statistics		
Genotype	**+ / +**	**+ / E8fs**
Number of values	2	6
Mean	73.5	75.67
Standard Deviation	21.92	17.67
Standard Error of Mean	15.5	7.214
Lower 95% CI of mean	-123.4	57.12
Upper 95% CI of mean	270.4	94.21

Inferential statistics		
Mann Whitney test		
	p-value	0.821

Supplementary Table 9.48 | Statistics of data shown in Figure 6.6 d.

Descriptive statistics			
Genotype	**+ / +**	**+ / E8fs**	**E8fs / E8fs**
Number of values	36	23	9
Mean	1	0.859	0.01556
Standard Deviation	0.2425	0.2204	0.0174
Standard Error of Mean	0.04041	0.04595	0.0058
Lower 95% CI of mean	0.918	0.7637	0.00218
Upper 95% CI of mean	1.082	0.9543	0.02893

D'Agostino & Pearson omnibus normality test			
p-value	0.2048	0.4438	0.4127

Inferential statistics		
One-way ANOVA test		
	p-value	< 0.0001

Tukey's multiple comparisons test		
Groups compared		Adjusted *p*-value
+ / +	+ / E8fs	0.0490
+ / +	E8fs / E8fs	< 0.0001
+ / E8fs	E8fs / E8fs	< 0.0001

Supplementary Table 9.49 | Statistics of data shown in Figure 6.7 a.

Descriptive statistics		
Genotype	**+ / +**	**+ / E8fs**
Number of values	3	3
Mean	20	35.33
Standard Deviation	18.68	28.99
Standard Error of Mean	10.79	16.74
Lower 95% CI of mean	-26.41	-36.68
Upper 95% CI of mean	66.41	107.3

Inferential statistics		
Mann Whitney test		
	p-value	0.400

Supplementary Table 9.50 | Statistics of data shown in Figure 6.7 b.

Descriptive statistics		
Genotype	**+ / +**	**+ / E8fs**
Number of values	3	3
Mean	133.3	131.3
Standard Deviation	7.024	5.033
Standard Error of Mean	4.055	2.906
Lower 95% CI of mean	115.9	118.8
Upper 95% CI of mean	150.8	143.8

Inferential statistics		
Mann Whitney test		
	p-value	0.800

Supplementary Table 9.51 | Statistics of data shown in Figure 6.7 c.

Descriptive statistics		
Genotype	**+ / +**	**+ / E8fs**
Number of values	5	7
Mean	89	112.9
Standard Deviation	16.85	20.68
Standard Error of Mean	7.537	7.818
Lower 95% CI of mean	68.08	93.73
Upper 95% CI of mean	109.9	132

Inferential statistics		
Mann Whitney test		
	p-value	0.082

Supplementary Table 9.52 | Statistics of data shown in Figure 6.7 d.

Descriptive statistics		
Genotype	**+ / +**	**+ / E8fs**
Number of values	5	7
Mean	146.6	152.6
Standard Deviation	8.355	5.381
Standard Error of Mean	3.736	2.034
Lower 95% CI of mean	136.2	147.6
Upper 95% CI of mean	157	157.5

Inferential statistics		
Mann Whitney test		
	p-value	0.160

Supplementary Table 9.53 | Descriptive statistics of data from Figure 6.9 a.

Descriptive statistics

morpholino	**control morphants**			***rps14* morphants**		
drug treatment	**DMSO**	**imiquimod**	**gardiquimod**	**DMSO**	**imiquimod**	**gardiquimod**
Number of values	17	17	9	17	20	17
Mean	2993.12	2994.00	2998.48	2925.09	2898.03	2820.53
Standard Deviation	152.36	174.33	181.87	98.61	108.65	164.68
Standard Error of Mean	36.95	42.28	60.62	23.92	24.30	39.94

Supplementary Table 9.54 | Inferential statistics of data from Figure 6.9 a.

Inferential statistics

Two-way ANOVA		
Source of Variation	% of total variation	*p*-value
Interaction	1.865	0.3627
morpholino	12.61	0.0003
treatment	1.512	0.4386

Dunnett's multiple comparisons test	
control morphants	Adjusted *p*-value
DMSO - imiquimod	0.9997
DMSO - gardiquimod	0.9942

rps14 morphants	Adjusted *p*-value
DMSO - imiquimod	0.7973
DMSO - gardiquimod	0.0719

Supplementary Table 9.55 | Descriptive statistics of data from Figure 6.9 b.

Descriptive statistics

morpholino	**control morphants**			***rps14* morphants**		
drug treatment	**DMSO**	**imiquimod**	**gardiquimod**	**DMSO**	**imiquimod**	**gardiquimod**
Number of values	16	17	9	17	20	17
Mean	211.56	207.96	212.71	158.13	157.06	154.87
Standard Deviation	12.59	15.85	8.79	22.55	13.58	12.67
Standard Error of Mean	3.15	3.84	2.93	5.47	3.04	3.07

Supplementary Table 9.56 | Inferential statistics of data from Figure 6.9 b.

Inferential statistics

Two-way ANOVA		
Source of Variation	% of total variation	*p*-value
Interaction	0.1932	0.6941
morpholino	73.47	< 0.0001
treatment	0.1065	0.8174

Dunnett's multiple comparisons test	
control morphants	Adjusted *p*-value
DMSO - imiquimod	0.7247
DMSO - gardiquimod	0.9769

rps14 morphants	Adjusted *p*-value
DMSO - imiquimod	0.9682
DMSO - gardiquimod	0.7619

Supplementary Table 9.57 | Descriptive statistics of data from Figure 6.9 c.

Descriptive statistics						
morpholino	**control morphants**			***rps14* morphants**		
drug treatment	**DMSO**	**imiquimod**	**gardiquimod**	**DMSO**	**imiquimod**	**gardiquimod**
Number of values	41	48	41	56	54	49
Mean	3536.39	3481.45	3242.16	3382.85	3460.71	3247.39
Standard Deviation	131.86	225.68	133.93	112.04	123.79	195.31
Standard Error of Mean	20.59	32.57	20.92	14.97	16.85	27.90

Supplementary Table 9.58 | Inferential statistics of data from Figure 6.9 c.

Inferential statistics

Two-way ANOVA		
Source of Variation	% of total variation	*p*-value
Interaction	3.217	0.0014
morpholino	2.136	0.003
treatment	28.33	< 0.0001

Dunnett's multiple comparisons test	
control morphants	Adjusted *p*-value
DMSO - imiquimod	0.1835
DMSO - gardiquimod	< 0.0001

rps14 morphants	Adjusted *p*-value
DMSO - imiquimod	0.0203
DMSO - gardiquimod	< 0.0001

Supplementary Table 9.59 | Descriptive statistics of data from Figure 6.9 d.

Descriptive statistics

morpholino	**control morphants**			***rps14* morphants**		
drug treatment	**DMSO**	**imiquimod**	**gardiquimod**	**DMSO**	**imiquimod**	**gardiquimod**
Number of values	41	48	42	55	53	48
Mean	246.97	240.14	237.07	211.81	217.24	215.01
Standard Deviation	13.00	9.00	13.01	17.37	16.68	16.56
Standard Error of Mean	2.03	1.30	2.01	2.34	2.29	2.39

Supplementary Table 9.60 | Inferential statistics of data from Figure 6.9 d.

Inferential statistics

Two-way ANOVA		
Source of Variation	% of total variation	*p*-value
Interaction	2.203	0.0034
morpholino	44.1	< 0.0001
treatment	0.498	0.2709

Dunnett's multiple comparisons test	
control morphants	Adjusted *p*-value
DMSO - imiquimod	0.0558
DMSO - gardiquimod	0.0048

rps14 morphants	Adjusted *p*-value
DMSO - imiquimod	0.1027
DMSO - gardiquimod	0.4407

Supplementary Table 9.61 | Statistics of data shown in Figure 6.10 e.

Descriptive statistics				
morpholino	**control**		***gata1a***	
drug treatment	**DMSO**	**imiquimod**	**DMSO**	**imiquimod**
Number of values	5	6	4	4
Mean	28.55	26.98	45.67	68.64
Standard Deviation	6.43	4.25	13.19	6.56
Standard Error of Mean	2.88	1.74	6.59	3.28

Inferential statistics		
Two-way ANOVA		
Source of Variation	% of total variation	*p*-value
Interaction	11.61	0.004
morpholino	66.55	< 0.0001
drug treatment	8.831	0.0098

Bonferroni's multiple comparisons test	
DMSO - imiquimod	Adjusted *p*-value
control MO	> 0.9999
gata1a MO	0.0016

Supplementary Table 9.62 | Statistics of data shown in Figure 6.10 f.

Descriptive statistics

morpholino	**control**		***gata1a***	
drug treatment	**DMSO**	**imiquimod**	**DMSO**	**imiquimod**
Number of values	5	6	4	4
Mean	71769.32	76193.46	74680.94	71939.48
Standard Deviation	3041.55	2227.45	8870.65	5628.74
Standard Error of Mean	1360.22	909.35	4435.33	2814.37

Inferential statistics

Two-way ANOVA		
Source of Variation	% of total variation	*p*-value
Interaction	12.74	0.1534
morpholino	0.4473	0.782
drug treatment	0.7028	0.7289

Bonferroni's multiple comparisons test	
DMSO - imiquimod	Adjusted *p*-value
control MO	0.3478
gata1a MO	0.921

Supplementary Table 9.63 | Statistics of data shown in Figure 6.11 a.

Descriptive statistics

rps14	**+ / +**			**+ / E8fs**		
drug treatment	**E3**	**DMSO**	**imiquimod**	**E3**	**DMSO**	**imiquimod**
Number of values	9	9	7	10	11	12
Mean	4.67	4.89	5.00	2.10	2.73	3.33
Standard Deviation	2.00	2.76	3.00	1.52	2.15	2.19
Standard Error of Mean	0.67	0.92	1.13	0.48	0.65	0.63

Inferential statistics

Two-way ANOVA		
Source of Variation	% of total variation	*p*-value
Interaction	0.2291	0.7614
rps14	13.7	0.0236
drug treatment	0.4809	0.6601

Supplementary Table 9.64 | Statistics of data shown in Figure 6.11 b.

Descriptive statistics

rps14	**+ / +**			**+ / E8fs**		
drug treatment	**E3**	**DMSO**	**imiquimod**	**E3**	**DMSO**	**imiquimod**
Number of values	9	9	7	10	11	12
Mean	41.00	39.44	36.29	39.00	38.91	37.50
Standard Deviation	8.17	8.06	6.02	11.41	7.19	9.09
Standard Error of Mean	2.72	2.69	2.28	3.61	2.17	2.62

Inferential statistics

Two-way ANOVA		
Source of Variation	% of total variation	*p*-value
Interaction	0.3228	0.7358
rps14	0.04861	0.8958
drug treatment	2.2	0.3807

Supplementary Table 9.65 | Statistics of data shown in Figure 6.11 c.

Descriptive statistics

rps14	**+ / +**			**+ / E8fs**		
drug treatment	**E3**	**DMSO**	**imiquimod**	**E3**	**DMSO**	**imiquimod**
Number of values	8	7	7	7	10	5
Mean	96.00	102.29	101.57	101.14	89.40	88.80
Standard Deviation	23.05	26.66	31.12	27.14	22.32	13.99
Standard Error of Mean	8.15	10.08	11.76	10.26	7.06	6.26

Inferential statistics

Two-way ANOVA		
Source of Variation	% of total variation	*p*-value
Interaction	3.174	0.5338
rps14	1.984	0.3773
drug treatment	0.3655	0.9293

Supplementary Table 9.66 | Statistics of data shown in Figure 6.14 c.

Descriptive statistics		
Genotype	**+ / +**	**+ / E8fs**
Number of values	12	17
Mean	0.553	0.387
Standard Deviation	0.193	0.225
Standard Error of Mean	0.056	0.055
Lower 95% CI of mean	0.431	0.272
Upper 95% CI of mean	0.676	0.503

D'Agostino & Pearson omnibus normality test		
p-value	0.7438	0.1128

Inferential statistics		
Unpaired t test		
	p-value	0.048

Supplementary Table 9.67 | Statistics of data shown in Figure 6.14 d.

Descriptive statistics		
Genotype	**+ / +**	**+ / E8fs**
Number of values	31	26
Mean	1.000	0.616
Standard Deviation	0.576	0.477
Standard Error of Mean	0.103	0.093
Lower 95% CI of mean	0.789	0.424
Upper 95% CI of mean	1.211	0.809

D'Agostino & Pearson omnibus normality test		
p-value	0.0089	0.1966

Inferential statistics		
Mann-Whitney test		
	p-value	0.004

9.3 Plasmid maps and sequences

Plasmid Sequence 9.1 | pT3TS-nCas9n

```
1        10        20        30        40        50
  |       |         |         |         |         |
  AATTAACCCTCACTAAAGGGAACAAAAGCTGGAGCTAAGCTTGCTTGTTC
  TTTTTGCAGAAGCTCAGAATAAACGCTCAACTTTGGCAGATCTAACTCGA
  CGCCACCATGGCTTCTCCACCTAAGAAGAAGAGAAAGGTGGGAAGCATGG
  ATAAGAAGTATAGCATCGGCCTGGATATTGGAACTAACTCCGTGGGTTGG
  GCAGTGATTACAGACGACTACAAGGTCCCTAGCAAGAAATTTAAGGTGCT
  GGGTAACACCGACAGGCACAGCATCAAGAAAAATCTGATTGGAGCCCTGC
  TGTTCGGTTCTGGAGAGACTGCCGAAGCAACACGCCTGAAAAGAACAGCA
  AGAAGGCGCTATACCAGAAGGAAGAATAGAATCTGTTACCTGCAGGAGAT
  TTTCTCTAACGAAATGGCTAAGGTGGACGATTCATTCTTTCATAGGCTGG
  AGGAAAGTTTCCTGGTCGAGGAAGATAAGAAACACGAGCGCCATCCTATC
  TTTGGAAACATTGTGGACGAGGTCGCCTATCACGAAAAATACCCAACCAT
  CTATCATCTGCGCAAGAAACTGGCTGACTCTACTGATAAAGCCGACCTGA
  GACTGATCTATCTGGCTCTGGCCCACATGATTAAGTTCAGGGGTCATTTT
  CTGATCGAGGGCGATCTGAACCCCGACAATTCCGATGTGGACAAGCTGTT
  CATCCAGCTGGTCCAGATTTACAATCAGCTGTTTGAGGAAAACCCTATTA
  ATGCTTCCAGAGTGGACGCAAAAGCTATCCTGTCAGCCAGGCTGTCCAAG
  TCACGCAGACTGGAGAACCTGATTGCACAGCTGCCCGGAGAAAAGAGGAA
  CGGTCTGTTTGGAAATCTGATCGCTCTGAGTCTGGGCCTGACTCCTAACT
  TCAAAAGCAATTTTGATCTGGCTGAGGACGCCAAACTGCAGCTGTCAAAG
  GACACATATGACGATGACCTGGATAACCTGCTGGCACAGATCGGAGATCA
  GTACGCTGACCTGTTCCTGGCTGCCAAAAATCTGTCCGACGCAATCCTGC
  TGTCAGATATTCTGAGAGTGAACAGCGAGATTACAAAAGCTCCTCTGAGT
  GCCAGCATGATCAAGAGATATGACGAGCACCATCAGGATCTGACCCTGCT
  GAAGGCTCTGGTCAGGCAGCAGCTGCCAGAGAAGTACAAGGAAATTTTCT
  TTGATCAGTCCAAGAACGGCTACGCCGGTTATATCGACGGAGGCGCATCA
  CAGGAGGAATTCTACAAGTTTATCAAACCTATTCTGGAGAAGATGGACGG
  AACTGAGGAACTGCTGGTGAAACTGAATAGAGAGGACCTGCTGAGGAAGC
  AGCGCACATTTGATAACGGTTCCATCCCACACCAGATTCATCTGGGAGAG
  CTGCACGCTATCCTGAGGCGCCAGGAAGACTTCTACCCCTTTCTGAAAGA
  TAACCGCGAGAAGATCGAAAAAATTCTGACCTTCAGAATCCCTTACTATG
  TGGGTCCACTGGCTCGCGGAAACAGCAGATTTGCCTGGATGACTCGCAAA
  TCCGAGGAAACCATTACTCCTTGGAACTTCGAGGAAGTGGTCGATAAGGG
  CGCCTCTGCACAGTCCTTCATCGAGAGAATGACTAATTTTGACAAAAACC
  TGCCCAATGAGAAAGTGCTGCCTAAGCACTCCCTGCTGTACGAGTATTTC
  ACTGTCTATAACGAACTGACAAAGGTGAAATACGTCACCGAGGGCATGAG
  AAAGCCAGCCTTCCTGTCAGGAGAGCAGAAGAAAGCAATCGTGGATCTGC
  TGTTTAAAACCAACAGGAAAGTGACTGTCAAGCAGCTGAAGGAGGACTAC
  TTCAAGAAAATTGAATGCTTCGATTCCGTGGAGATCAGCGGAGTCGAAGA
  CAGATTTAACGCAAGCCTGGGCGCTTACCACGATCTGCTGAAGATCATTA
  AGGATAAAGACTTCCTGGACAACGAGGAAAATGAGGATATCCTGGAAGAC
  ATTGTGCTGACACTGACCCTGTTTGAGGACAGAGGAATGATCGAGGAAAG
  ACTGAAAACCTATGCTCATCTGTTCGATGACAAGGTGATGAAACAGCTGA
  AGAGAAGGCGCTACACTGGCTGGGGTAGACTGAGCAGGAAGCTGATCAAC
  GGCATTAGGGATAAACAGTCAGGAAAGACAATCCTGGACTTTCTGAAAAG
  TGATGGCTTCGCCAACCGCAATTTTATGCAGCTGATTCACGATGACAGTC
  TGACCTTCAAAGAGGACATCCAGAAGGCTCAGGTGTCTGGACAGGGCCAC
  TCCCTGCATGAGCAGATTGCAAACCTGGCTGGAAGCCCAGCCATCAAGAA
  AGGCATTCTGCAGACAGTGAAAATCGTCGATGAGCTGGTGAAAGTCATGG
  GCCATAAGCCCGAAAACATCGTGATTGAGATGGCTCGCGAAAATCAGACA
  ACCCAGAAGGGTCAGAAGAACAGTAGAGAGAGGATGAAAAGAATCGAGGA
```

AGGCATTAAGGAGCTGGGTAGCCAGATCCTGAAAGAGCACCCAGTGGAAA
ACACACAGCTGCAGAATGAGAAGCTGTATCTGTACTATCTGCAGAATGGA
AGAGATATGTACGTGGACCAGGAGCTGGATATTAACAGGCTGTCTGATTA
CGACGTGGATCATATCGTCCCCCAGAGTTTCATCAAAGATGACAGCATTG
ACAACAAGGTGCTGACCAGGTCCGACAAAAACAGAGGAAAATCAGATAAT
GTCCCTAGTGAGGAAGTGGTCAAGAAAATGAAGAACTACTGGAGACAGCT
GCTGAATGCCAAACTGATCACTCAGAGGAAGTTTGATAACCTGACAAAAG
CAGAGCGCGGTGGACTGTCAGAACTGGACAAAGCTGGATTCATCAAGAGG
CAGCTGGTGGAAACACGCCAGATCACTAAACACGTCGCACAGATTCTGGA
TAGTCGCATGAACACAAAGTACGATGAGAATGACAAACTGATCAGAGAAG
TGAAGGTCATTACCCTGAAGAGTAAACTGGTCAGCGACTTTAGGAAAGAT
TTCCAGTTTTATAAGGTCCGCGAGATTAACAATTATCACCATGCCCATGA
CGCATACCTGAACGCCGTGGTCGGTACCGCACTGATCAAGAAATACCCAA
AACTGGAGAGCGAATTCGTGTACGGAGACTATAAGGTGTACGATGTCAGA
AAAATGATCGCCAAGTCCGAGCAGGAAATTGGAAAAGCTACTGCCAAGTA
TTTCTTTTACTCAAACATCATGAATTTCTTTAAGACAGAGATCACCCTGG
CCAATGGAGAAATCCGCAAAAGGCCCCTGATTGAGACAAACGGAGAGACA
GGCGAAATCGTGTGGGACAAAGGCAGAGATTTTGCAACCGTGAGGAAGGT
CCTGAGCATGCCTCAAGTGAATATCGTCAAGAAAACTGAGGTGCAGACAG
GCGGTTTCTCAAAAGAAAGTATTCTGCCAAAACGCAACTCTGATAAGCTG
ATCGCTAGAAAGAAAGACTGGGACCCTAAGAAGTATGGAGGCTTTGACTC
TCCCACTGTGGCATACTCCGTCCTGGTGGTCGCTAAGGTGGAGAAGGGCA
AAAGCAAGAAACTGAAATCTGTCAAGGAGCTGCTGGGTATCACAATTATG
GAGAGAAGCTCTTTCGAGAAGAACCCAATCGATTTTCTGGAGGCCAAAGG
TTATAAGGAAGTGAAGAAAGACCTGATCATTAAACTGCCCAAGTACAGTC
TGTTTGAGCTGGAAAACGGCAGGAAACGCATGCTGGCAAGCGCTGGAGAG
CTGCAGAAAGGCAATGAACTGGCCCTGCCTTCTAAGTACGTGAACTTCCT
GTATCTGGCAAGCCACTACGAGAAGCTGAAAGGATCTCCAGAGGATAACG
AACAGAAACAGCTGTTTGTGGAGCAGCACAAGCATTATCTGGACGAGATC
ATTGAACAGATTAGCGAGTTCTCTAAAAGAGTGATCCTGGCCGACGCAAA
TCTGGATAAGGTCCTGTCTGCTTACAACAAACACAGAGATAAGCCCATCA
GGGAGCAGGCCGAAAATATCATTCATCTGTTCACTCTGACAAACCTGGGC
GCACCTGCAGCTTTCAAGTACTTCGACACTACAATCGATAGAAAGAGGTA
CACCTCCACTAAGGAGGTGCTGGACGCTACACTGATCCATCAGAGTATTA
CCGGCCTGTACGAAACAAGGATTGACCTGTCTCAGCTGGGTGGCGACTCA
CCGGTGAGATCTCCTAAGAAGAAGAGAAAGGTGTGACCGCGGATCTGGTT
ACCACTAAACCAGCCTCAAGAACACCCGAATGGAGTCTCTAAGCTACATA
ATACCAACTTACACTTTACAAAATGTTGTCCCCCAAAATGTAGCCATTCG
TATCTGCTCCTAATAAAAAGAAAGTTTCTTCACATTCTAAAAAAAAAAAA
AAAAAAAAAAAAAAAAACCCCCCCCCCCCCCCTGCAGGGCCAAGTCGGCCT
CTAGAGGTACCCAATTCGCCCTATAGTGAGTCGTATTACAATTCACTGGC
CGTCGTTTTACAACGTCGTGACTGGGAAAACCCTGGCGTTACCCAACTTA
ATCGCCTTGCAGCACATCCCCCTTTCGCCAGCTGGCGTAATAGCGAAGAG
GCCCGCACCGATCGCCCTTCCCAACAGTTGCGCAGCCTGAATGGCGAATG
GAAATTGTAAGCGTTAATATTTTGTTAAAATTCGCGTTAAATTTTTGTTA
AATCAGCTCATTTTTTAACCAATAGGCCGAAATCGGCAAAATCCCTTATA
AATCAAAAGAATAGACCGAGATAGGGTTGAGTGTTGTTCCAGTTTGGAAC
AAGAGTCCACTATTAAAGAACGTGGACTCCAACGTCAAAGGGCGAAAAAC
CGTCTATCAGGGCGATGGCCCACTACGTGAACCATCACCCTAATCAAGTT
TTTTGGGGTCGAGGTGCCGTAAAGCACTAAATCGGAACCCTAAAGGGAGC
CCCCGATTTAGAGCTTGACGGGGAAAGCCGGCGAACGTGGCGAGAAAGGA
AGGGAAGAAAGCGAAAGGAGCGGGCGCTAGGGCGCTGGCAAGTGTAGCGG
TCACGCTGCGCGTAACCACCACACCCGCCGCGCTTAATGCGCCGCTACAG
GGCGCGTCAGGTGGCACTTTTCGGGGAAATGTGCGCGGAACCCCTATTTG
TTTATTTTTCTAAATACATTCAAATATGTATCCGCTCATGAGACAATAAC
CCTGATAAATGCTTCAATAATATTGAAAAAGGAAGAGTATGAGTATTCAA
CATTTCCGTGTCGCCCTTATTCCCTTTTTTGCGGCATTTTGCCTTCCTGT
TTTTGCTCACCCAGAAACGCTGGTGAAAGTAAAAGATGCTGAAGATCAGT
TGGGTGCACGAGTGGGTTACATCGAACTGGATCTCAACAGCGGTAAGATC

CTTGAGAGTTTTCGCCCCGAAGAACGTTTTCCAATGATGAGCACTTTTAA
AGTTCTGCTATGTGGCGCGGTATTATCCCGTATTGACGCCGGGCAAGAGC
AACTCGGTCGCCGCATACACTATTCTCAGAATGACTTGGTTGAGTACTCA
CCAGTCACAGAAAAGCATCTTACGGATGGCATGACAGTAAGAGAATTATG
CAGTGCTGCCATAACCATGAGTGATAACACTGCGGCCAACTTACTTCTGA
CAACGATCGGAGGACCGAAGGAGCTAACCGCTTTTTTGCACAACATGGGG
GATCATGTAACTCGCCTTGATCGTTGGGAACCGGAGCTGAATGAAGCCAT
ACCAAACGACGAGCGTGACACCACGATGCCTGTAGCAATGGCAACAACGT
TGCGCAAACTATTAACTGGCGAACTACTTACTCTAGCTTCCCGGCAACAA
TTAATAGACTGGATGGAGGCGGATAAAGTTGCAGGACCACTTCTGCGCTC
GGCCCTTCCGGCTGGCTGGTTTATTGCTGATAAATCTGGAGCCGGTGAGC
GTGGGTCTCGCGGTATCATTGCAGCACTGGGGCCAGATGGTAAGCCCTCC
CGTATCGTAGTTATCTACACGACGGGGAGTCAGGCAACTATGGATGAACG
AAATAGACAGATCGCTGAGATAGGTGCCTCACTGATTAAGCATTGGTAAC
TGTCAGACCAAGTTTACTCATATATACTTTAGATTGATTTAAAACTTCAT
TTTTAATTTAAAAGGATCTAGGTGAAGATCCTTTTTGATAATCTCATGAC
CAAAATCCCTTAACGTGAGTTTTCGTTCCACTGAGCGTCAGACCCCGTAG
AAAAGATCAAAGGATCTTCTTGAGATCCTTTTTTTCTGCGCGTAATCTGC
TGCTTGCAAACAAAAAAACCACCGCTACCAGCGGTGGTTTGTTTGCCGGA
TCAAGAGCTACCAACTCTTTTTCCGAAGGTAACTGGCTTCAGCAGAGCGC
AGATACCAAATACTGTCCTTCTAGTGTAGCCGTAGTTAGGCCACCACTTC
AAGAACTCTGTAGCACCGCCTACATACCTCGCTCTGCTAATCCTGTTACC
AGTGGCTGCTGCCAGTGGCGATAAGTCGTGTCTTACCGGGTTGGACTCAA
GACGATAGTTACCGGATAAGGCGCAGCGGTCGGGCTGAACGGGGGGTTCG
TGCACACAGCCCAGCTTGGAGCGAACGACCTACACCGAACTGAGATACCT
ACAGCGTGAGCTATGAGAAAGCGCCACGCTTCCCGAAGGGAGAAAGGCGG
ACAGGTATCCGGTAAGCGGCAGGGTCGGAACAGGAGAGCGCACGAGGGAG
CTTCCAGGGGGAAACGCCTGGTATCTTTATAGTCCTGTCGGGTTTCGCCA
CCTCTGACTTGAGCGTCGATTTTTGTGATGCTCGTCAGGGGGGCGGAGCC
TATGGAAAAACGCCAGCAACGCGGCCTTTTTACGGTTCCTGGCCTTTTGC
TGGCCTTTTGCTCACATGTTCTTTCCTGCGTTATCCCCTGATTCTGTGGA
TAACCGTATTACCGCCTTTGAGTGAGCTGATACCGCTCGCCGCAGCCGAA
CGACCGAGCGCAGCGAGTCAGTGAGCGAGGAAGCGGAAGAGCGCCCAATA
CGCAAACCGCCTCTCCCCGCGCGTTGGCCGATTCATTAATGCAGCTGGCA
CGACAGGTTTCCCGACTGGAAAGCGGGCAGTGAGCGCAACGCAATTAATG
TGAGTTAGCTCACTCATTAGGCACCCCAGGCTTTACACTTTATGCTTCCG
GCTCGTATGTTGTGTGGAATTGTGAGCGGATAACAATTTCACACAGGAAA
CAGCTATGACCATGATTACGCCAAGCTCGA

Plasmid Map 9.1 | pT3TS-nCas9n